

**Seismic Response Prediction Method of Buildings
with Floor Flexibility Based on Microtremor Measurement**

XIE Jinzhe

Contents

List of Figures	iv
List of Tables	vii
Chapter 1 Introduction	1
1.1 Background	1
1.2 Objectives.....	4
1.3 Thesis Organizing	5
Reference.....	7
Chapter 2 Dynamic Characteristics of Large-scale Low-rise Buildings Based on Microtremor	
Measurement	13
2.1 Introduction	13
2.2 Objective Buildings.....	13
2.2.1 Building A	13
2.2.2 Building B	15
2.2.3 Building C	15
2.2.4 Building D	15
2.2.5 Building E	15
2.2.6 Building F.....	16
2.3 Modal Identification Using Limited Sensors	16
2.3.1 Modal identification by multi-setup measurement procedures	16
2.3.2 Procedure demonstration by Building A	19
2.4 Modal Properties of Other Buildings	26
2.4.1 Building B	26
2.4.2 Building C	27
2.4.3 Building D	29
2.4.4 Building E	30
2.4.5 Building F.....	31
2.5 Needs of New Dynamic Response Model for Seismic Response Prediction	32
2.6 Conclusions	34
Reference.....	35
Chapter 3 Dynamic Response Modelling Based on Microtremor Measurement	39
3.1 Introduction	39
3.2 Seismic Response Prediction at Measured Locations	40

3.2.1 Modal equation of motion	40
3.2.2 Approximation of participation vector for seismic input	42
3.2.3 Seismic response prediction at sensor locations.....	44
3.3 Dimension Expansion of Modelling Considering Lateral-torsional Coupling Directly	45
3.3.1 2D modelling.....	45
3.3.2 Supplemented prediction procedures considering model selection.....	49
3.4 Conclusions.....	50
Reference.....	50
Chapter 4 Fundamental Properties of the Proposed Seismic Response Prediction Method	53
4.1 Introduction.....	53
4.2 Used 5-DOF Model.....	53
4.3 Influences of Participation Vector Approximation	54
4.3.1 Influence of limited modes.....	54
4.3.2 Influence of limited measurement points	55
4.4 Seismic Response Prediction with Approximated Participation Vector	60
4.5 Conclusions.....	63
Reference.....	64
Chapter 5 Verification with Numerical Model of Large-scale Low-rise Building	67
5.1 Introduction.....	67
5.2 Numerical Model.....	67
5.3 Measurement Points and Used Vibration Modes for Simulation	68
5.4 Participation Vector Approximation	71
5.4.1 1D model.....	71
5.4.2 2D model.....	73
5.5 Seismic Response Prediction.....	77
5.5.1 Single-directional ground motion.....	78
5.5.2 Two-directional ground motion.....	88
5.6 Conclusions.....	97
Reference.....	97
Chapter 6 Verification with Full-scale Shaking Table Test	99
6.1 Introduction.....	99
6.2 Test Specimen	99
6.3 Modal Identification Based on Microtremor Measurement	101
6.4 Participation Vector Approximation	106
6.5 Input Excitations to Shaking Table and Seismic Responses	108

6.6 Modal Properties Under the Shaking Table Tests	114
6.7 Verification with Different Intensities of Ground Motions.....	116
6.7.1 Using unmodified modal properties	117
6.7.2 Using updated modal properties.....	120
6.7.3 Using modified modal properties	123
6.8 Conclusions	127
Reference.....	128
Chapter 7 Conclusions	129
7.1 Summaries	129
7.2 Future Studies.....	131
Publications	133
Acknowledgements	135

List of Figures

Figure 1-1	Relationship among chapters.....	5
Figure 2-1	Atrium and skylight in Building E.....	16
Figure 2-2	Multi-setup measurement for mode shape identification.....	18
Figure 2-3	Measurement at Building A.....	20
Figure 2-4	Examples of microtremor acceleration time histories.....	21
Figure 2-5	Smoothing process.....	22
Figure 2-6	Distributions of the 1 st singular values in the 1 st and 2 nd measurements.....	22
Figure 2-7	Mode shapes of Building A.....	24
Figure 2-8	An example of RD method.....	25
Figure 2-9	Mode shapes of Building B.....	27
Figure 2-10	Modes at 1.51 Hz to 3.17 Hz of Building C.....	28
Figure 2-11	Modes at 3.58 Hz to 5.76 Hz of Building C.....	29
Figure 2-12	Mode shapes of Building D.....	30
Figure 2-13	Mode shapes of Building E.....	31
Figure 2-14	Mode shapes of Building F.....	32
Figure 3-1	General prediction procedure.....	39
Figure 3-2	Analytical model considering floor flexibility.....	41
Figure 3-3	Supplemented seismic response prediction considering model selection.....	49
Figure 4-1	Mode shapes of the 5-DOF model.....	54
Figure 4-2	Response spectrum of the input acceleration with 2% damping ratio.....	61
Figure 4-3	Predicted acceleration time histories.....	63
Figure 5-1	Outlook of the numerical model.....	68
Figure 5-2	Locations for the seismic response prediction.....	69
Figure 5-3	Mode shapes of the selected modes.....	70
Figure 5-4	Sums of approximated participation functions in the 1D model before/after removing the 4 th mode.....	72
Figure 5-5	Sums of <i>x</i> -directional approximated participation functions under the 2D model.....	74
Figure 5-6	Sums of <i>y</i> -directional approximated participation functions under the 2D model.....	75
Figure 5-7	Comparison of MSEs under the 2D models.....	75
Figure 5-8	Participation vector approximation with fewer nodes.....	76
Figure 5-9	Response spectra of input accelerations with 1% damping ratio.....	78

Figure 5-10	Peak acceleration distributions under single-directional ground motions (Unit: m/s^2) ...	79
Figure 5-11	Errors of peak response accelerations using the 1D model under single-directional ground motions (Unit: %)	80
Figure 5-12	Errors of peak response accelerations using the 2D model under single-directional ground motions (Unit: %)	81
Figure 5-13	Largest x -directional responses on the 4 th floor under the x -directional El Centro wave	84
Figure 5-14	Largest x -directional responses on the 4 th floor under the x -directional Taft wave	84
Figure 5-15	Largest x -directional responses on the 4 th floor under the x -directional Hachinohe wave	85
Figure 5-16	Largest x -directional responses on the 4 th floor under the x -directional JMA Kobe wave	85
Figure 5-17	Largest y -directional responses on the 4 th floor under the y -directional El Centro wave	86
Figure 5-18	Largest y -directional responses on the 4 th floor under the y -directional Taft wave	86
Figure 5-19	Largest y -directional responses on the 4 th floor under the y -directional Hachinohe wave	87
Figure 5-20	Largest y -directional responses on the 4 th floor under the y -directional JMA Kobe wave	87
Figure 5-21	Peak acceleration distributions under two-directional ground motions (Unit: m/s^2)	88
Figure 5-22	Errors of peak response accelerations using the 1D model under two-directional ground motions (Unit: %)	89
Figure 5-23	Errors of peak response accelerations using the 2D model under two-directional ground motions (Unit: %)	90
Figure 5-24	Largest x -directional responses on the 4 th floor under the two-directional El Centro wave	93
Figure 5-25	Largest x -directional responses on the 4 th floor under the two-directional Taft wave	93
Figure 5-26	Largest x -directional responses on the 4 th floor under the two-directional Hachinohe wave	94
Figure 5-27	Largest x -directional responses on the 4 th floor under the two-directional JMA Kobe wave	94
Figure 5-28	Largest y -directional responses on the 4 th floor under the two-directional El Centro wave	95
Figure 5-29	Largest y -directional responses on the 4 th floor under the two-directional Taft wave	95
Figure 5-30	Largest y -directional responses on the 4 th floor under the two-directional Hachinohe wave	96
Figure 5-31	Largest y -directional responses on the 4 th floor under the two-directional JMA Kobe wave	96
Figure 6-1	Test specimen outlook	100

Figure 6-2	Geometric information and the measurement points in the specimen	100
Figure 6-3	EXP.J at the connecting bridge.....	101
Figure 6-4	Accelerations in Measurement A.....	103
Figure 6-5	1 st singular value distribution.....	104
Figure 6-6	Mode shapes identified from microtremor measurements.....	105
Figure 6-7	Response spectra of input accelerations on the shaking table.....	109
Figure 6-8	x-directional accelerations in No.1 test.....	110
Figure 6-9	y-directional accelerations in No.3 test.....	110
Figure 6-10	Accelerations in No.5 test.....	111
Figure 6-11	Accelerations in No.6 test.....	112
Figure 6-12	x-directional accelerations with extreme peak amplitudes in No.6 test.....	113
Figure 6-13	x-directional modal properties in the 1 st mode under the Kobe waves	114
Figure 6-14	y-directional modal properties in the 1 st mode under the OS2 waves.....	115
Figure 6-15	Response prediction using unmodified modal properties in tests where no structural damage occurred.....	118
Figure 6-16	Response prediction using unmodified modal properties in tests where structural damage occurred	119
Figure 6-17	Response prediction using updated modal properties in tests where no structural damage occurred	121
Figure 6-18	Response prediction using updated modal properties in tests where structural damage occurred	122
Figure 6-19	Response prediction using modified modal properties in tests where no structural damage occurred.....	124
Figure 6-20	Response prediction using modified modal properties in tests where structural damage occurred	125
Figure 6-21	Predicted acceleration amplitudes corresponding to different natural frequencies and damping ratios	126

List of Tables

Table 2-1	Objective buildings.....	14
Table 2-2	Measurement plan	19
Table 2-3	Identified natural frequencies (Hz) from FDD method	23
Table 2-4	Identified natural frequencies and damping ratios from RD method	25
Table 2-5	Identified 1 st natural frequencies	33
Table 4-1	Mass and inter-story stiffness of the 5-DOF model.....	53
Table 4-2	Modal properties of the 5-DOF model	54
Table 4-3	Participation vector approximation using limited modes	54
Table 4-4	Sums of approximated participation functions using limited modes.....	55
Table 4-5	Participation vector approximation with different selected nodes.....	56
Table 4-6	Sums of approximated participation functions and corresponding MSE	57
Table 4-7	Participation vector approximation using mode shapes at selected nodes in limited modes	58
Table 4-8	Approximated participation functions before and after the 4 th mode is added.....	58
Table 4-9	Seismic response amplitude prediction using mode shapes at all nodes.....	60
Table 4-10	Seismic response amplitude prediction using mode shapes at Nodes 1, 2, 3 and 5	62
Table 5-1	Participation vector approximation using the 1D model.....	71
Table 5-2	Participation vector approximation using the 2D model.....	73
Table 5-3	Participation vector approximation with fewer nodes.....	76
Table 5-4	Participation vector approximation using mode shapes on upper floors.....	77
Table 5-5	Averaged/Peak prediction errors using the 1D model under single-directional ground motions	82
Table 5-6	Averaged/Peak prediction errors using the 2D model under single-directional ground motions	82
Table 5-7	Largest response amplitudes in the x - and y -directions on the 4 th floor.....	83
Table 5-8	Averaged/Peak prediction errors using the 1D model under two-directional ground motions	91
Table 5-9	Averaged/Peak prediction errors using the 2D model under two-directional ground motions	91
Table 5-10	Largest response amplitudes in the x - and y -directions on the 4 th floor.....	92
Table 6-1	Microtremor measurement plan	102
Table 6-2	Modes identified from microtremor measurements	104

Table 6-3	Preliminary participation vector approximation	106
Table 6-4	Participation vector approximation after removing modes	106
Table 6-5	Participation vector approximation using mode shapes at selected locations.....	107
Table 6-6	Sums of approximated participation functions.....	108
Table 6-7	Shaking table test	109
Table 6-8	Peak response amplitudes in the six tests.....	113
Table 6-9	Comparison of modal properties between under microtremor measurements and earthquakes.....	116
Table 6-10	Averaged prediction errors using unmodified modal properties.....	120
Table 6-11	Averaged prediction errors using updated modal properties.....	121
Table 6-12	Averaged prediction errors using modified modal properties.....	124

Chapter 1

Introduction

1.1 Background

In large Japanese cities like Tokyo and Osaka, it is recommended that building users stay in the building for a few days if its safety is confirmed after a large earthquake occurs [1-3]. However, it takes time and effort to secure the building safety when it has no obvious damage from the outlook. The quick seismic response estimation provides seismic responses at many locations on all floors, the information is helpful to estimate the structural damage for decision making and can improve the efficiency of building checking. In addition, the acceleration amplitude and the story drift at each location are related to the damage evaluation of non-structural components [4-6]. Therefore, the quick response estimations of accelerations and displacements also provide information to building owners to evaluate the losses of non-structural components that can be damaged before structural damage occurs [7-11].

The seismic response estimation requires a good understanding of the dynamic properties of the objective buildings. The direct way to understand the dynamic properties of a building under an earthquake is structural health monitoring. Sensors are installed at a building and the dynamic properties can be identified from the seismic response records. Imai *et al.* use four simulations with four different methods to demonstrate the applicability of modal parameter identification when the ground motion and vibration records at certain locations are given [12]. When structural damage occurs, the on-line modal parameter identification approaches can identify the equivalent dynamic properties to understand how they change during an earthquake [13].

Structural health monitoring is mainly applied to medium/high-rise buildings and the dynamic properties of these kinds of structures have been investigated well. Çelebi and Safak analysed the seismic response of a pyramid-shaped 60-story steel building under the 1989 Loma Prieta Earthquake [14, 15]. The soil-structure interaction was observed by comparing the free-field motion with the motion at the basement. The 1st natural frequencies in horizontal directions of the building identified from ambient vibration and forced vibration tests were identical when the living load and non-structural components were not loaded. The 1st natural frequencies were decreased by around 20% during the earthquake while the building had no obvious structural damage. They also analyzed the recorded accelerations of a 30-story building with the three-winged planar shape under the 1989 Loma Prieta Earthquake [16, 17]. It was observed that multiple modes, including lower modes below 2 Hz and higher modes around 5 Hz, were excited during the earthquake, and the identified modes exhibited lateral-torsional coupling. Çelebi *et al.* further compare the dynamic properties of five buildings subjected to the Loma Prieta Earthquake to these values from ambient vibration testing [18]. It was found that the natural frequencies from the testing are generally higher than

the values during an earthquake even if the building has no obvious structural damage. Trifunac *et al.* investigated the seismic response of a 7-story reinforced concrete (RC) building under 12 ground motions and found that the changes in identified natural frequencies could be caused by the soil-structure interaction [19-21]. The dynamic property amplitude dependency was investigated by Hisada *et al.* using the seismic response of the 29-story steel frame building under the 2011 Tohoku Earthquake [22]. The seismic responses of a 29-story building in Reference 22 and an additional 30-story neighboring building were further investigated by Çelebi *et al.* [23]. The changes in natural frequencies and damping ratios before, during and after the mainshock of the 2011 Tohoku Earthquake were studied. The 1st natural frequencies in the horizontal directions before the earthquake are around 10% larger than the values during the mainshock. However, the 1st damping ratios remained within 1-2% before, during and after the mainshock. The relationship between the response amplitudes and the dynamic properties was also investigated by Kashima using the seismic response at four high-rise steel buildings under the 2011 Tohoku Earthquake [24]. The seismic responses of high-rise buildings are more likely obtained because sensors can be installed for wind load monitoring and obtain the seismic responses by accident [25]. The identified dynamic properties contribute to the development of the structural design. For example, the Chilean seismic code NCh433 had major changes in 1993 and 1996 based on the lessons learnt after the 1985 Algarrobo Earthquake. Most of the high-rise buildings affected by the 2010 Maule Earthquake were designed by the updated code and those buildings performed well [26].

Structural health monitoring is not only used for dynamic property identification but also used to estimate the seismic responses at unmonitored locations. In practical situations, it is impossible to install many sensors for long-term monitoring because of the maintenance expenses. As a result, many methods are developed for the overall structural dynamic response estimation with limited sensors. They are classified by Limongelli into four kinds [27]: (1) methods that reduce the total number of degrees of freedom of the system so that the model parameters of the structure like stiffness matrix can be estimated using a limited amount of sensors [28-30]; (2) methods for the use of the extended Kalman filter method [31, 32]; (3) methods based on the expansion of measured mode shapes to the total dynamic degrees of freedom [33-35]; and (4) methods for sensor location optimization [36, 37]. Among the four categories, the third category is of particular interest because it can be used to predict the seismic response at unmonitored locations by using the mode superposition method. Ikeda and Hisada approximate the mode shapes by the sinusoidal waves to predict seismic responses of unmonitored floors, the prediction method was verified by using the recorded seismic responses of a 29-story building [38]. The prediction is not necessarily based on the expansion of mode shapes. Limongelli directly uses the spline function to interpolate the absolute accelerations at different floors in Reference 27, then the changes of parameters in the interpolation function are used for damage detection [39, 40]. Kodera *et al.* modify the boundary restriction of the spline function interpolation process in Reference 27 to consider the shear deformation near the ground [41]. The seismic response prediction can also be transformed into the modal response identification process when the mode shapes are available. An example is demonstrated by He *et al.* The mode shapes of the objective building were obtained by the finite element model. The modal responses were extracted by the empirical

mode decomposition and the seismic responses at unmonitored locations were obtained by the mode superposition method [42]. Morii *et al.* used the mode shapes obtained from the design documents to predict the seismic responses of a 1/3-scale 18-story steel building under shaking table tests [43]. The shaking table tests were also used to verify the sinusoidal wave approximation method in Reference 38 [44].

There also exist seismic response prediction methods that do not necessarily require sensors installed in the objective building to obtain seismic responses at some locations [45-48]. Those prediction methods use the modal properties from measurements to model the objective building. Michel *et al.* obtained the inter-story stiffness of a 9-story RC building using the identified dynamic properties from microtremor measurements and predicted its response under the ground motion caused by the nearby bridge demolition [45]. Then they used the method to predict the seismic response of a 13-story RC tower under the Vallorcine Earthquake [46]. The prediction method is further utilized to evaluate the vulnerability of buildings by the fragility estimation regarding inter-story drifts [47]. Mori and Spina used the probability approach to consider the natural frequency differences under microtremor measurements and an earthquake, then they predicted the seismic responses of a 3-story RC building under three earthquakes [48].

When the rigid-floor assumption is utilized, an individual floor or a group of floors is considered as a lumped mass and a building is modelled as the stick-shape lumped mass model. The seismic response estimation can be performed without any design document when the rigid-floor assumption is utilized [27, 38-41, 44-48]. The simplicity of the stick-shape lumped mass model makes it possible to identify the stiffness matrix, and the corresponding damping and mass matrices using the recorded accelerations at all floors. Ikeda transfers the mass identification problem into the conditional extremum problem. The mass matrix is identified using the mode shapes in limited modes [49], then the stiffness and damping matrices are estimated using the identified mass matrix and modal properties [50]. The difference between References 45 and 50 in the stiffness identification is that the former only uses the 1st mode while the latter utilizes multiple modes simultaneously. The mass and stiffness identification methods in References 49 and 50 were firstly verified by the shaking table test data of a 0.3-scale 6-story steel structure recorded in Reference [51] and then by the full-scale shaking table tests [52]. The convenience of the stick-shape lumped mass model is also exhibited in the nonlinear system. The nonlinear inter-story restoring force can be modelled by the Bouc-Wen model and the parameters in the Bouc-Wen model can be identified by using the recorded seismic responses [52, 53]. Despite the stick-shape lumped mass model, high-rise buildings can also be simplified by other models such as the elastic layered shear beam, a floor or a group of floors is simplified as a layer in the layered shear beam model [54, 55].

The existing seismic response prediction methods take the advantage of the geometric characteristics of the medium/high-rise buildings. They are generally based on the stick-shape lumped mass model by using the rigid-floor assumption. The rigid-floor assumption might not be applicable to all buildings such as the large-scale low-rise buildings because they have large planar areas with irregular shapes. However, there are few studies about the dynamic properties of large-scale low-rise buildings, whether the rigid-floor assumption is applicable to this kind of structure is unclear. Buildings under 60 m do not require time-series analysis for structural designs in Japan [56]. As a result, the seismic response records of low-rise

buildings are few and their dynamic properties are not well understood. Nonetheless, the seismic response estimation is still required when the structural condition is difficult to judge from the building outlook. The seismic responses of large-scale low-rise buildings are difficult to obtain, an alternative way to explore their dynamic properties is to use ambient vibration testing or so-called microtremor measurement. The word ‘ambient’ suggests the source of the vibration include wind, pedestrian, etc. The word ‘microtremor’ implies the level of the excitation is very small compared to an earthquake. Microtremor measurement is generally based on the output-only modal analysis because the source of the excitation is unmeasurable. One of the typical applications using microtremor measurement is to study the shift of dynamic properties before and after an earthquake [14-25, 57-59]. The identified dynamic properties from microtremor measurement are also used for other purposes such as investigating the dynamic properties under small-amplitude vibration such as weak ground motion and wind load [25, 60, 61] and numerical model calibration [62-64]. The seismic response prediction methods in References 45-48 have the advantage of not using design documents to establish mass, damping and stiffness matrices. The measured building is modelled by the modal properties from microtremor measurements. However, a new modelling method that considers floor flexibility might be required for the seismic response prediction when the objective building cannot assume floor rigid.

1.2 Objectives

The overall objective of this research is to propose a seismic response prediction method that utilizes the modal properties obtained from microtremor measurements. The method is not constrained by the rigid-floor assumption so it has wider applicability than the existing methods. The specific objectives of this research are:

- (1) To investigate the necessity of considering floor flexibility in the seismic response prediction. The modal properties of large-scale low-rise buildings are obtained from microtremor measurements. They are likely against the rigid-floor assumption because of their large-scale asymmetric planar shapes and components like expansion joints, large atria and skylights.
- (2) To propose the seismic response prediction method based on microtremor measurement, the method is based on the modal properties identified from microtremor measurements to model a multi-degree-of-freedom equivalently-linear building. The modelling is not constrained by the rigid-floor assumption. Then the seismic responses at the measured locations can be predicted under a given ground motion.
- (3) To study the fundamental properties of the proposed prediction method by numerical simulations. The applicability of the proposed prediction method is also preliminarily verified by numerical simulations that do not consider modal property variances.
- (4) To verify the proposed prediction method under different scales of ground motions and investigate the influence of the modal property variances on the seismic response prediction accuracy. The proposed method is applied to the specimen of full-scale shaking table tests. The predicted seismic responses are compared to the recorded responses for method verification.

1.3 Thesis Organizing

The present research mainly includes five chapters apart from the introduction in Chapter 1 and the conclusions in Chapter 7. The structure of the dissertation is shown in Figure 1-1 and the main contents of Chapters 2 to 6 are summarized below.

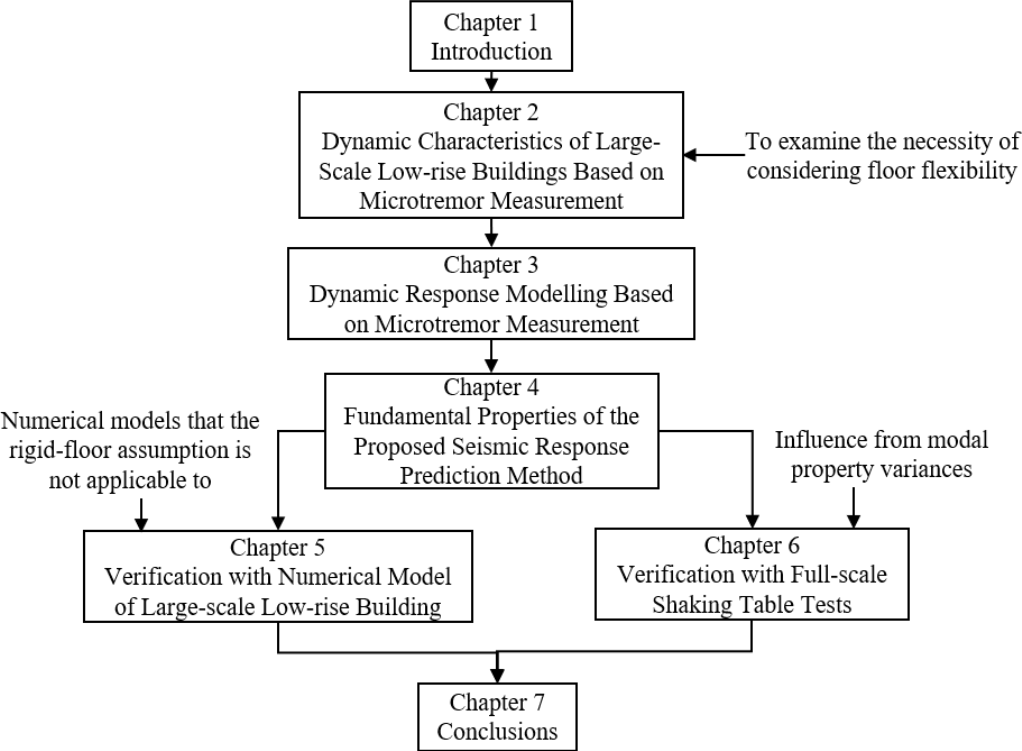


Figure 1-1 Relationship among chapters

In Chapter 2, the dynamic characteristics of large-scale low-rise buildings are studied by applying microtremor measurements to six actual commercial buildings in Japan. The natural frequencies, the corresponding damping ratios and the mode shapes in limited modes are identified to extract the general dynamic characteristics from these structures. Each building is different from others from structural perspective, their modal properties in common reflect the general dynamic characteristics. The measurements were conducted by multi-setups of measurements because the number of locations to measure exceeds the number of available accelerometers. Microtremors at several locations are measured simultaneously during one measurement and the corresponding mode shapes are obtained. The separately identified mode shapes via each measurement are assembled afterward to obtain the global mode shapes of the building. The assembled mode shapes are utilized to investigate whether the rigid-floor assumption in the existing seismic response prediction methods is applicable to this kind of structure. The implemented measurements explain the necessity of developing a new seismic response prediction method that is not constrained by the rigid-floor assumption.

In Chapter 3, a microtremor measurement-based seismic response prediction method is proposed. A multi-degree-of-freedom linear building is modelled by the modal equations of motion. The modal

equations of motion consist of the identified natural frequencies, damping ratios, mode shapes and participation factors for seismic input. The former three modal components in limited modes can be identified from microtremor measurements. The natural frequencies and damping ratios from measurements require their modifications to consider variances between modal properties under microtremor measurements and an earthquake even if the structure is not damaged. The participation factors are approximated by the identified mode shapes. Floor flexibility is interpreted by having multiple nodes on the same floor in the construction of the analytical model. All measured locations become the lumped nodes of the analytical model. The outline and concept of the prediction method are firstly introduced in one horizontal dimension. Then a two-dimensional (2D) model is utilized to fully consider the lateral-torsional coupling property that large-scale low-rise buildings with asymmetric planar shapes are likely to have. The selection of either the single-dimensional model (1D) or the 2D model depends on the microtremor measurement identification results.

In Chapter 4, the fundamental properties of the proposed seismic response prediction method are discussed by a simple numerical model. The fundamental properties include two parts: One is the proposed participation vector approximation method; and the other is the seismic response prediction using limited modes with the approximated participation vector. When the rigid-floor is not assumed, every location on a floor becomes a candidate to measure while only limited locations can be measured. In the numerical simulation, it means the participation factors in the limited modes are approximated by mode shapes at the selected nodes. In this chapter, the simulation firstly studies the influence of the limited modes on the participation vector approximation accuracy when using mode shapes at all nodes. It shows the applicability of the proposed participation vector approximation method. Next, the participation vector approximation is investigated when the mode shapes at the selected nodes are used. It shows how the selection of measured locations, which are node locations, influences the participation vector approximation accuracy. Lastly, the seismic response accuracy of the proposed seismic response prediction method is investigated. The study also shows how the prediction accuracy is influenced by the complicated interaction between participation factor approximation errors and the truncation errors in the mode superposition.

In Chapter 5, the proposed seismic response prediction method is further verified by a more complicated numerical model. The numerical model expresses a large-scale low-rise building and it has multiple modes with obvious lateral-torsional coupling. More importantly, the numerical model shows obvious floor flexibility. The main purpose of this simulation is to verify the advantage of the prediction method for not being constrained by the rigid-floor assumption. The simulation also confirms the necessity of the 2D model for buildings having multiple modes with lateral-torsional coupling. The necessity is reflected in two aspects: The 1D model approximates the participation vector in one direction using the same directional mode shape components. The 2D model approximates the participation vector in one direction by simultaneously using the mode shapes in two directions; The 2D model considers the vibrations induced by orthogonal ground motions while the 1D model cannot. The participation vector approximation results using the 1D and 2D models are firstly compared, then the seismic response prediction accuracies under the

single-directional ground motion are compared to show the consequence of participation factor approximation errors. Lastly, the predictions under the two-directional ground motions are performed to exhibit the necessity of considering vibrations caused by the orthogonal ground motions.

In Chapter 6, the prediction method is verified by the full-scale shaking table tests. The applicability of the prediction method in practical situations under different scales of ground motions is tested. The modal property variances are also investigated. The modal property variances here are mainly the natural frequency and damping ratio variances when they are under microtremor measurements and an earthquake. The variances are not considered in Chapters 4 and 5 because the two chapters are used to demonstrate the concept and preliminarily verify the proposed method. In this chapter, the natural frequencies and damping ratios identified from microtremor measurements are compared to the values identified from shaking table tests. Then, the seismic response predictions under three scenarios are performed: the first scenario directly uses the natural frequencies and damping ratios identified from microtremor measurements without the consideration of modal property variances; The second scenario uses the updated natural frequencies and damping ratios, providing that an observation system is installed for the modal property updating; The third scenario modifies the natural frequencies and damping ratios from microtremor measurements by factors that are based on engineering experience. The modified natural frequencies and damping ratios are slightly different from the actual values, but the prediction method using modified modal properties does not require instrumented sensors for seismic response recording.

In Chapter 7, the conclusions in Chapters 2 to 6 are summarized and integrated, then the future works related to this research are discussed.

Reference

- [1] Japan Cabinet Office (2015): Guidelines for people who have difficulty returning home after a large earthquake (in Japanese, translated by the author), http://www.bousai.go.jp/jishin/kitakukonnan/pdf/kitakukonnan_guideline.pdf (Accessed on 17 May 2022).
- [2] Tokyo Metropolitan (2020): Handbook for people who have difficulty returning home in Tokyo (in Japanese, translated by the author), https://www.bousai.metro.tokyo.lg.jp/_res/projects/default_project/_page_/001/001/369/202008.pdf (Accessed on 17 May 2022).
- [3] Osaka Prefecture Government (2018): Guidelines for people who have difficulty returning home in Osaka after a large earthquake (in Japanese, translated by the author), <https://www.pref.osaka.lg.jp/attach/23998/00000000/chirashi.pdf> (Accessed on 17 May 2022).
- [4] Lee TH, Kato M, Matsumiya T, Suita K, Nakashima M (2007): Seismic performance evaluation of non-structural components: drywall partitions, *Earthquake Engineering & Structural Dynamics*, Vol.36(3), pp.367-382.
- [5] Del Gobbo GM, Williams M, Blakeborough A (2016): Seismic performance assessment of a code compliant multistorey building, In: *The International Conference on Urban Risks* (Lisbon, Portugal), 8 pages, https://www.researchgate.net/profile/Giuseppe-Del-Gobbo/publication/301337059_Seismic_Performance_Assessment_of_a_Code_Compliant_Multistorey_Building/links/571239c108ae39beb87

- a40b3/Seismic-Performance-Assessment-of-a-Code-Compliant-Multistorey-Building.pdf (Accessed on 20 May 2022).
- [6] Derakhshan H, Walsh KQ, Ingham JM, Griffith MC, Thambiratnam DP (2020): Seismic fragility assessment of nonstructural components in unreinforced clay brick masonry buildings, *Earthquake Engineering & Structural Dynamics*, Vol.49(3), pp.285-300.
- [7] Naeim F (1999): Lessons learned from performance of nonstructural Components during the January 17, 1994 Northridge Earthquake-Case studies of six instrumented multistory buildings, *Journal of Seismology and Earthquake Engineering*, Vol.2(1), pp.47-57.
- [8] Achour N, Miyajima M, Kitaura M, Price A (2011): Earthquake-induced structural and nonstructural damage in hospitals, *Earthquake Spectra*, Vol.27(3), pp.617-634.
- [9] Kurata M, Hitomi M, Shimmoto S, Ohtsuru S, Shimoto M, Cho K, Sugiyama O, Aida S (2018): Hearing and analysis of hospital evacuation after the 2016 Kumamoto earthquake, In: *Proceedings of the 16th European Conference on Earthquake Engineering* (Thessaloniki, Greece), 9 pages, <http://papers.16ecee.org/files/10940%20final%20corr.pdf> (Accessed on 20 May 2022).
- [10] Qi L, Kunitomo K, Kurata M, Ikeda Y (2020): Investigating the vibration properties of integrated ceiling systems considering interactions with surrounding equipment, *Earthquake Engineering & Structural Dynamics*, Vol.49(8), pp.772-793.
- [11] Qi L, Kurata M, Ikeda Y, Kunitomo K, Takaoka M (2021): Seismic evaluation of two-elevation ceiling system by shake table tests, *Earthquake Engineering & Structural Dynamics*, Vol.50(4), pp.1147-1166.
- [12] Imai H, Yun CB, Maruyama O, Shinozuka M (1989): Fundamentals of system identification in structural dynamics, *Probabilistic Engineering Mechanics*, Vol.4(4), pp.162-173.
- [13] Loh CH, Lin HM (1996): Application of off-line and on-line identification techniques to building seismic response data, *Earthquake Engineering & Structural Dynamics*, Vol.25(3), pp.269-290.
- [14] Celebi M, Şafak E (1991): Seismic response of Transamerica building. I: Data and preliminary analysis, *Journal of Structural Engineering*, ASCE, Vol.117(8), pp.2389-2404.
- [15] Şafak E, Celebi M (1991): Seismic response of Transamerica building. II: system identification, *Journal of Structural Engineering*, ASCE, Vol.117(8), pp.2405-2425.
- [16] Celebi M, Şafak E (1992): Seismic response of Pacific Park Plaza. I: Data and preliminary analysis, *Journal of Structural Engineering*, ASCE, Vol.118(6), pp.1547-1565.
- [17] Şafak E, Celebi M (1992): Recorded seismic response of Pacific Park Plaza. II: system identification, *Journal of Structural Engineering*, ASCE, Vol.118(6), pp.1566-1589.
- [18] Celebi M, Phan LT, Marshall RD (1993): Dynamic characteristics of five tall buildings during strong and low-amplitude motions, *The Structural Design of Tall Buildings*, Vol.2(1), pp.1-15.
- [19] Luco JE, Trifunac MD, Wong HL (1987): On the apparent change in dynamic behavior of a nine-story reinforced concrete building, *Bulletin of the Seismological Society of America*, Vol.77(6), pp.1961-1983.
- [20] Trifunac MD, Ivanović SS, Todorovska MI (2001): Apparent periods of a building. I: Fourier analysis,

- Journal of Structural Engineering*, ASCE, Vol.127(5), pp.517-526.
- [21] Trifunac MD, Ivanović SS, Todorovska MI (2001): Apparent periods of a building. II: Time-frequency analysis, *Journal of Structural Engineering*, ASCE, Vol.127(5), pp.527-537.
- [22] Hisada Y, Yamashita T, Murakami M, Kubo T, Arata T, Shindo J, Aizawa K (2012): Seismic response and damage of high-rise buildings in Tokyo, Japan, during the 2011 Tohoku earthquake, *Proceedings of the 15th World Conference on Earthquake Engineering* (Lisbon, Portugal), 9 Pages, Paper ID: 4096
- [23] Çelebi M, Hisada Y, Omrani R, Ghahari SF, Taciroglu E (2016): Responses of two tall buildings in Tokyo, Japan, before, during, and after the M9.0 Tohoku Earthquake of 11 March 2011, *Earthquake Spectra*, Vol.32(1), pp.463-495.
- [24] Kashima T (2017): Study on changes in dynamic characteristics of high-rise steel-framed buildings based on strong motion data, *Procedia Engineering*, Vol.199, pp.194-199.
- [25] Brownjohn JMW, Pan TC (2001): Response of tall buildings to weak long distance earthquakes, *Earthquake Engineering & Structural Dynamics*, Vol.30(5), pp.709-729.
- [26] Lagos R, Kupfer M, Lindenberg J, Bonelli P, Saragoni R, Guendelman T, Massone L, Boroschek R, Yanez F (2012): Seismic performance of high-rise concrete buildings in Chile, *International Journal of High-Rise Buildings*, Vol.1(3), pp.181-194.
- [27] Limongelli MP (2003): Optimal location of sensors for reconstruction of seismic responses through spline function interpolation, *Earthquake Engineering & Structural Dynamics*, Vol.32(7), pp.1055-1074.
- [28] Kabe AM (1985): Stiffness matrix adjustment using mode data, *AIAA Journal*, Vol.23(9), pp.1431-1436.
- [29] Farhat C, Hemez FM (1993): Updating finite element dynamic models using an element-by-element sensitivity methodology, *AIAA Journal*, Vol.31(9), pp.1702-1711.
- [30] Yang CD, Yeh FB (1990): Identification, reduction, and refinement of model parameters by the eigensystem realization algorithm, *Journal of Guidance, Control, and Dynamics*, Vol.13(6), pp.1051-1059.
- [31] Hoshiya M, Saito E (1984): Structural identification by extended Kalman filter, *Journal of Engineering Mechanics*, ASCE, Vol.110(12), pp.1757-1770.
- [32] Hoshiya M, Sutoh A (1993): Kalman filter-finite element method in identification, *Journal of Engineering Mechanics*, ASCE, Vol.119(2), pp.197-210.
- [33] Shi ZY, Law SS, Zhang LM (2000): Damage localization by directly using incomplete mode shapes, *Journal of Engineering Mechanics*, ASCE, Vol.126(6), pp.656-660.
- [34] Law SS, Shi ZY, Zhang LM (1998): Structural damage detection from incomplete and noisy modal test data, *Journal of Engineering Mechanics*, ASCE, Vol.124(11), pp.1280-1288.
- [35] Levine-West M, Milman M, Kissil A (1996): Mode shape expansion techniques for prediction-experimental evaluation, *AIAA Journal*, Vol.34(4), pp.821-829.
- [36] Shah PC, Udawadia FE (1978): A methodology for optimal sensor locations for identification of

- dynamic systems, *Journal of Applied Mechanics*, ASME, Vol.45(1), pp.188-196.
- [37] Udawadia FE (1994): Methodology for optimum sensor locations for parameter identification in dynamic systems, *Journal of Engineering Mechanics*, ASME, Vol.120(2), pp.368-390.
- [38] Ikeda Y, Hisada Y (2013): Earthquake responses on all floors in a building estimated by observation records on some restricted floor, *Journal of Japan Association for Earthquake Engineering*, JAEE, Vol. 13(4), pp.38-54 (in Japanese).
- [39] Limongelli MP (2011): The interpolation damage detection method for frames under seismic excitation, *Journal of Sound and Vibration*, Vol.330(22), pp.5474-5489.
- [40] Limongelli MP (2014): Seismic health monitoring of an instrumented multistory building using the interpolation method, *Earthquake Engineering & Structural Dynamics*, Vol.43(11), pp.1581-1602.
- [41] Kodera K, Nishitani A, Okihara Y (2018): Cubic spline interpolation based estimation of all story seismic responses with acceleration measurement at a limited number of floors, *Journal of Structure Construction Engineering*, AIJ, Vol.83(746), pp. 527-535 (in Japanese).
- [42] He J, Guan X, Liu Y (2012): Structural response reconstruction based on empirical mode decomposition in time domain, *Mechanical Systems and Signal Processing*, Vol.28, pp.348-366.
- [43] Morii T, Okada K, Shiraishi M, Sugimoto K, Terada T, Sato T, Tobita J (2016): Seismic response estimation of whole building based on limited number of acceleration records for structural health monitoring system shortly after an earthquake-system application for large shaking table test of an 18-story steel building, *Journal of Structure Construction Engineering*, AIJ, Vol.81(730), pp.2045-2055 (in Japanese).
- [44] Hatada T, Ikeda Y, Hagiwara H, Nitta Y, Nishitani A (2018): Damage evaluation method based on acceleration measurement on some restricted floors, *Proceedings of the 16th European Conference on Earthquake Engineering* (Thessaloniki, Greece), 12 pages, Paper ID: 10305.
- [45] Michel C, Guéguen P, Bard PY (2008): Dynamic parameters of structures extracted from ambient vibration measurements: An aid for the seismic vulnerability assessment of existing buildings in moderate seismic hazard regions, *Soil Dynamics and Earthquake Engineering*, Vol.28(8), pp.593-604.
- [46] Michel C, Guéguen P, Arem SE, Mazars J, Kotronis P (2010): Full-scale dynamic response of an RC building under weak seismic motions using earthquake recordings, ambient vibrations and modelling, *Earthquake Engineering & Structural Dynamics*, Vol.39(4), pp.419-441.
- [47] Michel C, Gueguen P, Causse M (2012): Seismic vulnerability assessment to slight damage based on experimental modal parameters, *Earthquake Engineering & Structural Dynamics*, Vol.41(1), pp.81-98.
- [48] Mori F and Spina D (2015): Vulnerability assessment of strategic buildings based on ambient vibrations measurements, *Structural Monitoring and Maintenance*, Vol.2(2), pp.115-132.
- [49] Ikeda Y (2008): Mass identification for building on linear programming utilizing modal shapes, *Journal of Structural and Construction Engineering*, AIJ, Vol.73(627), pp.749-756 (in Japanese).
- [50] Ikeda Y (2009): Identification of story stiffness for MDOF shear building structures considering consistency with modal information, *Journal of Structural and Construction Engineering*, AIJ, Vol.74(646), pp.2237-2243 (in Japanese).

- [51] Whittaker AS, Uang CM, Bertero VV (1987): Earthquake simulation tests and associated studies of a 0.3-scale model of a six-story eccentrically braced steel structure, Report ID: UCB/EERC-87/02, Earthquake Engineering Research Center, College of Engineering, University of California.
- [52] Ikeda Y. (2016): Verification of system identification utilizing shaking table tests of a full-scale 4-story steel building, *Earthquake Engineering & Structural Dynamics*, Vol.45(4), pp.543-562.
- [53] Loh CH, Lin CY, Huang CC (2000): Time domain identification of frames under earthquake loadings, *Journal of Engineering Mechanics*, ASCE, Vol.126(7), pp.693-703.
- [54] Rahmani M, Todorovska MI (2013): 1D system identification of buildings during earthquakes by seismic interferometry with waveform inversion of impulse responses-method and application to Millikan library, *Soil Dynamics and Earthquake Engineering*, Vol.47, pp.157-174.
- [55] Rahmani M, Todorovska MI (2015): Structural health monitoring of a 54-story steel-frame building using a wave method and earthquake records, *Earthquake Spectra*, Vol.31(1), pp.501-525.
- [56] Hasegawa T (2013): Introduction to the Building Standard Law, Building Regulation in Japan, https://www.bcj.or.jp/upload/international/baseline/BSLIntroduction201307_e.pdf. (Accessed on 17 May 2022).
- [57] Sato T, Nakamura Y, Saita J (2008): The change of the dynamic characteristics using microtremor, In: *Proceedings of the 14th World Conference on Earthquake Engineering* (Beijing, China), 10 pages, https://sdr.co.jp/papers/14wcee/14wcee_microtremor.pdf (Accessed on 20 May 2022).
- [58] Ivanović SS, Trifunac MD, Novikova EI, Gladkov AA, Todorovska MI (2000): Ambient vibration tests of a seven-story reinforced concrete building in Van Nuys, California, damaged by the 1994 Northridge earthquake, *Soil Dynamics and Earthquake Engineering*, Vol.19(6), pp.391-411.
- [59] Kohler MD, Davis PM, Safak E (2005): Earthquake and ambient vibration monitoring of the steel-frame UCLA Factor building. *Earthquake Spectra*, Vol.21(3), pp.715-736.
- [60] Yang JN, Lei Y, Lin S, Huang N (2004): Identification of natural frequencies and dampings of in situ tall buildings using ambient wind vibration data, *Journal of Engineering Mechanics*, Vol.130(5), pp.570-577.
- [61] Aloisio A, Pasca D, Tomasi R, Fragiocomo M (2020): Dynamic identification and model updating of an eight-storey CLT building, *Engineering Structures*, Vol.213, 8 pages, Paper ID: 110593.
- [62] Jaishi B, Ren WX (2005): Structural finite element model updating using ambient vibration test results, *Journal of Structural Engineering*, Vol.131(4), pp.617-628.
- [63] Wu JR, Li QS (2004): Finite element model updating for a high-rise structure based on ambient vibration measurements, *Engineering Structures*, Vol.26(7), pp.979-990.
- [64] Wu JR, Li QS (2006): Structural parameter identification and damage detection for a steel structure using a two-stage finite element model updating method, *Journal of Constructional Steel Research*, Vol.62(3), pp.231-239.

Chapter 2

Dynamic Characteristics of Large-scale Low-rise Buildings Based on Microtremor Measurement

2.1 Introduction

In Japan, buildings less than 60 m high do not necessarily require vibration analysis in the structural design [1]. As a result, the dynamic characteristics of large-scale low-rise buildings are not fully understood. Some kinds of these structures are likely against the rigid-floor assumption. To understand the dynamic characteristics of large-scale low-rise buildings, microtremor measurements were taken to six existing commercial buildings in Japan [2]. Their dynamic characteristics are investigated by the identified modal properties. Section 2.2 introduces the basic information of the six objective buildings. Section 2.3 explains the modal identification methods using microtremor measurements when the number of measurement points exceeds the available sensors. The identification process in one measured building is introduced in detail as an example. Section 2.4 similarly introduces the identified modal properties of the other five buildings. Section 2.5 summarizes the dynamic characteristics of large-scale low-rise buildings to explain the need for a new seismic response prediction method that is not constrained by the rigid-floor assumption. Section 2.6 concludes this chapter.

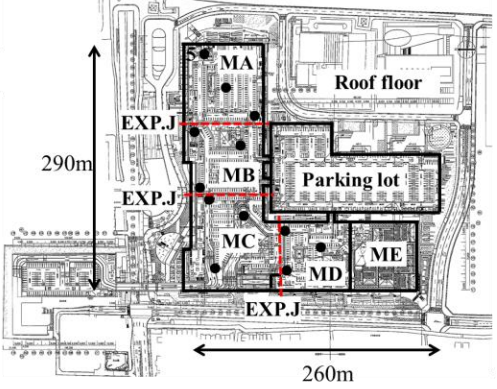
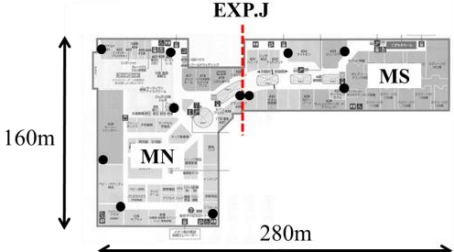
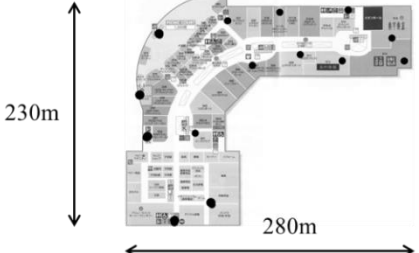
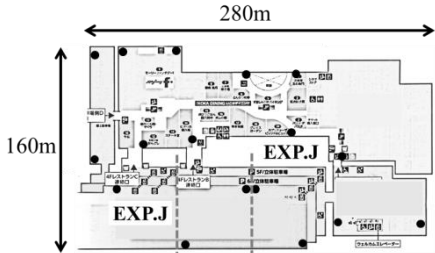
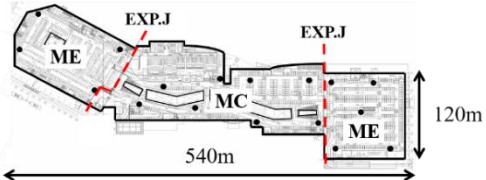
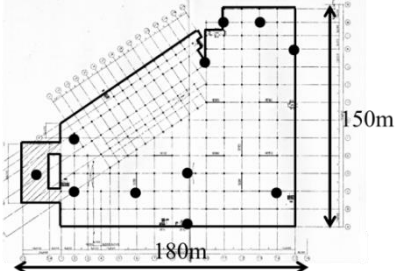
2.2 Objective Buildings

The six objective commercial buildings are named as Buildings A, B, C, D, E and F. Table 2-1 summarizes the basic information of these buildings, including the structure type, geometric information, functions at each floor and the existence of expansion joint (EXP.J).

2.2.1 Building A

Building A is a 3-story steel building. Three EXP.Js are installed at the 4th floor to reduce the influence of thermal stress. The divided areas are named as MA, MB, MC, MD and ME as shown in Table 2-1. The shopping and dining areas are on the 1st to 3rd floors, and the parking area is on the 4th floor (roof floor). The movie theater is in the ME area and there is a local roof on top of the 4th floor. It is L-shaped with the longitude length of 290 m and the transverse length of 260 m, and the spans between two close columns are equally 9 m. The building area is 40,800 m² and the gross floor area is around 126,500 m². The eave height is 23.8 m and the building height is 25.1 m. An independent structure for car-parking is near the main structure but they are not connected. Atria are set on the 2nd and 3rd floors. In the measurement plan, 42 measurement points were selected for microtremor measurements.

Table 2-1 Objective buildings

Name	Geometric characters	Planar view
A	<p>Frame: S (Steel) Plan: L-shape, 260 m by 290 m Height: 25 m Shopping area: 3 stories with atria Parking area: 4th (Roof) floor EXP.J: 3 only on the roof floor</p>	
B	<p>Frame: S Plan: L-shape, 280 m by 160 m Height: 29 m Shopping area: 4 stories with atria Parking: 5th & 6th (Roof) floors EXP.J: 1 on each floor</p>	
C	<p>Frame: SRC (Steel-framed reinforced concrete) & S Plan: L-shape, 280 m by 230 m Height: 25 m Shopping area: 3 Stories with atria Parking area: 4th to 6th (Roof) floors EXP.J: None</p>	
D	<p>Frame: SRC & S Plan: L-shape, 280 m by 160 m Height: 40 m Shopping area: 4 stories with atria Parking area: Beside shopping sections connected by contact bridges EXP.J: 2 only in parking area</p>	
E	<p>Frame: S Plan: 540 m by 120 m Height: 14 m Shopping area: 2 stories with atria & skylights Parking area: 3rd (Roof) floor EXP.J: 2 on each floor</p>	
F	<p>Frame: SRC & S Plan: Trapezoid, 180 m by 150 m Height: 24 m Shopping area: 3 stories with atria Parking area: 4th to 6th (Roof) floors EXP.J: None</p>	

2.2.2 Building B

Building B is a 5-story steel building. The 1st to 4th floors are shopping and dining areas, and the parking areas on the 5th and 6th floors. It is L-shaped in planar. The longitude length is 280 m and the transverse length is 160 m. The height is roughly estimated around 29 m. The gross floor area, including the parking area, is around 125,700 m². Unlike Building A, an EXP.J thoroughly divides the building to two parts named as MN and MS. Atria are set from the 1st to 4th floors. In the measurement plan, 60 measurement points were selected for microtremor measurements on the 1st to 5th floors because the 6th floor was not allowed to enter. One major interest is to investigate the influence of EXP.Js because they are installed differently in Buildings A and B.

2.2.3 Building C

Building C is a 4-story building with a partial underground floor. The 1st to 3rd floors are made of concrete-encased steel, and the 4th to 6th floors are made of steel as the parking area. It is also L-shaped in planar with the longitudinal length of 280 m and the transverse length of 230 m. The height is roughly estimated as 25 m and the gross floor area is 78,400 m². Atria are set on the 2nd and 3rd floors. Total of 82 measurement points were selected for microtremor measurements. The reason for selecting this building is to investigate the influence of EXP.Js because Building C has no EXP.J.

2.2.4 Building D

Building D is a 4-story building. It is mostly made of SRC while part of the large-scale area in the theater is made of steel. The bottom right part of the 4th and roof floors are the parking area and other parts are shops and a movie theater. Unlike other five buildings, only part of the roof floor is parking area. The longitudinal length is 280 m and the transverse length is 160 m, the height is around 40 m. The main structure is 4-story but the sub-structure, i.e., the parking lot has six stories. It is because the story height is different in the two structures and they are connected by corridors. The total number of measurement points was 71. No EXP.Js are installed at the main structure but there are two in the parking lot and they thoroughly separate the sub-structure.

2.2.5 Building E

Building E is a 2-story steel building. The 1st and 2nd floors are the shopping and dining areas. The parking area is on the 3rd floor. Two EXP.Js are installed and the building is divided thoroughly into three areas named as ME, MC and MW. The planar length is 540 m by 120 m, the span in the ME area is 12 m while the span in the MW and MC areas is 9 m. The gross floor area is around 120,000 m² with the maximum height of 23.1m. The height of the 3rd floor is 12.7 m. The total number of measurement points was 49. Atria and skylights are mostly in the MC area. Unlike previously introduced four buildings, the atria and skylights at Building E are long. Figure 2-1 shows the atrium and skylight in Building E.



(a) Atrium view from the 2nd floor

(b) Skylight view on the roof floor

Figure 2-1 Atrium and skylight in Building E

2.2.6 Building F

The 5-story Building F has two parts made of SRC and steel. The 1st to 3rd floors are made of SRC and the 4th to 6th floors are made of steel. The parking areas are on the 4th to 6th floors and part of the 3rd floor. The longitude length is 180 m and the transverse length is 150 m. The height is 24.1 m and the gross floor area is 99,000 m². The span is mostly 9.0 m and it is 7.2 m by 10.2 m at the areas close to the hypotenuse part. Atria are set on the 2nd and 3rd floors. 53 measurement points were selected on the 1st to 5th floors because the 6th floor was not allowed to enter. Building F is different from others because it is a trapezoid building without EXP.Js.

2.3 Modal Identification Using Limited Sensors

The microtremor measurement process is introduced in this section. The multi-setup measurements are utilized to obtain the mode shapes at different locations because the number of locations to measure significantly exceeds the number of available accelerometers. In each measurement, only parts of locations are measured simultaneously and the corresponding mode shapes are identified. There is at least one overlapped location that is constantly measured during the multi-setup measurements, which is named as the reference point. The separately identified mode shape amplitudes at other locations are assembled referring to the mode shape amplitudes of the reference point [3-5]. The multi-setup measurements have already been applied to a 22-story RC building [3], a 9-story SRC building [4], and masonry towers [5]. Although the objective buildings and the utilized modal identification methods are different from each other in References 3 to 5, the three references show the feasibility of using limited sensors to obtain the global mode shapes of the building. This section introduces the utilized modal identification methods and the multi-setup measurement procedure, then the multi-setup measurements in Building A are introduced in detail as an example.

2.3.1 Modal identification by multi-setup measurement procedures

The utilized modal identification methods are firstly introduced. The identification methods can be divided into two categories based on if the input is known: 1) the experimental modal analysis that requires full acknowledgement of input excitation and output response; 2) the output-only modal analysis that mostly

assumes the input is white noise and only uses the output data. The system identification based on microtremor measurement belongs to the latter category and its advantage is the applicability when the input excitation is unknown. In addition, microtremor measurements can be performed during working hour and have less interfere to the commercial buildings.

The modal identification methods based on output-only analysis have been developed for years. There are many different approaches to obtain modal properties such as: the Random Decrement (RD) method that makes modal free vibration from ambient vibration to identify natural frequencies and damping ratios [6], the fundamental properties of the RD method is studied by Tamura *et al.* [7]; The peak picking method to the power spectral density function for natural frequency identification [8]; The Natural Excitation Technique that extracts impulse response matrix from ambient vibrations [9]; Then the Eigensystem Realization Algorithm method utilizes the impulse response matrix to obtain mode shapes, natural frequencies and damping ratios [10]; The Frequency Domain Decomposition (FDD) method that applies singular value decomposition (SVD) to the power spectral density function to obtain natural frequencies and mode shapes [11]; The Enhanced Frequency Domain Decomposition method that apply the inverse Fourier transformation to the singular value distribution to obtain the free vibration curves so that the damping ratios can be identified in addition [12]; The Least-squares Complex Frequency Domain method that produces stable identifications using the weighted total least squares approach [13]; the Maximum Likelihood identification techniques that deal with non-stationary signal problems [14].

The utilized modal identification methods for the six buildings were the RD method in References 6 and 7, and the FDD method in Reference 11. The RD method was utilized to identify natural frequencies and damping ratios. The FDD method was utilized to identify natural frequencies and mode shapes. The FDD method was selected because of its simplicity for operation, it is a peak-picking method and effective when the two modes are close to each other, which is likely to happen for large-scale low-rise buildings. Some lateral modes of large-scale low-rise buildings might be close to the torsional modes. In addition, the corresponding mode shapes can be automatically extracted once the natural frequencies are picked. In Reference 5, many locations are constantly measured during the multi-setup measurements and the Modal Assurance Criterion (MAC) is utilized to validate the separately identified mode shapes [15]. When measuring large-scale low-rise buildings, there are only few locations are constantly measured during the multi-setup measurements so the MAC is not applicable. Instead, the identified natural frequencies from the FDD and RD methods are compared for validation. Besides, the application of the FDD method requires small damping ratios, the damping ratios identified from the RD method helps to verify this assumption.

The general procedure of the FDD method starts from the acceleration recording. Assuming the accelerations at l locations are recorded and they are denoted by a l -dimensional vector $a(t)$. The corresponding power spectral density matrix G is defined as:

$$A(i\omega) = F[a(t)] \quad (2-1)$$

$$G(i\omega) = E[A(i\omega)A^H(i\omega)] \quad (2-2)$$

F denotes the Fourier Transformation and it is calculated by the Fast Fourier Transformation for discrete data. E denotes the expectation and superscript H denotes the complex conjugate transpose. Equation (2-2) can be expressed by the following form for the discrete data.

$$G(i\omega) = A(i\omega)A^H(i\omega)/n \quad (2-3)$$

n is the length of the recorded data. The power spectral density matrix $G(f)$ is decomposed by SVD method:

$$G(i\omega) = U(i\omega)S(i\omega)U^H(i\omega) \quad (2-4)$$

In which, $S(i\omega)$ is the r -dimensional singular value matrix corresponding to different circular frequencies; and $U(i\omega)$ is the $l \times r$ singular left matrix. In this case, the singular right matrix is the same as the singular left matrix because $G(i\omega)$ is the $l \times l$ square matrix. When the 1st singular value distribution has peaks at specified frequencies, the corresponding frequencies are the resonance frequencies of the measured building and the corresponding singular vectors are the mode shape vectors.

The RD method assumes that the expectation of input excitation is zero. The vibration at a location includes the steady-state vibration and the transient vibration under a linear system. When the expectation of input excitation is zero, the expectation of the steady-state vibration caused by the input excitation is also zero. As a result, when accumulating the response acceleration at a location induced by random inputs, the steady-state vibration vanishes and only the transient vibration is left. The transient vibration is in the form of quasi free vibration. The obtained free vibration time history is then utilized in the system identification to obtain the natural frequencies and damping ratios by the auto-aggressive (AR) model. In the application of the RD method, the acceleration record from one sensor is used.

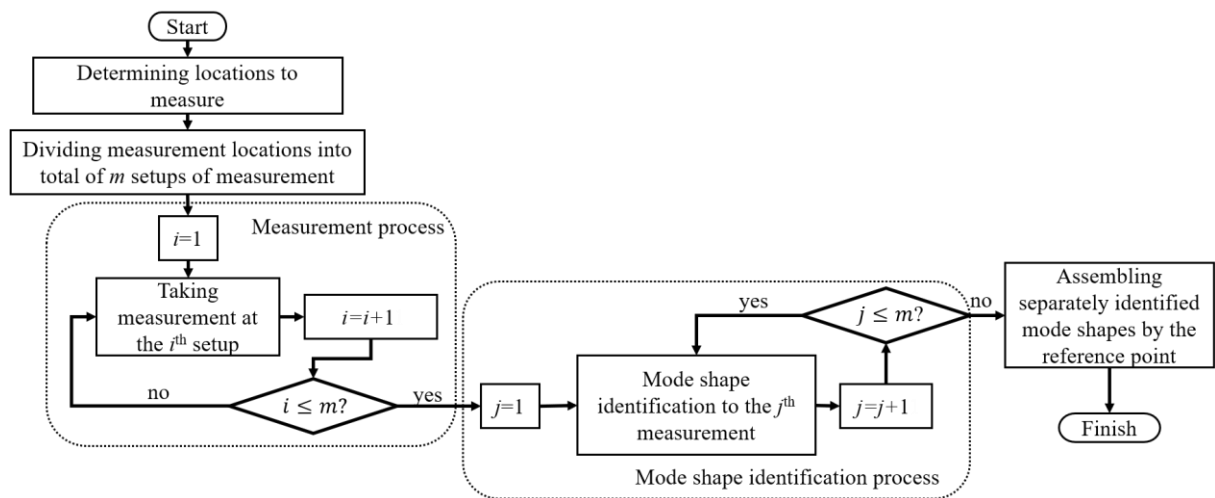


Figure 2-2 Multi-setup measurement for mode shape identification

Next, using multi-setup measurements to obtain mode shapes at many locations is introduced. The procedure can be illustrated by the following flowchart in Figure 2-2. In the measurement plan, the total measurement is divided into many setups of measurement. Each setup measures microtremor output responses at limited locations and at least one fixed location, which means at least one location is measured constantly among different setups of measurement. The constantly measured location is named as the reference point. The mode shapes in each setup are obtained by using the FFD identification method. The separately identified mode shapes are then unified by the mode shape amplitudes at the reference points.

For example, assuming there are total of 15 measurement points in the objective building while only eight sensors are available. The measurement points are named as Locations 0 to 14. The Location 0 is set as the reference point and mode shapes at Locations 1 to 7 are obtained from the 1st measurement. The mode shapes at Locations 0 to 7 are named as u_0 to u_7 , respectively. The mode shape matrix obtained from the 1st measurement is named as U_A . Mode shapes at Locations 8 to 14 are obtained from the 2nd measurement. The mode shapes at Locations 8 to 14 are named as u_8 to u_{14} , respectively. The corresponding mode shape matrix is named as U_B . The global mode shape U_{AB} are obtained by assembling U_A and U_B through u_0 :

$$\begin{cases} U_A = [u_0 & u_1 & \dots & u_7 & 0 & \dots & 0] \\ U_B = [u_0 & 0 & \dots & 0 & u_8 & \dots & u_{14}] \end{cases} \xrightarrow{\text{Assemble}} U_{AB} = [u_0 \quad \dots \quad u_{14}] \quad (2-5)$$

2.3.2 Procedure demonstration by Building A

The microtremor measurements were taken during business hours. In order not to interrupt the customers, wireless three-axis accelerometers were utilized and the sampling frequency was 200 Hz. There was a total of 42 measurement points while only eight sensors were available. The measurement plan used four fixed locations as reference points. Each location is named by a number as shown in Figure 2-3. The red dots indicate measurement points. The red dots highlighted by the blue circles are the reference points during the microtremor measurements. The green rectangle is the measured area during one measurement. Table 2-2 is the measurement plan. The accelerometers were set near the columns to avoid local vertical vibration from slabs. Due to the complexity of the buildings and the large number of measurement points, the mode shapes from two horizontal orthogonal directions were identified separately.

Table 2-2 Measurement plan

Measurement Sequence No.	Duration (min)	Main objective area	Sensor location
1	40	Roof	1, 2, 3, 4, 5, 6, 7, 8
2	40	Roof	1, 2, 3, 4, 9, 10, 11, 12
3	20	3 rd floor	2, 13, 23, 33, 15, 16, 17, 18
4	20	3 rd floor	3, 14, 24, 34, 19, 20, 21, 22
5	20	2 nd floor	2, 13, 23, 33, 25, 26, 27, 28
6	20	2 nd floor	3, 14, 24, 34, 29, 30, 31, 32
7	20	1 st floor	2, 13, 23, 33, 35, 26, 37, 38
8	20	1 st floor	3, 14, 24, 34, 39, 40, 41, 42

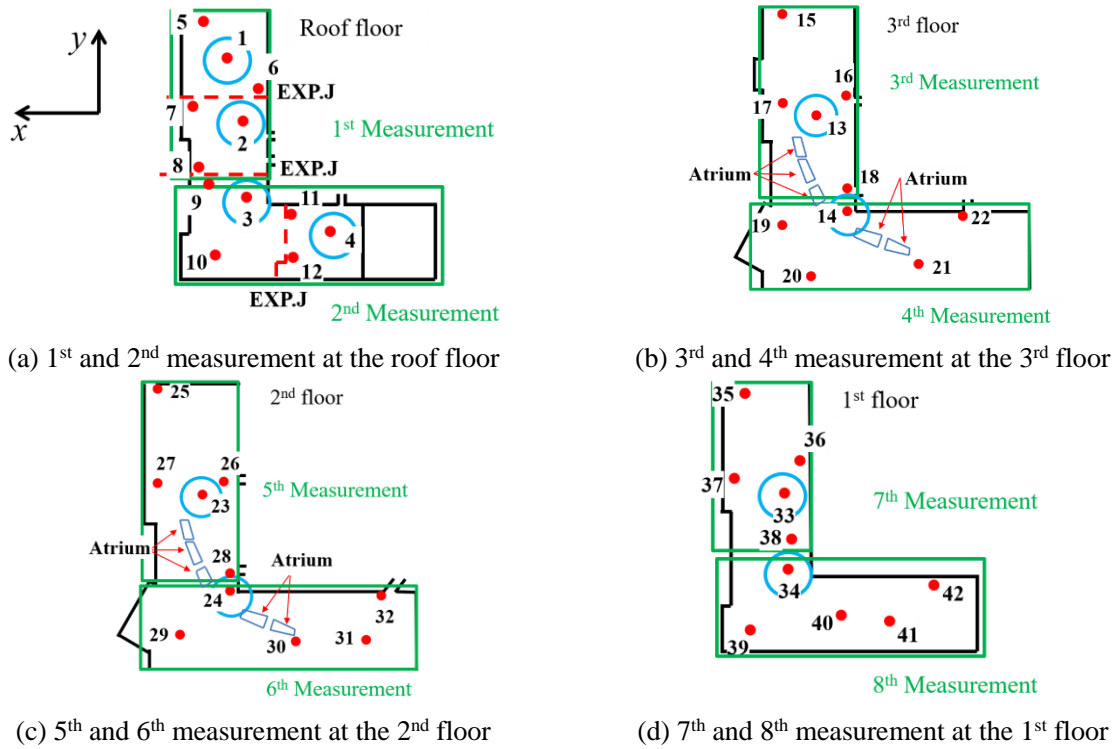


Figure 2-3 Measurement at Building A

When taking the 1st and 2nd measurements, four accelerometers were installed at same Locations 1 to 4 and the rest four sensors were installed on Locations 5-8 or 9-12, respectively. In the 3rd, 5th and 7th measurements, the reference points were Locations 2, 13, 23 and 33 in the MB area to secure the vertical distribution of mode shape. Similarly, Locations 3, 14, 24 and 34 in the MC area were the reference points in the 4th, 6th and 8th measurements. Figure 2-4 is the x -directional acceleration time histories on each floor in the 3rd measurement to exhibit the microtremor vibration amplitudes.

In order to reduce the influence of noise, the smoothing process was utilized. The recorded accelerations were divided into 20 window parts and each part contained 8,192 data (40.96 s). The SVD was applied to the divided data window, then the averaged singular values from the 20 windows passed the Hanning Window for five times. Figure 2-5 shows the smoothing process applied to the 1st measurement in the x -direction. Figure 2-6 is the 1st singular value distributions of the power spectral density matrix of acceleration in the 1st and 2nd measurements.

The peaks on the singular value curves find the resonance modes of the building. The identified modes might be either local modes or global modes because the identified modes imply vibrations in each measurement area. The identified natural frequencies from the eight measurements are summarized in Table 2-3 to investigate if the identified mode is a global mode or a local mode. When modes are found at many measurements, the corresponding modes are likely to be the global modes, or else they are local modes. The changes of natural frequency are expected because the customers in the buildings were time changing and the measurements were taken separately. The variance in the measurements is considered when summarizing. The notation ‘-’ means a mode was not found in the corresponding measurement.

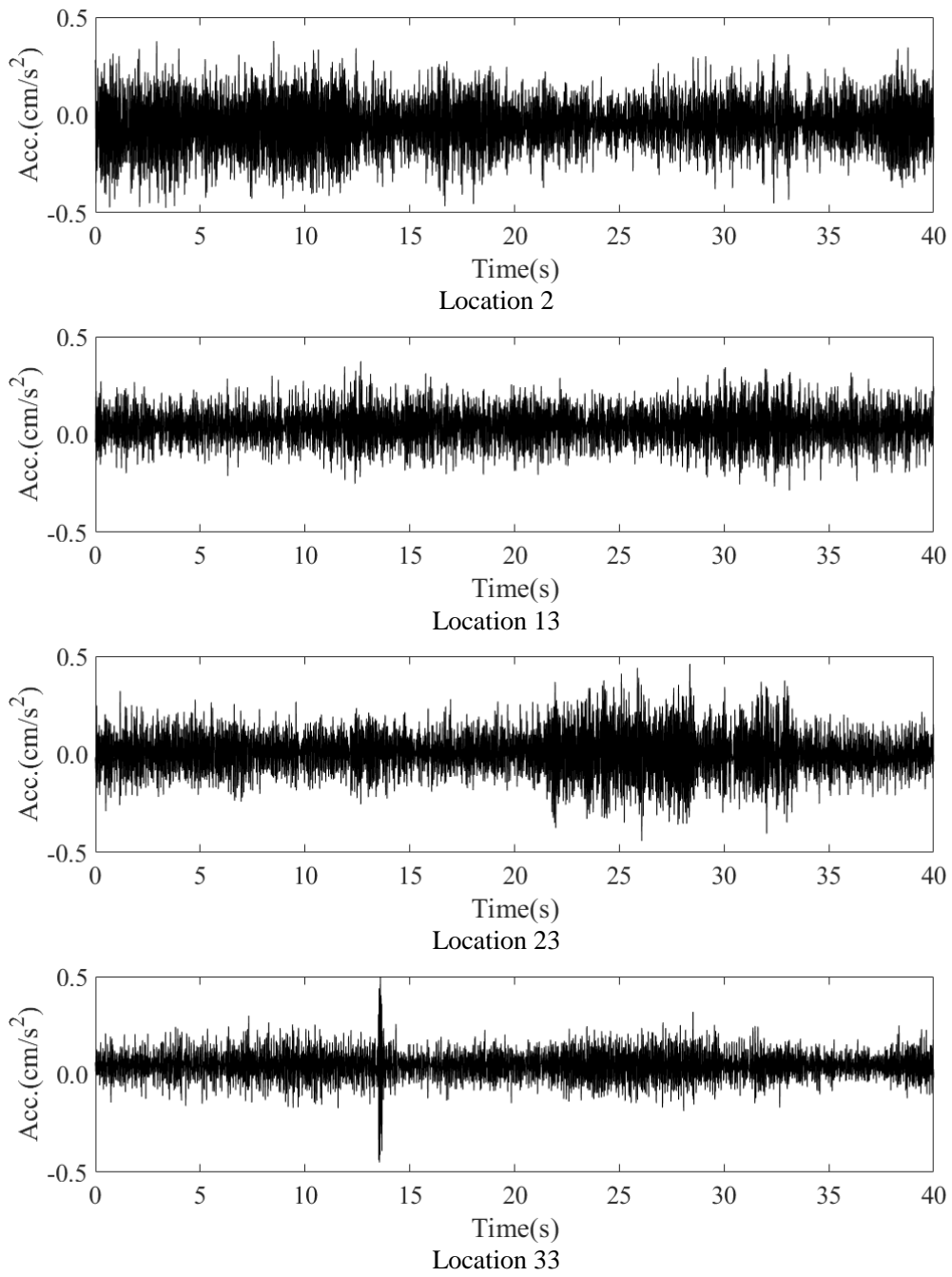


Figure 2-4 Examples of microtremor acceleration time histories

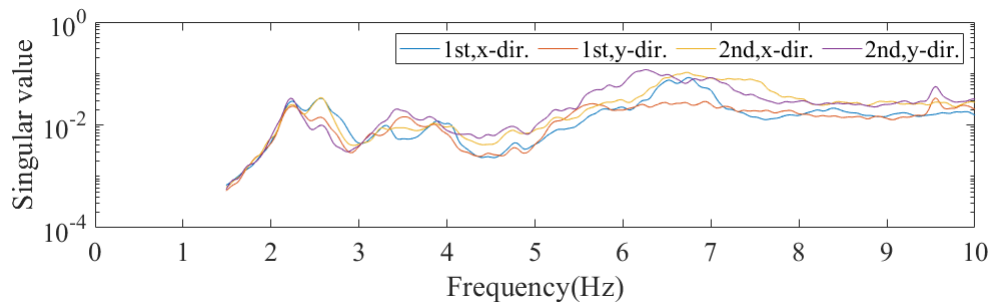
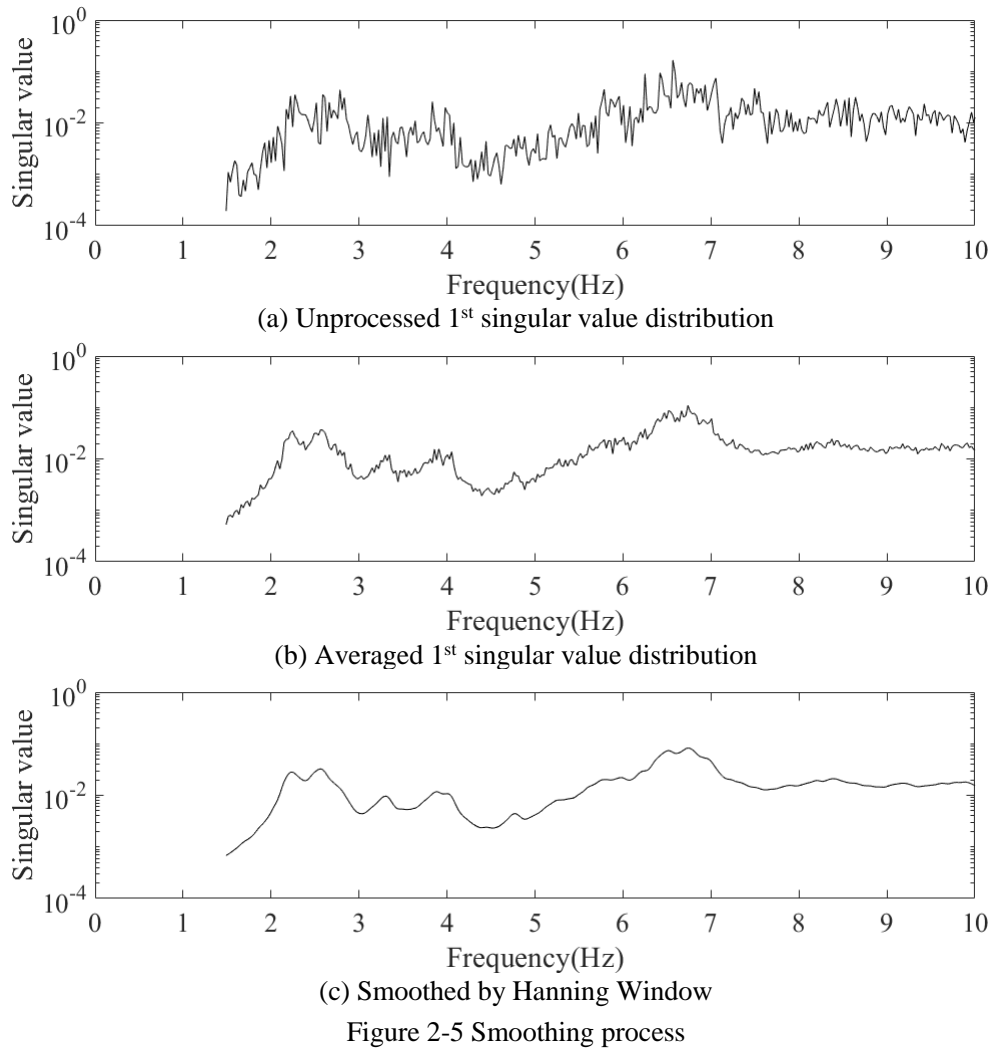


Table 2-3 provides the preliminary estimation to the modes of Building A. The next step is to obtain the global mode shapes of the identified modes. For Building A, the global mode shapes were obtained by the following procedure: Firstly, the mode shape amplitudes in the x - and y -directions at Location 1 was set as unity in the 1st and 2nd measurement. The mode shape amplitudes at other locations were assembled by the mode shape amplitude at Location 1. Next, the x - and y -directional mode shape amplitudes at Location 2 in the 3rd and 5th and 7th measurements were set as unity to assemble the mode shapes at other locations in the three measurements. Similarly, the x - and y -directional mode shape amplitudes at Location 3 in the 4th, 6th and 8th measurements were set as unity to assemble the mode shapes at other locations in the three

measurements. Then, the mode shape amplitudes at Locations 2, 13, 23 and 33 were averaged to obtain the vertical mode shape distribution in the MB area. The mode shapes at Locations 3, 14, 24, 34 were averaged for the vertical mode shape distribution in the MC area. Lastly, the mode shaped amplitudes obtained from the 3rd to 8th measurements were assembled according to the mode shape amplitudes among Locations 1, 2 and 3.

Table 2-3 Identified natural frequencies (Hz) from FDD method

Measurement sequential No.	1	2	3	4	5	6	7	8
x-direction	2.25	2.25	2.20	2.20	2.20	-	2.25	2.22
	2.56	2.56	2.59	2.54	-	2.59	2.56	2.56
	3.30	-	3.30	3.27	3.27	-	-	3.30
	-	-	-	3.54	-	3.52	-	-
	3.83	3.83	3.83	3.86	3.83	-	-	3.83
	-	-	-	-	3.98	-	-	-
	-	-	-	-	-	-	-	4.76
	-	5.27	-	-	-	-	-	-
	-	-	5.64	5.62	-	-	-	-
	-	-	-	-	-	5.76	5.81	5.71
	5.98	-	5.88	-	-	-	-	-
	6.52	-	-	-	-	-	-	-
	6.74	6.73	-	-	-	-	-	-
	-	-	-	-	-	6.86	6.93	6.91
y-direction	2.25	2.22	2.22	2.22	2.22	2.22	2.22	2.22
	2.56	2.56	2.59	2.56	-	2.56	-	2.59
	-	-	-	-	-	-	2.69	-
	3.52	-	3.52	3.54	3.56	3.54	3.52	-
	3.83	3.81	-	3.86	-	3.78	3.86	3.93
	-	-	-	-	-	5.35	-	-
	5.64	-	-	5.64	-	-	-	5.69
	-	-	-	-	5.98	-	-	-
	-	6.25	-	-	-	-	-	-

Figure 2-7 shows part of identified mode shapes in Building A. The red dots are the measured locations. The black arrows are the mode shape amplitudes at each measured location and the white arrows exhibit the general trend of the mode shape in the specific area. The mode shapes are normalized by the reference point (Location 1 in Figure 2-7), the reference point is highlighted by the green circle. The lengths of the black arrows at the reference point represent that the x- and y-directional mode shape amplitudes are unities. The mode shape identifications were conducted separately because of the multi-setup measurements. When the identified natural frequencies from the two directions are identical or close to each other, the mode shape vectors are drawn on the same figure.

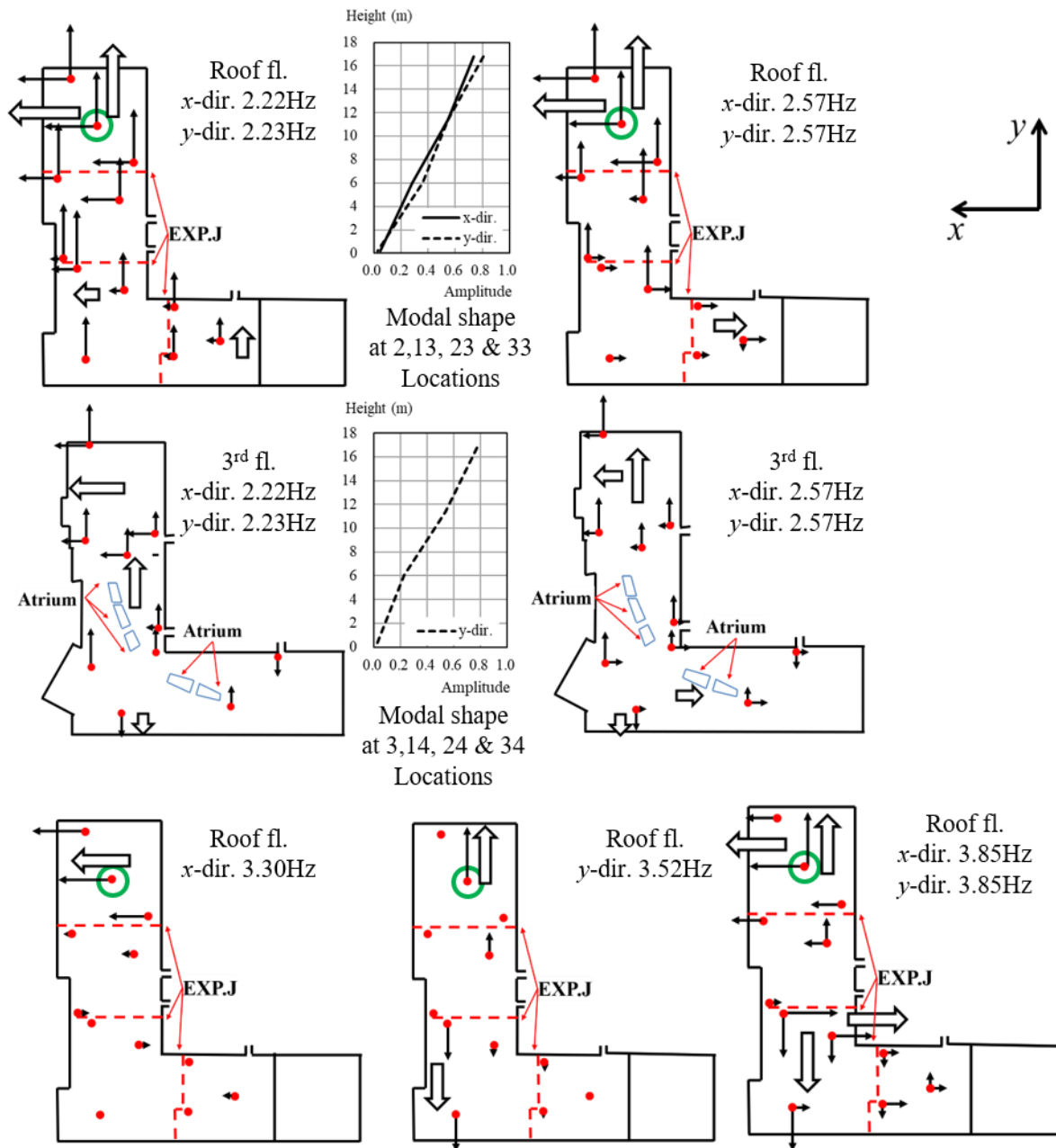


Figure 2-7 Mode shapes of Building A

The 1st global x - and y -directional modes are at 2.22 Hz and 2.23 Hz, respectively. This might be because of the asymmetric planar shape. Based on the vertical mode shape amplitude, the 2.22 Hz and 2.23 Hz modes are confirmed as the global lateral modes. It is also possible that the single mode actually appears with large mode shape amplitudes in two directions simultaneously at 2.22 Hz and 2.23 Hz. The global lateral modes are accompanied with torsion. The mode shape amplitudes in the MA are larger while the amplitudes in the MD and ME areas are smaller in the 2.22 Hz and 2.23 Hz modes. The 2.57 Hz mode is identified in both the x - and y -directions, the x -directional mode shape amplitudes in the MA and MB areas are in the opposite direction to the amplitudes in other areas, so this mode is considered the 1st torsional mode. Similar to the 2.23 Hz mode, the y -directional amplitudes in the MA and MB areas are in opposite

directions on the 3rd floor. At 3.30 Hz, the local *x*-directional mode is observed in the MA area on the roof floor, the mode is likely to be caused by the EXP.Js. In the 3.52Hz mode, the mode shape amplitudes in the MA and MB areas are opposite to the amplitudes in the MC area, which is also likely caused by the EXP.Js. Similar local modes are observed at 3.85 Hz in the *x*- and *y*-directions where the mode shape amplitudes in the MA, MB areas are in the opposite direction to the ones in the MC and MD areas. The measurement points were away from the atria and thus the influence of atria is not observed. Modes with frequencies higher than 5 Hz are also shown in Table 2-3. Most of them are local modes that have large amplitudes in specific areas. The 1st natural period of a building can be roughly estimated based on its height by multiplying a coefficient. For steel structures, the coefficient is 0.03 according to the Building Standard Law [16]. The height of the building is 23.1 m and the corresponding estimated 1st natural frequency 1.44 Hz. The estimated 1st natural frequency about 50% larger comparing to the identified values. The mode shapes in Figure 2-7 suggest that the rigid floor assumption is not applicable.

Table 2-4 Identified natural frequencies and damping ratios from RD method

Freq. (Hz) by FDD	<i>x</i> -direction		<i>y</i> -direction		
	Freq. (Hz) by RD	Damping ratio (%)	Freq. (Hz) by FDD	Freq. (Hz) by RD	Damping ratio (%)
2.22	2.25	2.5	2.23	2.24	2.2
2.57	2.60	2.4	2.57	2.59	2.6
3.30	3.40	2.0	3.42	3.45	1.8
3.85	3.84	1.6	3.85	3.81	1.7

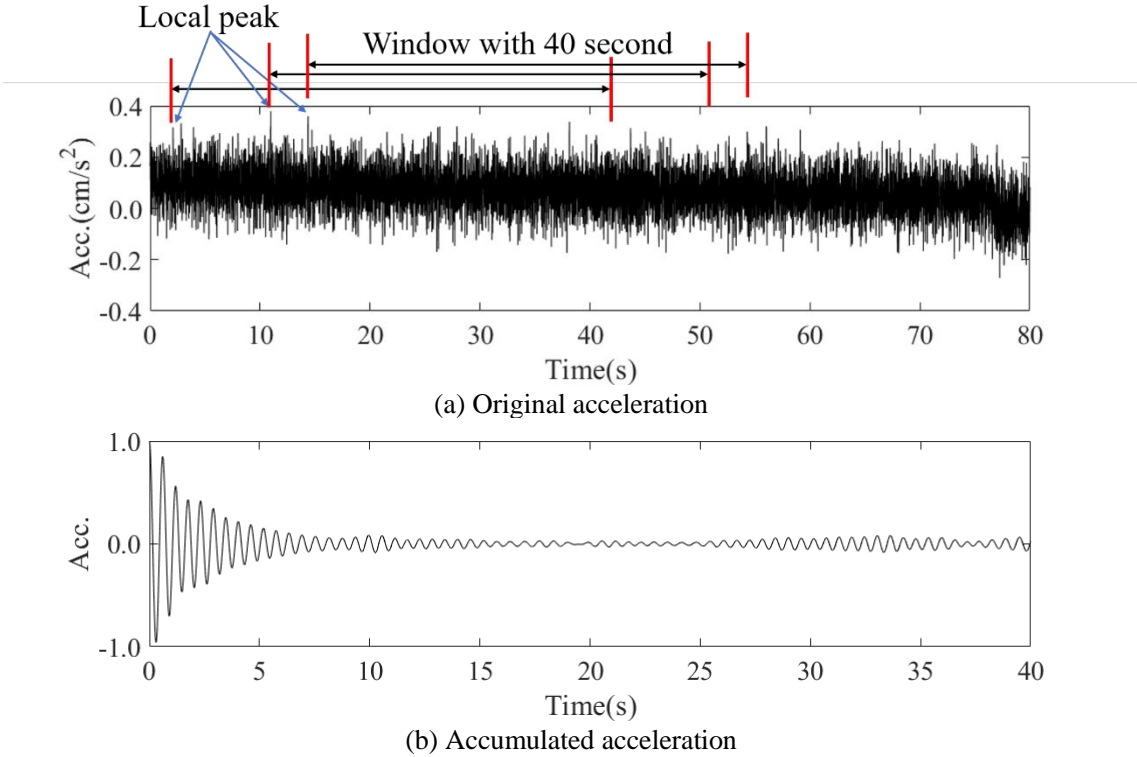


Figure 2-8 An example of RD method

The RD method was utilized to identify natural frequencies and damping ratios. When identifying a mode within a specific range, the recorded acceleration at a location firstly passed through a bandpass filter to neglect other mode components. Then 4,000 time-window pieces of data were picked from the acceleration time history. Those windows were picked based on the peaks in the acceleration time history, which means each window had a peak acceleration at the beginning. Figure 2-8(a) shows the x -direction acceleration time history at Location 1 in the 1st measurement and the demonstration of the window picking. To increase the number of pieces, there were overlapped parts during different windows. Figure 2-8(a) only shows part of the recorded microtremor data for the better demonstration. Figure 2-8(b) is the accumulated acceleration time history and the amplitude is normalized by the maximum value. The response of steady-state part vanished and only the transient vibration part was left in the form of free vibration. Then the natural frequency and damping ratio of the specified mode were identified by the AR model. The accelerations on the roof floor are utilized and the averaged natural frequencies and damping ratios are listed in Table 2-4. The RD identification results are close to the FDD identification results so the identified modal properties are reliable.

2.4 Modal Properties of Other Buildings

The identified modal properties of Building A have been introduced in Section 2.3 as an example of the multi-setup measurement process. This section introduces the identification results of the rest five buildings. The six buildings (including Building A) are different from each other from the structural viewpoint, their modal properties in common reflect the overall dynamic characteristics of large-scale low-rise buildings. Unlike Building A where the measurement process is introduced in detail, this section only shows the identification results. In addition, this section mainly focuses on the mode shapes at lower frequencies and exhibits the corresponding mode shapes. The reported modes mostly have mode shapes that are against the rigid-floor assumption.

2.4.1 Building B

Figure 2-9 shows the representative mode shapes of Building B. The EXP.J thoroughly divides the building into two parts along its height. The two parts are named as MN and MS as shown in Table 2-1. The effectiveness of the EXP.J can be observed because the mode shape amplitudes at the two sides of the joint are in opposite directions. For the MS part, the 1st y -directional mode with torsion is observed at 1.38 Hz. The 1st x -directional mode is at 1.50 Hz. The 1st torsional mode is at 1.54 Hz. For the MN part, the 1st x -directional mode is also at 1.50 Hz, which is same as the 1st x -directional mode at MS part. However, the 1st y -directional mode is at 1.54 Hz and the 1st torsional mode is at 1.92 Hz. Interactions between the two parts of the building are observed, the small mode shape amplitudes are observed in the one part and large amplitudes in the other. The mode shape amplitudes at the two sides of the EXP.J are in opposite directions in the 2.17 Hz mode. Local torsional mode is found at 2.60 Hz. A local lateral mode with large amplitudes in one sub-area is found at 3.99 Hz, the large amplitudes at specific area are likely because of the movie theater in the MS area and the large space dining area in the MN area on the 4th floor. The identified mode

shape amplitudes at the two sides of atria are in the same direction. The identified damping ratio in the 1.38 Hz mode is 1.1% and the values are 1.8-2.8% in the 1.54 Hz, 1.92 Hz and 2.17 Hz modes.

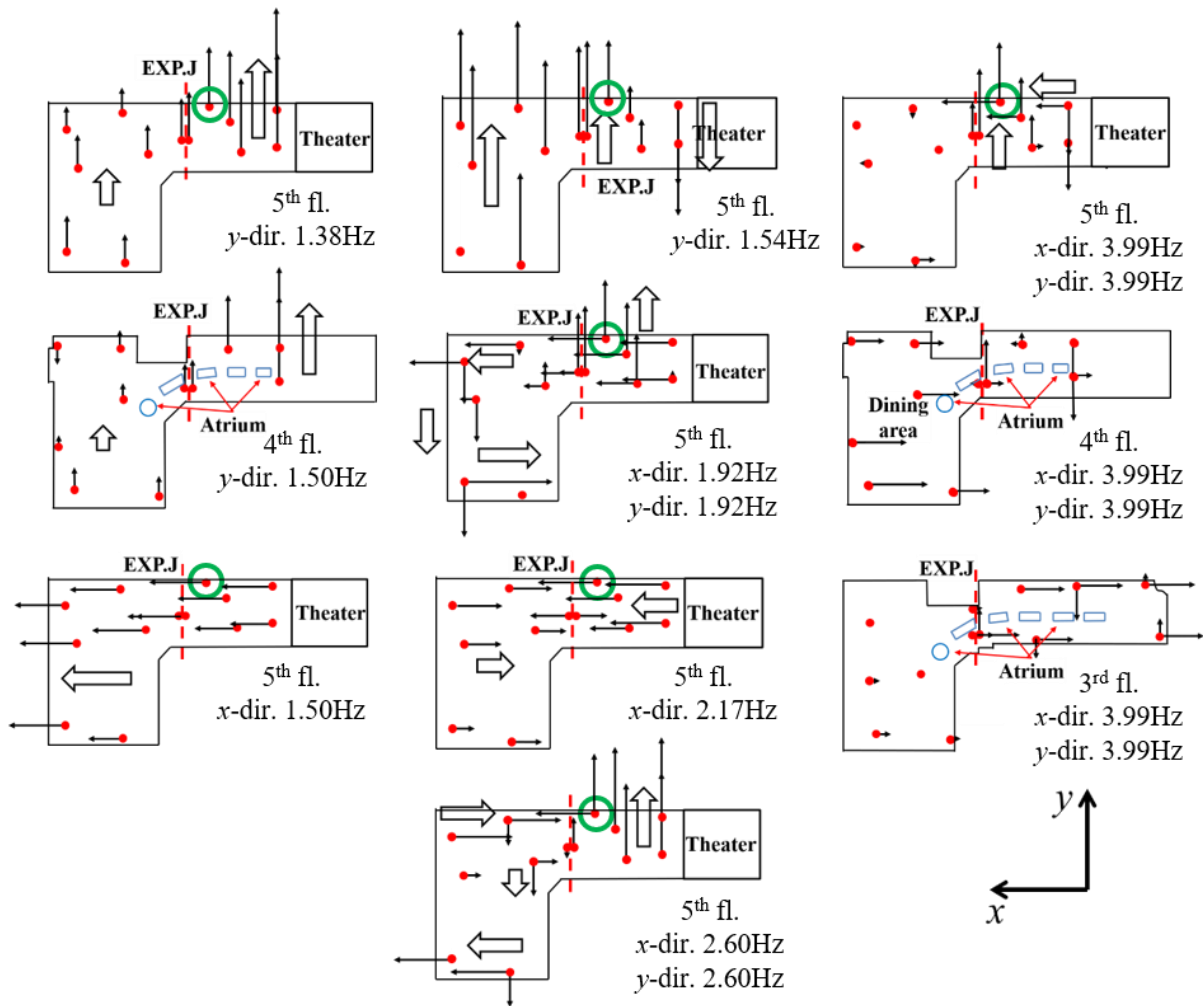


Figure 2-9 Mode shapes of Building B

2.4.2 Building C

Figures 2-10 and 2-11 shows the representative mode shapes of Building C. The local lateral mode on the 6th floor is observed at 1.51 Hz in both the x- and the y-directions simultaneously. The y-directional local mode in the parking area is observed at the 2.45 Hz and the x-directional modes are observed on the 4th floor at 2.63 Hz and on the 5th and 6th floors at 2.88 Hz. The three modes are the local modes in the parking area since they are not found on the lower floors. The reason is because the upper three floors are made of steel while the 1st to 3rd floors are made of SRC. The local modes are likely caused by the inconsistent stiffness.

The global lateral modes in the Building C are at 3.17 Hz in the y-direction and 3.58 Hz in the x-direction. The two modes are coupled with torsional components but the levels of lateral-torsional coupling are different at different areas. The damping ratios of the six modes mentioned above are around 1%.

The local torsional modes are observed at the right part of the building at 4.36 Hz and 4.92 Hz. A y-directional mode is found at 5.76 Hz, the mode shape amplitudes at the upper and bottom areas are in

opposite directions. Although the atria are set on the 1st to 3rd floors, mode shape amplitudes around the atria are in the same direction. Although the building has no EXP.Js, local modes that are only at specific area are observed at 2.88 Hz, 3.17 Hz, 3.58 Hz and 4.36 Hz.

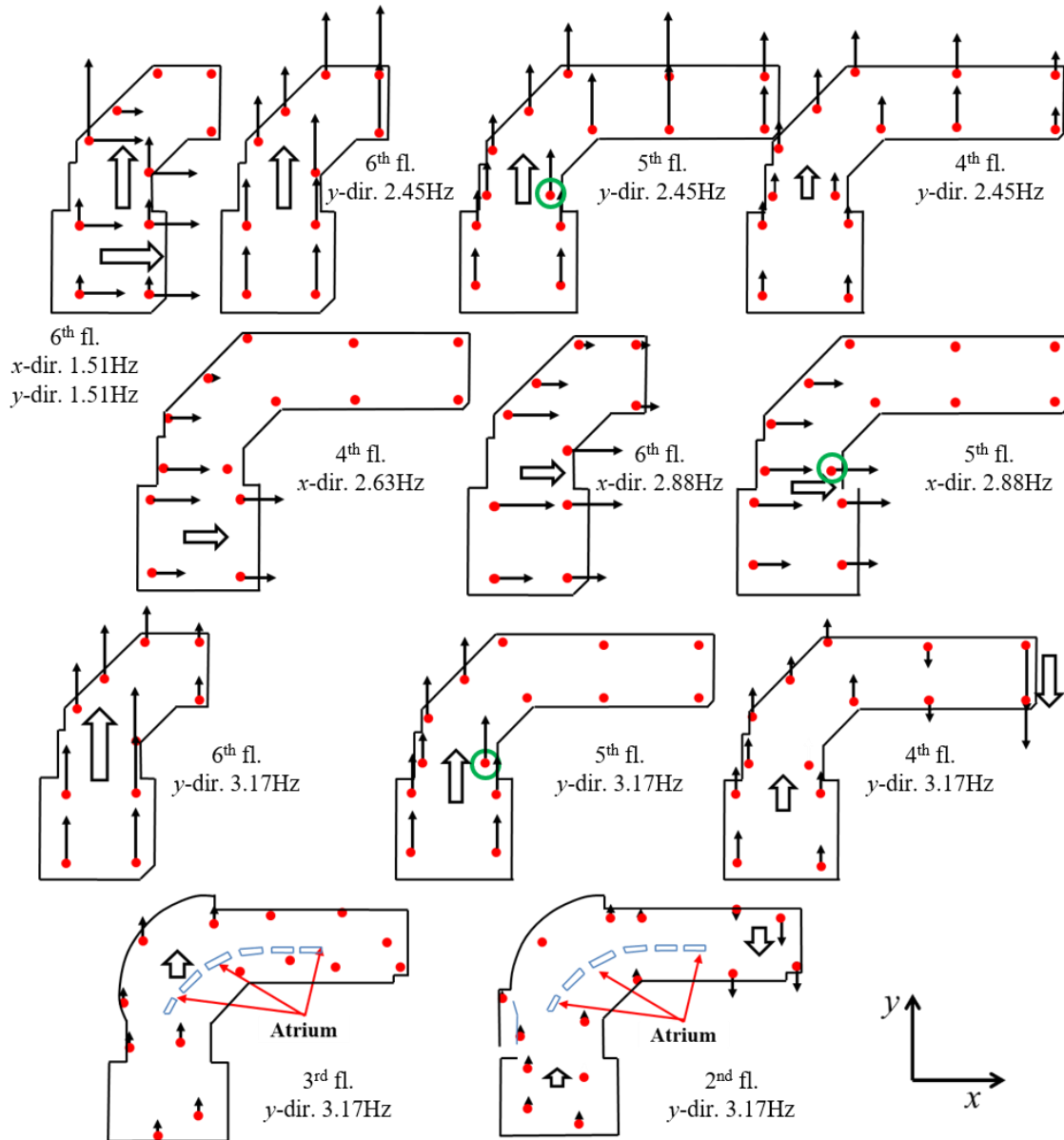


Figure 2-10 Modes at 1.51 Hz to 3.17 Hz of Building C

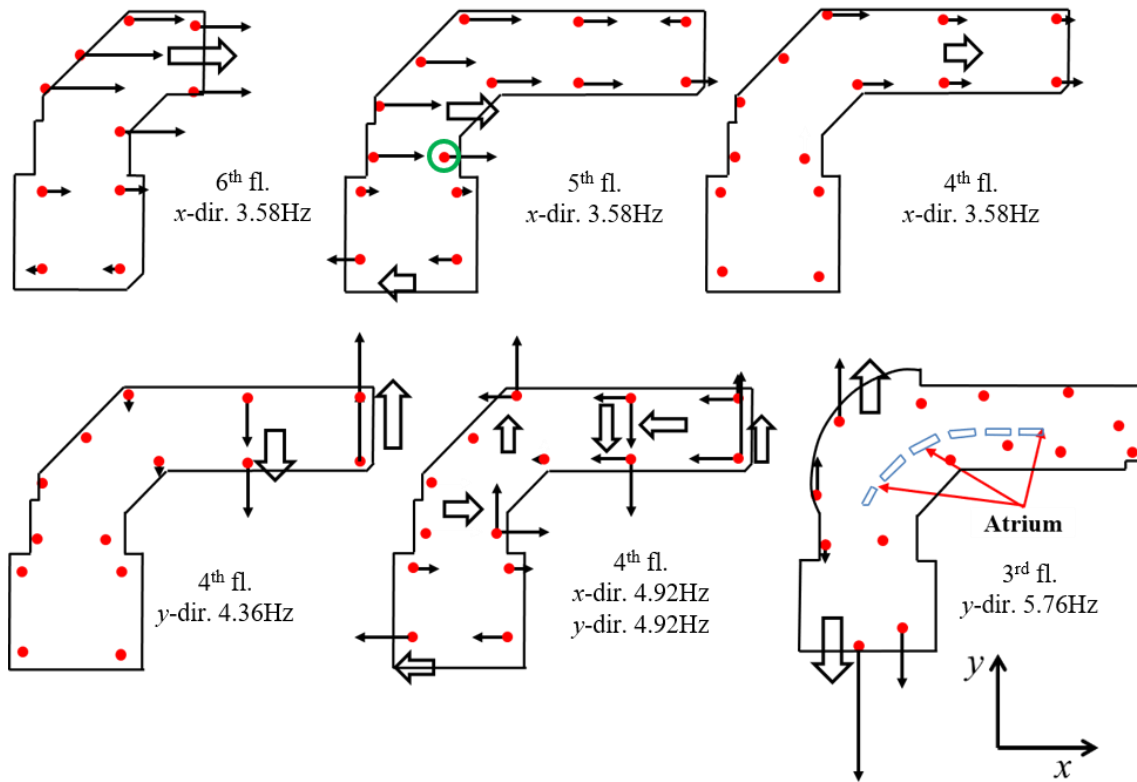


Figure 2-11 Modes at 3.58 Hz to 5.76 Hz of Building C

2.4.3 Building D

Figure 2-12 shows the representative mode shapes of Building D. The main structure is connected with a parking lot as a sub-structure and therefore the measurements were taken at both the main structure and the sub-structure. The mode shapes in the Building D are complicated because the height levels of the floors in the parking lot are different from ones of the main structure floors. The candidates of the 1st global torsional mode are the 2.39 Hz and 2.80 Hz modes, but the 1st global lateral modes are not found. Instead, many local modes are observed such as the y-directional mode at the left part of the main structure at 1.83 Hz. The measurement point on the left part of the parking lot, highlighted by the blue circle in Figure 2-12 is the slope end for the cars to move upwards and downwards, the mode shape amplitudes at this location are generally large. The x-directional global mode of the parking lot is at 2.08 Hz, the measurement points far from the main structure have obvious mode shape amplitudes as well. It implies the connection of the two structures. This phenomenon is also observed at 2.71 Hz. At 4.63 Hz, mode shape amplitudes at the two sides of the atrium are in opposite directions. The identified damping ratios for the modes mentioned above are 1-2%.

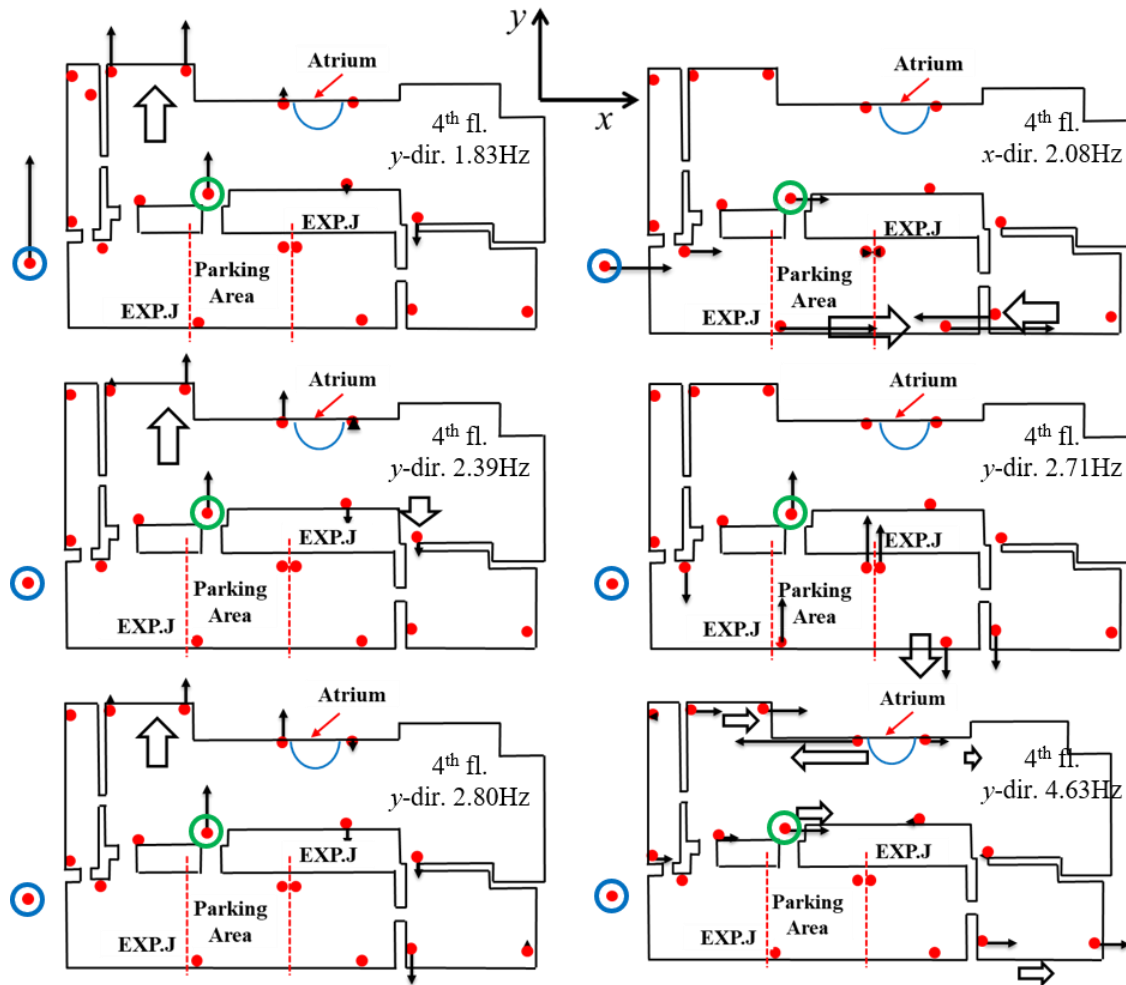


Figure 2-12 Mode shapes of Building D

2.4.4 Building E

Figure 2-13 shows the representative mode shapes of Building E. The building is divided into three areas by the EXP.Js. The three areas are named as MW, MC and ME as shown in Table 2-1. Many local modes in one or two of the three areas are identified. The 1st x -directional mode of the ME and MC areas is at 1.47 Hz. The mode shape amplitudes in the MW area are small and the MW area seems to be pulled by the MC area. The 1st x -directional mode of the MW area is at 2.09 Hz. The 1st torsional modes of the three areas are found at 2.71 Hz. Large atria and skylights are installed in the MC area and the local mode at one side of the skylights is observed at 3.56 Hz. The mode shape amplitudes near atria and skylights are generally different from each other. For example, the mode shape amplitudes around atria are different in lengths and directions in the local modes at 4.15 Hz, 5.37 Hz, 5.42 Hz and 5.71 Hz. The identified damping ratio in the 1st x -directional mode in the ME and MC areas is 1.0-1.2% while the damping ratio in the 1st x -directional mode of the MW area is 1.2-1.8%. The damping ratio in the 1st y -directional modes of the ME, MC and MW areas are 0.5%, 1.2-1.5% and 1.0-1.6%, respectively.

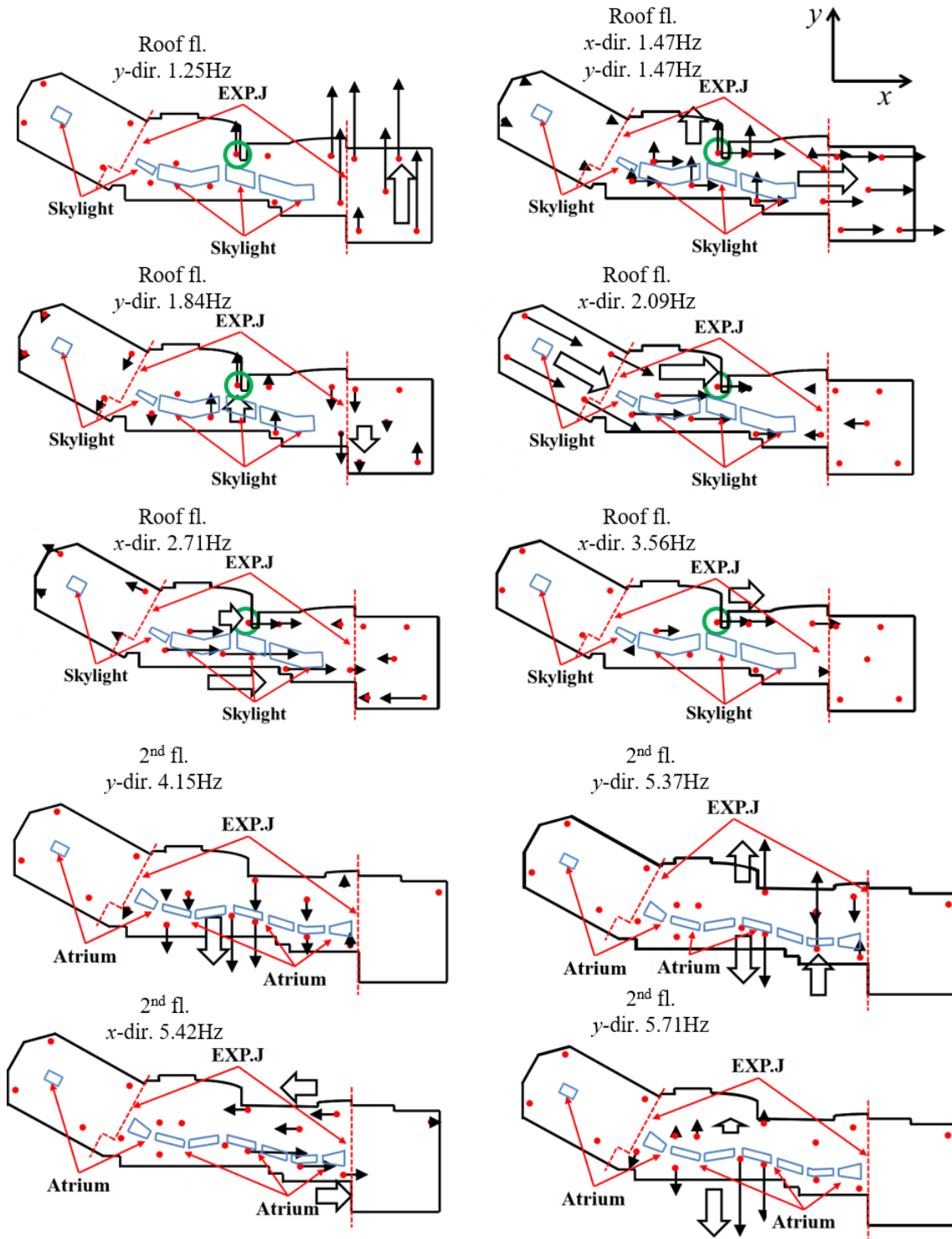


Figure 2-13 Mode shapes of Building E

2.4.5 Building F

Figure 2-14 shows the representative mode shapes of Building F. The 1st global x -directional mode is at 2.44 Hz. The influence of the atrium on the 3rd floor is observed in the 2.44 Hz mode, the mode shape amplitudes at the two sides of the atrium are in opposite directions. The 1st global y -directional mode is at 2.74Hz. The 1st torsional mode is at 3.39 Hz. In the x -directional mode at 4.28 Hz, the shape amplitudes in

the left part are in the opposite direction to the amplitudes in the right part. The damping ratios of 1st lateral modes are around 1.8% in both the *x*- and *y*-directions while the damping ratio of the 1st torsional mode is around 1.7%.

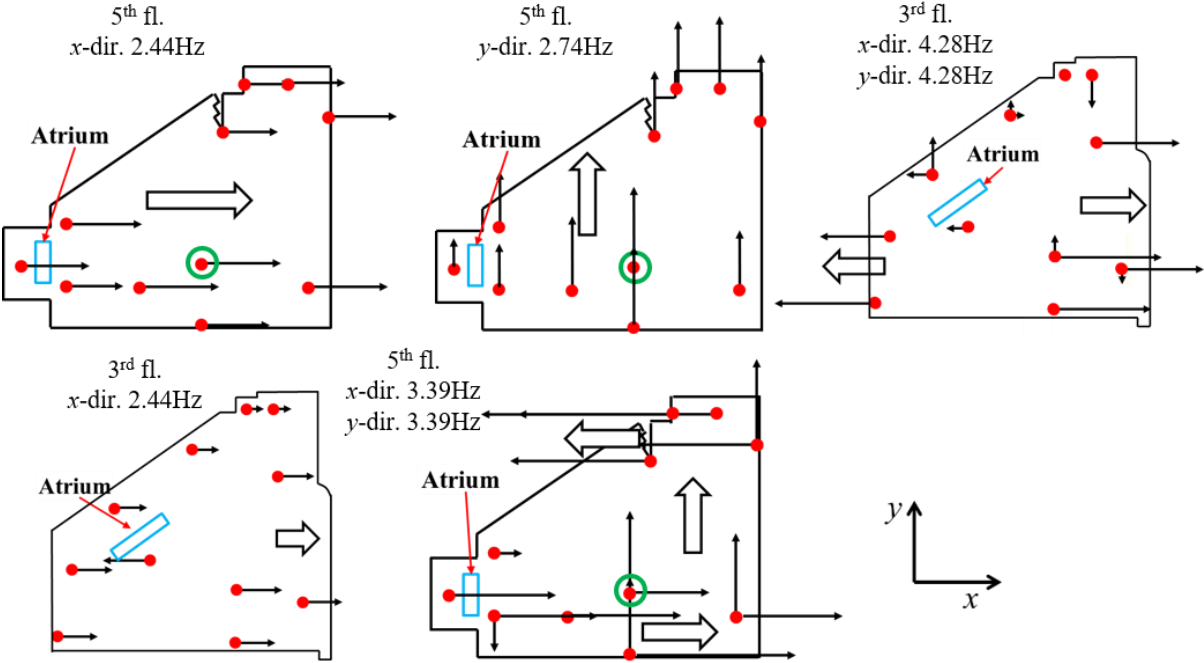


Figure 2-14 Mode shapes of Building F

2.5 Needs of New Dynamic Response Model for Seismic Response Prediction

The dynamic characteristics of the large-scale low-rise buildings are summarized based on the identified modal properties of the six measured buildings. The modal properties include the natural frequencies, damping ratios and mode shapes, among which the identified mode shapes are of particular interest. The identified mode shapes of the six buildings imply that the rigid-floor assumption is not applicable to this kind of structure. As a result, a new model is required for seismic response prediction.

The 1st natural period of a building can be estimated by multiplying the height of the building with a coefficient according to Reference 16. The coefficient is based on the type of the structure and the value is 0.03 for steel structures. For Building F, the coefficient is set as 0.025 because half of the building is made of steel and another half is made of SRC. Buildings C and D are not estimated because their structures are complicated. Half of Building C is made of steel and another half is made of SRC and there is a local 6th floor on the top. The two factors make it difficult to estimate the building height and determine the coefficient for the 1st natural period estimation. Building D is also made of steel and SRC, the height levels of the floors of the parking lot are different from the main structure floors so it is also difficult to estimate the 1st natural period. The heights of Building A and F are obtained from design documents while others are from observations. The identified 1st *x*- and *y*-directional modes are different in some of the buildings. Table 2-5 summarizes the lowest identified natural frequencies of the 1st global modes and the estimated values of the four buildings.

Table 2-5 Identified 1st natural frequencies

	Building A	Building B	Building E	Building F
Identified	2.22 Hz	1.38 Hz	1.47 Hz	2.44 Hz
Estimated	1.44 Hz	1.15 Hz	2.40 Hz	1.67 Hz
Variance	+54%	+20%	-39%	+46%

The identified 1st natural frequencies of Buildings A, B and E are higher than the estimated values. A reason is that the non-structural components would provide stiffness under small vibration. The filling walls might contribute 60% extra stiffness to the lateral load resisting system in a tall building according to the numerical simulation analysis [17]. Some experiments also suggest that the non-structural components influence the modal properties of a building [18, 19]. The non-structural components like infill walls are actually added in the numerical model when using the modal properties identified from ambient vibration testing to calibrate the numerical model [20]. The increased stiffness from the non-structural components is reduced during an earthquake and the estimated 1st natural frequency in Reference 16 considers the stiffness reduction. In fact, the stiffness provided by the non-structural components can be reduced even under wind loads [21]. Therefore, the overestimation of the 1st natural frequency from microtremor measurements are reasonable. However, Building E shows different trend because the identified 1st natural frequency is significantly smaller than the estimated value. Since there is not available data that records the modal properties of large-scale low-rise buildings under an earthquake, the inconsistent trend between the identified natural frequencies and estimated natural frequencies is difficult to explain.

Table 2-5 implies that the variances of 1st natural frequencies when under microtremor measurements and an earthquake might vary from 40% lower to 50% higher in large-scale low-rise buildings. The range of the variance is significantly larger compared to the observed 1st natural frequency variances in high-rise buildings. Celebi *et al.* compared the 1st natural frequency and damping ratio of five tall buildings under microtremor measurements and the 1989 Loma Prieta Earthquake. The decrease of the 1st natural frequency was 10-15% for steel structures and 20-30% for RC structures [22-25]. Kohler *et al.* compared the 1st natural frequency of a 17-story steel building identified from microtremor measurements and two earthquakes, the Encino Earthquake and the Yorba Linda Earthquake. The 1st natural frequency in one direction dropped from 0.55 Hz to 0.51 Hz and from 0.59 Hz to 0.52 Hz in the other direction [26]. Dunand *et al.* analyzed the changes in natural frequency of two buildings during more than ten earthquakes. One is a 12-story steel building and the other is a 9-story RC building. The decreases of their 1st natural frequencies were also around 20% compared to the values from microtremor measurements for steel structures [27, 28]. Celebi *et al.* investigated the changes in the natural frequencies of two tall steel buildings in Tokyo under the Tohoku Earthquake. The identified 1st natural frequencies of the two buildings under the mainshock were compared with the values obtained from the pre-shock. There were 10% decreases in both two buildings [29]. When the 1st natural frequencies under earthquakes are compared to ones under microtremor, the identified larger-scale low-rise buildings have larger variances in the natural frequencies than tall buildings.

The damping ratios for the 1st global modes (the 1st x- and y-direction lateral modes and the 1st torsion mode) are around 1-2.5%. The values are consistent with the conventional designed values. The differences caused by the types of the structure (steel structure and SRC structure) are not observed.

The lateral-torsional coupling property is observed in the 1st lateral modes in L-shaped buildings like Buildings A, B and C. The mode shape amplitudes at the measured locations on each floor have different values and the mode shape amplitudes at some locations are in the opposite direction to others. The influences of EXP.Js on the mode shapes are similar in Buildings A, B, D and E. Local modes are observed at the small sub-areas divided by the EXP.Js. Mode shape amplitudes at the two sides of the joint are sometimes in opposite directions. Local modes around atria and skylights are observed in Buildings E and F. Some identified modes show that the mode shape amplitudes at the two sides of the atria and skylights are in opposite directions, especially in Building E because it has relatively larger atria and skylights. The different mode shape amplitudes in lengths and directions on the same floor suggest that the rigid floor assumption is not applicable to large-scale low-rise buildings.

The effectiveness of EXP.Js is observed even at the microtremor level. In Building A where the EXP.Js are installed only on the roof floor, the mode shape amplitudes around the EXP.Js are different in lengths and directions in the identified modes. When the EXP.Js thoroughly divide the structure like Buildings B, D and E, the divided sub-areas have individual local modes. But the sub-areas are still weakly connected because modes with large mode shape amplitudes at one sub-structure also have small mode shape amplitudes at the nearby sub-substructures. In Building E, it is observed well that the local mode where two of the three sub-areas are excited.

Local modes are also found in large spaces such as the dining area, theater and shopping area are found. The reason is that those areas have fewer partition walls and thus the stiffness is relatively weak compared to other areas.

2.6 Conclusions

Six commercial buildings were selected and microtremor measurements were taken to investigate the dynamic characteristics of large-scale low-rise buildings. The six buildings are different from each other in planar shapes, the existence of EXP.Js and the structure types. The natural frequencies, and the corresponding damping ratios and mode shapes are identified to extract the dynamic characteristics in common. The global mode shapes were identified by applying multi-setup measurements because the measurements were performed using limited accelerometers. The main conclusions are summarized below:

- (1) Many locations on the same floor were measured. The mode shape amplitudes on the same floor are generally different and some locations have mode shape amplitudes in the opposite direction to others. The mode shape amplitude differences on the same floor are likely caused by the large planar area because they can be observed in both L-shaped buildings and other shaped buildings. Many identified modes have obvious lateral-torsional coupling. The mode shape amplitudes at the two sides of the EXP.Js, atria and skylights are in opposite directions in some identified modes. Local modes are also found in large areas like dining areas, and sub-areas divided by the EXP.Js, atria and skylights. The

identified mode shapes suggest that the rigid floor assumption is not applicable to large-scale low-rise buildings.

- (2) The identified 1st natural frequencies are different from the estimated values from the Building Standard Law. The variances vary from 40% lower to 50% higher. However, the 1st natural frequencies during an earthquake are generally 10-20% lower than the values identified from microtremor measurements of high-rise steel buildings.
- (3) The damping ratios in the 1st global modes are around 1.0-2.5%. The difference between steel structures and SRC structures is not found. Despite the possibility of measurement variances, an explanation is that the measurement is at the microtremor level.

Reference

- [1] Hasegawa T (2013): Introduction to the Building Standard Law, Building Regulation in Japan, *Building Center of Japan*, https://www.bcj.or.jp/upload/international/baseline/BSLIntroduction201307_e.pdf. (Accessed on 17 May 2022).
- [2] Xie J, Ikeda Y, Kurata M (2021): Modal identification of large-scale low-rise buildings through microtremor measurements, *Proceedings of the 14th World Conference on Earthquake Engineering* (Sendai, Japan), 12 pages, Paper ID: 3b-0015.
- [3] Sugumoto K, Okada K, Shiraishi M, Mori T (2014): Dynamic characteristics identification of buildings based on multipoint moving measurements and reconstructed transfer function, *Shimizu Corporation Research Report*, Vol.91, pp.37-44 (in Japanese).
- [4] Kurisu A, Maseiki R, Hibino H, Sakamoto S, Nagashima I (2017): Evaluation of building vibration characteristics by sequential partial measurement of microtremor, *The AIJ Journal of Technology and Design*, AIJ, Vol.23(54), pp.441-446 (in Japanese).
- [5] Gentile C, Saisi A (2007): Ambient vibration testing of historic masonry towers for structural identification and damage assessment, *Construction and Building Materials*, Vol.21(6), pp.1311-1321.
- [6] Ibrahim SR (1977): Random decrement technique for modal identification of structures, *Journal of Spacecraft and Rockets*, Vol.14(11), pp.696-700.
- [7] Tamura Y, Sasaki A, Tsukagoshi H (1993): Evaluation of damping ratios of randomly excited buildings using the random decrement technique, *Journal of Structure Construction Engineering*, AIJ, No.454, pp.29-38 (in Japanese).
- [8] Bendat JS, Piersol AG (1980): Engineering applications of correlation and spectral analysis, *New York*, Wiley.
- [9] James GH, Carne TG, Lauffer JP (1993): The natural excitation technique (NExT) for modal parameter extraction from operating turbines, *Sandia National Laboratories*, Technical Report: SAND92-1666.
- [10] Juang JN, Pappa RS (1985): An eigensystem realization algorithm for modal parameter identification and model reduction, *Journal of Guidance, Control, and Dynamics*, Vol.8(5), pp.620-627.

- [11] Brincker R, Zhang L, Andersen P (2000): Modal identification from ambient responses using frequency domain decomposition, *Proceedings of the 18th International Modal Analysis Conference* (San Antonio, USA), 6 pages, pp.625-630.
- [12] Brincker R, Ventura CE, Andersen P (2001): Damping estimation by frequency domain decomposition, *Proceedings of the 19th International Modal Analysis Conference* (Orlando, USA), 6 pages, pp.698-703.
- [13] Van Der Auweraer H, Guillaume P, Verboven P, Vanalanduit S (2001): Application of a fast-stabilizing frequency domain parameter estimation method, *Journal of Dynamic Systems, Measurement, and Control*, Vol.123(4), pp.651-658.
- [14] Parloo E, Verboven P, Guillaume P, Overmeire MV (2001): Maximum likelihood identification of modal parameters from non-stationary operational data, *Proceedings of the 19th International Modal Analysis Conference* (Orlando, USA), 7 pages, pp.425-431.
- [15] Allemang RJ (1982): A correlation coefficient for modal vector analysis, *Proceedings of the 1st International Modal Analysis Conference* (Orlando, USA), 7 pages, pp.110-116.
- [16] Building Standard Law. <https://www.mlit.go.jp/notice/noticedata/pdf/201703/00006623.pdf> (Accessed on 24 May 2022)
- [17] Li B, Hutchinson GL, Duffield CF (2011): The influence of non-structural components on tall building stiffness, *The Structural Design of Tall and Special Buildings*, Vol.20(7), pp.853-870.
- [18] Gad EF, Duffield CF, Chandler AM, Stark G (1998): Testing of cold-formed steel framed domestic structures, *Proceedings of the 11th European Conference on Earthquake Engineering* (Paris, France), 7 pages, pp.323-329.
- [19] Gad EF, Duffield CF (2000): Lateral behavior of light framed walls in domestic structures, *Proceedings of the 12th World Conference on Earthquake Engineering* (Auckland, New Zealand), 10 pages, Paper ID: 1663.
- [20] Yu H, Mohammed MA, Mohammadi ME, Moaveni B, Barbosa AR, Stavridis A, Wood RL (2017): Structural identification of an 18-story RC building in Nepal using post-earthquake ambient vibration and lidar data, *Frontiers in Built Environment*, Vol.3, 15 pages, Paper ID: 11.
- [21] Li QS, Wu JR, Liang SG, Xiao YQ, Wong CK (2004): Full-scale measurements and numerical evaluation of wind-induced vibration of a 63-story reinforced concrete tall building, *Engineering Structures*, Vol.26(12), pp.1779-1794.
- [22] Celebi M, Şafak E (1991): Seismic response of Transamerica building. I: Data and preliminary analysis, *Journal of Structural Engineering*, ASCE, Vol.117(8), pp.2389-2404.
- [23] Celebi M, Şafak E (1992): Seismic response of Pacific Park Plaza. I: Data and preliminary analysis, *Journal of Structural Engineering*, ASCE, Vol.118(6), pp.1547-1565.
- [24] Celebi M and Liu HP (1998): Before and after retrofit-response of a building during ambient and strong motions, *Journal of Wind Engineering and Industrial Aerodynamics*, Vol.77, pp.259-268.
- [25] Çelebi M, Phan LT, Marshall RD (1993): Dynamic characteristics of five tall buildings during strong and low-amplitude motions, *The Structural Design of Tall Buildings*, Vol.2(1), pp.1-15.

- [26] Kohler MD, Davis PM Safak E (2005): Earthquake and ambient vibration monitoring of the steel-frame UCLA Factor building, *Earthquake Spectra* 2005, Vol.21(3), pp.715-736.
- [27] Dunand F, Bard P, Rodgers J (2006): Comparison of the dynamic parameters extracted from weak, moderate and strong motion recorded in Buildings, *Proceedings of the 1st European Conference on Earthquake Engineering and Seismology* (Geneva, Switzerland), 6 pages, Paper ID: 1021
- [28] Dunand F, Rodgers JE, Acosta AV, Salsman M, Bard PY, Çelebi M (2004): Ambient vibration and earthquake strong-motion data sets for selected USGS extensively instrumented buildings, *US Geological Survey*, Open-File Report 2004-1375.
- [29] Çelebi M, Hisada Y, Omrani R, Ghahari SF, Taciroglu E (2016): Responses of two tall buildings in Tokyo, Japan, before, during, and after the M9. 0 Tohoku Earthquake of 11 March 2011, *Earthquake Spectra*, Vol.32(1), pp.463-495.

Chapter 3

Dynamic Response Modelling Based on Microtremor Measurement

3.1 Introduction

This chapter introduces a new modelling process to a building with floor flexibility based on the modal properties identified from microtremor measurements [1, 2]. The modelling is to establish modal equations of motion from the identified modal properties. After the modelling, the seismic response of the measured building under a given ground motion can be predicted. There are other different methods that use modal properties from microtremor measurements to model a building [3-5]. The proposed modelling process in References 1 and 2 is based on Reference [6]. The major difference among the prediction methods in References 1 to 5 is the participation vector approximation. In References 3 to 5, the objective building is modelled as a stick-shape lumped mass model under the rigid-floor assumption. The stick-shape lumped mass model is convenient for the mass matrix estimation and the estimated mass matrix is useful in the participation vector approximation. However, the rigid-floor assumption is not applicable to all kinds of structures as explained in Chapter 2. The participation vector approximation in References 1, 2 and 6 have the advantage which does not assume a certain floor rigid, but it requires further detailed discussion and supplements in the later chapters. Although the participation vector approximation methods are different, the seismic response prediction procedures in References 1 to 6 can be summarized by the flowchart in Figure 3-1:

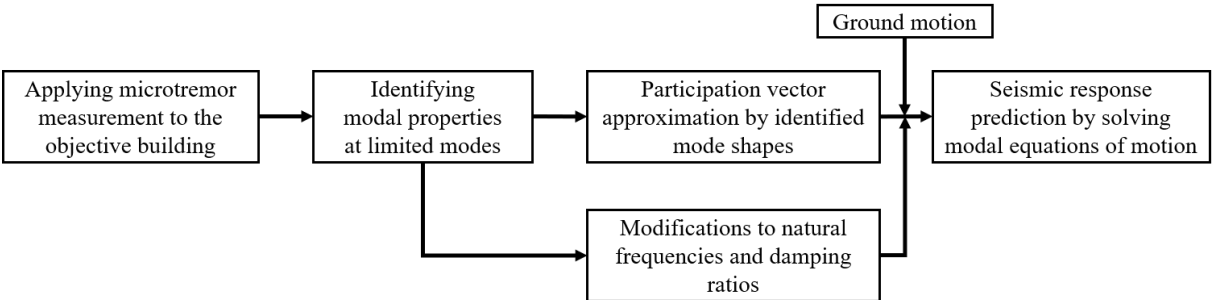


Figure 3-1 General prediction procedure

The prediction method starts with applying microtremor measurement to the objective building. The natural frequencies, and the corresponding damping ratios and mode shapes in lower vibration modes can be identified from microtremor measurements. Next, the participation vector corresponding to the identified modes is approximated via the mode shapes. The seismic response of the measured building under a given ground motion can be predicted by solving the introduced modal equations of motion. The

natural frequencies and damping ratios identified from measurements are expected to be modified for the seismic response prediction. It is because they are generally different when during microtremor measurements and earthquakes. The natural frequencies and damping ratios can be updated by using the recorded seismic responses and the input ground motion when a vibration observation system is installed. They can also be directly modified by factors determined by engineering viewpoints.

This chapter introduces the outline and concept of the modelling process based on microtremor measurement and is ranged as follows: The modelling to the measured buildings based on the modal properties from microtremor measurement is in Section 3.2. Section 3.3 expands the single-dimensional (1D) model used in Section 3.2 to the two-dimensional (2D) model. The expanded model fully considers the lateral-torsional coupling property that the modes in large-scale low-rise buildings are likely to have. Then a model selection process that decides if to use the 1D or 2D model is added to the general prediction procedure in Figure 3-1. Lastly, Section 3.4 concludes this chapter.

3.2 Seismic Response Prediction at Measured Locations

3.2.1 Modal equation of motion

The 1D model is utilized to demonstrate the modelling of a multi-degree-of-freedom (M-DOF) linear building based on the modal properties identified from microtremor measurements. In the 1D model, only the horizontal vibrations in the same direction of the input ground motion are considered. When the 1D model with n lumped masses is subjected to the single-directional ground motion, that is the x -directional ground motion, the equation of motion is written as:

$$M_x \ddot{x}(t) + C_x \dot{x}(t) + K_x x(t) = -M_x e \ddot{x}_0(t) \quad (3-1)$$

In which, M_x , C_x and K_x are the x -directional $n \times n$ mass, damping and stiffness matrices, respectively. e is the n -dimensional unit vector for an input. $x(t)$ is the n -dimensional relative displacement vector to the base and $\ddot{x}_0(t)$ is the seismic input acceleration in the x -direction. The dot means differential with respect to time.

The relative displacement vector $x(t)$ can be expressed by the $n \times n$ mode shape matrix U_x and the n -dimensional modal displacement vector $q(t)$ under a linear assumption:

$$x(t) = U_x q(t) \quad (3-2)$$

Equation (3-2) can be rewritten in the scalar form:

$$x_i(t) = \sum_{j=1}^n u_{i,j}^x q_j(t) \quad (3-3)$$

Here $x_i(t)$ is the relative displacement at the i^{th} node, $q_j(t)$ is the modal displacement in the j^{th} mode. $u_{i,j}^x$

is the mode shape component in the mode shape matrix U_x , it means mode shape amplitudes at the i^{th} node in the j^{th} mode. The n -DOF model assumes the lumped masses are located at the locations where microtremors are measured. For example, when multiple locations on each floor are measured in a L-shaped 4-story building as shown in Figure 3-2, the proposed method assumes multiple masses are lumped at those measured locations. All the nodes on a floor are connected by a flexible plate, the two nodes on two near floors are connected by a spring (the blue line) when they are at the same/near horizontal locations. However, the stick-shape lumped mass models in References 3 to 5 consider each floor as a single mass.

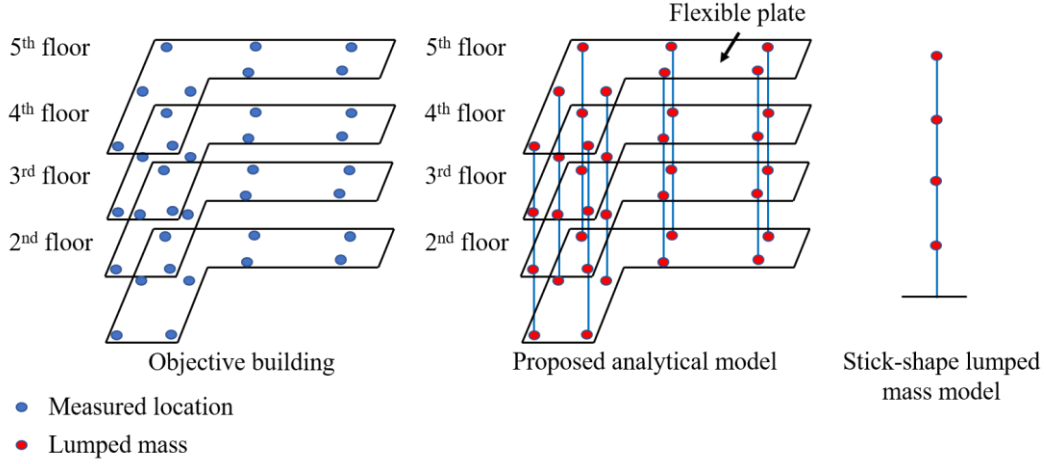


Figure 3-2 Analytical model considering floor flexibility

Therefore, the mode shape amplitude $u_{i,j}^x$ can be identified from microtremor measurements. When the damping matrix is assumed to be proportional to the mass and stiffness matrices, Equation (3-1) can be transformed to the modal equations of motion:

$$U_x^T M_x U_x \ddot{q}(t) + U_x^T C_x U_x \dot{q}(t) + U_x^T K_x U_x q(t) = -U_x^T M_x e \ddot{x}_0(t) \quad (3-4)$$

The superscript ‘ T ’ means transposing. By left multiplying the inverse matrix of $U_x^T M_x U_x$ to the both sides of Equation (3-4), Equation (3-4) is transformed from the differential equations with coupled n variables in Equation (3-1) into the decoupled differential equations in Equation (3-5):

$$\begin{Bmatrix} \ddot{q}_1(t) \\ \ddot{q}_2(t) \\ \vdots \\ \ddot{q}_n(t) \end{Bmatrix} + \begin{bmatrix} 2h_1\omega_1 & 0 & \cdots & 0 \\ 0 & 2h_2\omega_2 & \cdots & 0 \\ \vdots & \vdots & \ddots & \vdots \\ 0 & 0 & \cdots & 2h_n\omega_n \end{bmatrix} \begin{Bmatrix} \dot{q}_1(t) \\ \dot{q}_2(t) \\ \vdots \\ \dot{q}_n(t) \end{Bmatrix} + \begin{bmatrix} \omega_1^2 & 0 & \cdots & 0 \\ 0 & \omega_2^2 & \cdots & 0 \\ \vdots & \vdots & \ddots & \vdots \\ 0 & 0 & \cdots & \omega_n^2 \end{bmatrix} \begin{Bmatrix} q_1(t) \\ q_2(t) \\ \vdots \\ q_n(t) \end{Bmatrix} = - \begin{bmatrix} \beta_1^x \\ \beta_2^x \\ \vdots \\ \beta_n^x \end{bmatrix} \ddot{x}_0(t) \quad (3-5)$$

where

$$(U_x^T M_x U_x)^{-1} U_x^T C U_x = \begin{bmatrix} 2h_1\omega_1 & 0 & \cdots & 0 \\ 0 & 2h_2\omega_2 & \cdots & 0 \\ \vdots & \vdots & \ddots & \vdots \\ 0 & 0 & \cdots & 2h_n\omega_n \end{bmatrix} \quad (3-6)$$

$$(U_x^T M_x U_x)^{-1} U_x^T K U_x = \begin{bmatrix} \omega_1^2 & 0 & \cdots & 0 \\ 0 & \omega_2^2 & \cdots & 0 \\ \vdots & \vdots & \ddots & \vdots \\ 0 & 0 & \cdots & \omega_n^2 \end{bmatrix} \quad (3-7)$$

$$(U_x^T M_x U_x)^{-1} U_x^T M_x e = U_x^{-1} M_x^{-1} (U_x^T)^{-1} U_x^T M_x e = U_x^{-1} e = \begin{bmatrix} \beta_1^x \\ \beta_2^x \\ \vdots \\ \beta_n^x \end{bmatrix} \quad (3-8)$$

ω_j and h_j are the circular natural frequency and the corresponding damping ratio in the j^{th} mode, respectively. β_j^x is the x -directional participation factor in the j^{th} mode, it represents the weight of the x -direction ground motion in the j^{th} modal equation of motion. Equation (3-5) can be rewritten in the scalar equation for the j^{th} mode ($j=1, 2, \dots, n$):

$$\ddot{q}_j(t) + 2h_j\omega_j\dot{q}_j(t) + \omega_j^2q_j(t) = -\beta_j^x\ddot{x}_0(t) \quad (3-9)$$

The relationship between the participation vector and the mode shape matrix can be written in two ways, one is based on Equation (3-8) using the following form:

$$\begin{bmatrix} u_{1,1}^x & u_{1,2}^x & \cdots & u_{1,n}^x \\ u_{2,1}^x & u_{2,2}^x & \cdots & u_{2,n}^x \\ \vdots & \vdots & \ddots & \vdots \\ u_{n,1}^x & u_{n,2}^x & \cdots & u_{n,n}^x \end{bmatrix} \begin{bmatrix} \beta_1^x \\ \beta_2^x \\ \vdots \\ \beta_n^x \end{bmatrix} = \begin{Bmatrix} 1 \\ 1 \\ \vdots \\ 1 \end{Bmatrix} \quad (3-10)$$

The other utilizes the orthogonal property of the mode shape matrix so that the participation factor β_j^x is only related to the corresponding n -dimensional mode shape vector u_j^x :

$$\beta_j^x = \frac{u_j^{xT} M_x e}{u_j^{xT} M_x u_j^x} \quad (3-11)$$

The mass, damping and stiffness matrices are required when the measured building is interpreted by the equations of motion as Equation (3-1). However, the measured building can also be described by the modal equations of motion as Equation (3-5) when natural frequencies, damping ratios, mode shapes and participation vector are available. Then the mass, damping and stiffness matrices are not needed for the proposed seismic prediction method.

3.2.2 Approximation of participation vector for seismic input

As shown in Equation (3-5), the seismic response under a given ground motion can be calculated when the natural frequencies, the corresponding damping ratios, mode shapes and participation vector are available. The former three properties can be obtained from microtremor measurements while the participation vector cannot be directly obtained. The participation vector relates to the input excitation while the microtremor measurement belongs to the ambient vibration testing. It is noted that the natural frequencies and damping

ratios require modification because they are generally different during microtremor measurements and earthquakes even if no structural damage occurs as explained in Chapter 2.

References 3 to 5 approximate the participation factor of each identified mode using Equation (3-11). However, when not using the rigid-floor assumption and setting multiple nodes on each floor to consider floor flexibility, the mass matrix estimation becomes difficult for an actual building without its design documents. The participation vector approximation needs to be based on Equation (3-10) rather than Equation (3-11) to avoid accessing the mass matrix.

When n locations are selected in microtremor measurements, the number of identified modes is generally smaller than the number of measurement points as implied in Chapter 2. It is not guaranteed that using mode shapes at all measured locations has the best participation vector approximation accuracy. Therefore, the proposed participation vector approximation method considers the possibility that mode shapes at some locations are neglected. Assuming that m ($m \leq n$) modes identified from microtremor measurements with mode shapes at l ($l \leq n$) locations are utilized in the participation vector approximation, Equation (3-10) is approximated by

$$U'_x \beta'_x \approx e' \quad (3-12)$$

wherein

$$U'_x = \begin{bmatrix} u_{1,1}^{x'} & u_{1,2}^{x'} & \cdots & u_{1,m}^{x'} \\ u_{2,1}^{x'} & u_{2,2}^{x'} & \cdots & u_{2,m}^{x'} \\ \vdots & \vdots & \ddots & \vdots \\ u_{l,1}^{x'} & u_{l,2}^{x'} & \cdots & u_{l,m}^{x'} \end{bmatrix} \quad (3-13)$$

$$\beta'_x = [\beta_1^{x'} \quad \beta_2^{x'} \quad \cdots \quad \beta_m^{x'}]^T \quad (3-14)$$

U'_x is the identified $l \times m$ mode shape matrix and β'_x is the corresponding approximated m -dimensional participation vector. e' is the l -dimensional unit vector. $\beta_j^{x'}$ is the approximated x -directional participation factors in the j^{th} mode. $u_{i,j}^{x'}$ is the identified x -directional mode shape amplitude at the i^{th} node in the j^{th} mode. The superscript ‘ $'$ ’ for x distinguishes the mode shape amplitudes in Equation (3-12) from amplitudes in Equation (3-10). In general, the sums of participation functions, i.e., $U_x \beta_x$ in the left part of Equation (3-10) are not influenced by the mode shape normalization. This generality is followed by the proposed method: the sums of approximated participation functions, i.e., $U'_x \beta'_x$ in the left part of Equation (3-12) are not influenced by the mode shape normalization. To simplify the mode shape normalization, the identified mode shape vector in the j^{th} mode, is recommended to be normalized by:

$$\sum_{j=1}^n u_{j,i}^{x'^2} = 1 \quad (3-15)$$

The approximated participation vector in Equation (3-12) is obtained by using the Least Squares Method

(LSM):

$$\beta'_x = (U_x'^T U_x')^{-1} U_x'^T e' \quad (3-16)$$

The application of LSM requires the number of identified variables be less than or equal to the number of equations, i.e., $m \leq l$, which is generally satisfied in practical situations. For example, less than 10 modes for l can be identified while there are often more than 40 measurement points for n in microtremor measurements for large-scale low-rise buildings in Chapter 2. The LSM aims to minimize the errors between left part of Equation (3-12) and the right part at all selected nodes. However, the errors on the higher floors are generally smaller while the errors on the lower floors are larger when a few lower modes are utilized [7]. Therefore, only applying LSM to mode shapes at higher floors might lead to better participation vector approximation results, which is the reason that mode shapes at l ($l \leq n$) locations are utilized in the approximation.

3.2.3 Seismic response prediction at sensor locations

After the participation vector is approximated by the identified mode shapes, the modal displacements of the identified modes under a given ground motion can be obtained by solving the modal equations of motion with the approximated participation factors:

$$\ddot{q}'_j(t) + 2h_j \omega_j \dot{q}'_j(t) + \omega_j^2 q'_j(t) = -\beta'_j \ddot{x}_0(t) \quad (3-17)$$

$q'_j(t)$ is the modal displacement in the j^{th} mode obtained from the approximated participation factor. Then the seismic responses at the measured locations can be obtained by the mode superposition method:

$$\begin{Bmatrix} x_1(t) \\ x_2(t) \\ \vdots \\ x_n(t) \end{Bmatrix} = \begin{bmatrix} u_{1,1}^{x'} & u_{1,2}^{x'} & \dots & u_{1,m}^{x'} \\ u_{2,1}^{x'} & u_{2,2}^{x'} & \dots & u_{2,m}^{x'} \\ \vdots & \vdots & \ddots & \vdots \\ u_{n,1}^{x'} & u_{n,2}^{x'} & \dots & u_{n,m}^{x'} \end{bmatrix} \begin{Bmatrix} q'_1(t) \\ q'_2(t) \\ \vdots \\ q'_m(t) \end{Bmatrix} \quad (3-18)$$

It is important to understand that the natural frequencies and damping ratios identified from microtremor measurements are generally different from the ones under an earthquake even if no structural damage occurs. The natural frequencies and damping ratios used in Equation (3-17) need to be either updated when an observation system is installed to identify the natural frequencies and damping ratios during the earthquake, or modified by factors based on massive case studies.

In summary, it is possible to model a M-DOF linear building by the modal equations of motion using natural frequencies, damping ratios, mode shapes as discussed in this section. Those properties can be identified from microtremor measurements. As a result, the seismic response of the objective building under a given ground motion can be predicted. The modal equations of motion are the step stone in the modelling because the mass matrix, stiffness matrix and damping matrix inevitably require the design

documents of the objective building.

3.3 Dimension Expansion of Modelling Considering Lateral-torsional Coupling Directly

The 1D model is utilized in Section 3.2 to demonstrate the concept of building modelling based on microtremor measurement. However, some large-scale low-rise buildings have asymmetric planar shapes, which means the identified modes are likely to have lateral-torsional coupling. The lateral-torsional coupling property means the seismic responses in one direction, at those measured locations, might be induced by orthogonal ground motions. However, the 1D model cannot consider the vibrations induced by orthogonal ground motions.

The researches on lateral-torsional coupling are mainly based on the stick-shaped lumped mass model that uses the rigid-floor assumption [8-14]. A floor or a group of floors is lumped as a node and the torsion of the node is added as the additional degree of freedom. The lateral-torsional coupling occurs when the center of mass and resistance do not coincide. Penzien uses the two-degree-of-freedom model to simplify a multi-story building with lateral-torsional coupling [8]. Reinhorn *et al.* propose a simplified seismic response calculation method for lateral-torsional coupling building using the properties of the uncoupled counterparts [9]. Kan and Chopra simplify a multi-story building with lateral-torsional coupling into a multi-story uncoupled system and a single-story coupled system [10]. Rutenberg *et al.* use the shear beam model to analyse the lateral-torsional coupling property [11]. The parametric study of a single-story building model subjected to both harmonic ground motions and earthquakes was conducted by Chandler and Hutchinson [12], the research suggests that the qualitative effects of the controlling parameters on the maximum translational and torsional responses are not affected by the nature of the loading. The parametric analysis based on a 5-story model was performed by Hejal and Chopra [13, 14]. The analysis suggests that the seismic response mainly depends on the eccentricity, uncoupled torsional to lateral frequency ratio, the joint rotation index, fundamental vibration period and the corresponding damping ratio. The shaking table tests of a 4-story frame structure aluminium model with asymmetric mass distribution shaken by a single-directional ground motion were conducted by Maheri *et al.* [15]. The results suggest that the 1st lateral mode and the 1st torsional mode contribute mostly to the total response, especially to the peak response at the edges. The phenomenon was also observed by Mola *et al.* from pseudo-dynamic tests [16]. The single-/multi-story rigid floor model is commonly used in many derivative studies such as the base isolation design or viscoelastic damper design for asymmetric buildings [17, 18]; The simplified seismic response calculation [8-11, 19, 20]; The parameter identification [21, 22].

Being different from the past research, the proposed seismic response prediction method set multiple nodes on each floor to consider floor flexibility as introduced in Section 3.2. The 1D in Section 3.2 is expanded to two-dimension to fully consider the lateral-torsional coupling, especially the vibrations induced by orthogonal ground motions.

3.3.1 2D modelling

Similar to Section 3.2, a linear model with n lumped nodes is established. In the 2D model, the two

orthogonal horizontal motions of each node are considered. When the model is subjected to the bidirectional ground motions, the equations of motion are:

$$\widehat{M} \begin{Bmatrix} \ddot{\hat{x}}(t) \\ \ddot{\hat{y}}(t) \end{Bmatrix} + \widehat{C} \begin{Bmatrix} \dot{\hat{x}}(t) \\ \dot{\hat{y}}(t) \end{Bmatrix} + \widehat{K} \begin{Bmatrix} \hat{x}(t) \\ \hat{y}(t) \end{Bmatrix} = -\widehat{M} \begin{bmatrix} e & o \\ o & e \end{bmatrix} \begin{Bmatrix} \ddot{x}_0(t) \\ \ddot{y}_0(t) \end{Bmatrix} \quad (3-19)$$

The ‘ $\widehat{}$ ’ means the parameters are under the 2D model. \widehat{M} , \widehat{C} and \widehat{K} are the $2n \times 2n$ mass, damping and stiffness matrices that contain x - and y - directional components, respectively. o is the n -dimensional null vector and e is the unit n -dimensional vector. $\hat{x}(t)$ and $\hat{y}(t)$ correspond to the n -dimensional relative displacement vector in the x - and y -directions to the base, respectively. $\ddot{x}_0(t)$ and $\ddot{y}_0(t)$ are the seismic input accelerations in two lateral directions. When the damping matrix is assumed proportional to the mass and stiffness matrices, Equation (3-19) is transformed to the modal equations of motion, which can be written in the scalar equation in the j^{th} ($i=1, 2 \dots 2n$) mode:

$$\ddot{\hat{q}}_j(t) + 2\hat{h}_j\hat{\omega}_j\dot{\hat{q}}_j(t) + \hat{\omega}_j^2\hat{q}_j(t) = -\hat{\beta}_j^x\ddot{x}_0(t) - \hat{\beta}_j^y\ddot{y}_0(t) \quad (3-20)$$

In which, $\hat{\beta}_j^x$ and $\hat{\beta}_j^y$ are the x - and y -directional participation factors in the j^{th} mode, respectively. \hat{h}_j and $\hat{\omega}_j$ are the damping ratio and circular frequency in the j^{th} mode. \hat{q}_j is the j^{th} modal displacement. The seismic response can be expressed by the $2n \times 2n$ mode shape matrix \widehat{U} and the $2n$ -dimensional modal displacement vector \hat{q} :

$$\begin{Bmatrix} \hat{x}(t) \\ \hat{y}(t) \end{Bmatrix} = \widehat{U}\hat{q} \quad (3-21)$$

Equation (3-21) can be rewritten in the following form:

$$[\hat{x}_1(t) \ \hat{x}_2(t) \ \dots \ \hat{x}_n(t) \ \hat{y}_1(t) \ \hat{y}_2(t) \ \dots \ \hat{y}_n(t)]^T = \begin{bmatrix} \widehat{U}_x \\ \widehat{U}_y \end{bmatrix} [\hat{q}_1(t) \ \hat{q}_2(t) \ \dots \ \hat{q}_{2n}(t)]^T \quad (3-22)$$

Here \hat{x}_i and \hat{y}_i are the x - and y -directional seismic responses at the i^{th} node, respectively. \widehat{U}_x and \widehat{U}_y are the $n \times 2n$ sub-matrices of the mode shape matrix \widehat{U} , indicating the x - and y -directional mode shape components. The relationship between the participation vector and the mode shapes can be expressed in the following form:

$$\begin{bmatrix} \widehat{U}_x \\ \widehat{U}_y \end{bmatrix} \begin{bmatrix} \hat{\beta}_1^x & \hat{\beta}_1^y \\ \hat{\beta}_2^x & \hat{\beta}_2^y \\ \vdots & \vdots \\ \hat{\beta}_{2n}^x & \hat{\beta}_{2n}^y \end{bmatrix} = \begin{bmatrix} e & o \\ o & e \end{bmatrix} \quad (3-23)$$

When applying microtremor measurements to a building, the measurements are usually performed in the

x - and y -directions separately. The lateral-torsional coupling in the 2D model implies that a same natural frequency can be identified in both the x - and the y -directions simultaneously. In practical situations, it is not necessary that each identified natural frequency is simultaneously found in both two directions. The lateral-torsional coupling might be weak in some modes so that they have large mode shape amplitudes in one direction and small amplitudes in the other direction. As a result, those modes are likely identified only in one direction. Nonetheless, the 2D model is needed when a same natural frequency is identified simultaneously in both the x - and the y -directions especially at a low frequency. It is because modes at low frequencies generally contribute the most to the seismic responses. For example, the 2D model is recommended for Building A in Chapter 2 because three low frequencies (2.22 Hz, 2.57 Hz and 3.85 Hz) are simultaneously identified in both directions and the three modes show obvious lateral-torsional coupling. When using the 2D model while some modes are only identified in one direction, the unfounded mode shape amplitudes are considered to be small and set as zeros. When the global mode shapes are obtained by multi-measurements described in Chapter 2, it is possible that certain modes are not found in some measurements, then the mode shapes at those locations are set as zeros.

When m ($m \leq 2n$) modes identified from microtremor measurements with mode shapes at l ($l \leq n$) locations are utilized in the participation vector approximation, the identified mode shape matrix and the approximated participation vector are assumed approximately satisfying the following equation:

$$\begin{bmatrix} \hat{U}'_x \\ \hat{U}'_y \end{bmatrix} [\hat{\beta}'_x \quad \hat{\beta}'_y] \approx \begin{bmatrix} e' & o' \\ o' & e' \end{bmatrix} \quad (3-24)$$

The $l \times m$ matrices \hat{U}'_x and \hat{U}'_y are the x - and y -directional mode shape matrices identified from the microtremor measurements. o' is the l -dimensional null vector. The m -dimensional vectors $\hat{\beta}'_x$ and $\hat{\beta}'_y$ are the x - and y -directional approximated participation vectors, respectively. They are obtained by using the LSM:

$$\hat{\beta}'_x = \left(\begin{bmatrix} \hat{U}'_x \\ \hat{U}'_y \end{bmatrix}^T \begin{bmatrix} \hat{U}'_x \\ \hat{U}'_y \end{bmatrix} \right)^{-1} \begin{bmatrix} \hat{U}'_x \\ \hat{U}'_y \end{bmatrix}^T \begin{bmatrix} e' \\ o' \end{bmatrix} \quad (3-25)$$

$$\hat{\beta}'_y = \left(\begin{bmatrix} \hat{U}'_x \\ \hat{U}'_y \end{bmatrix}^T \begin{bmatrix} \hat{U}'_x \\ \hat{U}'_y \end{bmatrix} \right)^{-1} \begin{bmatrix} \hat{U}'_x \\ \hat{U}'_y \end{bmatrix}^T \begin{bmatrix} o' \\ e' \end{bmatrix} \quad (3-26)$$

The application of LSM requires $m \leq 2l$, which is usually satisfied because it means the identified modes are no larger than twice of the measured locations. The predicted seismic response in the 2D model is expressed as follows:

$$\ddot{q}'_j(t) + 2h_j\omega_j\dot{q}'_j(t) + \omega_j^2q'_j(t) = -\hat{\beta}_j^{x'}\ddot{x}_0(t) - \hat{\beta}_j^{y'}\ddot{y}_0(t) \quad (i = 1, 2 \dots m) \quad (3-27)$$

$$[\hat{x}'_1(t) \quad \hat{x}'_2(t) \quad \dots \quad \hat{x}'_n(t) \quad \hat{y}'_1(t) \quad \hat{y}'_2(t) \quad \dots \quad \hat{y}'_n(t)]^T = \begin{bmatrix} \hat{U}'_x \\ \hat{U}'_y \end{bmatrix} [\hat{q}'_1(t) \quad \hat{q}'_2(t) \quad \dots \quad \hat{q}'_m(t)]^T \quad (3-28)$$

$\hat{x}'_i(t)$ and $\hat{y}'_i(t)$ are the predicted x - and y - directional seismic responses at the i^{th} node, respectively. $\hat{\beta}_j^{x'}$ and $\hat{\beta}_j^{y'}$ are the approximated x - and y -directional participation factors in the j^{th} mode, respectively. $\hat{q}'_j(t)$ is the modal displacement obtained from Equation (3-27) with the approximated participation factors.

The differences between the 1D and 2D models are understood from two aspects. One is that the 2D model can consider the vibrations caused from the orthogonal ground motions in the seismic response prediction; The other is that the 2D model utilizes the x - and y -directional mode shapes simultaneously to approximate the participation vector in one direction. When using the 1D model, the participation vector in one direction is approximated by the corresponding directional mode shapes as shown in Equations (3-16). The 2D model approximates the participation vector in one direction using mode shapes in two directions simultaneously as shown in Equations (3-25) and (3-26).

The participation vector approximation difference can be explained by the errors in the LSM process. In the 2D model, the errors in the LSM mean the difference between the left part of Equation (3-24) and the right part. The errors can be expressed by the two $2l$ -dimensional vectors ε_x^{2D} and ε_y^{2D} in Equations (3-29) and (3-30). The superscript 2D means that the errors are evaluated under the 2D model and are related to the x - or y -directional participation vector. As shown in both Equations (3-29) and (3-30), the errors in the LSM regarding the participation vector in one direction are related to the mode shapes in both the x - and y -directions.

$$\varepsilon_x^{2D} = \begin{bmatrix} e' \\ o' \end{bmatrix} - \begin{bmatrix} \hat{U}'_x \\ \hat{U}'_y \end{bmatrix} \hat{\beta}'_x \quad (3-29)$$

$$\varepsilon_y^{2D} = \begin{bmatrix} o' \\ e' \end{bmatrix} - \begin{bmatrix} \hat{U}'_x \\ \hat{U}'_y \end{bmatrix} \hat{\beta}'_y \quad (3-30)$$

However, the LSM in the 1D model only considers the errors relating to the considered directional mode shape components as shown below:

$$\varepsilon_x^{1D} = e' - U'_x \beta'_x \quad (3-31)$$

$$\varepsilon_y^{1D} = e' - U'_y \beta'_y \quad (3-32)$$

ε_x^{1D} and ε_y^{1D} are the l -dimensional vectors representing the errors in the LSM in the 1D model. Comparing to the 2D model, the errors relating to the orthogonal mode shapes are not considered in the 1D model. The LSM aims to minimize the sums of squared errors. In the 2D model, the sum of squared errors means $\sum_{i=1}^{2l} (\varepsilon_{x,i}^{2D})^2$ or $\sum_{i=1}^{2l} (\varepsilon_{y,i}^{2D})^2$. $\varepsilon_{x,i}^{2D}$ and $\varepsilon_{y,i}^{2D}$ are the i^{th} element in the $2l$ -dimensional vectors ε_x^{2D} and ε_y^{2D} , respectively. When substituting the approximated participation vector from the 1D model to Equations (3-29) and (3-30), the sum of squared errors is likely larger than using the approximated participation vector from the 2D model. As a result, the approximated participation vector from the 1D model is similarly different from the approximation result using the 2D model. When the utilized modes show weak lateral-torsional coupling, a mode would either contain small mode shape components in the orthogonal direction, or it is a torsional mode that has very small participation factor. Then the errors related to the

orthogonal mode shapes are automatically small. However, when the utilized modes show obvious lateral-torsional coupling, the approximated participation vector from the 1D model may not be the optimized values in the 2D model from the LSM viewpoint. As a result, the participation vector approximation difference occurs. The approximation result using the 2D model is believed having better accuracy because it uses more mode shape amplitudes.

3.3.2 Supplemented prediction procedures considering model selection

The general seismic response prediction shown in Figure 3-1 is supplemented by the model selection process based on if a same natural frequency is identified in two horizontal directions and the mode shows lateral-torsional coupling. The participation vector approximation and the seismic response prediction parts in Figure 3-1 are supplemented by the model selection procedures:

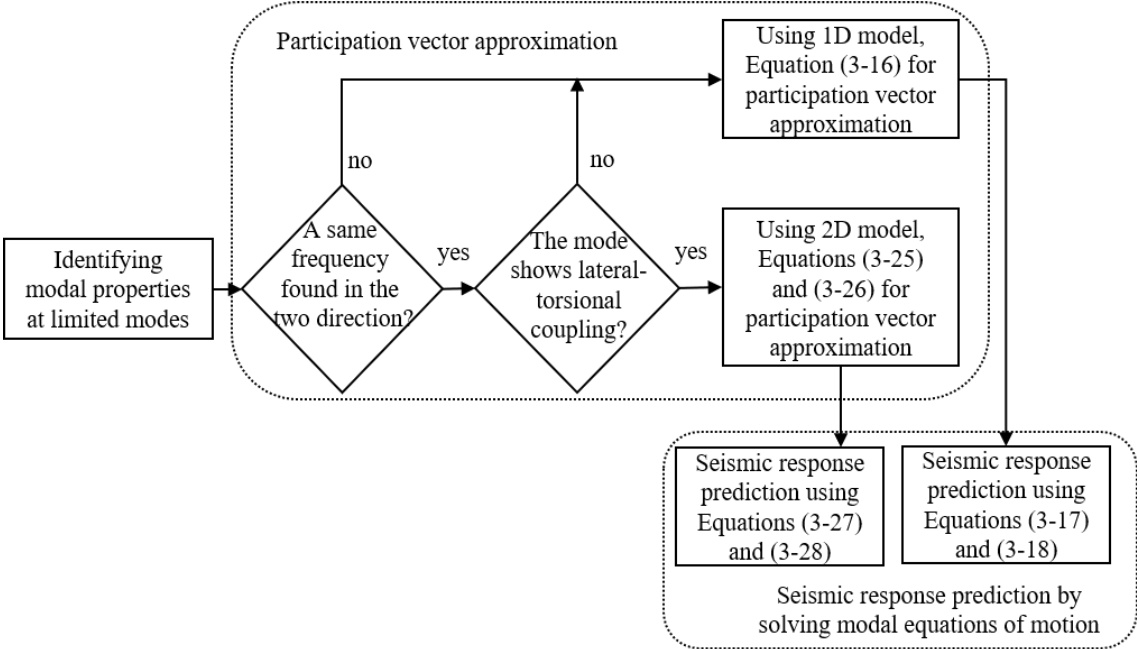


Figure 3-3 Supplemented seismic response prediction considering model selection

The proposed seismic response prediction method is summarized as follow: Firstly, microtremor measurements are applied to the objective building to obtain its natural frequencies, the corresponding damping ratios and the mode shapes in limited modes. the sensors are recommended to be installed as many as possible because the prediction method can only predict the seismic responses at the measured locations; Then, the selection of the 1D and 2D models is based on the identification result. The 2D model is recommended when a same natural frequency is identified in two horizontal directions and the corresponding mode shape shows lateral-torsional coupling, or else the 1D model is preferred; The participation vector corresponding to identified modes are approximated by the mode shapes; Lastly, the seismic responses at the measured locations under a given ground motion are predicted using the modified natural frequencies and damping ratios, identified mode shapes and approximated participation vector.

3.4 Conclusions

This chapter proposes the seismic response prediction method based on microtremor measurement. The measured building is modelled as an M-DOF linear model based on the modal properties identified from microtremor measurements. The modelling allows the seismic response prediction under a given ground motion to be performed. The advantages of the prediction method include three parts: (1) It is a fast response estimation method that does not require design documents; (2) It is not constrained by the rigid floor assumption so it can be used for large-scale low-rise buildings; and (3) It does not necessarily require instrumented sensors for the seismic response recording. The conclusions of this chapter are summarized as follows:

- (1) The objective building is modelled by using the modal equations of motion using the natural frequencies, the corresponding damping ratios and the mode shapes, and the approximated participation vector. The former three properties are based on the identified modal properties from microtremor measurements. Multiple nodes are set on each floor to consider floor flexibility. The masses are lumped at the locations where microtremors are measured, but mass information is not used in the proposal.
- (2) The LSM is utilized to approximate the participation vector. The approximation requires mode shape vectors only. The approximation method does not require estimating the mass matrix to model the objective building, which does not need the traditional stick-shape lumped mass model. Therefore, the participation vector approximation method allows multiple nodes set on each floor to consider floor flexibility.
- (3) The prediction method can predict the seismic response at the measured locations under a given ground motion. Two models are proposed based on the modal parameter identification results. The 2D model is recommended when a same natural frequency is simultaneously identified in the two horizontal directions and the mode shape shows lateral-torsional coupling, or else the 1D model is utilized in the seismic response prediction.

Reference

- [1] Xie J, Ikeda Y, Kurata M (2021): Multi-degree-of-freedom linear building model based on microtremor measurement for seismic response analysis, *Journal of structural engineering*, AIJ, Vol.67(B), pp.509–518. (in Japanese).
- [2] Ikeda Y, Kurata M, Xie J (2022): Verification of multi-degree-of-freedom building modelling for seismic response prediction based on microtremor measurement, *Earthquake Engineering & Structural Dynamics*, Vol.51(7), pp.1610-1635.
- [3] Michel C, Guéguen P, Bard PY (2008): Dynamic parameters of structures extracted from ambient vibration measurements: An aid for the seismic vulnerability assessment of existing buildings in moderate seismic hazard regions, *Soil Dynamics and Earthquake Engineering*, Vol.28(8), pp.593-604.

- [4] Michel C, Guéguen P, El Arem S, Mazars J, Kotronis P (2010): Full-scale dynamic response of an RC building under weak seismic motions using earthquake recordings, ambient vibrations and modelling, *Earthquake Engineering & Structural Dynamics*, Vol.39(4), pp.419-441.
- [5] Mori F, Spina D (2015): Vulnerability assessment of strategic buildings based on ambient vibrations measurements, *Structure Monitoring and Maintenance*, Vol.2(2), pp.115-132.
- [6] Ikeda Y, Kurata M (2019): A multi-degree-of-freedom building model based on microtremor measurement for seismic response estimation, *Annual Meeting*, Disaster Prevention Research Institute, Kyoto University, Paper ID: B04, <https://www.dpri.kyoto-u.ac.jp/hapyo/19/pdf/B04.pdf>. (in Japanese, accessed on 31 May 2022)
- [7] Suzuki K (1983): A study on problems of load combination in a seismic design. *Comprehensive Urban Studies*, Tokyo Metropolitan University, Vol.20, pp.181–192. <https://www.usp-tmu.jp/archivepdf/docs/20-12.pdf>. (in Japanese, accessed on 31 May 2022)
- [8] Penzien J (1969): Earthquake response of irregularly shaped buildings, *Proceedings of the 4th World Conference on Earthquake Engineering* (Santiago, Chile), Vol.2, pp.75-88.
- [9] Reinhorn A, Rutenberg A, Glück J (1977): Dynamic torsional coupling in asymmetric building structures, *Building and Environment*, Vol.12(4), pp.251-261.
- [10] Kan CL, Chopra AK (1977): Elastic earthquake analysis of a class of torsionally coupled buildings, *Journal of the Structural Division*, ASCE, Vol.103(4), pp.821-838.
- [11] Rutenberg A, Hsu TI, Tso WK (1978): Response spectrum techniques for asymmetric buildings, *Earthquake Engineering & Structural Dynamics*, Vol.6(5), pp.427-435.
- [12] Chandler AM, Hutchinson GL (1986): Torsional coupling effects in the earthquake response of asymmetric buildings, *Engineering Structures*, Vol.8(4), pp.222-236.
- [13] Hejal R, Chopra AK (1989): Earthquake response of torsionally coupled, frame buildings, *Journal of Structural Engineering*, ASCE, Vol.115(4), pp.834-851.
- [14] Hejal R, Chopra AK (1989): Lateral-torsional coupling in earthquake response of frame buildings, *Journal of Structural Engineering*; ASCE, Vol.115(4), pp.852-867.
- [15] Maheri MR, Chandler AM, Bassett RH (1991): Coupled lateral-torsional behaviour of frame structures under earthquake loading, *Earthquake Engineering & Structural Dynamics*, Vol.20(1), pp.61-85.
- [16] Mola E, Negro P, Pinto AV (2004): Evaluation of current approaches for the analysis and design of multi-storey torsionally unbalanced frames, *Proceedings of the 13th World Conference of on Earthquake Engineering* (Vancouver, Canada), 15 pagers, Paper ID: 3304.
- [17] Segúin CE, Juan C, Almazán JL (2008): Base-structure interaction of linearly isolated structures with

- lateral–torsional coupling, *Engineering Structures*, Vol.30(1), pp.110-125.
- [18] Alam Z, Zhang C, Samali B (2020): The role of viscoelastic damping on retrofitting seismic performance of asymmetric reinforced concrete structures, *Earthquake Engineering & Engineering Vibration* Vol.19(1), pp.223-237.
- [19] Trombetti TL, Conte JP (2005): New insight into and simplified approach to seismic analysis of torsionally coupled one-story, elastic systems, *Journal of sound and vibration*, Vol.286(1-2), pp.265-312.
- [20] Yiu CF, Chan CM, Huang M, Li G (2014): Evaluation of lateral-torsional coupling in earthquake response of asymmetric multistory buildings, *The Structural Design of Tall and Special Buildings*, Vol.23(13), pp.1007-1026.
- [21] Omrani R, Hudson RE, Taciroglu E (2012): Story-by-story estimation of the stiffness parameters of laterally-torsionally coupled buildings using forced or ambient vibration data: I. Formulation and verification, *Earthquake engineering & structural dynamics*, Vol.41(12), pp.1609-1634.
- [22] Shintani K, Yoshitomi S, Takewaki I (2017): Direct linear system identification method for multistory three-dimensional building structure with general eccentricity, *Frontiers in Built Environment*, Vol.3, 8 pages, Paper ID: 17.

Chapter 4

Fundamental Properties of the Proposed Seismic Response Prediction Method

4.1 Introduction

The proposed method in Chapter 3 has arbitrary in selecting both the used modes and the measurement points (the node selection in numerical simulations) to approximate participation vector for seismic inputs. Before considering floor flexibility in an analytical model, Chapter 4 focuses on the selections of modes and nodes. These fundamental properties include two parts: one is the participation vector approximation by using mode shapes in limited modes and/or at limited locations; and the other is the seismic response prediction accuracy by using limited modes with approximated participation vector. The fundamental properties are studied by the numerical simulation. The basic information of the utilized numerical model is introduced in Section 4.2. Section 4.3 discusses how the participation vector approximation results are influenced by the limited number of modes with mode shapes at limited locations. Section 4.4 exhibits the seismic response prediction accuracy with the approximated participation vector, and Section 4.5 concludes the fundamental properties of the seismic response prediction method.

4.2 Used 5-DOF Model

The fundamental properties of the proposed seismic response prediction method are explored by the numerical simulation of a simple 5-degree-of-freedom (5-DOF) lumped mass model [1]. The 5-DOF model represents a 5-story building [2]. The basic information of the model is shown in Table 4-1. The modal properties in each mode are shown in Table 4-2. The damping ratio is assumed to be 2% in each mode to discuss the influence of truncation errors on the mode superposition. The mode shape vector in each mode is normalized by setting the sum of squared mode shape amplitudes as unity. Figure 4-1 shows the mode shapes of the model in the form of the participation functions.

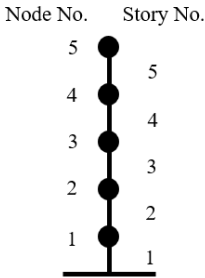


Table 4-1 Mass and inter-story stiffness of the 5-DOF model

Node number	Mass 10 ³ kg (t·s ² /cm)	Story number	Stiffness kN/m (t/cm)
5	53.937 (0.055)	5	117,680 (120)
4	44.130 (0.045)	4	147,100 (150)
3	44.130 (0.045)	3	176,520 (180)
2	44.130 (0.045)	2	205,940 (210)
1	49.033 (0.050)	1	205,940 (210)

Table 4-2 Modal properties of the 5-DOF model

Node number	1 st mode	2 nd mode	3 rd mode	4 th mode	5 th mode
5	0.643	-0.553	0.369	0.175	0.035
4	0.550	0.018	-0.588	-0.610	-0.198
3	0.425	0.462	-0.355	0.552	0.481
2	0.286	0.572	0.342	0.170	-0.705
1	0.149	0.391	0.524	-0.514	0.480
Participation factor	2.021	0.747	0.408	-0.237	0.150
Natural frequency (Hz)	2.82	7.55	11.98	15.74	19.21
Damping ratio	0.02	0.02	0.02	0.02	0.02

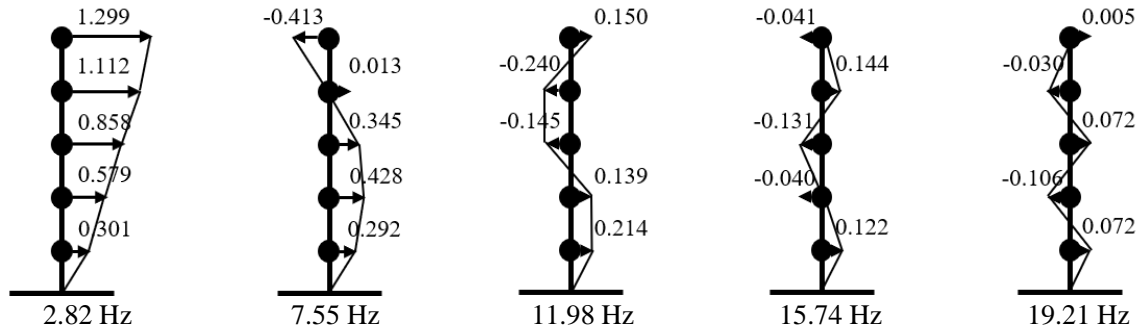


Figure 4-1 Mode shapes of the 5-DOF model

4.3 Influences of Participation Vector Approximation

4.3.1 Influence of limited modes

The microtremor measurements can identify a limited number of modes only. The proposed participation vector approximation method utilizes the mode shapes of multiple modes simultaneously. The approximated participation factor in a mode is influenced by the number of utilized modes. In addition, the number of the identified and used modes affects the seismic response prediction due to the mode superposition. Therefore, the fundamental properties of the proposed seismic response prediction method are firstly exhibited by investigating the changes of approximated participation vector with different numbers of modes.

Table 4-3 selects 1 to 5 as the number of used lower modes in the participation vector approximation to simulate the limitation of modal parameter identification via microtremor measurement. Since the model is single-dimensional (1D), the participation vector is approximated by Equation (3-16). The approximation starts from using the 1st mode to using the 1st to 4th modes. ‘-’ means the mode is not considered.

Table 4-3 Participation vector approximation using limited modes

Considered modes	1 st mode	1 st and 2 nd modes	1 st to 3 rd modes	1 st to 4 th modes	True value
1 st mode	2.052	1.999	2.024	2.019	2.021
2 nd mode	-	0.745	0.734	0.745	0.747
3 rd mode	-	-	0.400	0.403	0.408
4 th mode	-	-	-	-0.233	-0.237
5 th mode	-	-	-	-	0.150

When only the 1st mode is considered in the participation factor approximation, the factor of 2.052 has already had an adequate accuracy in comparison to the true value of 2.021. This approximation accuracy suggests the effectiveness of using the LSM in the approximation. Increasing the number of the used modes vibrates the approximated participation factors within a small range. The approximation accuracy of the 2nd mode is slightly decreased when the 3rd mode is added. The slightly decreased approximation accuracy in the 2nd mode is acceptable in the seismic response prediction because the use of the 1st to 3rd modes in the seismic response prediction may be better than the use of only the 1st and 2nd modes.

Table 4-4 shows the sums of participation functions indicated as $U'_x\beta'_x$ in Equation (3-12) corresponding to different numbers of utilized modes. For a comparison, the sums of participation functions using the accurate participation vector are indicated in the ‘True’ columns.

Table 4-4 Sums of approximated participation functions using limited modes

Considered modes	1 st mode		1 st and 2 nd modes		1 st to 3 rd modes		1 st to 4 th modes	
	True	Approx.	True	Approx.	True	Approx.	True	Approx.
Node 5	1.299	1.319	0.886	0.872	1.036	1.042	0.995	0.994
Node 4	1.112	1.129	1.125	1.113	0.886	0.891	1.030	1.029
Node 3	0.858	0.871	1.203	1.193	1.059	1.056	0.928	0.930
Node 2	0.579	0.588	1.007	0.999	1.146	1.137	1.106	1.103
Node 1	0.301	0.305	0.593	0.589	0.806	0.798	0.928	0.922

In Table 4-4, the approximated sums of participation functions at higher nodes are closer to unity and lower nodes are away from unity when lower modes are utilized. The sum of participation functions at Node 2 is significantly increased when the 2nd mode is added because the 2nd mode has large mode shape amplitudes at Node 2. However, the sum at Node 1 gets closer to unity after the 4th mode is added because the 2nd to 4th modes have large mode shape amplitudes at Node 1. The distribution of sums of participation function is helpful to estimate missing modes. In the 1D model, the sums of participation functions at certain locations might be away from unity, which implies that some modes are missing and those modes are likely to have large mode shape amplitudes at those locations.

4.3.2 Influence of limited measurement points

When a floor is not modeled as a node, every location on a floor is a candidate for microtremor measurement. However, the measurements can be implemented at limited locations, which means the participation vector of the objective building is approximated by the mode shapes at the selected locations. In the numerical simulation, it means the number of selected nodes is less than the number of total nodes in the numerical model and the mode shapes at the selected nodes are utilized in the participation vector approximation. Table 4-5 shows the participation vector approximation results using the 1st and 2nd modes when the mode shapes at two to four nodes are available. It demonstrates the influence of the limited measurement points (selected nodes) on the participation vector approximation. Node 5 is selected in all the cases because it has the largest 1st mode shape amplitude and the vibration at the top floor is generally the largest. Then another node is selected among Nodes 1 to 4 in the two-node cases to preliminarily

investigate the influence of the selected nodes on the approximation accuracy. Next, one additional node is selected based on the two-node cases to investigate if the participation vector approximation accuracy is improved when more nodes are utilized. The participation vector approximation using four nodes is also used to investigate if the approximation accuracy is improved.

Table 4-5 Participation vector approximation with different selected nodes

		Two nodes					
Mode	True value	Nodes 1 &5	Nodes 2 &5	Nodes 3 &5	Nodes 4 &5		
1 st mode	2.021	2.830	2.139	1.909	1.808		
2 nd mode	0.747	1.481	0.677	0.411	0.293		
		Three nodes					
Mode	True value	Nodes 1, 2 &5	Nodes 1, 3 &5	Nodes 1,4 &5	Nodes 2, 3 &5	Nodes 2, 4 &5	Nodes 3, 4 &5
1 st mode	2.021	2.320	2.101	2.243	2.001	1.998	1.872
2 nd mode	0.747	0.915	0.763	1.091	0.558	0.632	0.398
		Four nodes					
Mode	True value	Nodes 1, 2, 3 &5	Nodes 1, 2, 4 &5	Nodes 1, 3, 4 &5	Nodes 2, 3, 4 &5		
1 st mode	2.021	2.088	2.118	1.998	1.939		
2 nd mode	0.747	0.742	0.877	0.744	0.556		

Table 4-5 suggests that the selected nodes influence the participation vector approximation accuracy and different modes are influenced differently. The participation factors are related to the mode shapes at all nodes. As a result, the approximation accuracy may be higher when the mode shapes at the selected nodes well reflect the overall mode shapes. For example, the mode shapes at Nodes 5 and 2 well reflect the 1st and 2nd modes. Node 2 has the largest mode shape amplitude that is opposite to Node 5. The approximation result, especially for the 2nd mode, is the best when using Nodes 2 and 5 among the two-node cases. The mode shapes at Nodes 4 and 5 cannot consider the amplitudes in the 2nd mode, so the approximation accuracy in the 2nd mode is lowest in the two-node cases.

When more nodes are selected, the mode shapes at the selected nodes are more likely to well reflect the overall mode shapes and the approximation accuracy is generally improved. As shown in Table 4-5, the participation vector approximation accuracy is generally improved when an additional node is utilized. For example, the approximation accuracy using Nodes 1, 2 and 5, Nodes 1, 3 and 5 or Nodes 1, 4 and 5 is obviously higher than using Nodes 1 and 5. There is only one exception that the approximation accuracy is slightly decreased when an additional node is selected, which is when Nodes 3 and 5 are utilized and when Nodes 3, 4 and 5 are utilized. It is because the mode shapes at Node 4 can be linearly approximated by the mode shapes at Nodes 4 and 5 in the 1st and 2nd modes as shown in Figure 4-1. Node 4 is little informative to the overall mode shapes so the approximation results when using the Nodes 3 and 5 is only slightly changed when Node 4 is added and the changes decrease the approximation accuracy in this case.

It is difficult to theoretically determine measurement points on the same floor because they are usually determined only based on the planar shape of each floor. Unlike the vertical mode shape distribution, horizontal mode shape amplitude distribution in a rectangle area is already complicated [3, 4]. Nonetheless, evenly distributed measurement points on each floor are more likely to capture the overall mode shapes. In

addition, it is encouraged to select as many measurement points as possible to increase the chances of capturing those mode shape amplitudes in opposite directions.

To explain the influence of selected nodes, the sum of participation functions at each node is shown in Table 4-6 when only two nodes are utilized to approximate the participation factors in the 1st and 2nd modes. The objective of the LSM is to find a set of approximated participation factors that minimizes the sums of the absolute values of ε_x^{1D} in Equation (3-31). Therefore, the Mean Squared Errors (MSEs) in the LSM are attached to evaluate the performance of different node selections from the LSM viewpoint. The MSE in the 1D model is obtained by $\sum_{i=1}^N (\varepsilon_{x,i}^{1D})^2 / N$. $\varepsilon_{x,i}^{1D}$ is the i^{th} element in the ε_x^{1D} vector. N is the length of the ε_x^{1D} . Although the ε_x^{1D} is usually evaluated only at the selected nodes, Table 4-6 discusses the MSEs of the ε_x^{1D} at all five nodes to explain the participation vector approximation differences when using different sets of nodes.

Table 4-6 Sums of approximated participation functions and corresponding MSE

Selected nodes	All	Nodes 4 & 5	Nodes 3 & 5	Nodes 2 & 5	Nodes 1 & 5
Node 5	0.886	1.000	1.000	1.000	1.000
Node 4	1.125	1.000	1.058	1.189	1.583
Node 3	1.203	0.903	1.000	1.221	1.886
Node 2	1.007	0.686	0.782	1.000	1.658
Node 1	0.593	0.384	0.445	0.583	1.000
MSE	0.047	0.098	0.072	0.052	0.311

Since two modes are utilized and two nodes are selected, the sums of participation functions at the selected nodes are equal to 1.000 but the sums at unselected locations are away from 1.000. When using mode shapes at all nodes, the sum of participation functions at each node are not equal to 1.000 but the MSE in the LSM is the smallest comparing to using two nodes. The smallest MSE usually means the highest participation vector approximation accuracy when the utilized modes are fixed. When using mode shapes at Nodes 2 and 5, the MSE is the smallest in the two-node cases and the corresponding participation vector approximation accuracy is the highest.

The use of all identified modes does not necessarily produce higher approximation accuracy than the use of some identified modes when only limited nodes are selected. The participation factor approximation results in some modes might be greatly changed before and after a mode is added and their approximation accuracies are largely decreased. Then the decreased participation factor approximation accuracies might decrease the seismic response prediction accuracy.

For example, the 1st to 4th modes at Nodes 1, 2, 3 and 5 are utilized. Table 4-7 shows the participation vector approximation results under different numbers of modes when Node 4 is neglected. As a comparison, the approximation results using mode shapes at all nodes are also attached. The MSEs using different numbers of modes are attached to show the contribution of each mode. Unlike Table 4-6, the MSE in Table 4-7 evaluates the $\varepsilon_{x,i}^{1D}$ at the selected nodes. Therefore, the MSEs at the upper lines evaluate the $\varepsilon_{x,i}^{1D}$ at Nodes 1, 2, 3 and 5 and the MSEs at the lower lines evaluate the $\varepsilon_{x,i}^{1D}$ at all nodes.

Table 4-7 Participation vector approximation using mode shapes at selected nodes in limited modes

Considered modes	1 st mode	1 st and 2 nd modes	1 st to 3 rd modes	1 st to 4 th modes	True value
1 st mode	2.154	2.088	1.879	2.411	2.021
	2.052	1.998	2.024	2.019	
2 nd mode	-	0.742	0.736	0.760	0.747
	-	0.745	0.734	0.745	
3 rd mode	-	-	0.555	-0.023	0.408
	-	-	0.400	0.403	
4 th mode	-	-	-	-0.694	-0.237
	-	-	-	-0.233	
MSE	0.191	0.054	0.011	0.000	
	0.158	0.047	0.015	0.005	

Note: The upper lines use the Nodes 1, 2, 3 and 5 and lower lines use all nodes.

When Node 4 is neglected, the participation factor approximation accuracies of the 1st and 3rd modes are greatly changed after adding the 4th mode. The decreased participation factor approximation accuracies in the 1st and 3rd modes can be directly observed by comparing to the true values. Although the example in Table 4-7 implies that the participation vector approximation accuracy might be greatly decreased after adding a mode, the decreased approximation accuracy does not occur in the examples in Table 4-5 so the discussion about Table 4-5 is effective.

However, one need to decide if the large changes after a mode is added means improved approximation accuracy or decreased approximation accuracy in practical situations. Therefore, the MSE is utilized. The small reduction of MSE from 0.011 to 0.000 implies that the 4th mode is unimportant, then the changes in the 1st and 3rd modes are likely decreasing their approximation accuracies.

To further investigate if the changes caused by adding the 4th mode decrease the participation vector approximation accuracy, the sums of participation functions before and after the 4th mode is added can be helpful. Since large changes occur in the 1st and 3rd modes after the 4th mode is added, Table 4-8 shows the approximated participation functions in the 1st and 3rd modes before adding the 4th mode and the approximated participation functions in the 1st, 3rd and 4th modes after adding the 4th mode. Before the 4th mode is added in the participation vector approximation, the approximated participation functions of the 4th mode are set as zeros.

Table 4-8 Approximated participation functions before and after the 4th mode is added

	Before adding the 4 th mode				After adding the 4 th mode			
	1 st mode	3 rd mode	4 th mode	Sums	1 st mode	3 rd mode	4 th mode	Sums
Node 5	1.208	0.205	0.000	1.412	1.550	-0.009	-0.121	1.420
Node 3	0.798	-0.197	0.000	0.601	1.024	0.008	-0.383	0.649
Node 2	0.538	0.190	0.000	0.728	0.691	-0.008	-0.118	0.565
Node 1	0.280	0.291	0.000	0.571	0.359	-0.012	0.357	0.703

As shown in Table 4-8, the approximated participation functions in the 1st and 3rd modes are changed after the 4th mode is added. However, the sums of approximated participation functions in the 1st and 3rd modes before the 4th mode is added are similar to the sums of approximated participation functions in the

1st, 3rd and 4th modes. The small changes in the sums of approximated participation functions also imply that the 4th mode is unimportant. Therefore, the changes in the 1st and 3rd modes after adding the 4th mode are more likely decreasing their participation factor approximation accuracies.

An explanation to the decreased participation factor approximation accuracies is that the 4th mode is little informative because its mode shape vector can be linearly approximated by the linear combination of the 1st and 3rd modes as shown in Equation (4-1). The parameters of 0.771 and 0.834 in Equation (4-1) are obtained by the LSM. From Table 4-2, the mode shape vector in the 1st, 3rd and 4th modes after removing the Node 4 are $\{0.643, 0.425, 0.286, 0.149\}^T$, $\{0.369, -0.355, 0.342, 0.524\}^T$ and $\{0.175, 0.552, 0.170, -0.514\}^T$, respectively,

$$\begin{pmatrix} 0.643 \\ 0.425 \\ 0.286 \\ 0.149 \end{pmatrix} \times 0.771 - \begin{pmatrix} 0.369 \\ -0.355 \\ 0.342 \\ 0.524 \end{pmatrix} \times 0.834 = \begin{pmatrix} 0.188 \\ 0.623 \\ -0.064 \\ -0.323 \end{pmatrix} \quad (4-1)$$

The right part in Equation (4-1) is similar to the mode shape vector in the 4th mode so that the 4th mode is indeed little informative. Then the changes in the 1st and 3rd modes after adding the 4th mode are unlikely to improve the participation factor approximation accuracies. Some researches call the mode shape linear approximation relationship among the 1st, 3rd and 4th modes as the collinearity [5-9]. On the other hand, the mode shape vector in the 4th mode cannot be well linearly approximated by the 1st and 3rd modes when Node 4 is not neglected. Equation (4-2) shows the linear approximation results using the 1st and 3rd modes to the 4th mode when the mode shape amplitudes at all nodes are utilized. Similar to Equation (4-1), the parameters of -0.0156 and 0.0146 in Equation (4-2) are obtained from using the LSM. As a result, the approximated participation factors in the 1st and 3rd modes do not change largely after the 4th mode is added when not neglecting Node 4.

$$\begin{pmatrix} 0.643 \\ 0.550 \\ 0.425 \\ 0.286 \\ 0.149 \end{pmatrix} \times (-0.0156) + \begin{pmatrix} 0.369 \\ -0.588 \\ -0.355 \\ 0.342 \\ 0.524 \end{pmatrix} \times 0.0146 = \begin{pmatrix} -0.005 \\ -0.017 \\ -0.012 \\ 0.001 \\ 0.005 \end{pmatrix} \neq \begin{pmatrix} 0.175 \\ -0.610 \\ 0.552 \\ 0.170 \\ -0.514 \end{pmatrix} \quad (4-2)$$

The example in Table 4-7 shows that using more modes does not necessarily lead to higher participation vector approximation accuracy. Some modes should be removed because they decrease the participation factor approximation accuracies in other modes. The simplest way to find modes that decrease the participation vector approximation accuracy is to start the participation vector approximation by using the lowest mode and then gradually adding higher modes. When approximated participation factors in some modes greatly change after a mode is added, the reduction of MSE decides if the changes decrease the approximation accuracy and the mode should be removed. For example, the approximation results in the 1st and 3rd mode changes greatly after the 4th mode is added while the MSE is only slightly reduced in Table 4-7, which means the 4th mode is unimportant. The changes after adding the 4th mode are likely to decrease

the approximation accuracy so the 4th mode should be removed. As the supplements for decision making, the sums of approximated participation functions before and after the 4th mode is added are investigated in Table 4-8, the slightly changed sums of approximated participation functions further suggest that the 4th mode is indeed unimportant. In practical situations, the changes of approximation results after adding a mode and the corresponding reduction of MSE are recommended for preliminary judgement. The MSE can be simultaneously calculated when the participation vector approximation starts with the lowest mode and gradually adding higher modes so the MSE requires little effort. The utilized participation vector approximation procedure tends to remove higher modes because lower modes are believed to contribute the most in the seismic responses.

4.4 Seismic Response Prediction with Approximated Participation Vector

This section discusses the influences of both the participation vector approximation errors and the truncation errors in the mode superposition on the seismic response prediction accuracy. Table 4-9 uses different number of modes for the seismic response prediction, the table shows the peak absolute accelerations in the 5-DOF model under the El Centro wave (NS component) with the peak acceleration of 1 m/s². Figure 4-2 shows the response spectrum of the El Centre wave with the 2% damping ratio. Section 4.2 describes the natural frequencies, damping ratios and mode shapes in Table 4-2. The sampling time is 0.005 s for response analysis and the average acceleration method is utilized to solve the modal equations of motion. The accurate results are obtained by using all five modes.

Table 4-9 Seismic response amplitude prediction using mode shapes at all nodes

	Considered modes	Accurate	1 st mode	1 st and 2 nd	1 st to 3 rd	1 st to 4 th
Acceleration (m/s ²)	Node 5	3.454	2.837	3.385	3.407	3.448
	Node 4	2.477	2.431	2.369	2.535	2.488
	Node 3	2.270	1.879	2.297	2.219	2.261
	Node 2	2.334	1.416	2.185	2.284	2.334
	Node 1	1.634	1.013	1.541	1.701	1.631
	Ave. errors (%)			-23	-3	+0
Velocity ×10 ⁻¹ (m/s)	Node 5	1.518	1.430	1.492	1.514	1.516
	Node 4	1.211	1.224	1.192	1.215	1.210
	Node 3	1.018	0.944	1.000	1.017	1.017
	Node 2	0.769	0.637	0.760	0.763	0.768
	Node 1	0.442	0.331	0.429	0.447	0.441
	Ave. errors (%)			-11	-2	+1
Displacement ×10 ⁻³ (m)	Node 5	8.878	9.037	8.790	8.887	8.869
	Node 4	7.636	7.737	7.535	7.652	7.629
	Node 3	5.928	5.969	5.841	5.926	5.922
	Node 2	4.001	4.027	3.958	4.000	3.993
	Node 1	2.067	2.092	2.065	2.081	2.068
	Ave. errors (%)			+1	-1	+0

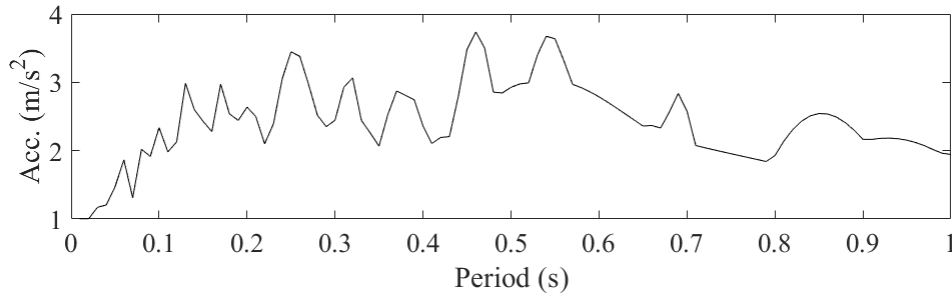


Figure 4-2 Response spectrum of the input acceleration with 2% damping ratio

The 1st and 2nd modes are the mostly excited modes according to Figure 4-2 because the corresponding natural periods are around 0.36 s and 0.13 s, respectively. The natural periods of 3rd to 5th modes are lower than 0.1 s. Besides, the 1st and 2nd modes have large participation functions as shown in Figure 4-1. When only the 1st mode is considered, the prediction underestimates the response accelerations and the averaged relative error is 23%. The error is caused by the truncation error in the mode superposition because the approximated 1st participation factor has high accuracy. The simulation uses the constant damping ratio so that the influence of the truncation error in the mode superposition is large. The errors of velocity and displacement amplitudes are smaller even if only the 1st mode is utilized. After the 2nd mode is added, the prediction errors are significantly reduced and the averaged relative errors are reduced from 23% to 3% regarding acceleration amplitudes. Although the numerical simulation uses the constant damping ratios to consider the influence of higher modes, Table 4-9 shows the applicability of the proposed seismic response prediction method when using two lowest modes.

Next, the prediction accuracy using more modes with less accurate approximated participation vector is compared to the accuracy using fewer modes with more accurate approximation participation vector. As shown in Table 4-7, the participation factor accuracies using the 1st to 4th modes are lower than using the 1st to 3rd modes when Node 4 is neglected. The 4th mode should be removed due to the decreased participation factor approximation accuracies. However, the seismic response prediction method hopes to use more modes in the mode superposition. Therefore, Table 4-10 predicts the seismic responses using the approximated participation vectors in Table 4-7 that neglects Node 4. Since Node 4 is neglected in Table 4-7 to simulate the only limited nodes can be measured, Table 4-10 only evaluates the seismic responses at Nodes 1, 2, 3 and 5.

The prediction accuracies of acceleration, velocity and displacement amplitudes in Table 4-10 are similar to Table 4-9 before the 4th mode is added because the utilized approximated participation factors are similar. However, the prediction errors are obviously increased when the 4th mode is added in Table 4-10. The increased errors are mainly caused by the increased participation factor approximation error in the 1st mode. The 1st mode is the mostly excited mode and the approximated participation factor in the 1st mode changes greatly after the 4th mode is added in Table 4-7. The errors at Nodes 3 and 5 are more increased than Nodes 1 and 2, which also implies that the increased prediction errors are caused by the 1st mode. Table 4-10 suggests that the use of the 1st to 3rd modes has the highest prediction accuracy. The participation vector

approximation errors in the 1st mode influences the prediction accuracy more than the truncation error caused by neglecting the 4th mode.

Table 4-10 Seismic response amplitude prediction using mode shapes at Nodes 1, 2, 3 and 5

	Considered modes	Accurate	1 st	1 st and 2 nd	1 st to 3 rd	1 st to 4 th
Acceleration (m/s ²)	Node 5	3.454	2.977	3.475	3.272	3.976
	Node 3	2.270	1.972	2.336	2.119	2.802
	Node 2	2.334	1.459	2.210	2.286	2.425
	Node 1	1.634	1.030	1.551	1.745	1.742
	Ave. errors (%)		-25	-2	-2	+12
Velocity ×10 ⁻¹ (m/s)	Node 5	1.518	1.501	1.549	1.423	1.773
	Node 3	1.018	0.991	1.037	0.959	1.186
	Node 2	0.769	0.669	0.784	0.731	0.880
	Node 1	0.442	0.347	0.440	0.434	0.509
	Ave. errors (%)		-10	+1	-5	+16
Displacement ×10 ⁻³ (m)	Node 5	8.878	9.486	9.183	8.244	10.618
	Node 3	5.928	6.265	6.101	5.509	7.072
	Node 2	4.001	4.227	4.132	3.714	4.779
	Node 1	2.067	2.196	2.155	1.932	2.461
	Ave. errors (%)		+6	+3	-7	+19

Figure 4-3 shows the predicted response accelerations at the four selected nodes using the approximated participation factors in Table 4-7 that neglects the Node 4. The predicted acceleration using the 1st to 3rd modes and the 1st to 4th modes are compared. The difference between the two cases is small in the time history.

Table 4-7 shows that using more modes does not necessarily lead to higher participation vector approximation accuracy when mode shapes at limited nodes are utilized, the participation factor approximation results in some modes might be greatly decreased when a mode is added. Then Table 4-10 and Figure 4-3 demonstrate that the less accurate approximated participation vector is likely to decrease the seismic response prediction accuracy, even though more modes are utilized. As a result, using more modes does not necessarily lead to the higher seismic response prediction accuracy when mode shapes at limited nodes are utilized.

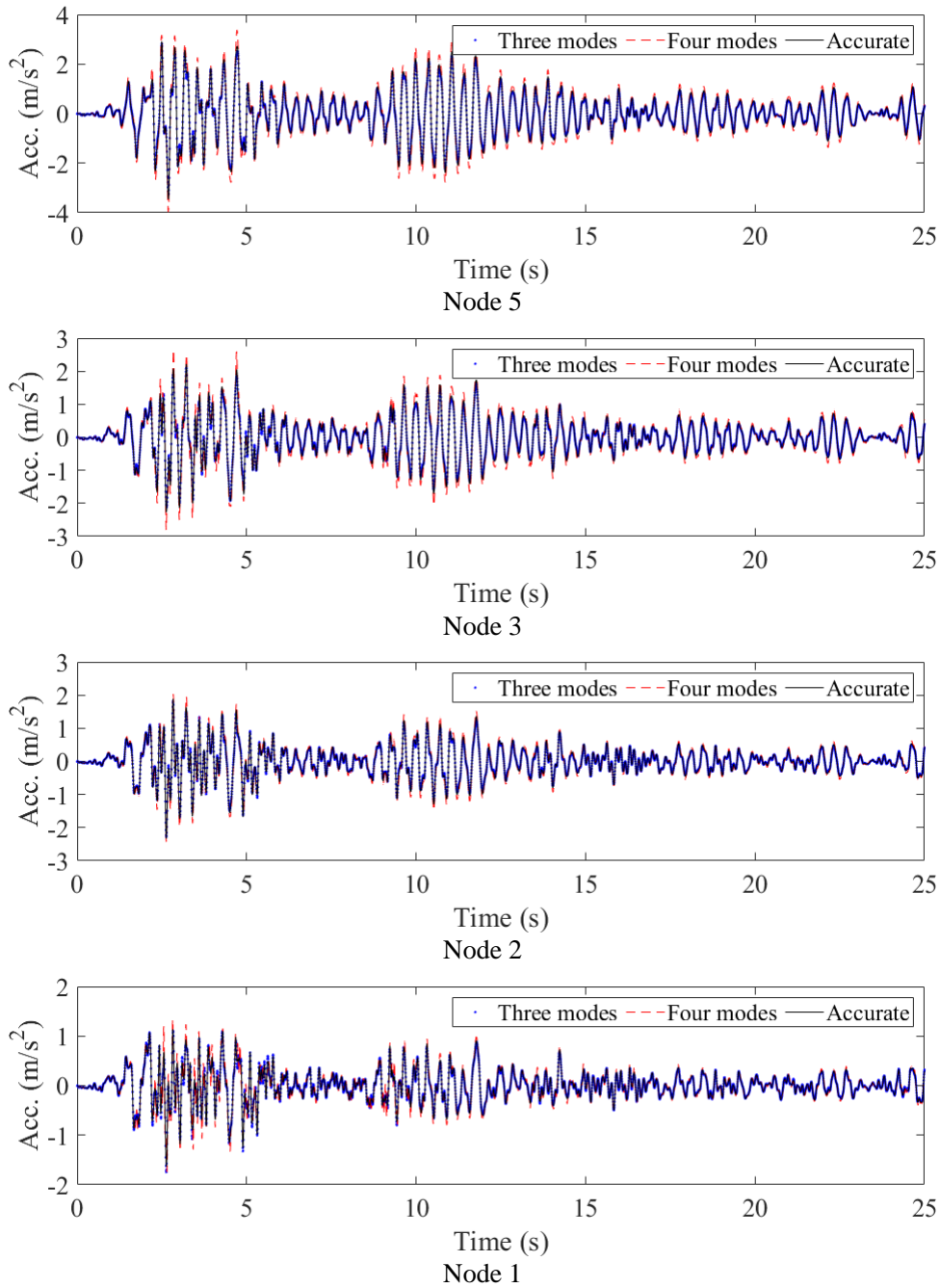


Figure 4-3 Predicted acceleration time histories

4.5 Conclusions

This chapter explores the fundamental properties of the proposed seismic response prediction method. The properties include two aspects: one relates to the participation vector approximation and the other relates to the seismic response prediction. The properties are demonstrated by the numerical simulation of the 5-DOF model and the conclusions are summarized as follows:

- (1) When mode shapes at all nodes are used, the participation vector approximation has high accuracy even if only a few modes are available. When the approximation starts with only using the lowest mode and gradually adding higher modes, the approximated participation factors vibrate within small

ranges when higher modes are gradually added. The sums of approximated participation functions at higher nodes reach unity quickly when using a few lower modes while lower nodes require more higher modes. In return, the distribution of sums of approximated participation functions can be used to estimate the missing modes. When the sums of approximated participation functions at some locations are away from unity in the 1D model, some modes with large mode shape amplitudes at those locations are likely missing.

- (2) When a floor is not modelled as a node, the participation vector is approximated by the mode shapes at measured locations on each floor and only limited locations are selected for measurement. In the numerical simulation, the participation vector approximation using mode shapes at selected nodes is investigated. The node selection (the selection of measurement points) indeed influences the approximation accuracy but different modes are influenced differently. The lower modes are less influenced by the node selection. Therefore, it is possible to use mode shapes at limited locations to approximate participation factors of lower modes with high accuracy. The approximation accuracy is generally improved by having more measurement points.
- (3) The use of all identified modes does not necessarily produce higher participation vector approximation accuracy than the use of some identified modes when only limited nodes are selected. It is recommended to start the approximation with only the lowest mode, then gradually adding higher modes to investigate the changes in approximation results. When the approximation results significantly change after a mode is added while the corresponding MSE in the LSM is not or slightly reduced, the mode should be removed.
- (4) The seismic response prediction accuracy is high even if only using a few modes when not considering the modal property variances. The lower modes are mostly excited under an earthquake and the approximated participation factors of lower modes are good when using the corresponding mode shapes. The seismic response prediction accuracies between using more modes with less accurate approximated participation vector and using fewer modes with more accurate approximated participation vector are compared. The former case has lower participation factor approximation accuracies in lower modes and thus the prediction accuracy is lower than the latter case. The simulation suggests that using more modes does not necessarily lead to higher seismic response prediction accuracy when mode shapes at limited nodes are utilized.

Reference

- [1] Xie J, Ikeda Y, Kurata M (2021): Multi-degree-of-freedom linear building model based on microtremor measurement for seismic response analysis, *Journal of structural engineering*, AIJ, Vol.67(B), pp.509–518 (in Japanese).
- [2] Ohsaki Y (1980): Vibration Theory (in Japanese, translated by the author), *Shokokusha*, 302pp.
- [3] Wang G, Wereley NM (2002): Free in-plane vibration of rectangular plates, *AIAA journal*, Vol.40(5), pp.953-959.

- [4] Du J, Li WL, Jin G, Yang T, Liu Z (2007): An analytical method for the in-plane vibration analysis of rectangular plates with elastically restrained edges, *Journal of sound and vibration*, Vol.306(3-5), pp.908-927.
- [5] Mackinnon MJ, Puterman ML (1989): Collinearity in generalized linear models, *Communications in Statistics-Theory and Methods*, Vol.18(9), pp.3463-3472.
- [6] Lesaffre E, Marx BD (1993): Collinearity in generalized linear regression, *Communications in Statistics-Theory and Methods*, Vol.22(7), pp.1933-1952.
- [7] Mason CH, Perreault Jr WD (1991): Collinearity, power, and interpretation of multiple regression analysis, *Journal of marketing research*, Vol.28(3), pp.268-280.
- [8] Næs T, Mevik BH (2001): Understanding the collinearity problem in regression and discriminant analysis, *Journal of Chemometrics: A Journal of the Chemometrics Society*, Vol.15(4), pp.413-426.
- [9] Damodar N (2009): Basic Econometrics Fifth Edition, *McGraw-Hill* 922pp.

Chapter 5

Verification with Numerical Model of Large-scale Low-rise Building

5.1 Introduction

In Chapter 5, the applicability of the proposed prediction method to buildings that exhibit floor flexibility is verified by the numerical simulation of the large-scale low-rise building [1]. The fundamental properties summarized in Chapter 4 are utilized in the verification. The model has an asymmetric planar shape and its mode shapes have obvious lateral-torsional coupling. The prediction results when using the single-dimensional (1D) and two-dimensional (2D) models are compared. This chapter is arranged as follows: Section 5.2 introduces the basic information about the numerical model. The prediction method can only predict the seismic responses at the selected nodes and Section 5.3 introduces the selected nodes and modes in the seismic response prediction. The node and mode selections simulate that the microtremor measurements can be taken only at limited locations in a building and only a limited number of modes can be identified. The participation vector approximation results using the 1D and 2D models are compared in Section 5.4. Then the seismic response prediction accuracy is discussed in Section 5.5. Two cases are considered in the seismic response prediction, one considers the single-directional ground motions and only evaluates the corresponding directional seismic response prediction accuracies. It exhibits how the prediction accuracy is influenced by the participation vector approximation errors. The other case considers the two-directional ground motions. It exhibits the necessity of considering the vibrations induced by orthogonal ground motion. Lastly, Section 5.6 concludes this chapter.

5.2 Numerical Model

The outlook of the numerical model is shown in Figure 5-1. The model originates from the Building A in Chapter 2 but without EXP.Js on the roof floor. The reason of neglecting the joints is that the simulation preliminarily verifies the applicability of the proposed method to buildings that the rigid-floor assumption is not applicable to. EXP.Js inevitably complicate the simulation. For example, the collision between the two sides of the joints needs to be considered. The numerical model without EXP.Js is adequate for the preliminary method verification as long as it exhibits floor flexibility.

For the convenience of description, the model is divided into three parts by the black dash lines, the divided areas are circled by the blue rings and named as P1, P2 and P3 areas in Figure 5-1. The 3-story L-shaped steel structure is 270 m by 280 m in planar and 20.2 m in height. The spans between two close columns are mostly 9 m in the x - and y -directions. The model has a local roof (5th floor) installed at the right corners on the roof floor (4th floor). The hollow area on the 4th floor simulates a movie theatre. The

weights from the 2nd to the local roof floors are 240,000 kN, 240,000 kN, 220,000 kN and 30,000 kN, respectively. The numerical model utilizes fixed supports at its base nodes. The information of structural components is obtained from actual structural design drawings. Three types of beams are utilized at different areas: Beams in the P2 area utilize H-396×199×7×1 with SS400, beams in the P1 and P3 areas utilize H-346×174×6×9 with SS400, and edge beams utilize H-580×300×12×20 with SM490A. The edge beams are expected to resist relatively large deformation in practical situations so they have larger cross-section with SM490A that has higher yield strength. Columns on the 1st and 2nd floors utilize □-400×16 with SS400, columns on the 3rd and 4th floors and the local roof utilize □-400×14 with SS400. Braces utilize □-350×12 with STKR400. Floor slabs are RC slabs with 130 mm thick. The 5.6 mm SS400 plates are used as shear walls.

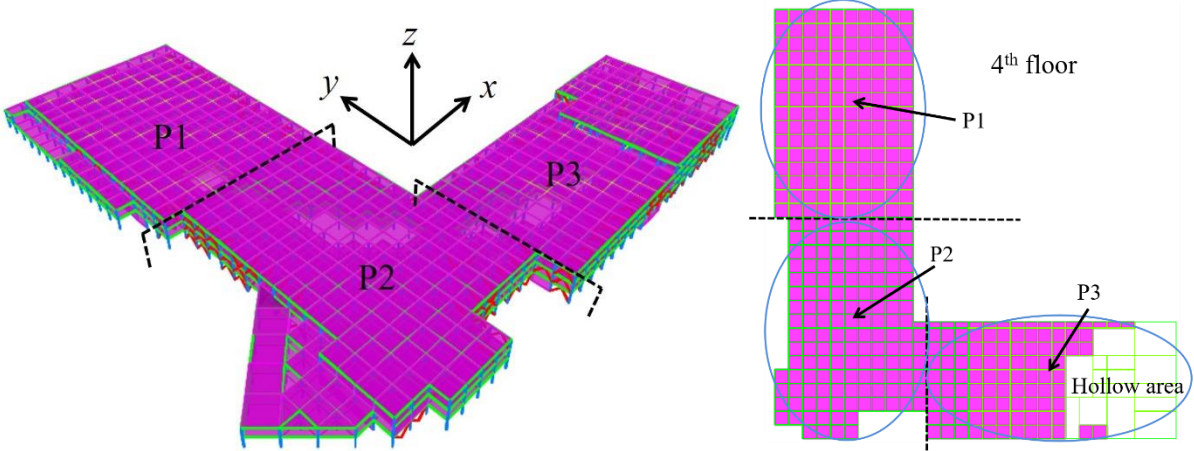


Figure 5-1 Outlook of the numerical model

5.3 Measurement Points and Used Vibration Modes for Simulation

In the numerical simulation, the measurement points coincide with the nodes of the finite element model so the measurement point selection equals to the node selection. The nodes represent the column locations in the numerical model and the green dots in Figure 5-2 represent the selected nodes. The nodes on the 4th (the roof floor) and the 5th (the local roof) floors are evenly selected near the edges, the nodes on the 2nd and 3rd floors are horizontally consistent with the nodes on the 4th and 5th floors. Each selected node is attached with a name for the convenience of description. The name of each selected nodes contains a number and a character, the number indicates the floor number and the character means the horizontal location. The span between the columns at Location k, j or i and the close column at the edges are 4 m in the y-direction. Therefore, the selected nodes at the three horizontal locations look closer to edges comparing to other selected nodes. The selected nodes are used for not only the participation vector approximation, but also the seismic response prediction. Therefore, the selected nodes are based on three factors: The seismic responses near the edges are generally large; It is impossible to apply microtremor measurements at the edges in practical situations so the nodes near the edges are selected; The lateral-torsional coupling is more obvious near the edges.

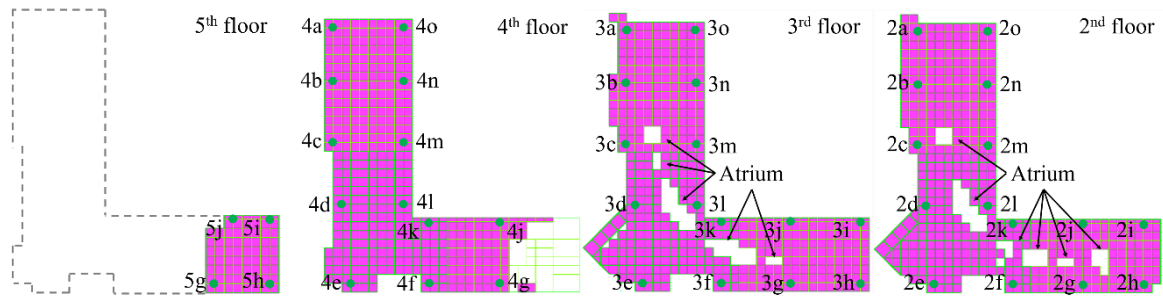
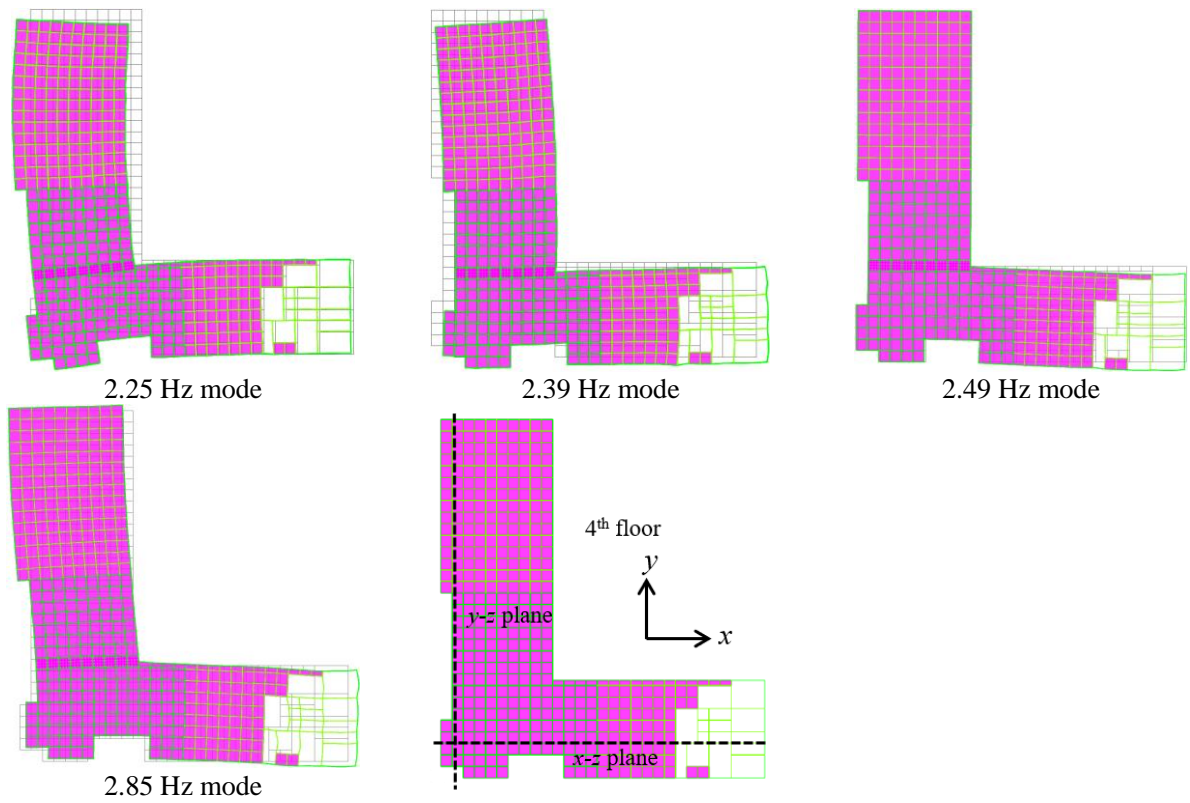


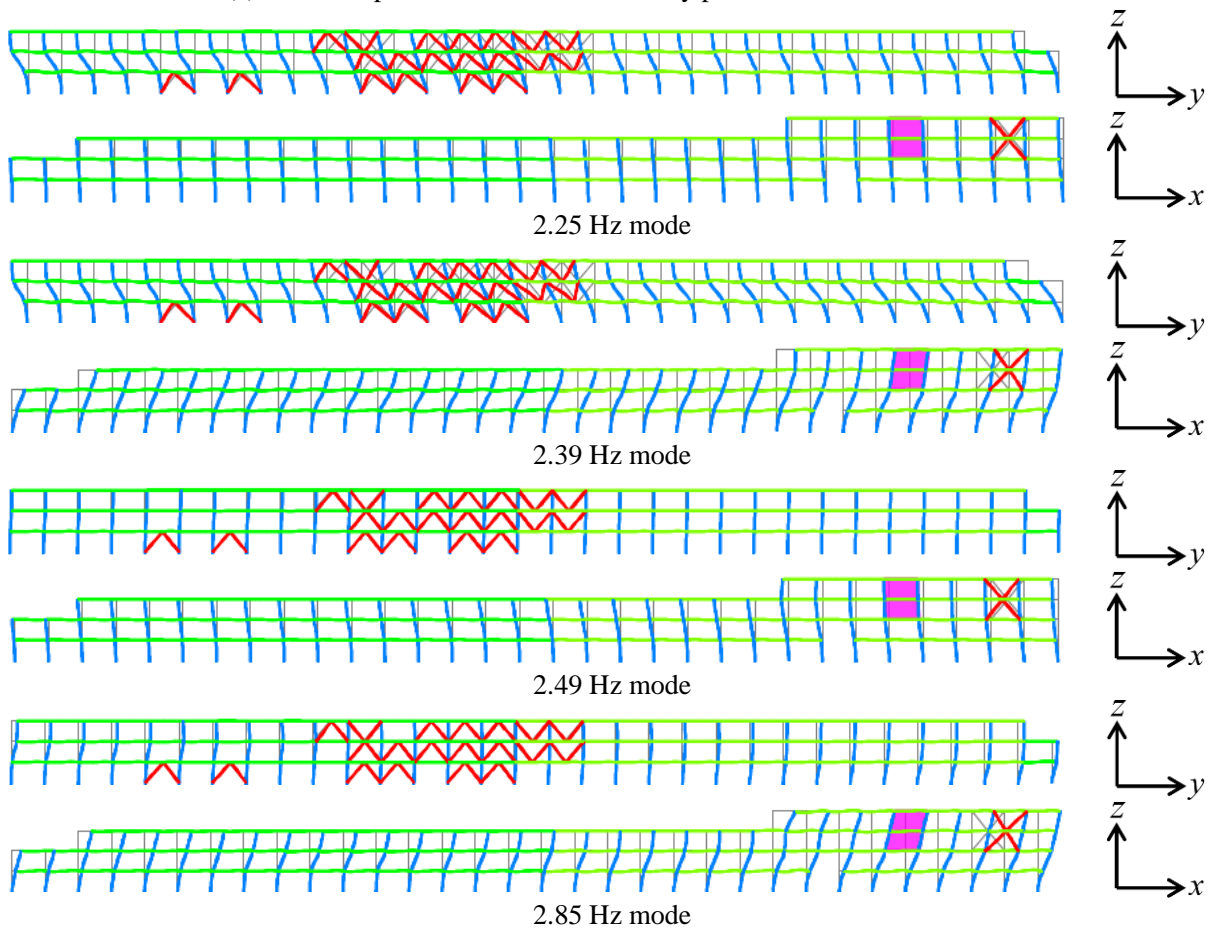
Figure 5-2 Locations for the seismic response prediction

Unlike the 5-DOF model in Chapter 4 that only has 5 modes to select, the numerical model has 78 modes within 10 Hz and most of them are local modes with mode shape amplitudes in small areas. To simulate the seismic response prediction using modal properties in limited modes, four modes at the lowest frequencies are selected and their mode shapes are shown in Figure 5-3(a) by plane view and Figure 5-3(b) by elevation. The four lowest modes have large mode shape amplitudes at many locations in at least one of the P1, P2 and P3 areas. The selection considers that modes with large mode shape amplitudes at many locations at low frequencies are more likely identified in practical situations. Neither local modes with large amplitudes in small areas nor global modes at higher frequencies with large amplitudes at many locations are selected. As a result, the seismic response prediction at specific locations might be less accurate.

Figure 5-3(a) shows the obvious floor flexibility of the numerical model by plane view because the selected modes have large amplitudes in P1, P2 or P3 areas and small amplitudes in other areas. For example, the 2.25 Hz mode has large amplitudes in P1 and P2 areas while the amplitudes in P3 area is small. Although atria are installed on the 2nd and 3rd floors as shown in Figure 5-2, floor flexibility is mainly caused by the large scale asymmetric planar shape of the numerical model according to the amplitudes on the 4th floor. The 2.25 Hz, 2.39 Hz and 2.85 Hz modes show obvious lateral-torsional coupling property since they have large x - and y -directional amplitudes simultaneously. The 2.25 Hz mode has obvious x - and y -directional mode shape amplitudes in P1 and P2 areas while the amplitudes in P3 area is small. The 2.39 Hz mode has obvious x - and y -directional amplitudes in the all three areas. The 2.49 Hz mode is the local y -directional mode in P3 area. The x -directional amplitudes in P1 area are in the opposite direction to the amplitudes in P3 area in the 2.85 Hz mode. The amplitudes on the 4th floor are generally larger than the 2nd and 3rd floors in the four modes.



(a) Mode shapes of the selected modes by plane view on the 4th floor



(b) Mode shapes of the selected modes by elevation

Figure 5-3 Mode shapes of the selected modes

5.4 Participation Vector Approximation

The 1D and 2D modellings are proposed in Chapter 3 based on whether the objective building has modes with obvious lateral-torsional coupling or not. The lateral-torsional coupling of a mode implies having large x - and y -directional components simultaneously. The 2.25 Hz, 2.39 Hz and 2.85 Hz modes show obvious lateral-torsional coupling and have large x - and y -directional mode shape amplitudes as shown in Figure 5-3(a). The participation vector approximation results are likely different when using the 1D and 2D models. The 2D model uses x - and y -directional mode shape components simultaneously to approximate the participation vector in one direction. On the other hand, the 1D model only uses the mode shape components in the same direction of the participation vector. This section compares the approximation differences when using the two models.

The mode shapes from the numerical model are directly used so that the approximated participation vectors can be compared to the true values. The numerical model is actually a 6-dimensional model [2], the translations of each node along the x -, y - and z -directional axes and the rotations about the three axes are considered in the numerical model. Nonetheless, the comparison between the approximated participation vector and the true values helps to anticipate the seismic response prediction accuracy.

5.4.1 1D model

The participation vector approximation results using Equation (3-16) from the 1D model are shown in Table 5-1. Similar to the simulation in Chapter 4, the modes are sorted from the lowest frequency to the highest frequency, the approximation starts with using the lowest mode and gradually adding higher modes. It helps to monitor the changes of approximation results when using different number of modes. The MSEs in the LSM corresponding to different number of utilized modes are also attached to judge if the large changes in the approximation results after adding a mode means improved approximation accuracy. As introduced in Chapter 4, the x -directional MSE in the LSM when using the 1D model is $\sum_{i=1}^N (\varepsilon_{x,i}^{1D})^2 / N$. $\varepsilon_{x,i}^{1D}$ is the i^{th} element in the ε_x^{1D} vector in Equation (3-31). N is the length of the ε_x^{1D} and equal to the number of selected nodes in the 1D model. The MSE in the y -direction follows the similar definition by replacing ε_x^{1D} with ε_y^{1D} in Equation (3-32). ‘-’ means the mode is not considered.

Table 5-1 Participation vector approximation using the 1D model

Mode freq. (Hz)	x -direction					y -direction				
	Total number of utilized modes					Total number of utilized modes				
	1	2	3	4	True	1	2	3	4	True
2.25	-9.15	-2.74	-3.64	-1.97	-4.94	-9.65	3.35	-3.60	-2.09	-4.28
2.39	-	8.81	7.35	9.22	5.56	-	-13.88	-6.86	-5.61	-5.27
2.49	-	-	-2.17	-1.49	-1.75	-	-	-2.69	-4.20	-3.64
2.85	-	-	-	-0.82	1.06	-	-	-	5.29	1.73
MSE	0.22	0.09	0.09	0.09		0.26	0.11	0.08	0.07	

As explained in Chapter 4, the large changes of approximation results are considered decreasing the approximation accuracy when the corresponding MSE is only slightly reduced. The approximated y -

directional participation factor in the 1st mode (2.25 Hz mode) changes significantly when the 2nd mode (2.39 Hz mode) is added. Then the approximation results in the 1st and 2nd modes change when the 3rd mode (2.49 Hz mode) is added. The changes after the 2nd and 3rd modes are added are considered improving the approximation accuracy because MSE is obviously reduced. However, the approximated participation factors in the 1st and 3rd modes change when the 4th mode (2.85 Hz mode) is added while the MSE is only reduced from 0.08 to 0.07. Therefore, the 4th mode is considered as the candidate to remove from the y-directional participation vector approximation. Similar to the discussion in the y-directional approximation, the 4th mode is also considered as a candidate to remove from the x-directional participation vector approximation. Although the approximated x-directional participation factors in the 1st and 2nd modes change when the 3rd mode is added, the changes are relatively small comparing to the changes when the 4th mode is added. Since the seismic response prediction hopes to use more modes in the mode superposition, the 3rd mode is kept in the x-directional participation vector approximation.

To help decide if the 4th mode should be removed from the x- and y-directional participation vector approximation, Figure 5-4 shows the sums of approximated participation functions in the x- and y-directions before and after the 4th mode is removed.

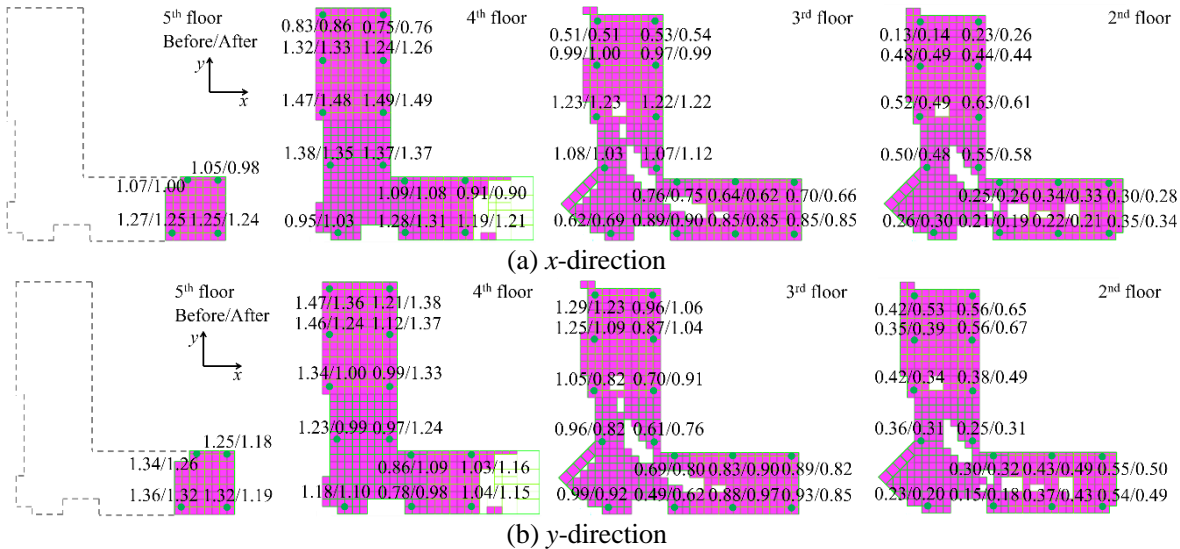


Figure 5-4 Sums of approximated participation functions in the 1D model before/after removing the 4th mode

The x-directional sums of approximated participation functions before and after removing the 4th mode have slight differences, which suggests that the 4th mode is indeed unimportant in the x-direction. The changes in the x-directional approximation results when the 4th mode is added are likely decreasing the approximation accuracy. On the other hand, the 4th mode obviously changes the y-directional sums of approximated participation functions especially on the 4th floor. The sums at some locations are closer to unity while other locations are farther from unity on the same floor after the 4th mode is added. Therefore, the 4th mode is considered contributing to the participation vector approximation. Based on Table 5-1 and Figure 5-4, the 4th mode is removed from the x-directional participation vector approximation and kept in

the y-directional approximation. As a result, the 4th mode is removed from the x-directional seismic response prediction when using the 1D model.

The approximation accuracy in Table 5-1 is still low even if the 4th mode is removed in the x-direction. An explanation to the low approximation accuracies is that the selected modes simultaneously have x- and y-directional amplitudes while the 1D model only uses single directional amplitudes in the corresponding directional participation vector approximation. As a result, the amplitudes in the selected modes are not well utilized and likely causing the low approximation accuracies.

Figure 5-4 shows that the sums of approximated participation functions on the 4th floor are closer to unity while the sums on the 2nd floor are farther from unity. This phenomenon is consistent with the simple numerical simulation in Chapter 4. An explanation is that lower floors are more influenced by the higher modes while the utilized modes are at low frequencies with large mode shape amplitudes on higher floors as shown in Figure 5-3(b). Figure 5-4 also shows that the x-directional sums of approximated participation functions in P1 area are farther from unity than the sums in P2 and P3 areas, which suggests that some modes might be missing and those modes have large amplitudes in P1 area.

5.4.2 2D model

The participation vector approximation results using Equations (3-25) and (3-26) from the 2D model are shown in Table 5-2. Similar to Table 5-1, the approximations using different number of modes are listed and the corresponding MSEs are attached. However, the MSE under the 2D model is different from the ones under the 1D model. For example, the MSE in the x-direction is obtained by $\sum_{i=1}^{2N} (\epsilon_{x,i}^{2D})^2 / 2N$. $\epsilon_{x,i}^{2D}$ is the *i*th element in the ϵ_x^{2D} vector in Equation (3-29). In the 2D model, ϵ_x^{2D} relates to both x- and y-directional mode shapes so the length of ϵ_x^{2D} is 2*N* where *N* is the number of selected nodes.

The 2D model outperforms the 1D model because the approximation accuracies of the utilized modes are significantly improved in Table 5-2 comparing to Table 5-1. The approximation accuracies in Table 5-2 show the applicability of the proposed participation vector approximation method when the utilized modes have obvious lateral-torsional coupling. The reason of the improved accuracy is likely because the two-directional mode shape amplitudes are simultaneously utilized. Unlike Table 5-1, the approximation results have small changes before and after a mode is added so that the 2D model does not need removing modes.

Table 5-2 Participation vector approximation using the 2D model

Mode freq. (Hz)	x-direction					y-direction				
	Total number of utilized modes					Total number of utilized modes				
	1	2	3	4	True	1	2	3	4	True
2.25	-5.16	-5.15	-5.18	-5.19	-4.94	-4.21	-4.22	-4.28	-4.29	-4.28
2.39	-	5.65	5.75	5.66	5.56	-	-5.36	-5.13	-5.32	-5.27
2.49	-	-	-1.59	-1.64	-1.75	-	-	-3.32	-3.42	-3.64
2.85	-	-	-	0.88	1.06	-	-	-	1.78	1.73
MSE	0.34	0.13	0.11	0.10		0.39	0.21	0.10	0.08	

The reason behind the participation vector approximation differences when using the 1D and 2D model is explained in Chapter 3. In the 2D model, the sums of approximated participation functions related to the participation vector in one direction contain two parts, one relates to the x -directional mode shapes and the other relates to the y -directional mode shapes. For example, the sums of approximated participation functions relating to the x -directional participation functions are $[\hat{U}_x^T \quad \hat{U}_y^T]^T \hat{\beta}'_x$. As noted in Equation (3-24), \hat{U}_x is the utilized x -directional mode shape matrix, \hat{U}_y is the utilized y -directional mode shape matrix and $\hat{\beta}'_x$ is the x -directional approximated participation vector. The 2D model not only requires the sums of approximated participation functions related to the mode shapes in one direction close to unity, but also requires the sums related to the other direction close to null. However, the 1D model only requires the sums of approximated participation functions related to the mode shapes in one direction close to unity.

Figure 5-5 shows the sums of approximated participation functions under the 2D model when using the approximated x -directional participation vector in Tables 5-1 and 5-2. The approximated x -directional participation vector in Tables 5-1 and 5-2 are substituted into $\hat{\beta}'_x$ so that the corresponding sums of approximated participation functions are compared in Figure 5-5. Then Figure 5-6 compares the sums of approximated y -directional participation functions. The comparisons help to discuss the differences in Tables 5-1 and 5-2. The sums of approximated participation functions in one direction is divided into two parts, one relates to the mode shapes in the same direction of the considered participation vector and the other relates to the orthogonal mode shapes. For example, the x -directional participation functions are expressed by $\hat{U}_x' \hat{\beta}'_x$ in Figure 5-5(a) and $\hat{U}_y' \hat{\beta}'_x$ in Figure 5-5(b). The participation vectors in Table 5-1 utilize the 1st to 3rd modes in the x -direction and the 1st to 4th modes in the y -direction as explained in Sub-section 5.4.1. The participation vectors in Table 5-2 utilize the 1st to 4th modes in both x - and y -directions.

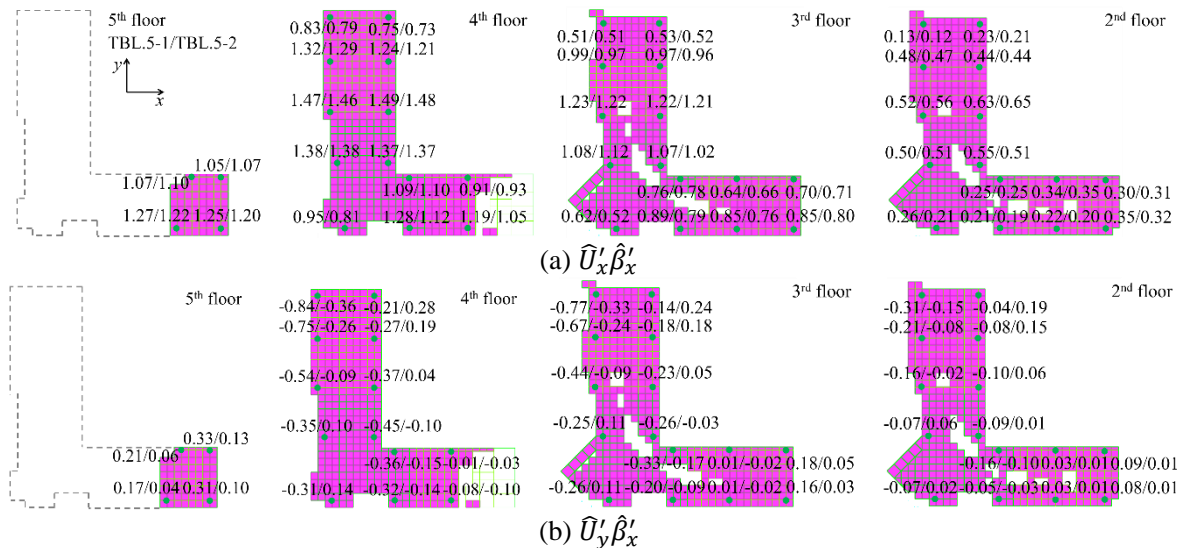


Figure 5-5 Sums of x -directional approximated participation functions under the 2D model

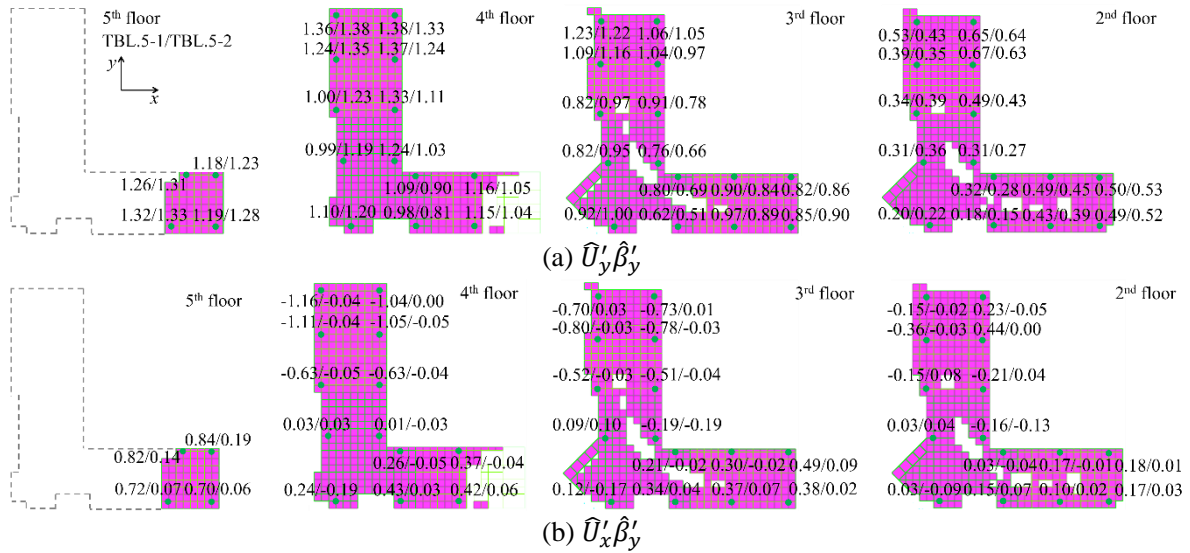


Figure 5-6 Sums of y-directional approximated participation functions under the 2D model

The sums of approximated participation functions in the same direction of the considered directional participation vector, i.e., $\hat{U}'_x \hat{\beta}'_x$ in Figure 5-5(a) and $\hat{U}'_y \hat{\beta}'_y$ in Figure 5-6(a), are similarly close to unity. However, the $\hat{U}'_y \hat{\beta}'_x$ in Figure 5-5(b) and $\hat{U}'_x \hat{\beta}'_y$ in Figure 5-6(b) are obviously different. The 2D model requires the $\hat{U}'_y \hat{\beta}'_x$ and $\hat{U}'_x \hat{\beta}'_y$ close to null while the values are farther from null when using the approximated participation vector from Table 5-1. As a result, the approximated participation vector in Table 5-1 is unlikely the optimal one under the 2D model and the participation vector approximation results are different.

Figure 5-7 compares the x- and y-directional MSEs under the 2D model when using the approximated participation vectors from Tables 5-1 and 5-2. The MSE corresponding to different number of utilized modes are shown in Figure 5-7. Since the 4th mode is not used in the x-directional approximation in Table 5-1, the MSEs only have three dots in Figure 5-7(a) when using the approximated participation vector from Table 5-1. The MSEs using approximated participation vector in Table 5-1 are larger than the MSEs using Table 5-2, which corresponds to the different approximation results between Tables 5-1 and 5-2. Figure 5-7(b) shows that the 4th mode obviously increases the MSE when using Table 5-1. The increased MSE corresponds to the fact that the differences in the y-directional approximation results between Tables 5-1 and 5-2 become larger after the 4th mode is added. The y-directional approximation results in Tables 5-1 and 5-2 are actually more similar before the 4th mode is added.

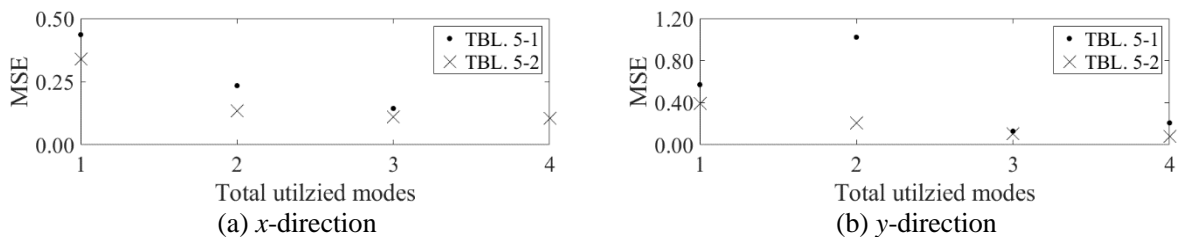


Figure 5-7 Comparison of MSEs under the 2D models

Figures 5-5 and 5-6 show that the sums of approximated participation functions are different on different floors in different areas. For example, the sums of approximated participation functions in P1 area are obviously farther from unity in Figures 5-5(a) and 5-6(a), which imply there are missing local modes with large mode shape amplitudes. Figures 5-5(a) and 5-6(a) also show that the sums on the 4th floor are closer to unity while the sums on the 2nd floor are farther, which implies the higher modes with large mode shape amplitudes on the 2nd floor are not considered.

Next, the participation vector approximation using fewer nodes are tested. Figure 5-8 selects fewer nodes for the participation factor approximation comparing to Figure 5-2. The selected nodes are still evenly distributed near the edges of each floor but the density of selected nodes is smaller comparing to Figure 5-2.

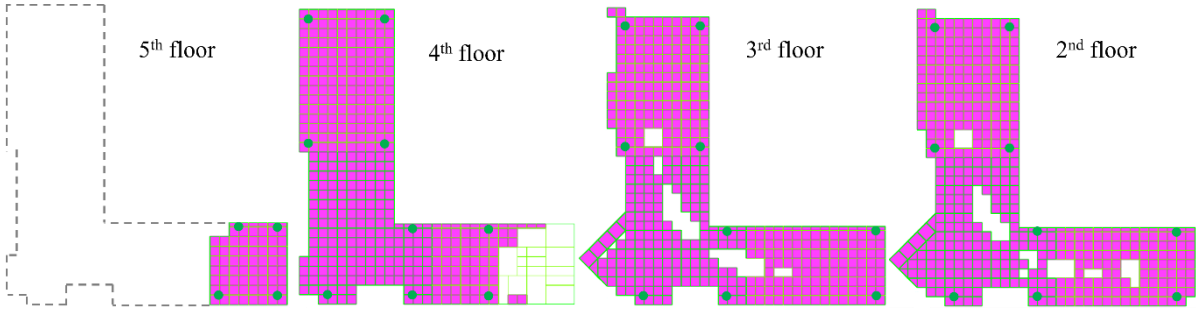


Figure 5-8 Participation vector approximation with fewer nodes

The participation vector approximation results using the fewer nodes are shown in Table 5-3. The accuracy is slightly reduced comparing to Table 5-2, the comparison shows the improved participation vector approximation accuracy by using more measurement points.

Table 5-3 Participation vector approximation with fewer nodes

Mode freq. (Hz)	x-direction					y-direction				
	Total number of utilized modes					Total number of utilized modes				
	1	2	3	4	True	1	2	3	4	True
2.25	-5.21	-5.37	-5.41	-5.38	-4.94	-4.34	-4.20	-4.29	-4.21	-4.28
2.39	-	5.76	5.92	5.72	5.56	-	-5.19	-4.86	-5.35	-5.27
2.49	-	-	-1.55	-1.60	-1.75	-	-	-3.12	-3.22	-3.64
2.85	-	-	-	0.72	1.06	-	-	-	1.79	1.73

Lastly, the participation vector approximation only using mode shapes on upper floors are tested. In Chapter 4, the approximated participation factor in the 1st mode has good accuracy when only using mode shapes at upper floors. Table 5-4 shows the approximation results with the selected nodes in Figure 5-2 under two cases: One uses mode shapes on the 3rd to 5th floors, the other uses mode shapes on the 4th and 5th floors.

Table 5-4 Participation vector approximation using mode shapes on upper floors

Mode freq. (Hz)	x-direction					y-direction				
	Total number of utilized modes					Total number of utilized modes				
	1	2	3	4	True	1	2	3	4	True
2.25	-4.72	-4.73	-4.75	-4.77	-4.94	-3.83	-3.82	-3.87	-3.91	-4.28
	-4.42	-4.31	-4.33	-4.34		-3.42	-3.51	-3.54	-3.57	
2.39	-	5.16	5.25	5.15	5.56	-	-4.83	-4.66	-4.84	-5.27
	-	4.75	4.84	4.69		-	-4.38	-4.18	-4.45	
2.49	-	-	-1.48	-1.52	-1.75	-	-	-3.05	-3.13	-3.64
	-	-	-1.31	-1.34		-	-	-2.74	-2.81	
2.85	-	-	-	0.83	1.06	-	-	-	1.57	1.73
	-	-	-	0.77		-	-	-	1.40	

Note: The upper lines for 3rd to 5th floors and the lower lines for 4th and 5th floors

Similar to the numerical simulation in Chapter 4, the approximation accuracy is lower when only using upper floors than using all floors. An explanation is that the utilized mode shapes are not strictly triangle-shaped in vertical as shown in Figure 5-3(b), the mode shapes on upper floors cannot perfectly capture the mode shapes on lower floors. Based on the participation vector approximation results in Tables 5-2 to 5-4, the approximated participation vector in Table 5-2 is utilized in the seismic response prediction when using the 2D model because of its highest accuracy.

5.5 Seismic Response Prediction

The seismic response prediction has two major purposes: the applicability of the proposed seismic response prediction method for buildings with flexible floors; and the necessity of the 2D model for the buildings with multiple lateral-torsional coupling modes. The seismic response prediction accuracies at the selected nodes in Figure 5-2 are investigated. The seismic response prediction accuracies using the 1D and 2D models are compared. The utilized participation vectors for the seismic response prediction are indicated in Table 5-1 for the 1D model and in Table 5-2 for the 2D model.

The 2D model utilizes the four modes introduced in Section 5.3 while the 4th mode (2.85 Hz mode) is removed in the x -direction when using the 1D model as discussed in Sub-section 5.4.1. The damping ratios are assumed frequency-proportional and the damping ratio in the 1st mode is set as 1%. The modal property variances are not considered in this simulation. The variances of modal parameters appear in modal parameter identification itself and the response amplitude difference between microtremor and an earthquake. The simulation assumes an observation system is installed at the objective building so that the natural frequencies and damping ratios are updated. The building remains linearly elastic because the purpose of the prediction method is to provide seismic response estimation when the building has no obvious structural damage, it is also the reason that the mode shapes are assumed unchanged.

The El Centro, Taft, Hachinohe and JMA Kobe waves are utilized as the input ground motions. The NS and EW components are used as the x - and y -directional input ground motions, respectively. The x - and y -directional acceleration amplitudes are scaled down by setting the peak ground velocity as 0.25 m/s in both directions. The corresponding x -directional peak accelerations of the four ground motions are 2.55, 2.43, 1.67 and 2.12 m/s², respectively, the corresponding y -directional peak accelerations are 1.42, 2.48, 1.19 and

1.92 m/s², respectively. The response spectra of the four ground motions with a damping ratio of 1% are shown in Figure 5-9.

Two cases are considered: One assumes the ground motion is single-directional, only the corresponding directional seismic responses are evaluated and the corresponding prediction accuracies when using the 1D and 2D models are compared. This case investigates the influence of the participation vector approximation errors on the seismic response prediction accuracy; The other case considers the two-directional ground motions to explore the necessity of considering vibrations induced by orthogonal ground motions.

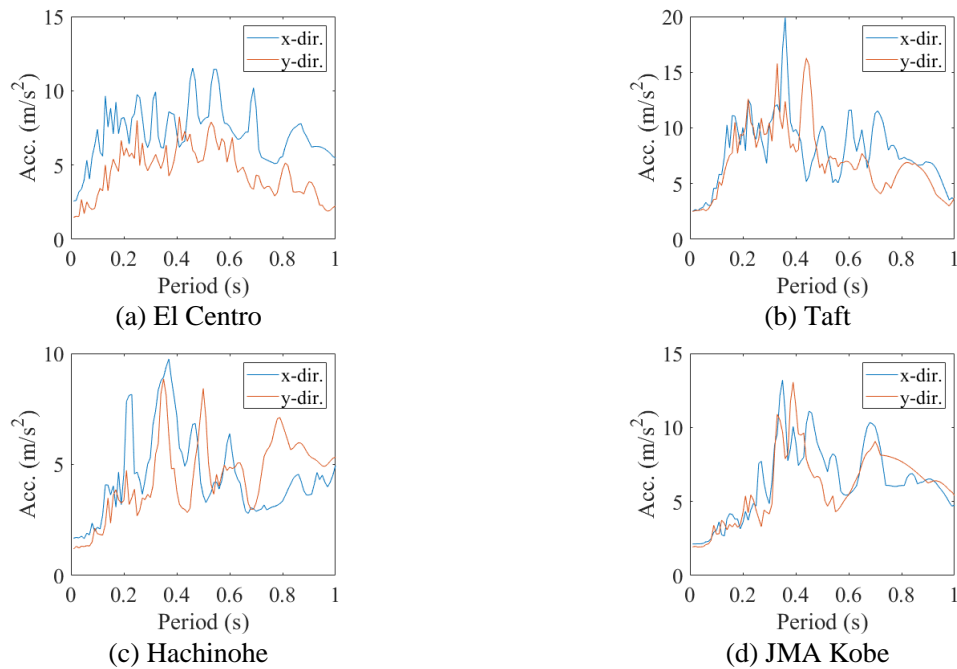


Figure 5-9 Response spectra of input accelerations with 1% damping ratio

5.5.1 Single-directional ground motion

In this section, the ground motion is single-directional and only the same directional responses are evaluated. The single-directional ground motion simulation aims to exhibit the influence of participation vector approximation errors on the seismic response prediction accuracy. The 1D model cannot consider the orthogonal vibrations induced by single-directional ground motions so this section only considers the vibrations in the same direction of the input ground motion. Figure 5-10 shows the peaks of the seismic response absolute accelerations at the selected nodes. The x -directional amplitudes mean the amplitudes caused by the x -directional ground motion, they are not the x -directional amplitudes from the y -directional ground motion. The acceleration amplitudes in P1 and P3 areas are large than the amplitudes in P2 area under the four ground motions. Specifically, the x -directional amplitudes in P1 area and the y -directional amplitudes in P3 areas are obviously large, which implies the lateral-torsional coupling of the modes in the model.

The predicted responses are compared to the true responses. The predicted acceleration amplitude errors at the selected nodes when using the 1D and 2D models are shown in Figures 5-11 and 5-12, respectively.

The negative value means the prediction underestimates the response and positive value means overestimating. Tables 5-5 and 5-6 summarize the averaged errors and the peak errors on each floor in the seismic response amplitude prediction when using the 1D and 2D models, respectively.

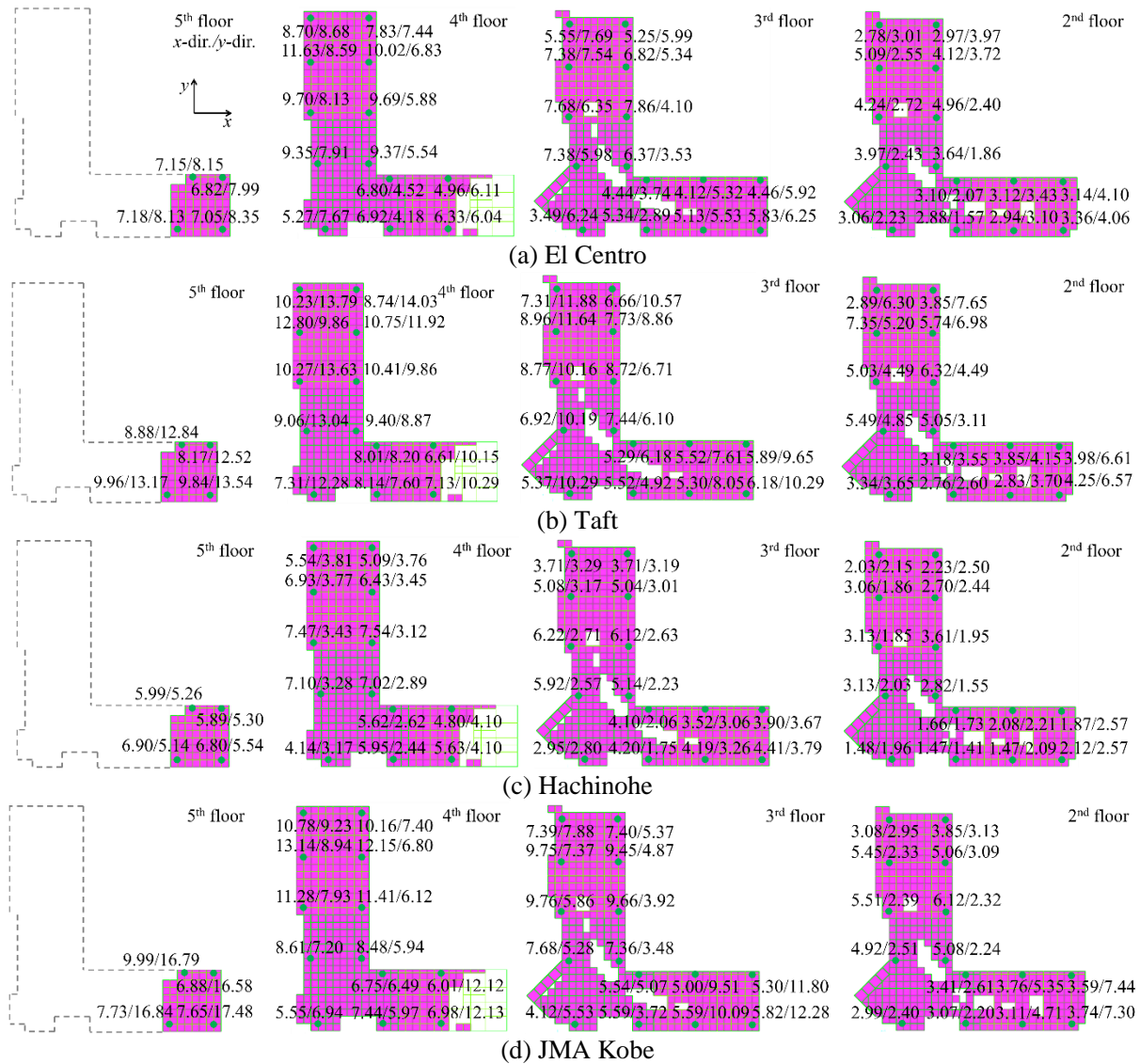


Figure 5-10 Peak acceleration distributions under single-directional ground motions (Unit: m/s^2)

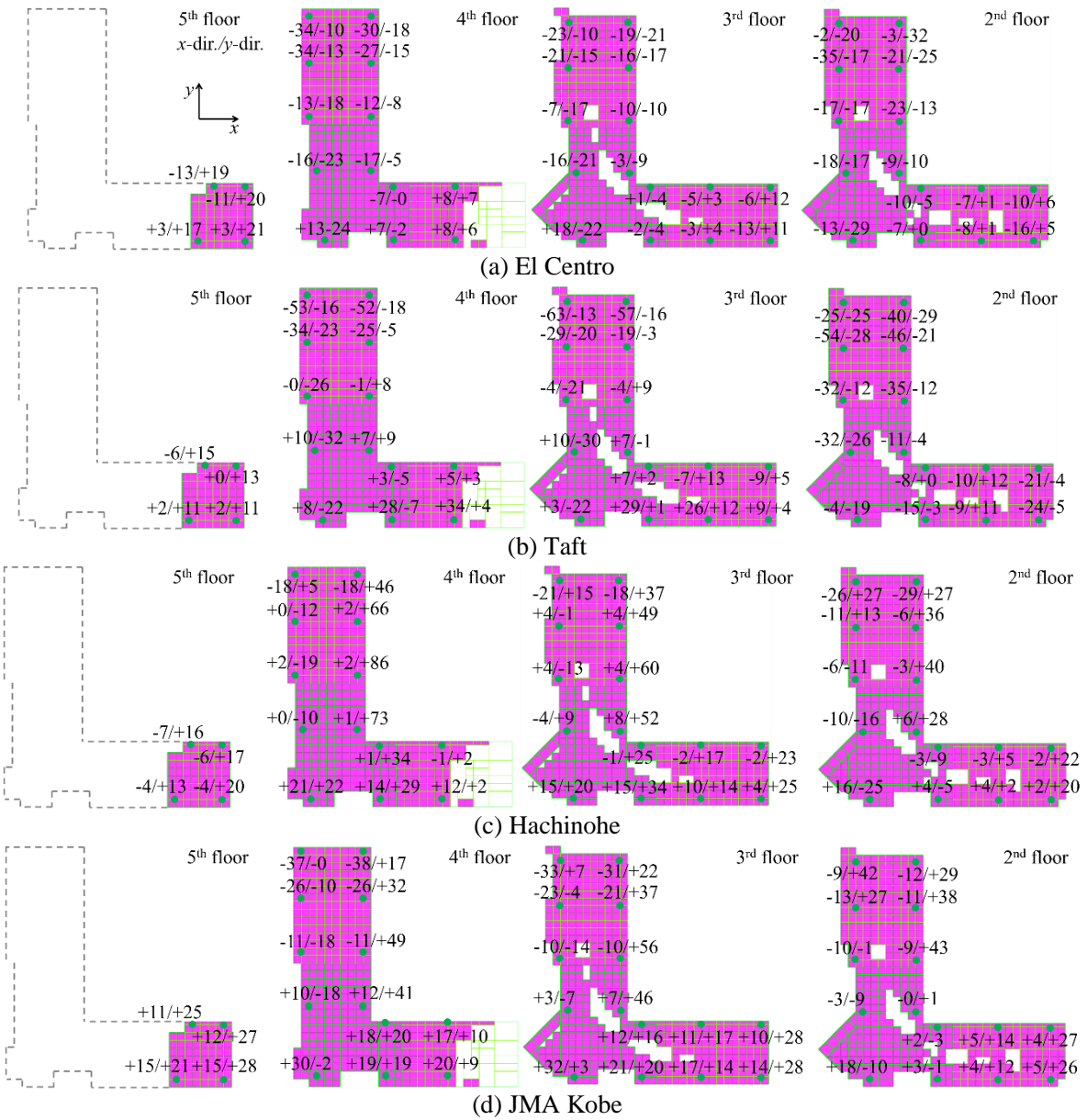


Figure 5-11 Errors of peak response accelerations using the 1D model under single-directional ground motions (Unit: %)

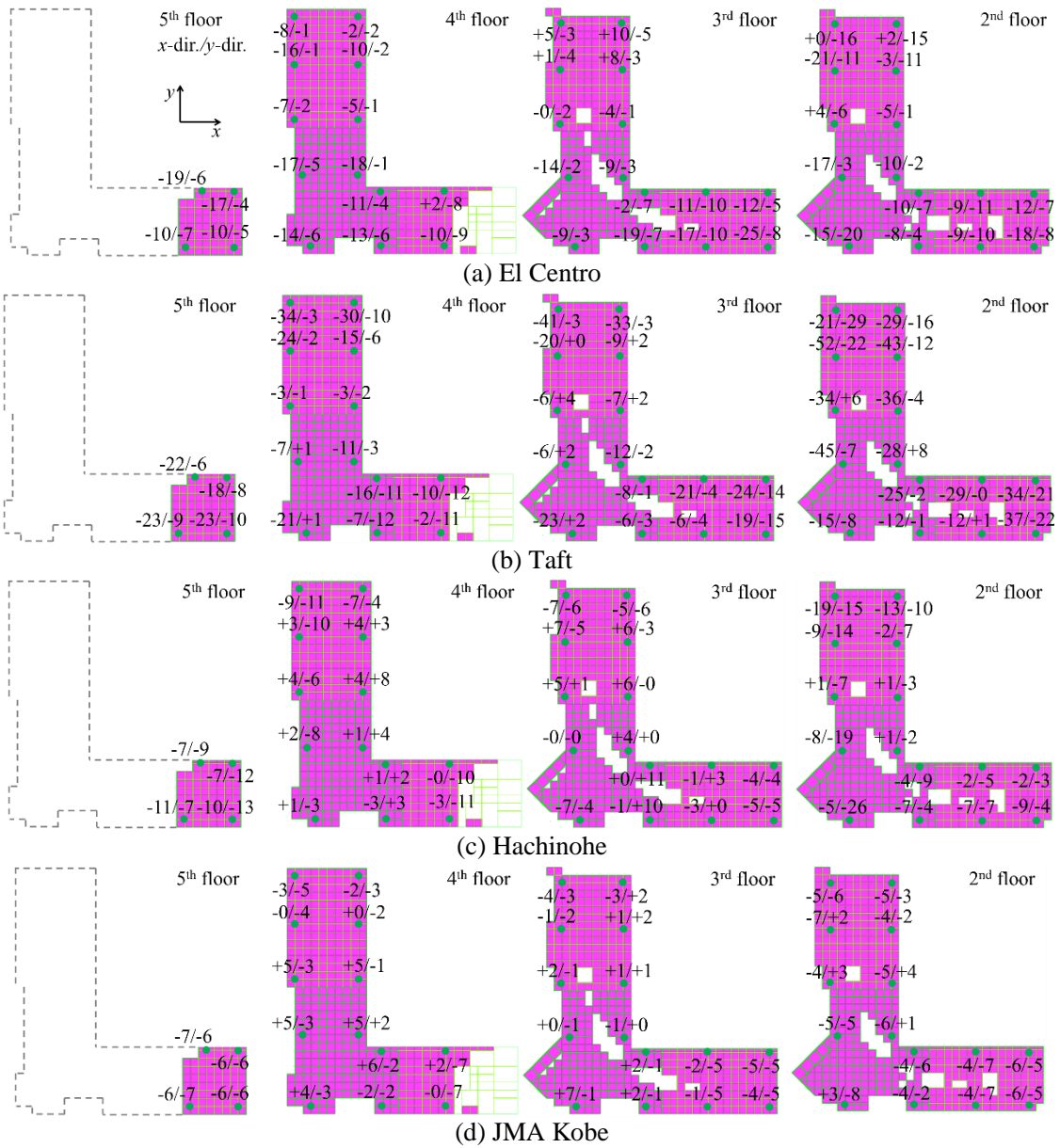


Figure 5-12 Errors of peak response accelerations using the 2D model under single-directional ground motions (Unit: %)

Table 5-5 Averaged/Peak prediction errors using the 1D model under single-directional ground motions

(Unit: %)

First value: Average, Second value in parenthesis: Peak

Fl.	x-direction				y-direction				
	El Centro	Taft	Hachinohe	JMA Kobe	El Centro	Taft	Hachinohe	JMA Kobe	
Acc.	5	-5(-13)	-0(-6)	-5(-7)	+13(+15)	+19(+21)	+12(+15)	+16(+20)	+25(+28)
	4	-12(-34)	-5(-53)	+1(+21)	-2(-38)	-9(-24)	-10(-32)	+25(+86)	+11(+49)
	3	-8(-23)	-7(-63)	+1(-21)	-0(-33)	-8(-22)	-5(-30)	+24(+60)	+7(+26)
	2	-13(-35)	-24(-54)	-5(-29)	-2(+18)	-11(-32)	-11(-29)	+10(+40)	+16(+43)
Vel.	5	-3(-13)	+14(+22)	+1(+5)	+19(+23)	+19(+20)	+14(+16)	+19(+22)	+23(+26)
	4	-3(-23)	+2(-40)	-1(-21)	-4(-36)	-11(-24)	-11(-34)	+25(+81)	+5(+28)
	3	-6(-32)	+4(-38)	+1(-23)	-1(-36)	-5(+25)	-10(-37)	+22(+75)	+18(+56)
	2	-14(-44)	+1(-34)	+1(+20)	-3(-33)	-8(-32)	-10(-39)	+21(+67)	+11(+36)
Disp.	5	+15(+17)	+24(+26)	+3(+6)	+17(+20)	+17(+19)	+16(+16)	+11(+12)	+23(+25)
	4	-1(+39)	+8(+35)	+4(+24)	+1(-31)	-10(-24)	-12(-34)	+14(+58)	+2(+23)
	3	+4(+37)	+11(+37)	+3(+18)	+1(-32)	-7(-23)	-9(-35)	+11(+48)	+5(+24)
	2	+1(+31)	+9(+37)	+3(+16)	-3(-30)	-7(-24)	-8(-38)	+12(+40)	+10(+35)

Table 5-6 Averaged/Peak prediction errors using the 2D model under single-directional ground motions

(Unit: %)

First value: Average, Second value in parenthesis: Peak

Fl.	x-direction				y-direction				
	El Centro	Taft	Hachinohe	JMA Kobe	El Centro	Taft	Hachinohe	JMA Kobe	
Acc.	5	-14(-19)	-21(-23)	-9(-11)	-6(-7)	-5(-7)	-8(-10)	-11(-13)	-6(-7)
	4	-10(-18)	-14(-34)	-0(-9)	+2(+6)	-4(-9)	-6(-12)	-3(-11)	-3(-7)
	3	-7(-25)	-16(-41)	-0(-7)	-0(+7)	-5(-10)	-2(-15)	-1(+11)	-2(-5)
	2	-9(-21)	-30(-52)	-6(-19)	-4(-7)	-9(-20)	-9(-29)	-9(-26)	+1(+6)
Vel.	5	-10(-16)	-9(-13)	-2(-2)	-2(-3)	-7(-8)	-6(-7)	-7(-10)	-6(-7)
	4	+0(-13)	-6(-18)	+0(-5)	+0(+3)	-3(-7)	+1(-6)	+1(+30)	-2(-4)
	3	-5(-19)	-5(-11)	+1(-4)	+1(+7)	-2(-5)	-2(-6)	-1(-8)	-2(-5)
	2	-13(-30)	-8(-23)	+0(-6)	+0(-10)	-6(-15)	-5(-12)	-7(-17)	+0(+9)
Disp.	5	+2(+4)	-6(-8)	-4(-5)	-2(-3)	-1(-2)	-4(-5)	-6(-7)	-5(-5)
	4	+2(+7)	-1(-8)	+2(+6)	+3(+7)	-2(-5)	+0(-3)	+1(+7)	-2(-5)
	3	+5(+12)	-1(-6)	+1(+6)	+1(+4)	-2(-6)	-0(-6)	-1(-7)	-2(-5)
	2	+3(+14)	-3(-12)	+1(+6)	-3(-10)	-3(-9)	-1(-7)	-5(-14)	-3(-8)

The comparisons of Figure 5-11 to Figure 5-12 and Table 5-5 to Table 5-6 show the influence of the participation vector approximation errors on the seismic response prediction accuracy. The 1D model has the less accurate approximated participation vector in the two directions and the prediction accuracies are indeed lower than using the 2D model. For example, the 1st and 2nd modes have large mode shape amplitudes in P1 area, the large participation factor approximation errors in the 1st and 2nd modes in Table 5-1 lead to the large prediction errors in P1 area in Figure 5-11. Although the y-directional participation vector approximation errors are larger than the x-directional errors in the 1D model, the y-directional prediction accuracies are not similarly lower than the x-directional accuracies. The y-directional prediction accuracies are actually slightly better than x-directional accuracies under the El Centro and Taft waves. It might be because the 4th mode is neglected in the x-directional prediction.

As discussed in Sub-section 5.4.2, there might exist missing local modes with large x -directional mode shape amplitudes in the P1 area. It is because the sums of approximated participation functions in this area are obviously farther from unity in Figure 5-5(a). Those missing modes are likely excited under the Taft wave while they are less excited under the other three waves. As a result, the x -directional prediction accuracies in P1 area is low in Figure 5-12(b) but the prediction accuracies are higher under the other three ground motions. The relatively larger prediction errors on the 2nd floor comparing to other floors are likely caused by the neglecting of higher modes with large mode shape amplitudes on the 2nd floor. Figure 5-12 also shows that the large errors generally occur in P1 and P3 areas under the four ground motions. It is because the mode shape amplitudes in the two areas are larger than P2 area and the large amplitudes magnify the mis-estimated modal responses.

The largest seismic response amplitudes on the 4th floor under the four ground motions are summarized in Table 5-7, and the prediction errors when using the 2D model are attached. Although the y -directional seismic responses on the 5th floor are the largest as shown in Figure 5-10, the 5th floor is local so it is less representative than the 4th floor. The locations of the largest acceleration, velocity and displacement amplitudes are generally in P1 and P3 areas because the influence of the lateral-torsional coupling is stronger in the two areas.

Figures 5-13 to 5-20 show the predicted time history at the locations where they have the largest amplitudes on the 4th floor, the corresponding locations names are listed in Table 5-7. The figures demonstrate the effectiveness of the proposed seismic response prediction method and the influence of participation vector errors on the response prediction. The predicted responses are similar to the true responses from the time history viewpoint even if using the 1D model that has low participation vector approximation accuracy. An explanation is that the natural frequency and damping ratio variances are not considered and the selected four modes are likely the dominating modes to the seismic responses. The influence of the participation vector approximation errors is mainly reflected by the response amplitudes. However, a mode with large participation factor approximation error is not necessarily excited by a particular earthquake and causes large response prediction error. For example, the y -directional prediction accuracy using the 1D model is similar to the result using the 2D model in Figure 5-20 even though the former one has large the approximated participation factors variances.

Table 5-7 Largest response amplitudes in the x - and y -directions on the 4th floor

Response	El Centro			Taft			Hachinohe			JMA Kobe		
	Amp.	Err.	Loc.	Amp.	Err.	Loc.	Amp.	Err.	Loc.	Amp.	Err.	Loc.
Acc. (m/s ²)	11.63	-16	4b	12.80	-24	4b	7.54	+4	4m	13.14	-1	4b
	8.68	-1	4a	14.03	-10	4o	4.10	-11	4g	12.13	-7	4g
Vel. (×10 ⁻¹ m/s)	6.41	+4	4b	6.83	-2	4m	4.95	+3	4m	8.96	+1	4b
	5.77	-2	4b	9.26	+4	4b	2.08	+0	4a	7.46	-4	4g
Disp. (×10 ⁻² m)	4.83	+3	4b	4.55	-0	4m	3.64	+6	4m	6.02	+4	4b
	3.95	-1	4b	6.49	+2	4b	1.72	+1	4b	4.94	-5	4g

Note: the upper lines for x -direction and lower lines for y -direction

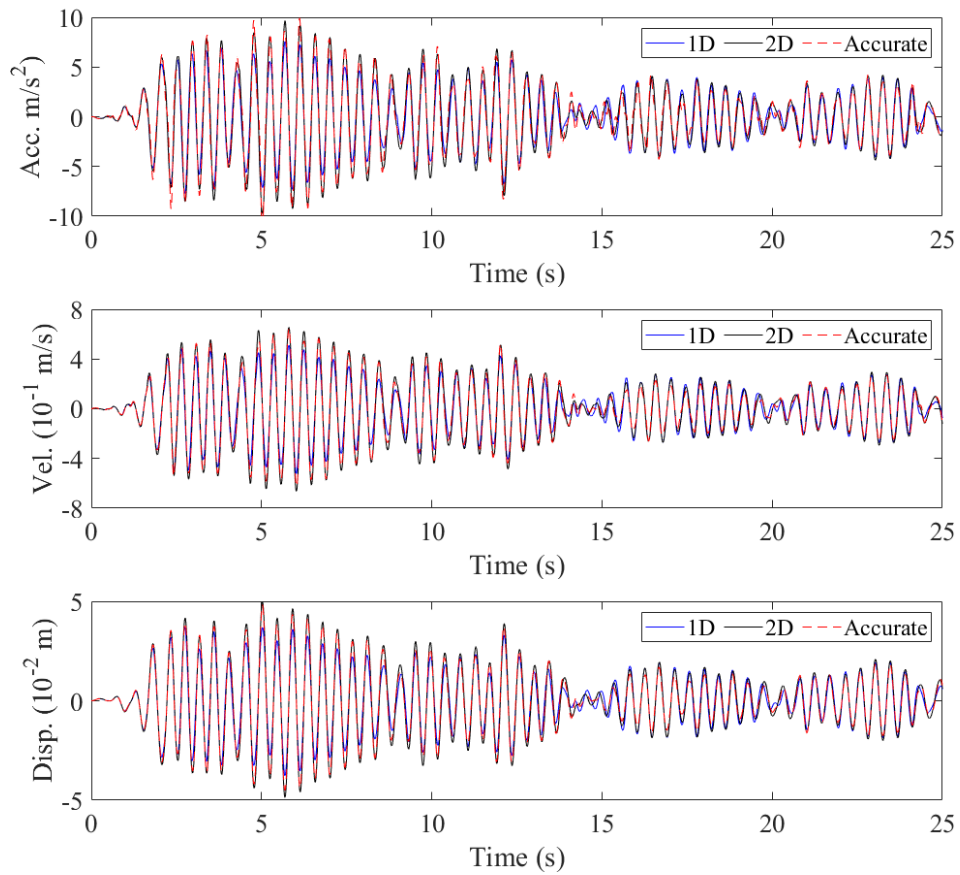


Figure 5-13 Largest x -directional responses on the 4th floor under the x -directional El Centro wave

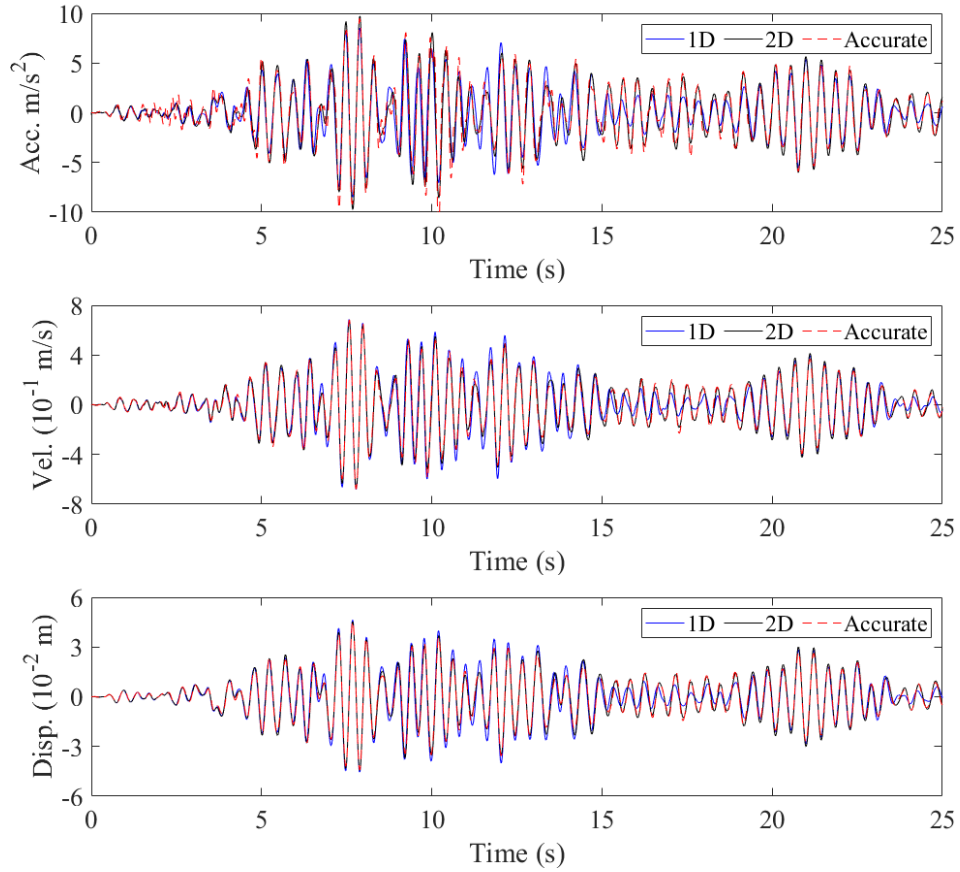


Figure 5-14 Largest x -directional responses on the 4th floor under the x -directional Taft wave

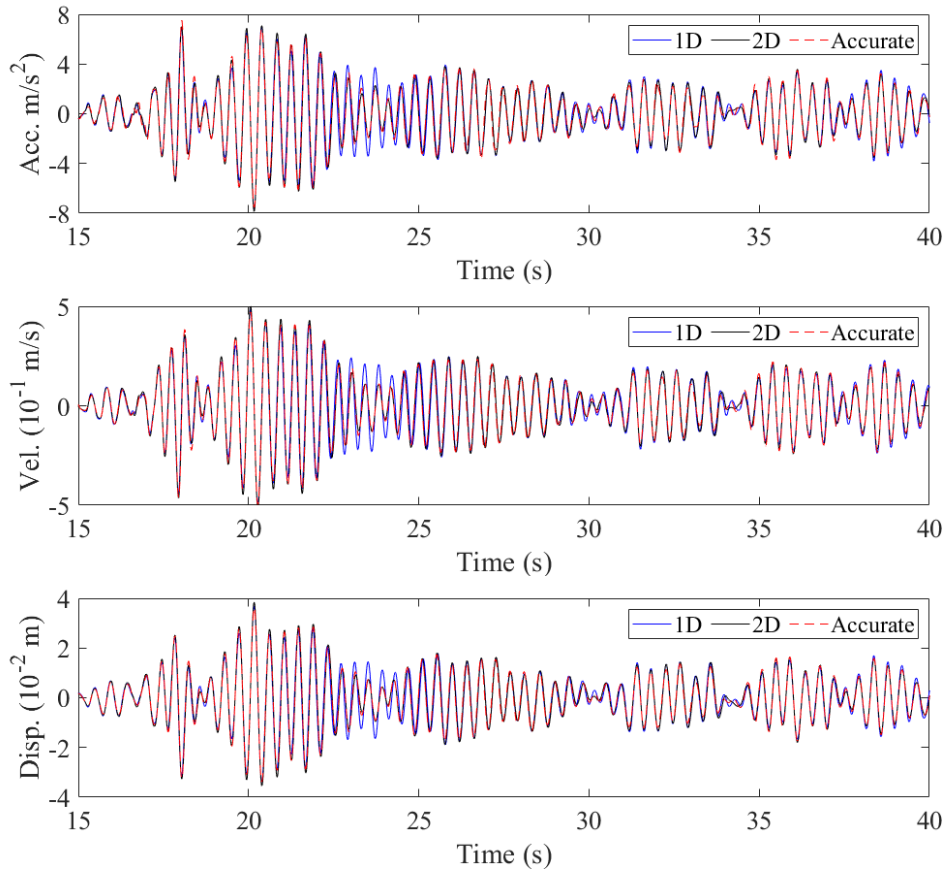


Figure 5-15 Largest x -directional responses on the 4th floor under the x -directional Hachinohe wave

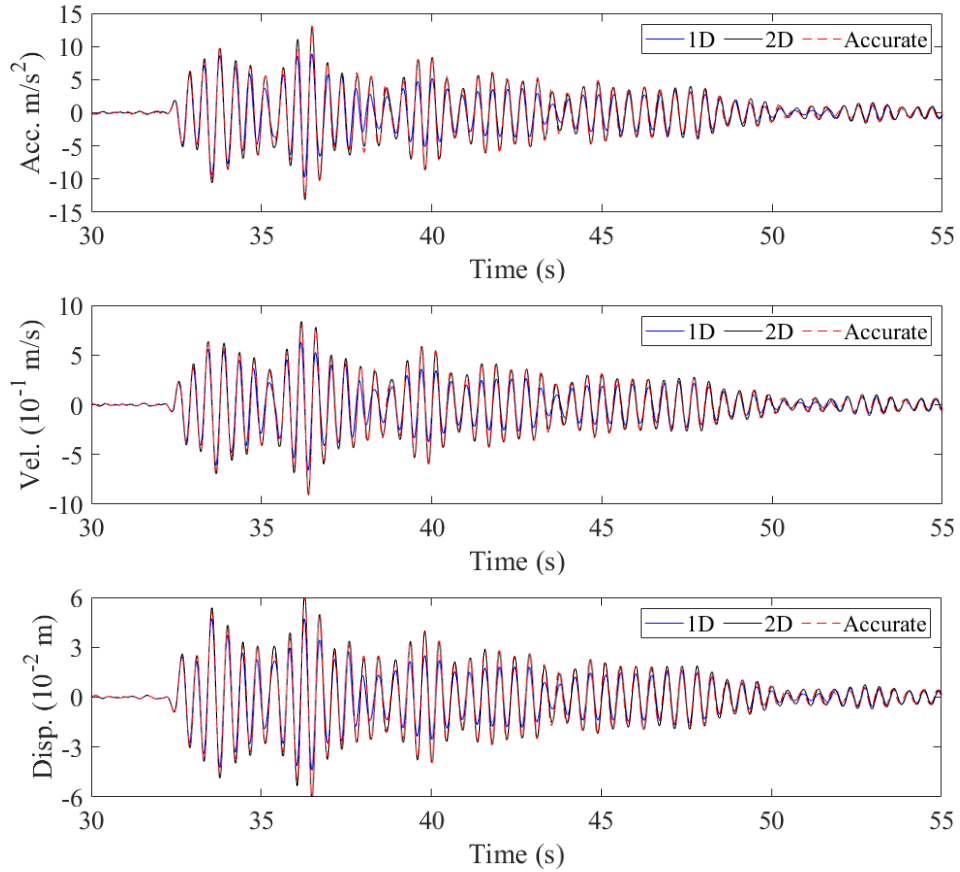


Figure 5-16 Largest x -directional responses on the 4th floor under the x -directional JMA Kobe wave

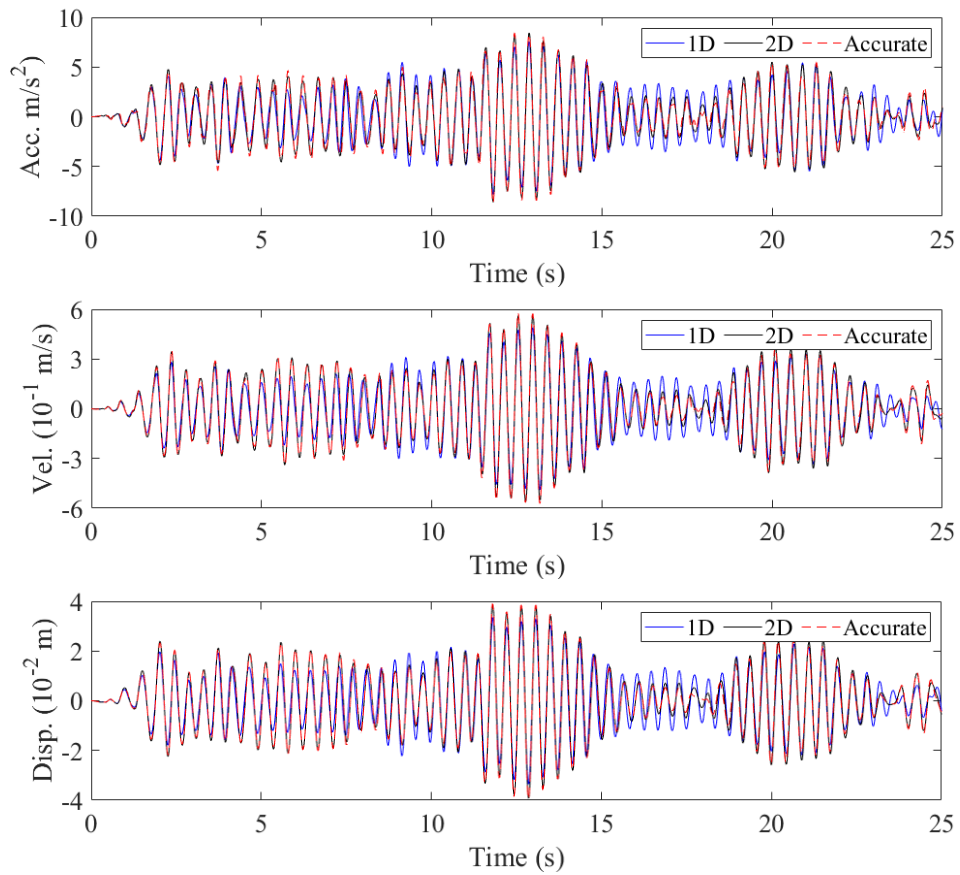


Figure 5-17 Largest y-directional responses on the 4th floor under the y-directional El Centro wave

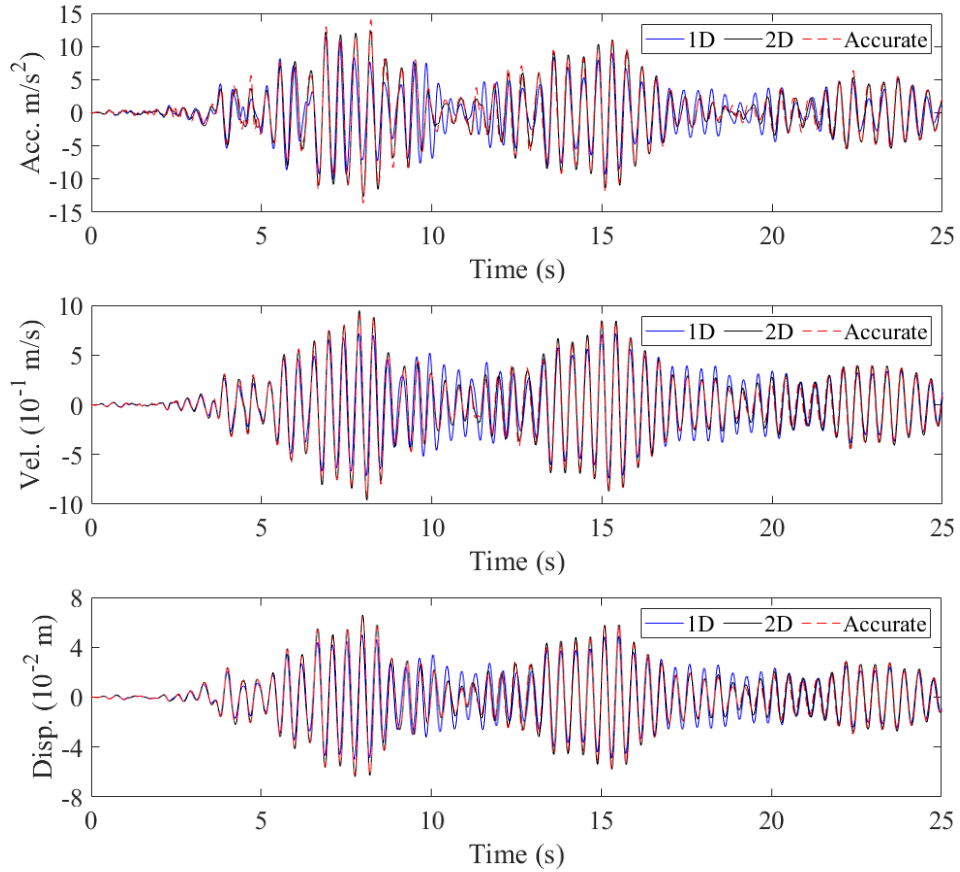


Figure 5-18 Largest y-directional responses on the 4th floor under the y-directional Taft wave

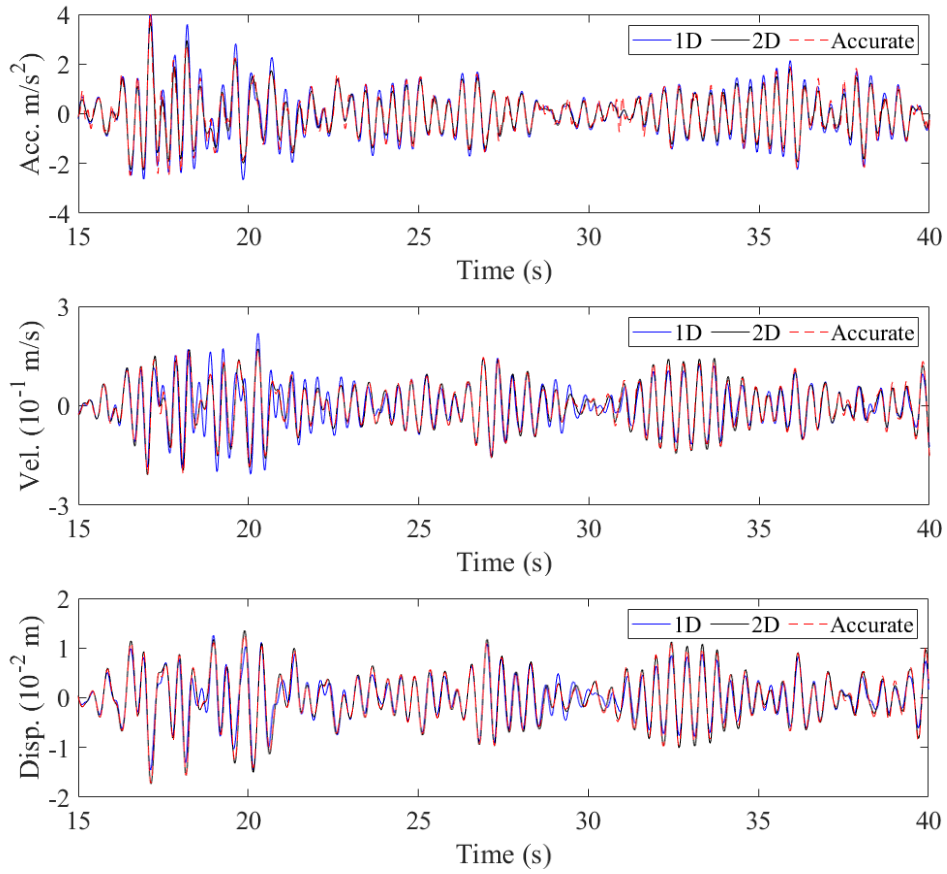


Figure 5-19 Largest y-directional responses on the 4th floor under the y-directional Hachinohe wave

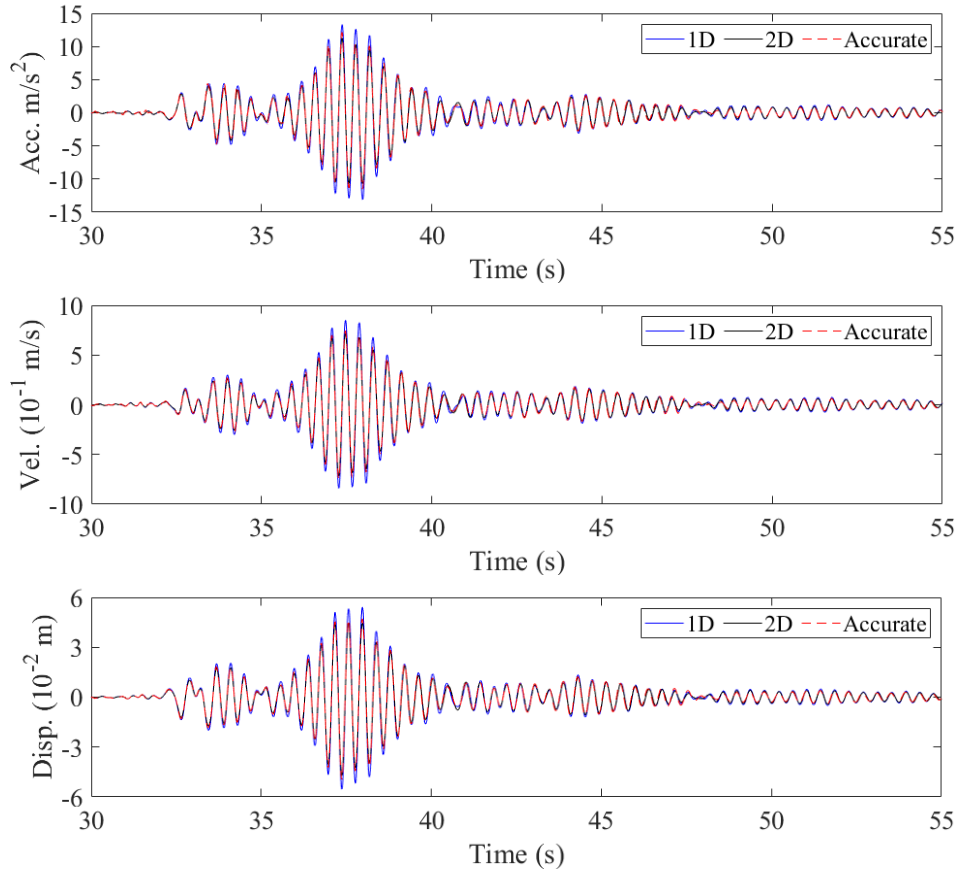


Figure 5-20 Largest y-directional responses on the 4th floor under the y-directional JMA Kobe wave

5.5.2 Two-directional ground motion

The single-directional ground motion simulation is mainly used to explore the influence of the participation vector approximation errors on the seismic response prediction accuracy. In this section, the applicability of the proposed seismic response prediction method is further tested by the two-directional ground motions. The simulation compares the prediction accuracies when using the 1D and 2D models to discuss the necessity of considering vibrations induced by orthogonal ground motions. The four ground motions in Sub-section 5.5.1 are utilized, the NS and EW components are simultaneously applied to the numerical model as the x - and y -directional input ground motions, respectively.

The peaks of absolute accelerations at the selected nodes are shown in Figure 5-21. The increased amplitudes under the two-directional ground motion comparing to Figure 5-10 shows that the vibrations in one direction is increased by the ground motion in the orthogonal direction. The increased response amplitudes are particularly obvious under the Taft wave in Figure 5-21(b) comparing to Figure 5-10(b). The predicted amplitudes using the 1D model are the same when the input ground motions are changed from single-directional to two-directional. Therefore, the increased response amplitudes imply the increased prediction errors when using the 1D model.

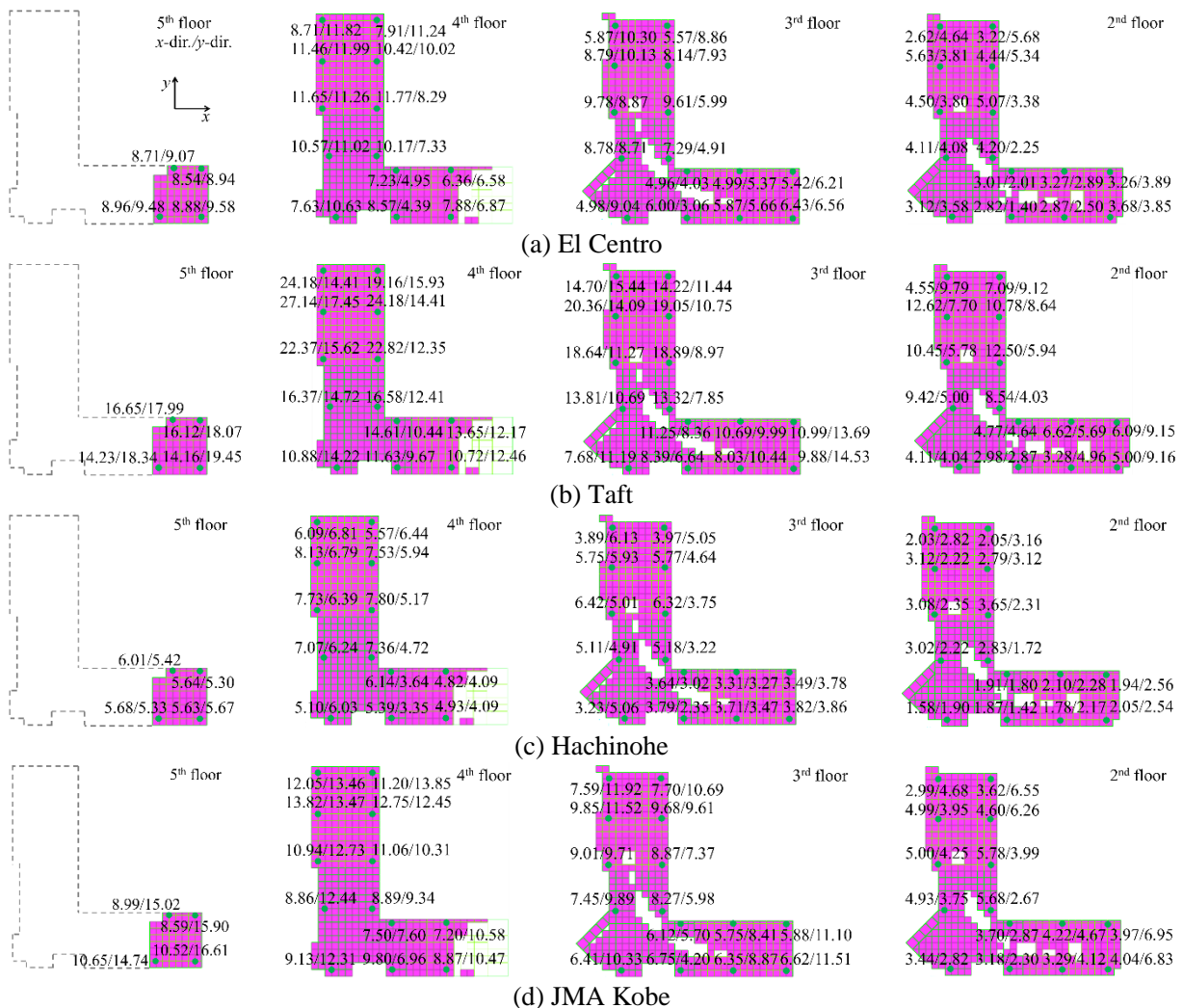


Figure 5-21 Peak acceleration distributions under two-directional ground motions (Unit: m/s^2)

The prediction errors when using the 1D and 2D models are in Figures 5-22 and 5-23, respectively. Tables 5-8 and 5-9 summarize the averaged errors and the peak errors on each floor in the seismic response amplitude prediction when using the 1D and 2D models, respectively.

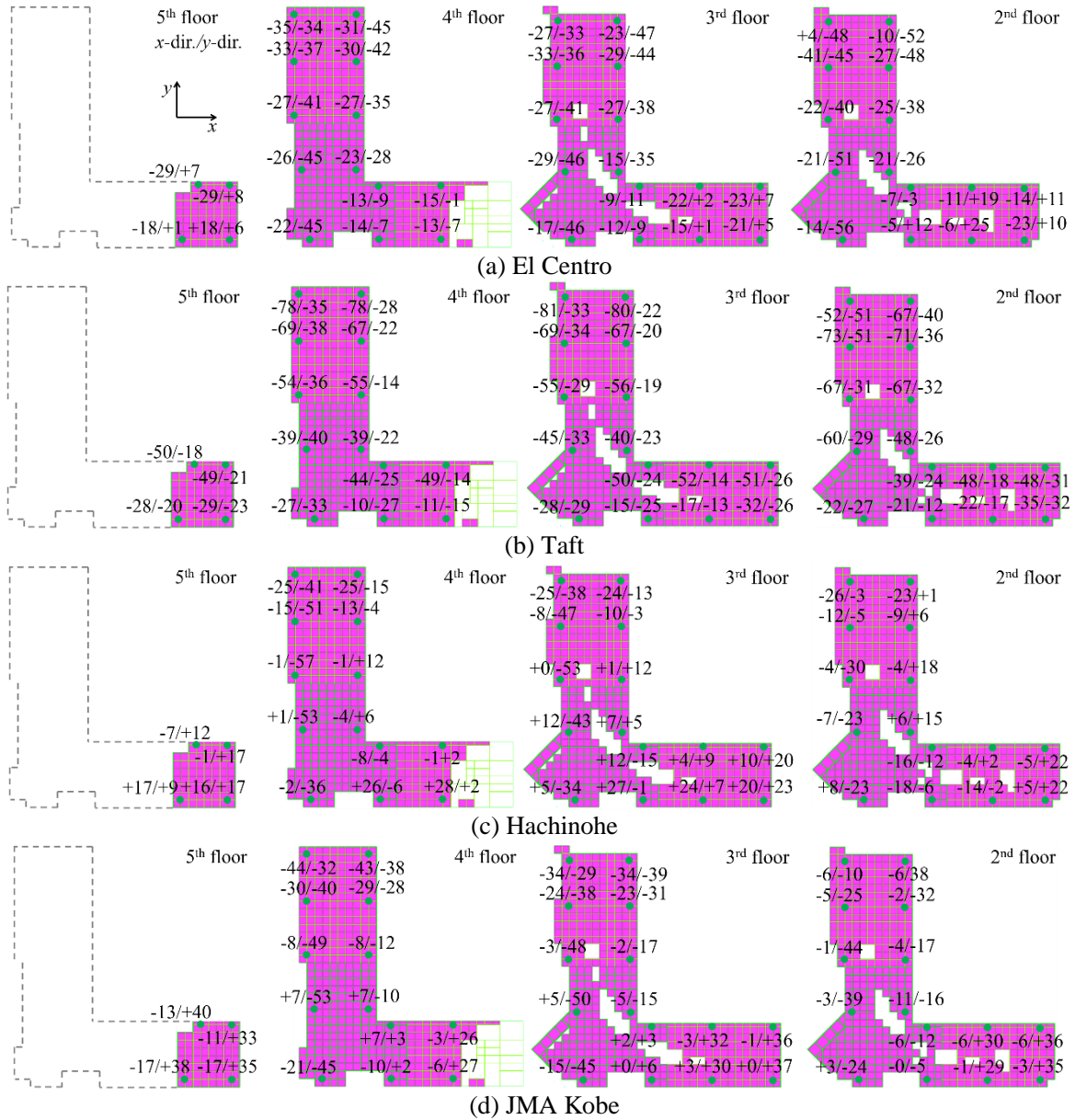


Figure 5-22 Errors of peak response accelerations using the 1D model under two-directional ground motions (Unit: %)

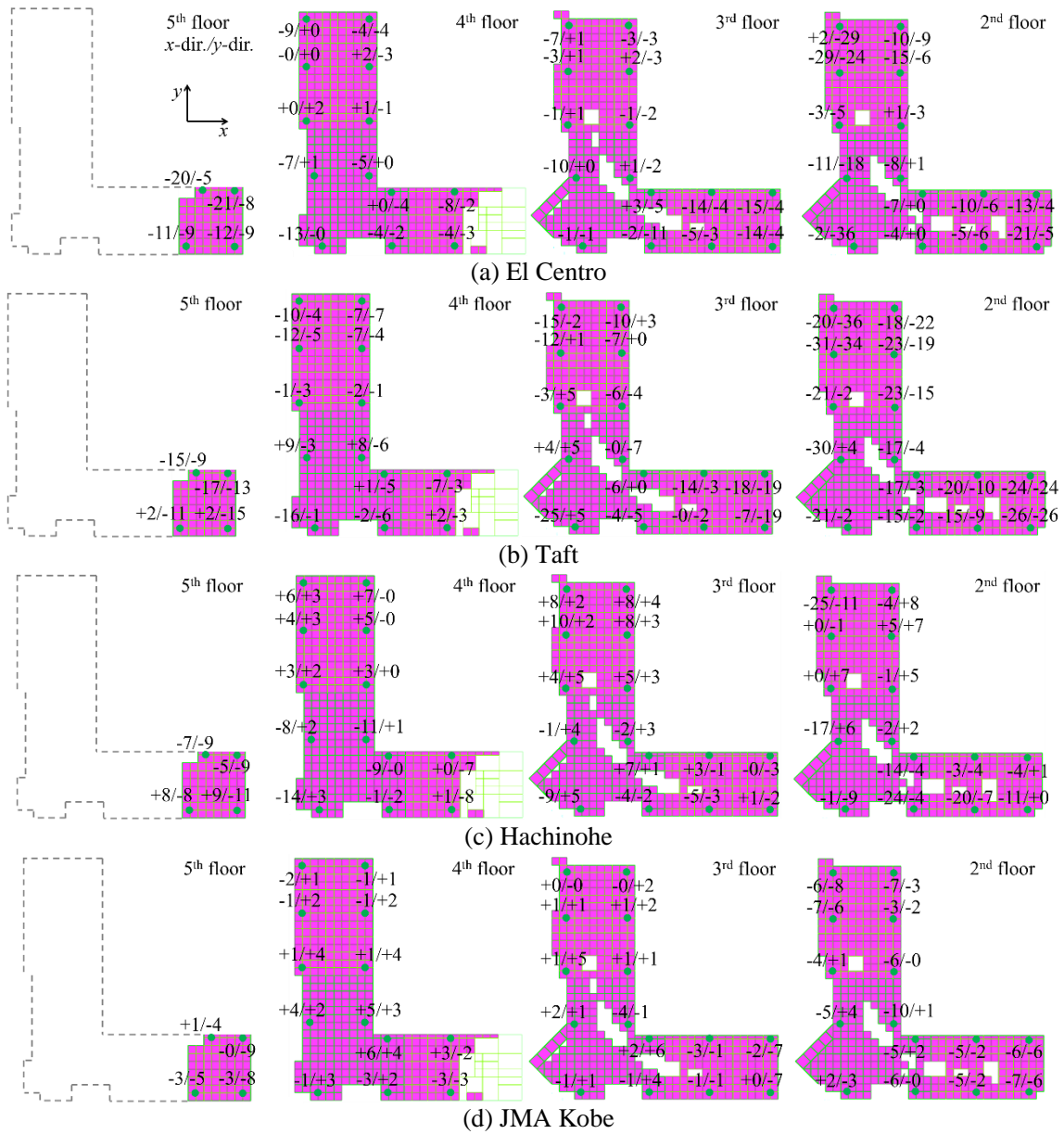


Figure 5-23 Errors of peak response accelerations using the 2D model under two-directional ground motions (Unit: %)

Table 5-8 Averaged/Peak prediction errors using the 1D model under two-directional ground motions

(Unit: %)

First value: Average, Second value in parenthesis: Peak

Fl.	x-direction				y-direction				
	El Centro	Taft	Hachinohe	JMA Kobe	El Centro	Taft	Hachinohe	JMA Kobe	
Acc.	5	-23(-29)	-39(-50)	+6(+17)	-14(-17)	+5(+8)	-21(-23)	+14(+17)	+36(+40)
	4	-24(-35)	-48(-78)	-3(+28)	-14(-44)	-29(-45)	-27(-40)	-19(-57)	-19(-53)
	3	-22(-33)	-49(-81)	+4(+27)	-9(-34)	-25(-47)	-25(-34)	-11(-53)	-11(-50)
	2	-16(-41)	-49(-73)	-8(-26)	-4(-11)	-22(-56)	-30(-51)	-1(-30)	-9(-44)
Vel.	5	-19(-20)	-37(-48)	+15(+21)	-18(-19)	+10(+11)	-17(-20)	+17(+21)	+35(+38)
	4	-23(-32)	-45(-75)	+1(+30)	-17(-41)	-33(-48)	-24(-35)	-27(-64)	-24(-55)
	3	-22(-30)	-42(-76)	+4(+30)	-17(-41)	-27(-49)	-25(-39)	-23(-63)	-16(-54)
	2	-26(-38)	-41(-71)	+5(+33)	-18(-38)	-28(-52)	-27(-42)	-20(-62)	-13(-55)
Disp.	5	-9(-13)	-31(-41)	+18(+24)	+1(+4)	+6(+9)	-14(-15)	+9(+12)	+35(+36)
	4	-18(-26)	-44(-73)	+6(+27)	-8(-36)	-30(-47)	-26(-37)	-28(-59)	-26(-56)
	3	-17(-27)	-43(-75)	+8(+26)	-7(-36)	-25(-48)	-25(-38)	-24(-57)	-18(-56)
	2	-19(-28)	-44(-71)	+8(+34)	-9(-32)	-25(-50)	-26(-40)	-22(-57)	-16(-56)

Table 5-9 Averaged/Peak prediction errors using the 2D model under two-directional ground motions

(Unit: %)

First value: Average, Second value in parenthesis: Peak

Fl.	x-direction				y-direction				
	El Centro	Taft	Hachinohe	JMA Kobe	El Centro	Taft	Hachinohe	JMA Kobe	
Acc.	5	-16(-21)	-7(-17)	+1(+9)	-1(-3)	-8(-9)	-12(-15)	-9(-11)	-7(-9)
	4	-4(-13)	-3(-16)	-1(-14)	+1(+6)	-1(-4)	-4(-7)	-0(-8)	+2(+4)
	3	-5(-15)	-8(-25)	+2(+10)	-0(-4)	-3(-11)	-3(-19)	+1(+5)	+0(-7)
	2	-9(-29)	-21(-31)	-8(-25)	-5(-10)	-10(-36)	-14(-36)	-0(-11)	-2(-8)
Vel.	5	-4(-5)	-11(-18)	+7(+9)	-1(-2)	-2(-4)	-8(-11)	-5(-7)	-7(-8)
	4	+3(+5)	-2(-8)	+1(+6)	+0(+2)	-1(-7)	+1(+7)	+0(-6)	+2(+5)
	3	+3(+9)	+0(-10)	+3(+8)	+0(+8)	-0(-6)	-1(-8)	-1(-11)	+1(-7)
	2	-2(-7)	+0(+11)	+3(+11)	-0(-5)	-3(-8)	-5(-14)	-2(-11)	+1(-7)
Disp.	5	-4(-7)	+1(+8)	+6(+7)	-1(-1)	-3(-4)	-5(-7)	-4(-4)	-5(-6)
	4	+3(+7)	+1(+6)	+3(+7)	+2(+7)	+2(+4)	+1(+3)	+2(-6)	+3(+5)
	3	+2(+6)	+0(+6)	+4(+7)	+1(+6)	+1(+3)	+1(-8)	+1(-6)	+2(-6)
	2	+2(+7)	-3(-9)	+4(+10)	-2(-8)	+0(+4)	-0(-10)	-1(-8)	+2(+7)

Figure 5-22 and Table 5-8 show the increased prediction errors comparing to the single-directional ground motion simulations when using the 1D model, especially under the Taft wave. The x -directional response amplitudes are not significantly increased under the Hachinohe and JMA Kobe waves in Figure 5-21 comparing to Figure 5-10. As a result, the prediction accuracies under the two waves are not largely decreased in Figure 5-22 comparing to Figure 5-11.

The seismic response prediction errors when using the 1D model are caused by the complicated interaction among three factors: The participation factor approximation errors; The mode truncation errors in the mode superposition; The neglecting of vibrations induced by orthogonal ground motions. Due to the complicated interaction among the three factors, the prediction errors at some locations might be smaller under a two-directional ground motion. For example, the x -directional prediction errors on the 2nd floor

under the JMA Kobe wave are slightly decreased under the two-directional ground motion in Figure 5-22 comparing to Figure 5-11.

Comparing to the 1D model, the prediction errors are similar under the two-directional ground motion when using the 2D model. Similar to Figure 5-12, large errors are also found in P1 area in Figure 5-23. The large errors in P1 area is likely caused by the neglecting of local modes with large mode shape amplitudes in this area. Nonetheless, the overall errors are under 20% in Figure 5-23 and Table 5-9, the low errors show the applicability of the prediction method. The *x*-directional prediction accuracies are actually improved comparing to the single-directional ground motions. It is because the *x*-directional responses induced by the *y*-directional ground motions are predicted well so that the overall *x*-directional prediction accuracy is improved.

The largest seismic response amplitudes on the 4th floor under the four ground motions are shown in Table 5-10 with their location names. The corresponding prediction errors when using the 2D model are attached. Then Figures 5-24 to 5-31 show the predicted time history at the locations where they have the largest amplitudes on the 4th floor, the corresponding location names are listed in Table 5-10. The figures further demonstrate the influence of the vibrations induced by orthogonal ground motions. Comparing to Figures 5-13 to 5-20, the prediction errors are more obvious in Figures 5-24 to 5-31 when using the 1D model. On the other hand, the predicted responses using the 2D model shows high accuracy from the time history viewpoint.

Table 5-10 Largest response amplitudes in the *x*- and *y*-directions on the 4th floor

Response	El Centro			Taft			Hachinohe			JMA Kobe		
	Amp.	Err.	Loc.	Amp.	Err.	Loc.	Amp.	Err.	Loc.	Amp.	Err.	Loc.
Acc. (m/s ²)	11.77	+1	4m	27.14	-12	4b	8.13	+4	4b	13.82	-1	4b
	11.99	+0	4b	17.82	-4	4a	6.81	+3	4a	13.85	+1	4o
Vel. (×10 ⁻¹ m/s)	7.90	+2	4m	16.56	-4	4b	4.97	+3	4m	9.30	+0	4b
	8.08	+1	4b	10.88	-1	4a	4.72	-2	4a	9.34	+4	4b
Disp. (×10 ⁻² m)	5.40	+2	4m	10.69	-1	4b	3.54	+6	4b	6.16	+0	4b
	5.42	+3	4b	7.43	+0	4a	3.19	+4	4a	6.21	+5	4b

Note: the upper lines for *x*-direction and lower lines for *y*-direction

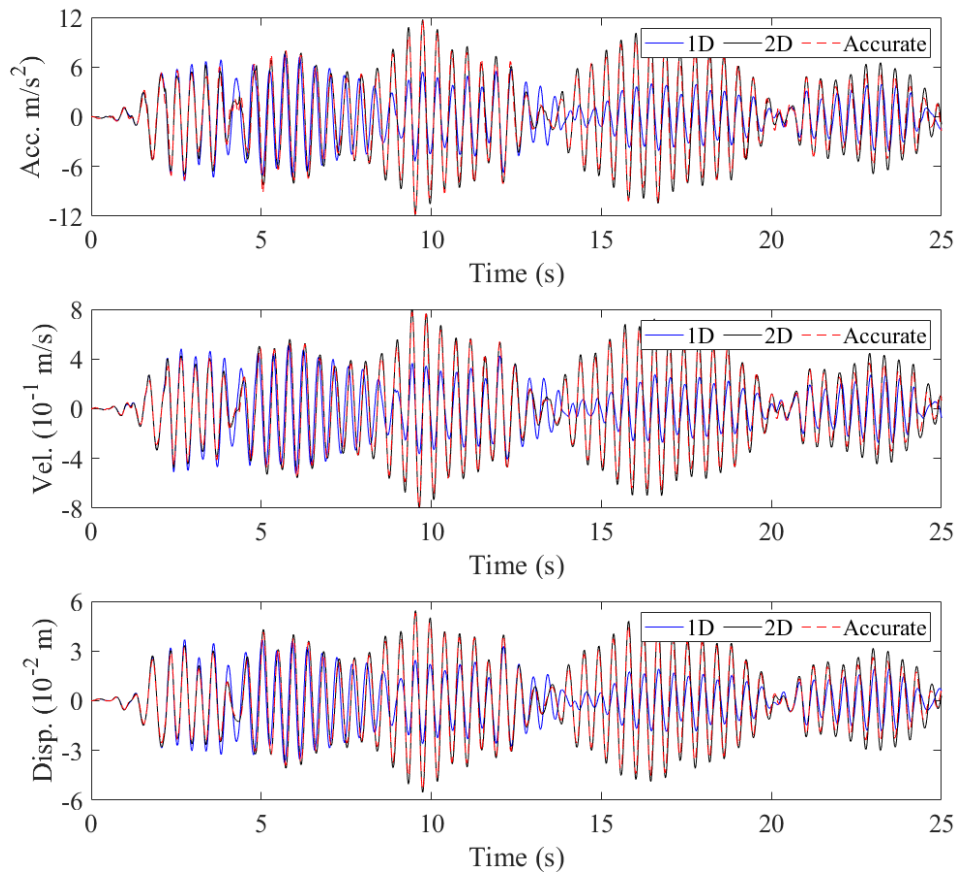


Figure 5-24 Largest x -directional responses on the 4th floor under the two-directional El Centro wave

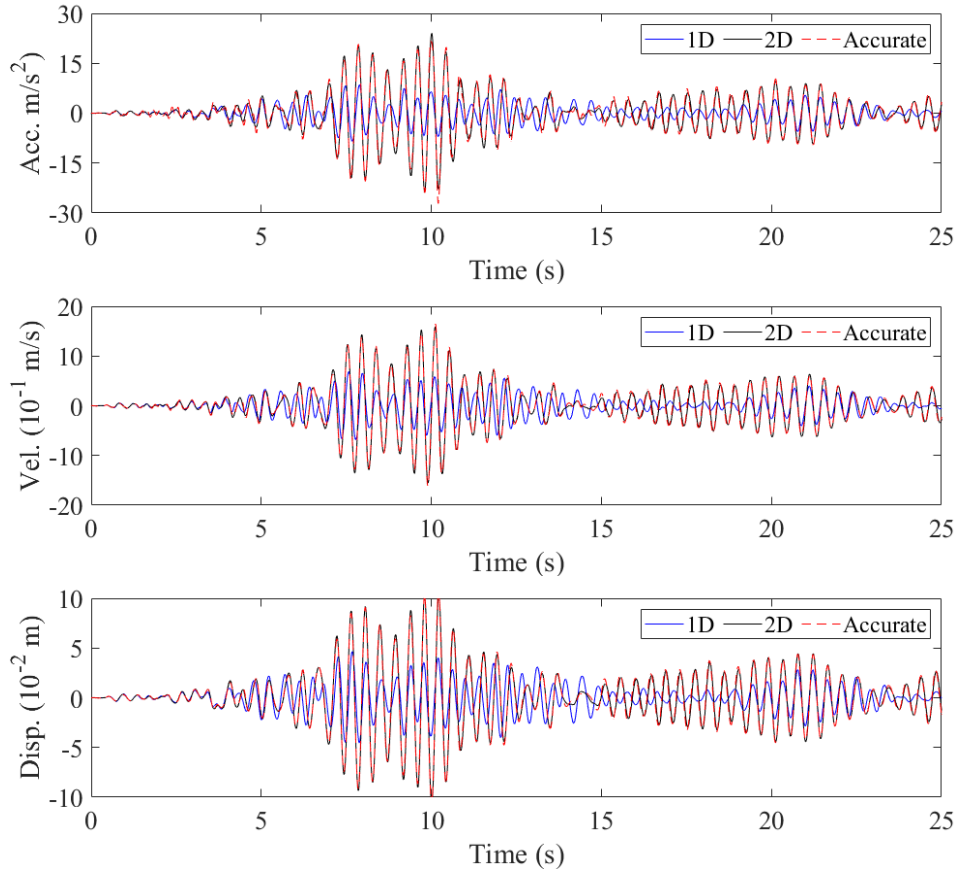


Figure 5-25 Largest x -directional responses on the 4th floor under the two-directional Taft wave

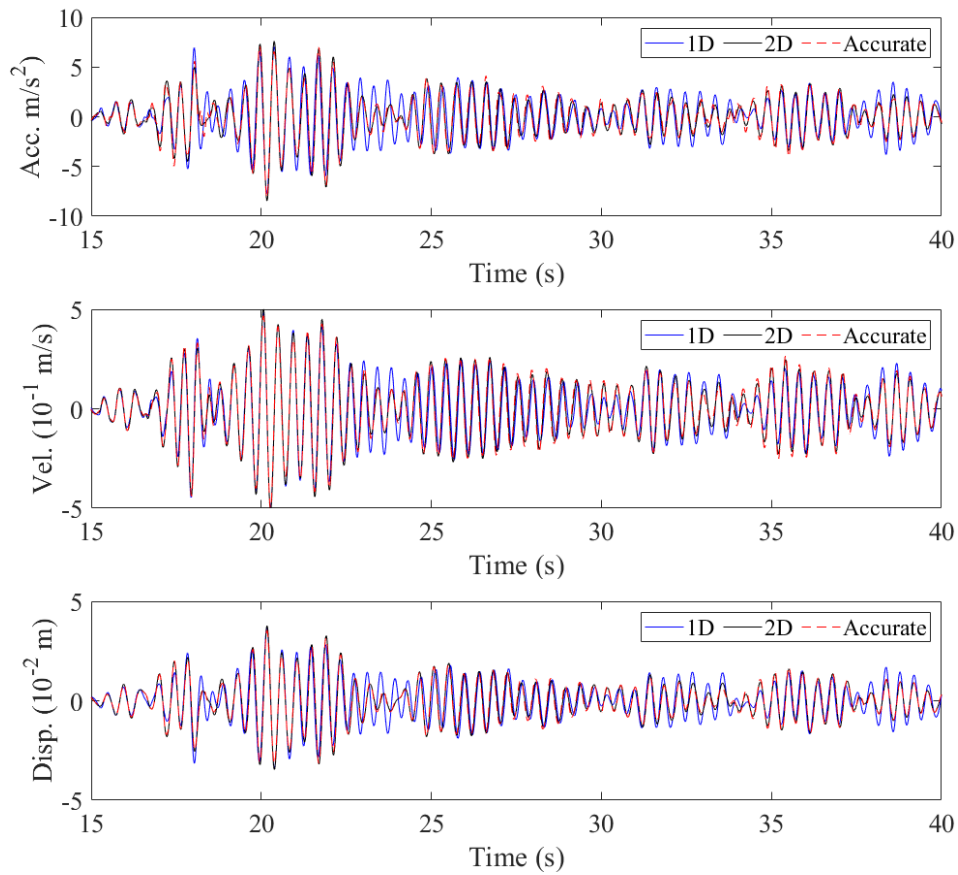


Figure 5-26 Largest x -directional responses on the 4th floor under the two-directional Hachinohe wave

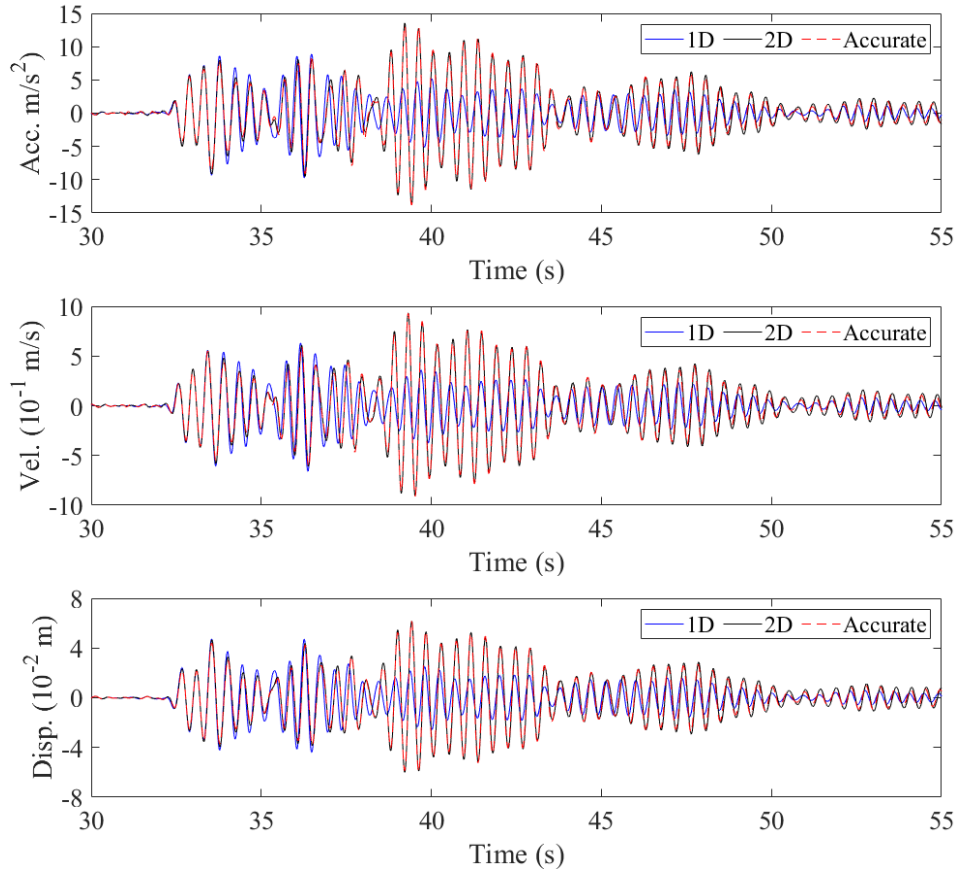


Figure 5-27 Largest x -directional responses on the 4th floor under the two-directional JMA Kobe wave

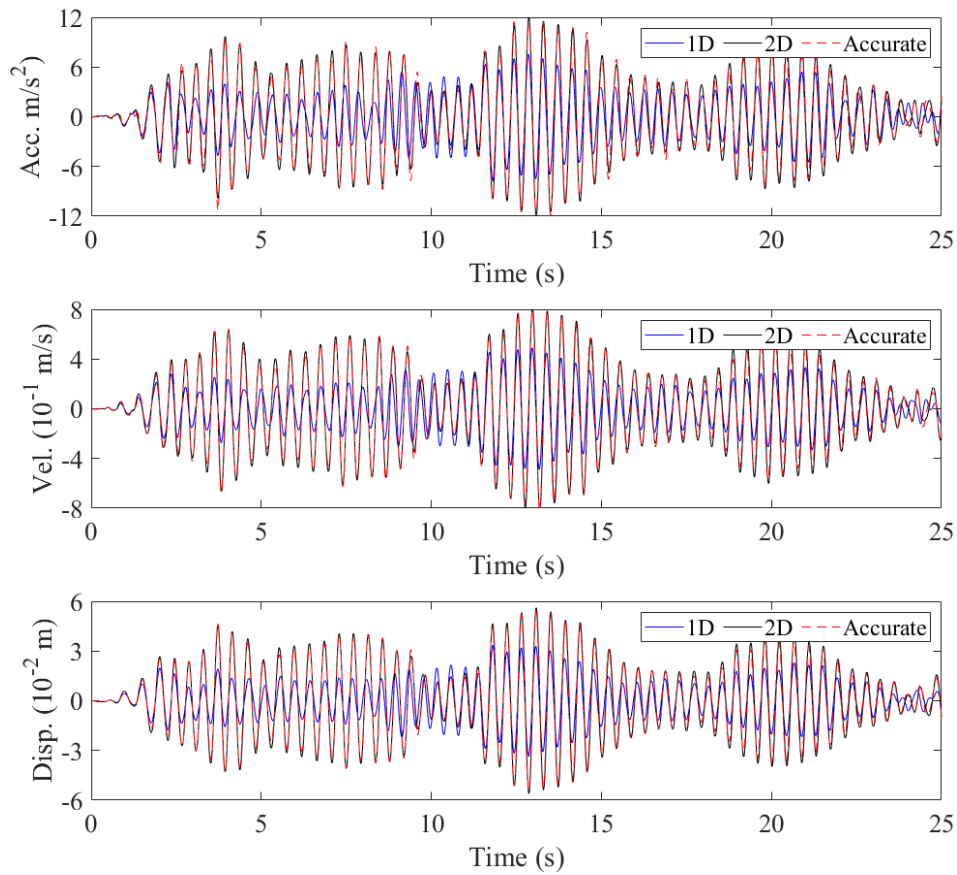


Figure 5-28 Largest y-directional responses on the 4th floor under the two-directional El Centro wave

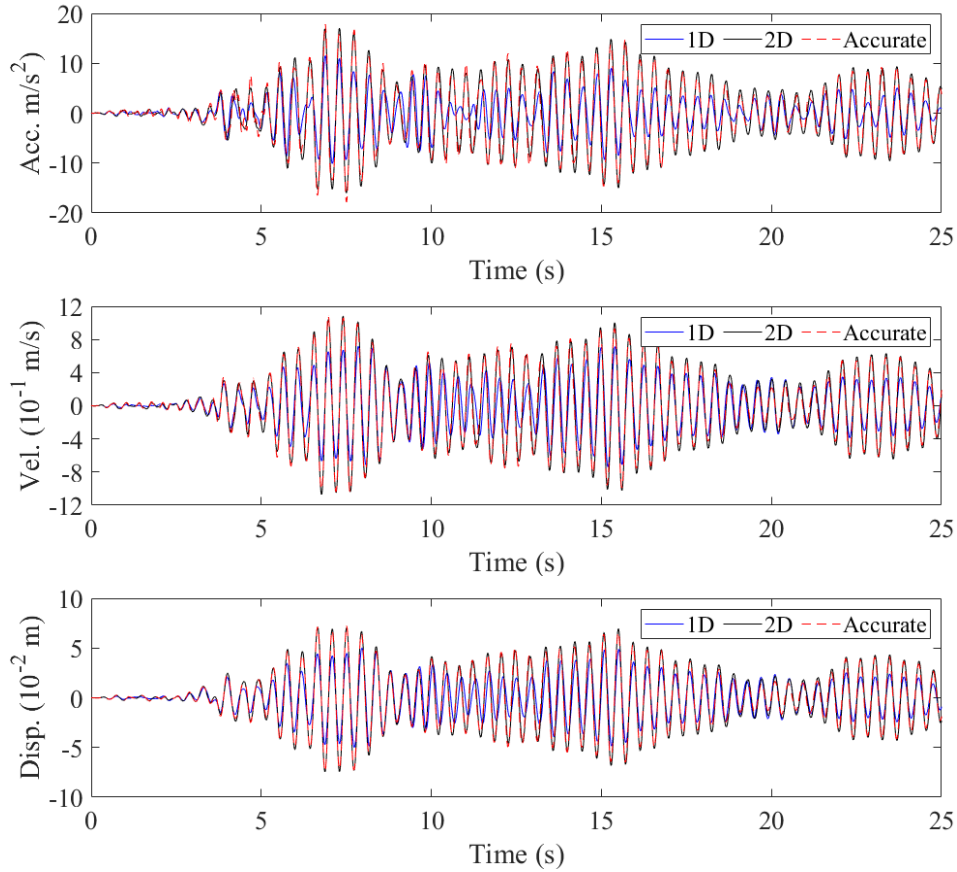


Figure 5-29 Largest y-directional responses on the 4th floor under the two-directional Taft wave

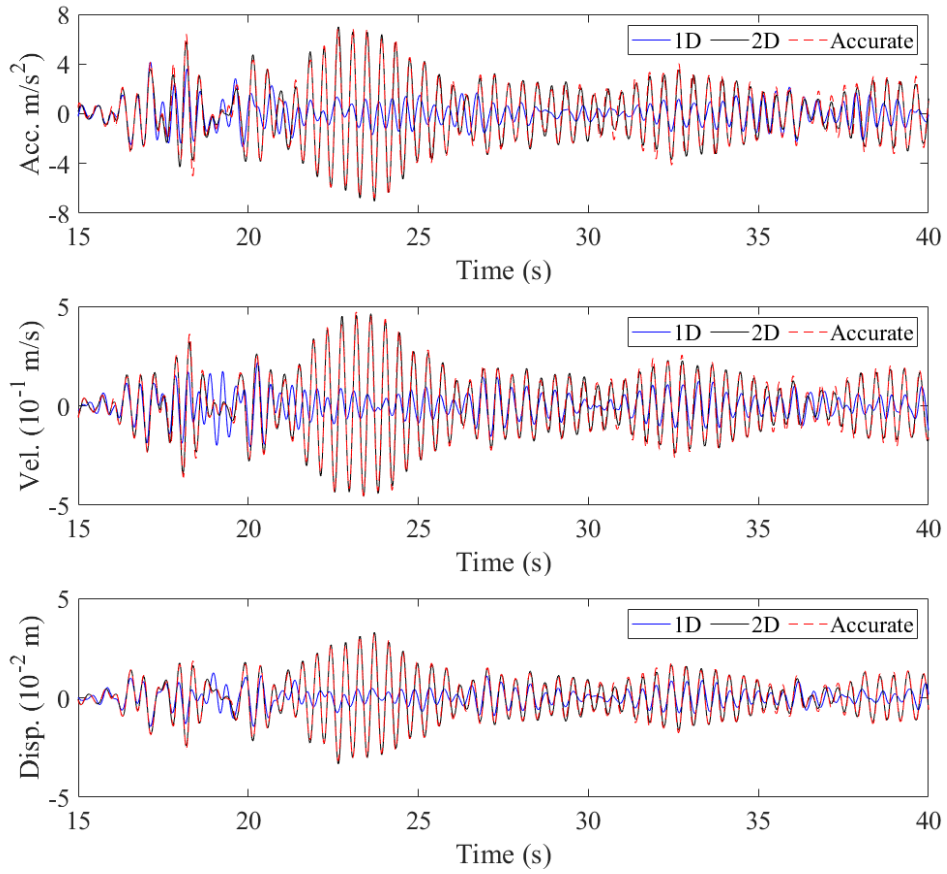


Figure 5-30 Largest y-directional responses on the 4th floor under the two-directional Hachinohe wave

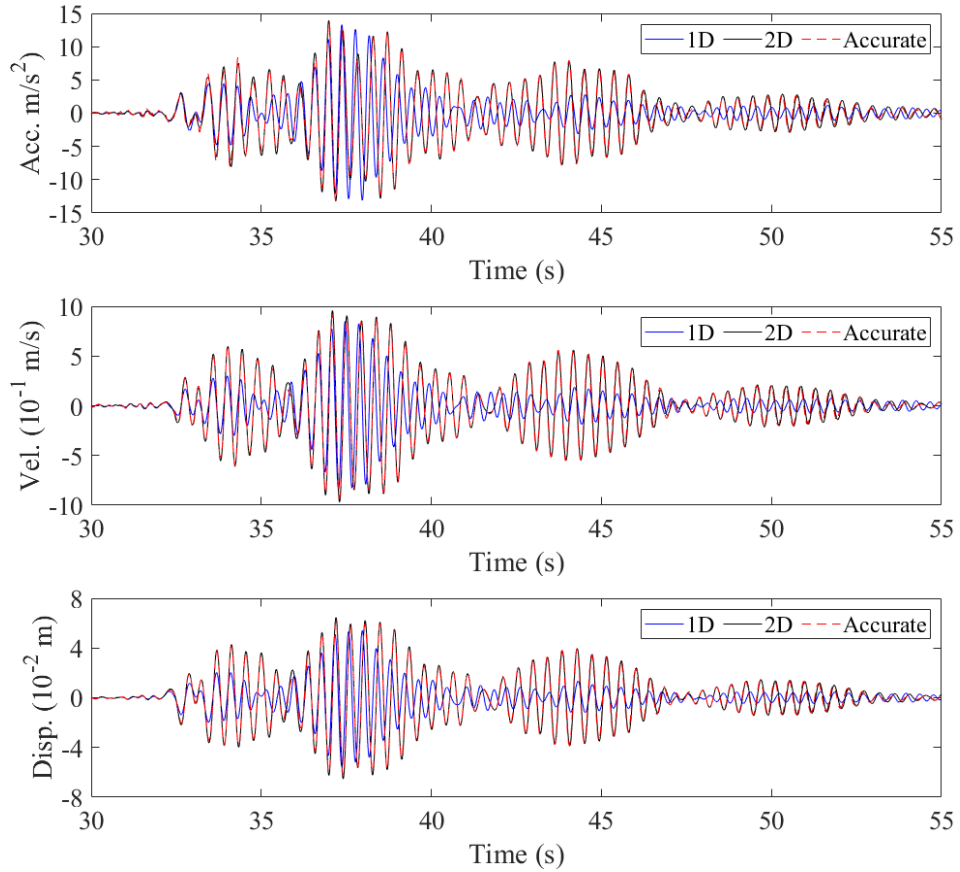


Figure 5-31 Largest y-directional responses on the 4th floor under the two-directional JMA Kobe wave

5.6 Conclusions

In this chapter, the proposed seismic response prediction method is verified by using the numerical model of the large-scale low-rise building. The numerical model shows floor flexibility and its mode shapes show lateral-torsional coupling. The approximated participation vectors using the 1D and 2D models are firstly compared. Then the seismic response prediction accuracies using the 1D and 2D models are investigated by the single- and two-directional ground motions. The main conclusions are summarized as follows:

- (1) In participation vector approximation, the 2D model has higher accuracy than the 1D model. The used modes show lateral-torsional coupling with large amplitudes in both horizontal directions. The higher approximation accuracy is produced by the fact that the 2D model utilizes the two directional mode shape components simultaneously to approximate the participation vector in one direction. On the other hand, the 1D model only utilizes the mode shape components in the same direction of the participation vector.
- (2) The influence of the participation vector approximation errors on the seismic response prediction accuracy is firstly explored by the single-directional ground motion. The simulation considers the seismic responses in the same direction of the input ground motion. The 2D model has higher seismic response prediction accuracy because of the higher participation vector approximation accuracy. However, the prediction accuracies at some locations are lower under certain ground motions, because some modes with large amplitudes at those locations are neglected while those modes are excited under certain ground motions.
- (3) The seismic response prediction accuracies using the 1D and 2D models are further compared by using the two-directional ground motions. The 2D model has better prediction accuracies not only because of the higher participation vector approximation accuracy, but also because the 2D model considers the vibrations induced by orthogonal ground motions. The prediction errors of the 1D model are significantly increased mainly because the 1D model cannot consider the vibrations induced by orthogonal ground motions.

Reference

- [1] Xie J, Ikeda Y (2021): Seismic Response Prediction of Large-scale Low-rise Buildings Based on Microtremor Measurement, *Summaries of Technical Papers of Annual Meeting Kinki Branch, AIJ*, 2 pages, Paper ID:2066.
- [2] CSI Analysis Reference Manual (2016): <https://docs.csiamerica.com/manuals/sap2000/CSiRefer.pdf> (Accessed on 22 June, 2022).

Chapter 6

Verification with Full-scale Shaking Table Test

6.1 Introduction

In Chapter 4, the fundamental properties of the proposed seismic response prediction method are explored by a 5-DOF stick-shaped lumped mass model. The participation vector approximation by using the mode shapes in limited modes and/or at limited locations and the seismic response prediction using the approximated participation vector are discussed. In Chapter 5, the prediction method is applied to a numerical model of a large-scale low-rise building to verify its applicability to buildings with floor flexibility. The necessity of the two-dimensional model when the objective building has modes with lateral-torsional coupling is also demonstrated. However, the modal property variances are not considered in the two chapters. The modal property variances here mean the natural frequency and damping ratio variances between under measurements and an earthquake. As explained in Chapter 2, the natural frequencies and damping ratios under microtremor measurements are generally different from the values under an earthquake even if the objective building has no structural damage. Therefore, this chapter investigates the influence of the modal property variances on the prediction accuracy and verifies the applicability of the prediction method in practical situations by the full-scale shaking table tests [1]. The specimen is a conventional 4-story steel structure with a rectangular planar shape. Although the specimen does not reflect floor flexibility, the shaking table tests are adequate to fulfill the objectives. In this chapter, Section 6.2 introduces the basic information about the specimen. Section 6.3 shows the modal properties of the specimen by applying microtremor measurements before the shaking table tests began. Section 6.4 discusses the participation vector approximation using the identified mode shapes. Section 6.5 introduces the input excitations and the seismic response performances of the specimen. Section 6.6 compares the modal properties identified during tests to the properties from microtremor measurements. Section 6.7 compares the predicted seismic responses to the recorded responses and Section 6.8 concludes the study.

6.2 Test Specimen

The experiment was conducted at a three-dimensional full-scale earthquake testing facility nicknamed 'E-Defense' in December 2020, in the National Research Institute for Earth Science and Disaster Prevention (NIED) near Kobe in Japan. The shaking table tests aimed to simulate the seismic performance of a hospital with medical equipment, dummy human bodies on each floor and a water tank filled with sand located on the roof. The outlook of the specimen is shown in Figure 6-1.

The specimen included two steel buildings: one was the base-fixed 4-story building and the other one was the base-isolated 3-story building. The geometric information of the base-fixed structure is in Figure 6-

2. The two buildings were connected by a bridge on the 2nd floor. An expansion joint (EXP.J) was installed at the bridge. Figure 6-3 is a photo of the EXP.J. The blue circle in Figure 6-2 represents the location where the photo was taken and the blue arrow represents the shooting angle. The two buildings were independent of each other because of the EXP.J. The objective building is the base-fixed building.

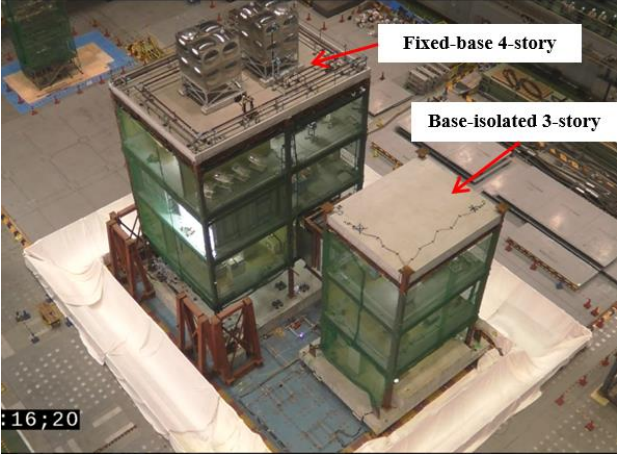


Figure 6-1 Test specimen outlook

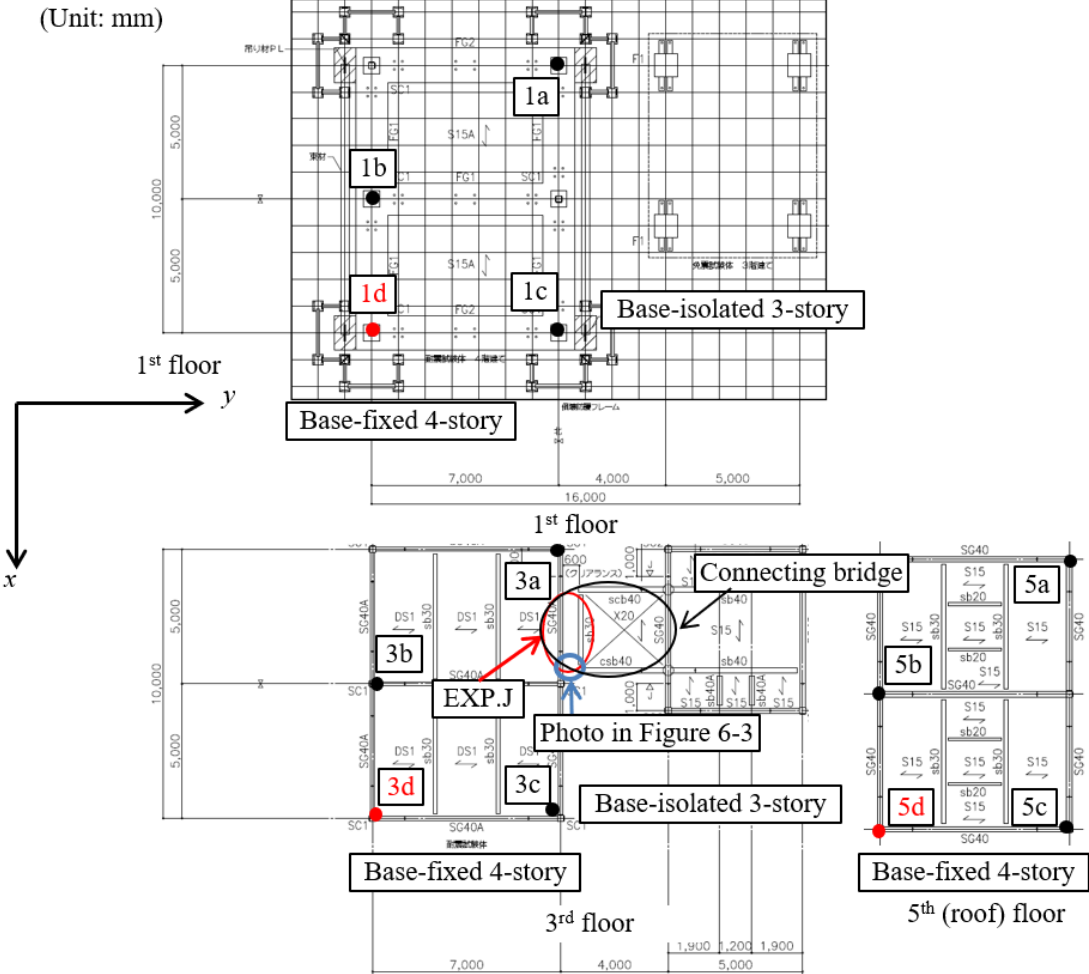


Figure 6-2 Geometric information and the measurement points in the specimen



Figure 6-3 EXP.J at the connecting bridge

The fixed-base building had a 10.0 m (two bays in the x -direction) by 7.0 m (one bay in the y -direction) floor plan and it was 16.1 m in height. The estimated weights from the 1st (including the concrete foundation) to 5th (roof) floors were 1,602 kN, 377 kN, 371 kN, 376 kN and 512 kN, respectively. As a result, the total weight of the building is 3,238 kN. The building's structure was a 4-story moment-resisting frame designed and constructed according to the current Japanese seismic codes. The frame was composed of steel hollow structural section (HSS) columns and H-shaped steel beams. All column-beam connections had through-diaphragms, and all fixed column bases were designed as the exposed type. All floors were made of 150 mm reinforced concrete slabs on steel deck plates. No claddings were installed. However, the x -directional frame was covered with partition walls in the 2nd to 4th stories. The columns were made of 250×16 mm cold-rolled HSS with BCR295 steel at a nominal strength of 295 MPa. The main beams utilized H-400×200×8×13 with SN490B steel at a nominal strength of 325 MPa or equivalent built-up steel sections. Floor beams utilized H-300×150×6.5×19 with SN490B. The column bases were the exposed-type used in Japan where anchor bolts embedded in the concrete foundation were connected to the base plates welded to the 1st story columns. The column bases were designed to yield prior to the columns.

6.3 Modal Identification Based on Microtremor Measurement

Total of 15 measurement points were deployed at the base-fixed building. The measured locations on the 1st, 3rd and 5th floors are shown in Figure 6-2 by the black dots. The measured locations on the other floors were horizontally identical to the three floors. Each measured location is attached with a name that consists of a number and a character, the number indicates the floor number and the character indicates the horizontal location. For example, Location 5a means Location a on the 5th floor and Location 4a means Location a on the 4th floor. Locations 5a and 4a are horizontally identical. The red dots represent the accelerometer locations deployed for the seismic response recording, they are named following the same rule of the measured locations. Four simultaneous measurements (Measurements A, B, C, and D) were repeated by fixing one accelerometer at Location 5a as the reference point to obtain the global mode shapes of the structure with a limited number of sensors. Location 5a was selected as the reference point because

the mode shape amplitudes on the 5th floor are likely larger. The locations for each measurement are shown in Table 6-1.

Table 6-1 Microtremor measurement plan

Sequence	Sensor 1	Sensor 2	Sensor 3	Sensor 4	Sensor 5
A	5a	4a	3a	2a	1a
B	5a	5b	5c	4b	4c
C	5a	3b	3c	2b	2c
D	5a	1b	1c	-	-

The sampling frequency was 200 Hz. Figure 6-4 shows the x -directional microtremor accelerations at Locations 5a to 1a under Measurement A. The peak accelerations were less than 0.020 m/s^2 on the 5th floor and less than 0.001 m/s^2 on the 1st floor during the four measurements. The sources of vibration were mostly indoor construction activities and ground vibrations. The input load can be assumed as the white noise so that the modal identification method based on the ambient vibration is applicable.

Similar to the identification process in Chapter 2, the natural frequencies and the corresponding mode shapes of the measured building were identified by the Frequency Domain Decomposition (FDD) method. The damping ratios were obtained by the Random Decrement (RD) method. Figure 6-5 shows the 1st singular value distributions of the four measurements. Total of 15 time-windows were utilized and each time-window contains 40.96 s long with 8192 data so that total utilized data contained around 10 minutes long. The FDD method was applied to each window and the singular value distribution was smoothed by the averaging process and the Hanning window five times. Comparing the four distributions of the 1st singular values in each horizontal direction, similar peaks appear at slightly different frequencies in the specific frequency ranges. Similar peak frequencies were averaged. The maximum difference is 0.1221 Hz around the relatively high frequency of 8.4 Hz.

Figure 6-6 shows the selected and averaged natural frequencies with the corresponding mode shapes. The mode shapes are normalized to the amplitudes at Location 5a. Table 6-2 summarizes the identified modes based on Figures 6-5 and 6-6. The dominant natural frequencies are 1.57 Hz in the y -direction and 1.65 Hz in the x -direction. The 1st torsional mode is at 2.25 Hz. As shown in Figure 6-6, there are two candidates of the 2nd lateral modes in the x -direction according to the identified mode shapes. The identified damping ratios in the 1st x - and y -directional modes were around 1.0%. However, the identified damping ratios are not used in the seismic response prediction because the damping ratios under medium/large excitations cannot be estimated by the microtremor. The purpose of using the RD method is to validate the natural frequency identified by the FDD method and the identified 1st natural frequencies are similar when using the two methods.

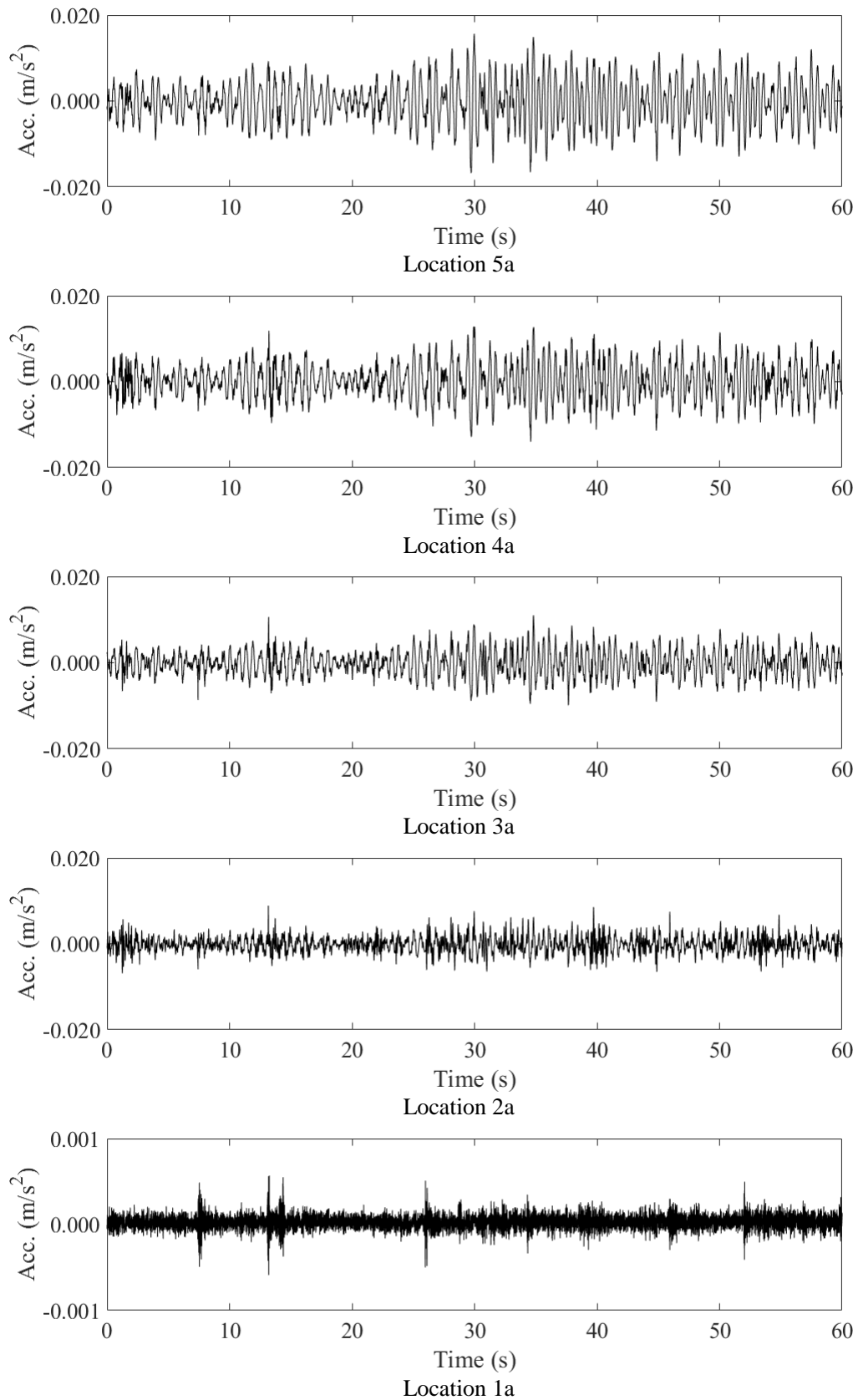


Figure 6-4 Accelerations in Measurement A

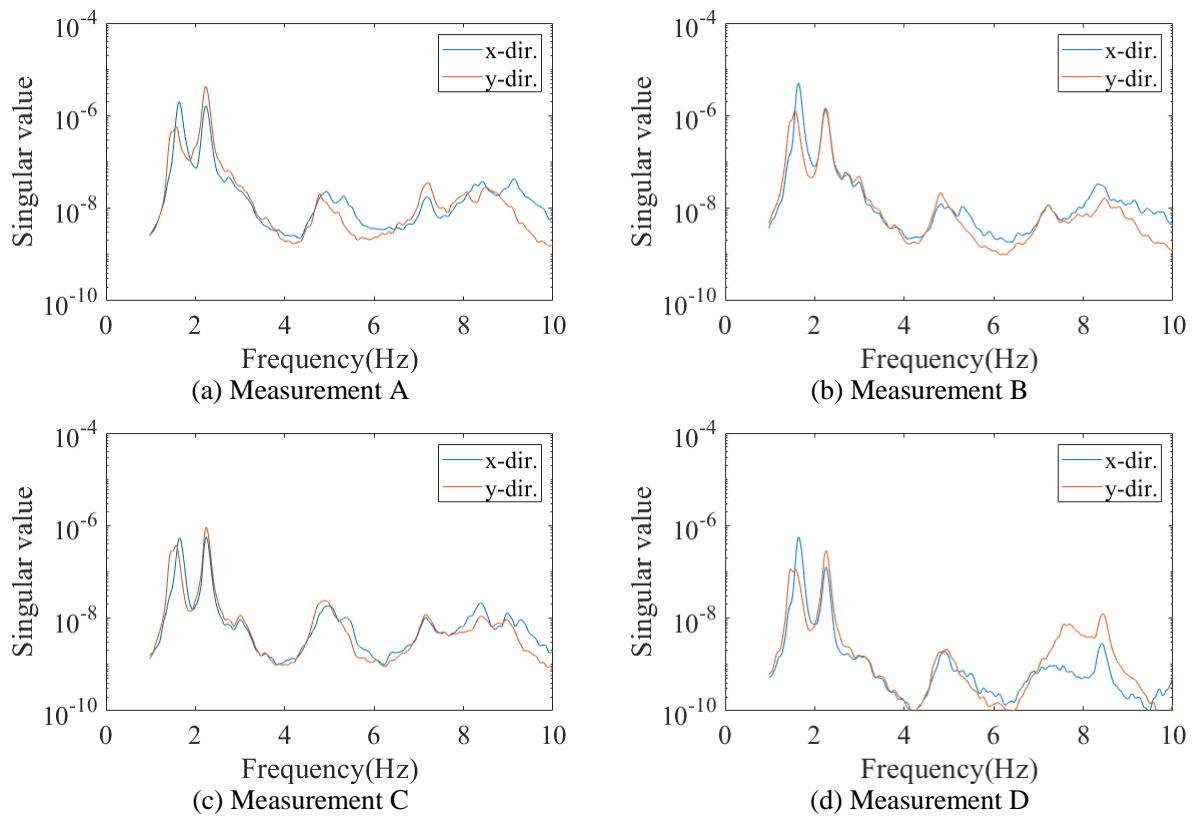
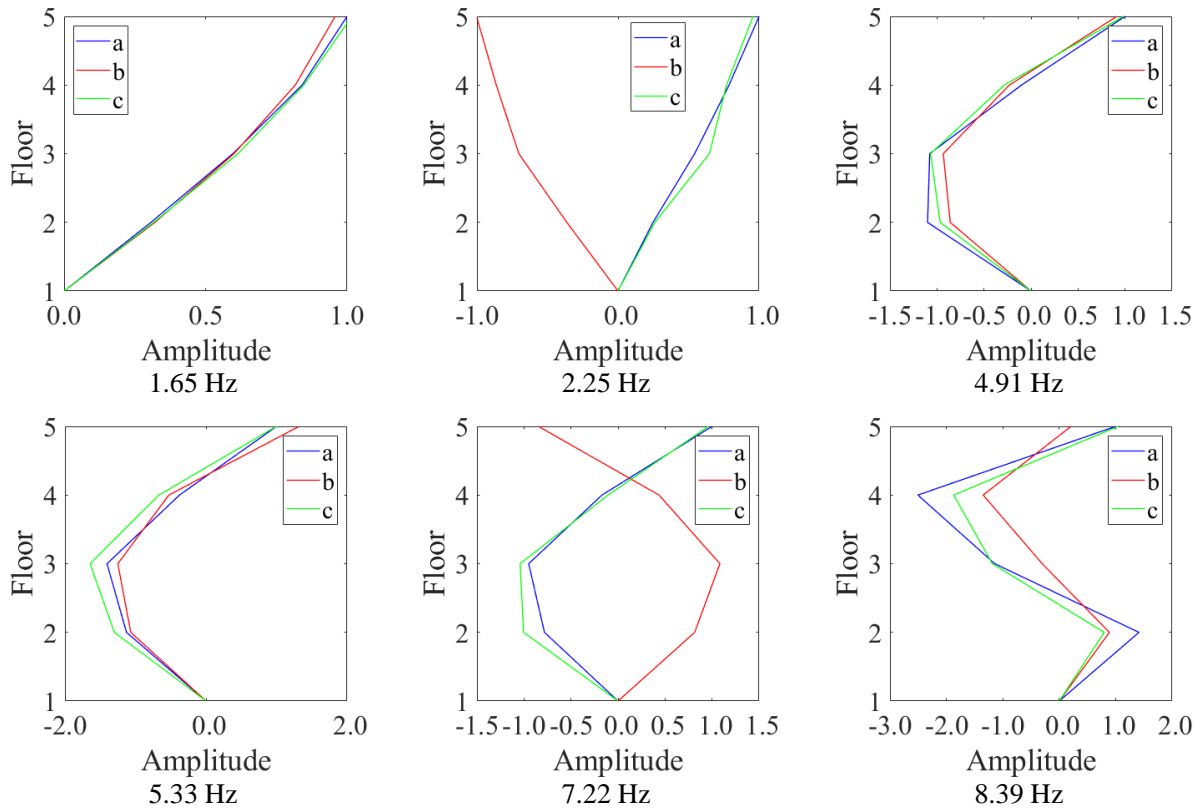


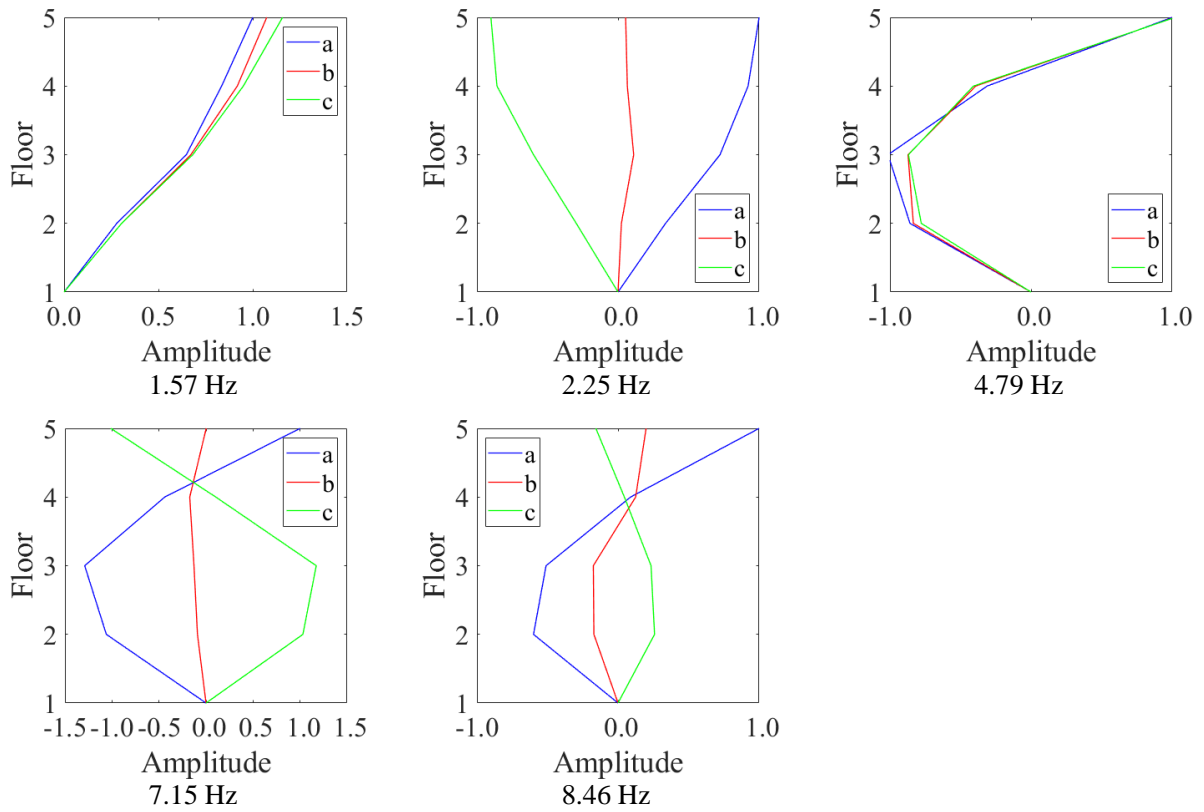
Figure 6-5 1st singular value distribution

Table 6-2 Modes identified from microtremor measurements

x-direction		y-direction	
Frequency (Hz)	Mode	Frequency (Hz)	Mode
1.65	Lateral 1 st	1.57	Lateral 1 st
2.25	Torsional 1 st	2.25	Torsional 1 st
4.91	Lateral 2 nd (Candidate)	4.79	Lateral 2 nd
5.33	Lateral 2 nd (Candidate)	7.15	Torsional 2 nd
7.22	Torsional 2 nd	8.46	Not determined
8.39	Lateral 3 rd with torsion		



(a) x-directional mode shapes



(b) y-directional mode shapes

Figure 6-6 Mode shapes identified from microtremor measurements

6.4 Participation Vector Approximation

As shown in Figure 6-6, the identified mode shapes have little lateral-torsional coupling in lower modes. Therefore, the single-dimensional model is utilized in participation vector approximation and seismic response prediction. There are two candidates for the 2nd lateral mode in the *x*-direction, which is not expected because the specimen is regular from the structure viewpoint. Nevertheless, the two candidates are simultaneously used in the participation vector approximation as the preliminary investigation. The mode shapes are normalized by setting the sum of squared mode shape amplitudes in each mode as unity as shown in Equation (3-15). Table 6-3 uses mode shapes at all measured locations and starts the participation vector approximation from using only the 1st mode, then higher modes are added to investigate the changes of the approximation results. The corresponding MSE in the LSM is also attached.

Table 6-3 Preliminary participation vector approximation

Freq. (Hz)	<i>x</i> -direction						Freq. (Hz)	<i>y</i> -direction				
	Total utilized modes							Total utilized modes				
	1	2	3	4	5	6	1	2	3	4	5	
1.65	3.25	3.28	3.21	3.47	3.49	3.38	1.57	3.21	3.21	3.17	3.18	3.63
2.25	-	-0.10	-0.07	0.12	0.18	-0.02	2.25	-	0.18	0.14	0.16	0.55
4.91	-	-	-1.06	-3.57	-4.09	-1.53	4.79	-	-	-1.03	-1.04	-0.42
5.33	-	-	-	2.56	3.03	0.39	7.15	-	-	-	0.11	1.31
7.22	-	-	-	-	0.17	-0.05	8.46	-	-	-	-	-1.47
8.39	-	-	-	-	-	0.49	MSE	0.14	0.14	0.05	0.05	0.04
MSE	0.12	0.12	0.03	0.02	0.02	0.01						

The abrupt changes in the approximation occur when the 4th (5.33 Hz) mode is added in the *x*-direction and the 5th (8.46 Hz) mode is added in the *y*-direction. Since the 3rd (4.91 Hz) and 4th modes have similar mode shapes, the 4th mode is little informative. Therefore, the abrupt changes in the *x*-direction after the 4th mode is added are considered decreasing the approximation accuracies in other modes. The slight changes in the *x*-directional MSE after adding the 4th mode suggests that the 4th mode is indeed unimportant. As a result, the 4th mode in the *x*-direction is removed from the participation vector approximation and the seismic response prediction. In the *y*-direction, the 5th mode also contributes little to the MSE reduction, which also means the changes in the participation vector approximation results are unlikely to improve the approximation accuracy. Therefore, the 5th mode in the *y*-direction is also removed. The approximation results after removing the two modes are shown in Table 6-4.

Table 6-4 Participation vector approximation after removing modes

Freq. (Hz)	<i>x</i> -direction					Freq. (Hz)	<i>y</i> -direction			
	Total utilized modes						Total utilized modes			
	1	2	3	4	5	1	2	3	4	
1.65	3.25	3.28	3.21	3.21	3.35	1.57	3.21	3.21	3.17	3.18
2.25	-	-0.10	-0.07	-0.07	-0.05	2.25	-	0.18	0.14	0.16
4.91	-	-	-1.06	-1.07	-1.15	4.79	-	-	-1.03	-1.04
7.22	-	-	-	0.01	-0.08	7.15	-	-	-	0.11
8.39	-	-	-	-	0.52					

Despite using mode shapes at all measured locations, three cases in each direction are considered in Table 6-5. The participation vector approximation using mode shapes on all measured locations is named as Case 0. Case 1 uses mode shapes at one location on each floor and only considers lateral modes so that Case 1 makes a good validation to Case 0. Case 2 uses mode shapes on the 3rd to 5th floors and Case 3 uses mode shapes on the 4th and 5th floors.

Table 6-5 Participation vector approximation using mode shapes at selected locations

		Natural frequencies of considered modes (Hz)					
Dir.	Case	1.65	2.25	4.91	7.22	8.39	Utilized sensor locations
x	0	3.35	-0.05	-1.15	-0.08	0.52	All (12) locations
	1	3.33	-	-1.13	-	0.38	5a, 4a, 3a, 2a
	2	3.16	-0.04	-0.81	-0.05	0.19	5a, 5b, 5c, 4a, 4b, 4c, 3a, 3b, 3c
	3	2.80	-0.07	-0.20	0.06	-0.16	5a, 5b, 5c, 4a, 4b, 4c
		Natural frequencies of considered modes (Hz)					
		1.57	2.25	4.79	7.15		
y	0	3.18	0.16	-1.04	0.11		All (12) locations
	1	3.39	-	-0.98	-		5a, 4a, 3a, 2a
	2	3.04	0.15	-0.62	0.08		5a, 5b, 5c, 4a, 4b, 4c, 3a, 3b, 3c
	3	2.89	0.16	-0.38	0.02		5a, 5b, 5c, 4a, 4b, 4c

As shown in Table 6-5, the approximated participation vector in Case 1 is similar to Case 0 and makes a good validation to Case 0. The *x*-directional approximation results in the 3rd and 5th modes (the 4.91 Hz and 8.39 Hz modes) and the *y*-directional approximation results in the 3rd mode (4.79 Hz mode) are obviously different among Cases 0, 2 and 3. An explanation is that upper floors cannot reflect the overall mode shape amplitudes in higher modes. For example, Figure 6-6(a) shows that the 3rd *x*-directional mode at 8.39 Hz has large mode shape amplitudes on the 2nd and 3rd floors, and the amplitudes are in opposite direction to the ones on 4th and 5th floors, respectively. However, Case 3 does not consider the amplitudes on the 2nd and 3rd floors with smaller sums of participation functions, and thus the approximation results in the 3rd mode is obviously different from Case 0. Similarly, Case 2 does not consider the amplitude on the 2nd floor that is in opposite direction to the amplitudes on the 3rd and 4th floors in the 5th *x*-directional mode at 8.39 Hz. As a result, the approximated participation factor in the 5th mode in Case 2 is different from Case 0. Figure 6-6(b) shows that the amplitudes at Location a (blue line) in the 3rd *y*-directional mode at 8.46 Hz are large on the 2nd and 3rd floors and in opposite direction to the amplitudes on the 4th and 5th floors. The 3rd *y*-directional mode is not well reflected in Cases 2 and 3 with smaller sums of participation functions and there are obvious differences among Cases 0, 2 and 3 in the 3rd *y*-directional mode.

The sums of approximated participation functions in Cases 0 to 3 are compared in Table 6-6 to decide the approximated participation vector for the seismic response prediction. The sums of approximated participation functions in Table 6-6 suggests that using mode shapes at all floors is likely to overestimate the seismic responses on the 3rd floor since the values exceeds the unity. In addition, Table 6-6 shows that the sums on the 2nd floor and the sums on the 4th and 5th floors are similarly close to unity in Case 0. However, the values on lower floors are expected to be lower than higher floors when using a limited

number of modes. It is because lower floors are more influenced by the truncation errors. In this regard, Case 2 is preferable because the corresponding sums of approximated participation functions match the expected distributions on each floor. In Case 3, the sums at Locations 2a, 2b and 2c are too small. Since the participation vector approximation results in Table 6-5 and the approximated sums of participation functions in Table 6-6 are similar between Cases 0 and 1, it is unnecessary to utilize both two cases in the seismic response prediction. Therefore, Cases 0 and 2 are selected as the two candidate models for the seismic response prediction.

Table 6-6 Sums of approximated participation functions

Dir.	Case	Measured location											
		5a	5b	5c	4a	4b	4c	3a	3b	3c	2a	2b	2c
x	0	1.01	0.98	1.05	0.84	1.01	0.99	1.08	1.10	1.09	1.00	0.84	0.90
	1	1.02	0.93	1.05	0.93	1.05	1.06	1.09	1.11	1.11	0.94	0.82	0.85
	2	0.99	0.99	1.02	0.96	1.03	1.04	0.99	0.98	1.00	0.75	0.66	0.70
	3	0.99	1.00	1.01	1.00	1.00	1.00	0.74	0.78	0.76	0.34	0.41	0.36
y	0	0.90	0.87	0.86	1.13	1.21	1.19	1.13	1.10	1.11	0.62	0.66	0.66
	1	0.89	0.97	1.07	1.14	1.27	1.31	1.15	1.13	1.14	0.64	0.67	0.65
	2	0.99	0.97	0.96	1.04	1.10	1.08	0.95	0.94	0.94	0.49	0.52	0.52
	3	1.00	1.00	1.00	0.99	1.02	0.99	0.86	0.83	0.80	0.43	0.43	0.41

6.5 Input Excitations to Shaking Table and Seismic Responses

Table 6-7 lists the input ground motions and their sequences in the shaking table tests. The NS component of the JMA Kobe wave was adapted as the earthquake ground motion for simulating the earthquake at Tokyo metropolitan area. The other ground motion (OS2) is an artificial ground motion used to evaluate the seismic damage of relatively long-period structures in the Osaka region for a mega subduction-zone earthquake along the Nankai Trough. ‘OS’ stands for Osaka and ‘2’ stands for the relatively soft ground in the area. OS2 is an original ground motion prepared by the Ministry of Land Infrastructure Transport and Tourism, Japan, for the engineering bedrock is scaled up considering Type 2 soil conditions.

The ground motions were scaled down to simulate the elastic limit corresponding to the allowable stress design (Level 1) and the inelastic limit corresponding to the ultimate strength design (Level 2) in the Japanese seismic design. Nos.1 and 2 tests used the JMA Kobe motion in a single horizontal direction for the Level 1 design check; No.3 test used the small OS2 wave in a single horizontal direction for evaluating the immediate functionality limit; Then the scale of the JMA Kobe motion was increased and applied to the specimen in a single horizontal direction for the Level 2 design check in No.4 test; The OS2 motion was scaled up and applied in two horizontal directions for evaluating the functionality limit in No.5 test and; The JMA Kobe motions was scale up and applied in two horizontal directions with a vertical motion to evaluate the failure mechanism in No.6 test. In Nos.5 and 6 tests, the y-directional input was same as the x-directional input.

Table 6-7 Shaking table test

Test sequential No.	Earthquake name	Input direction		Input scale		Peak acceleration on 1 st floor (m/s ²)	
		x-dir.	y-dir.	x-dir.	y-dir.	x-dir.	y-dir.
1	Kobe	Input	-	16%	-	1.37	0.16
2	Kobe	-	Input	-	16%	0.34	1.49
3	OS2	-	Input	-	20%	0.22	0.89
4	Kobe	Input	-	50%	-	4.06	0.76
5	OS2	Input	Input	50%	50%	2.25	2.07
6	Kobe	Input	Input	50%	50%	5.44	4.74

Figure 6-7 shows the acceleration response spectra of Nos.5 and 6 tests by using the recorded accelerations on the 1st floor. The utilized damping ratio is set as 2%. The designed *x*- and *y*-directional input ground motions are the same in Nos. 5 and 6 tests so the corresponding response spectra are similar.

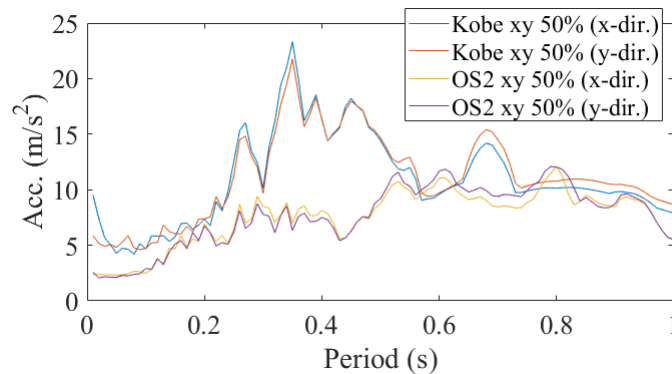


Figure 6-7 Response spectra of input accelerations on the shaking table

The sensors for the seismic response recording were at Locations 5d, 4d, 3d and 2d in red dots in Figure 6-2. They recorded the accelerations on the 5th to 2nd floors, respectively. Location 1d was set on the 1st floor and the corresponding accelerations are utilized as the input ground motions in the seismic response prediction. Figures 6-8 to 6-11 show the measured acceleration time histories in Nos.1, 3, 5 and 6 tests when the input Kobe and the OS2 waves were at small scale and large scale. Several anchor bolt fractures caused the intense shaking at 14.3 s at the column bases in No.6 test. The anchor bolt fractures lead to extreme peak amplitudes on lower floors. Figure 6-12 shows the *x*-directional accelerations with extreme peak amplitudes in No.6 test, which was caused by the anchor bolt fractures. The extreme peak amplitude on the 2nd floor was also observed in *y*-direction.

Table 6-8 summarizes the response amplitudes of absolute accelerations, relative velocities and relative displacements on the 2nd to 5th floors. The recorded *y*-directional acceleration on the 2nd floor and the *x*-directional accelerations on the 2nd and 3rd floors are not listed because they were significantly influenced by the anchor bolt fractures. The relative accelerations were filtered by the 4-order high-pass Butterworth filter with the cutoff frequency of 0.5 Hz, then the filtered accelerations are integrated by the numerical integration method to obtain the velocity and displacement amplitudes.

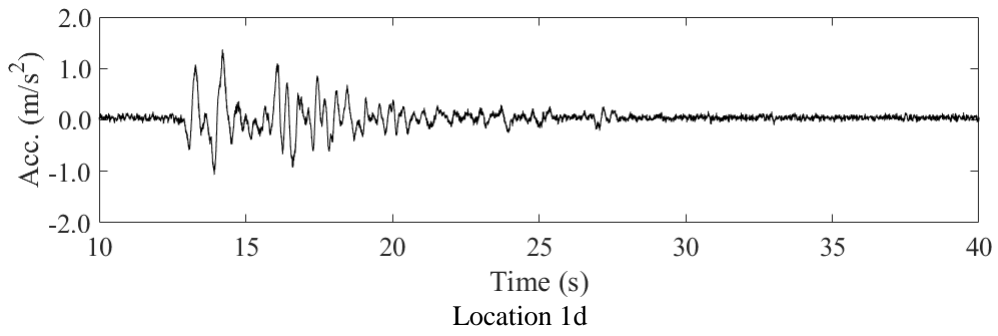
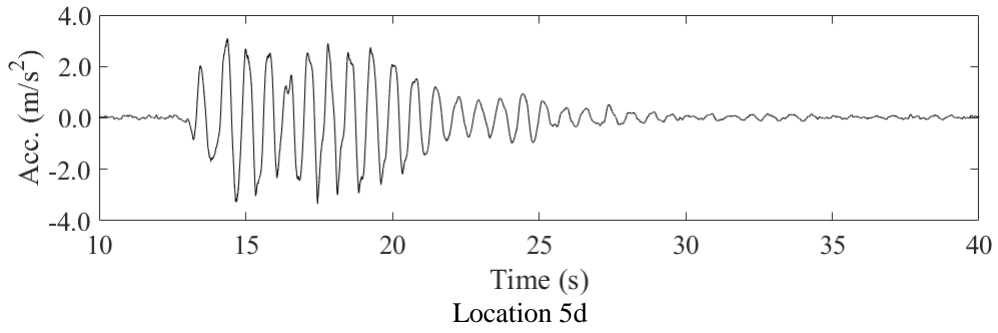


Figure 6-8 *x*-directional accelerations in No.1 test

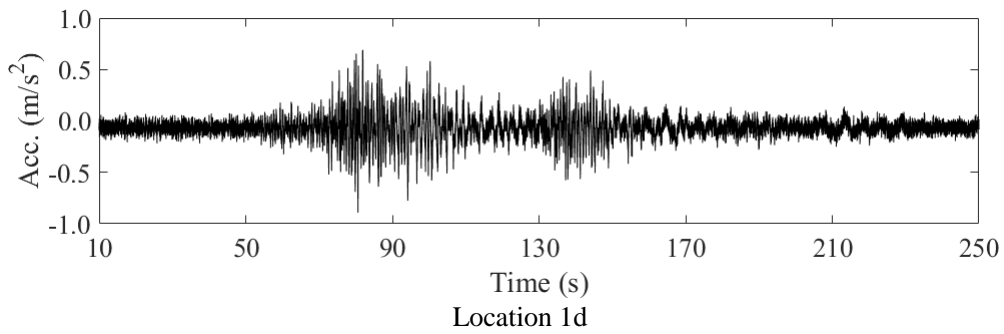
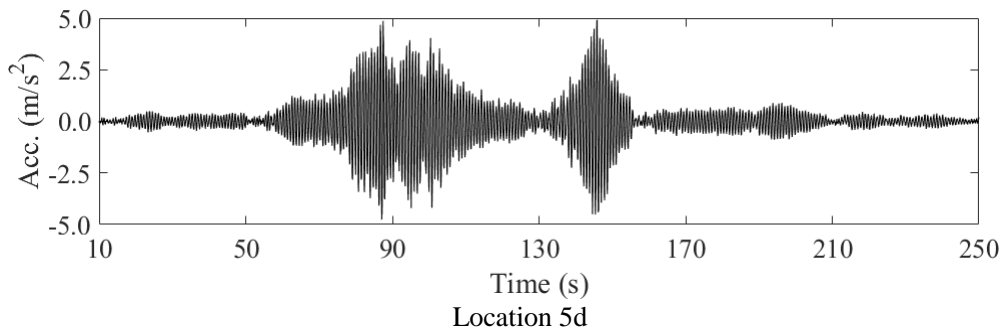


Figure 6-9 *y*-directional accelerations in No.3 test

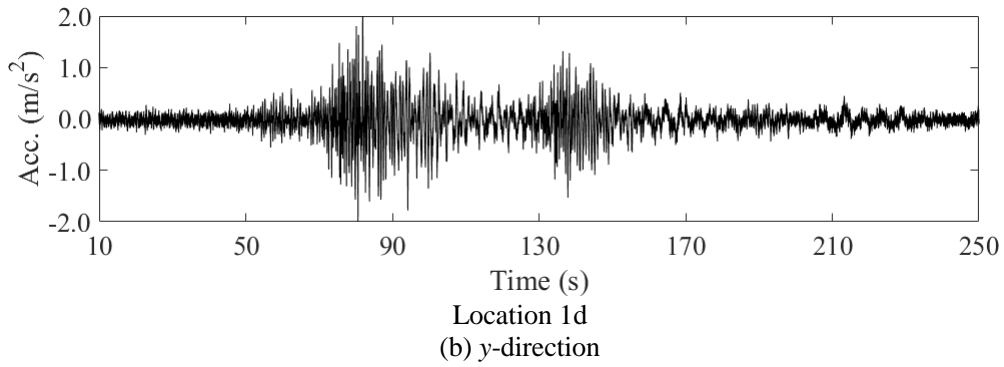
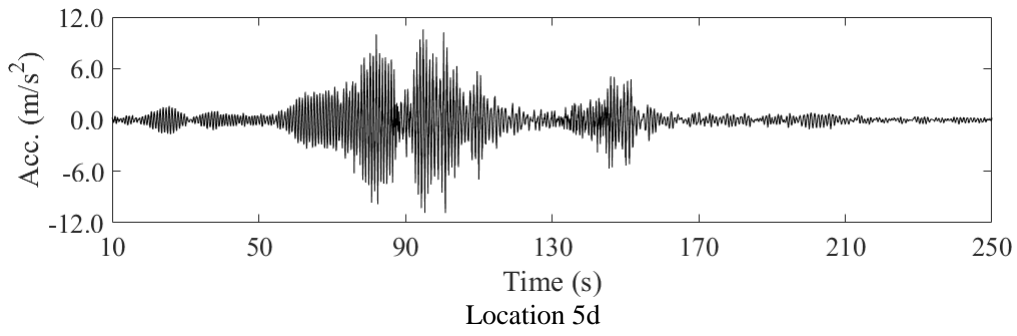
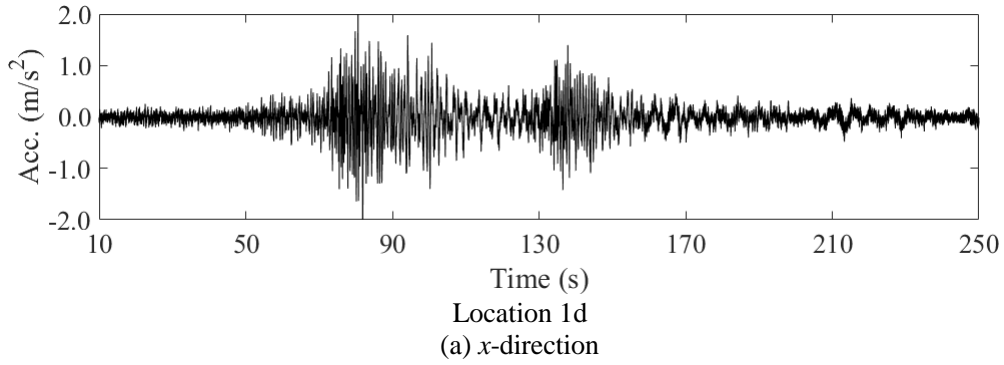
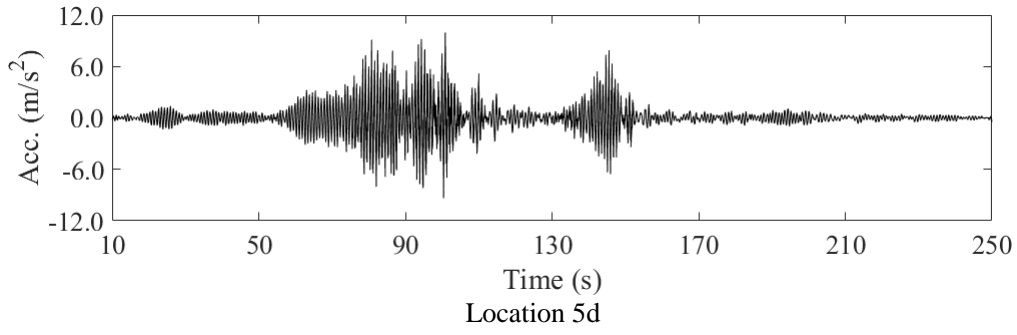


Figure 6-10 Accelerations in No.5 test

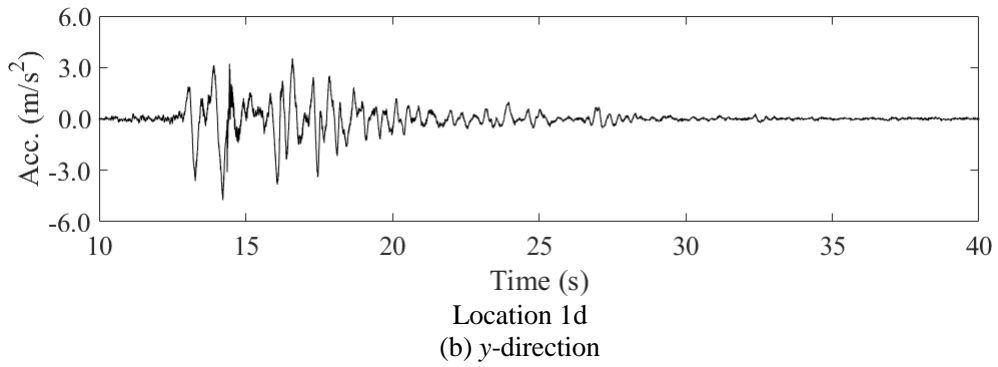
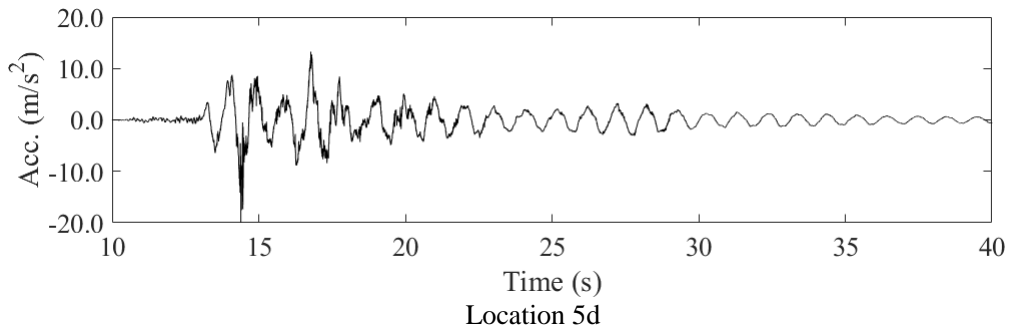
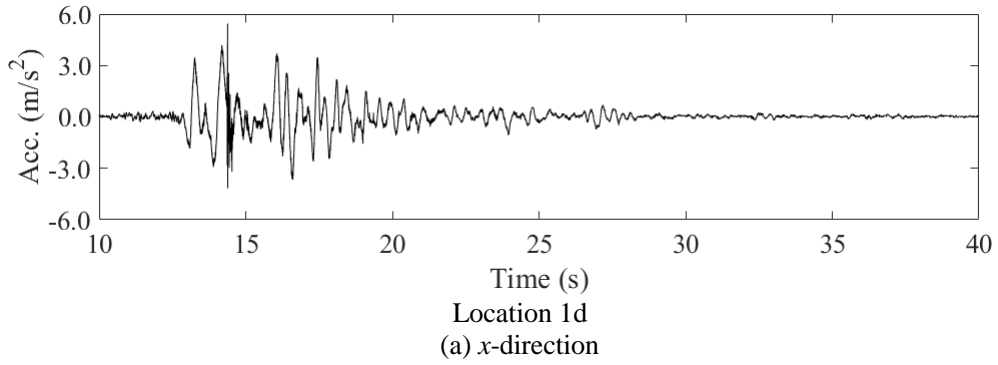
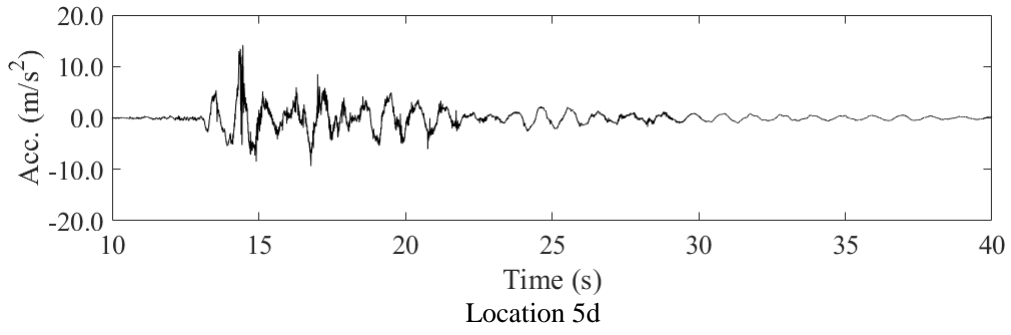


Figure 6-11 Accelerations in No.6 test

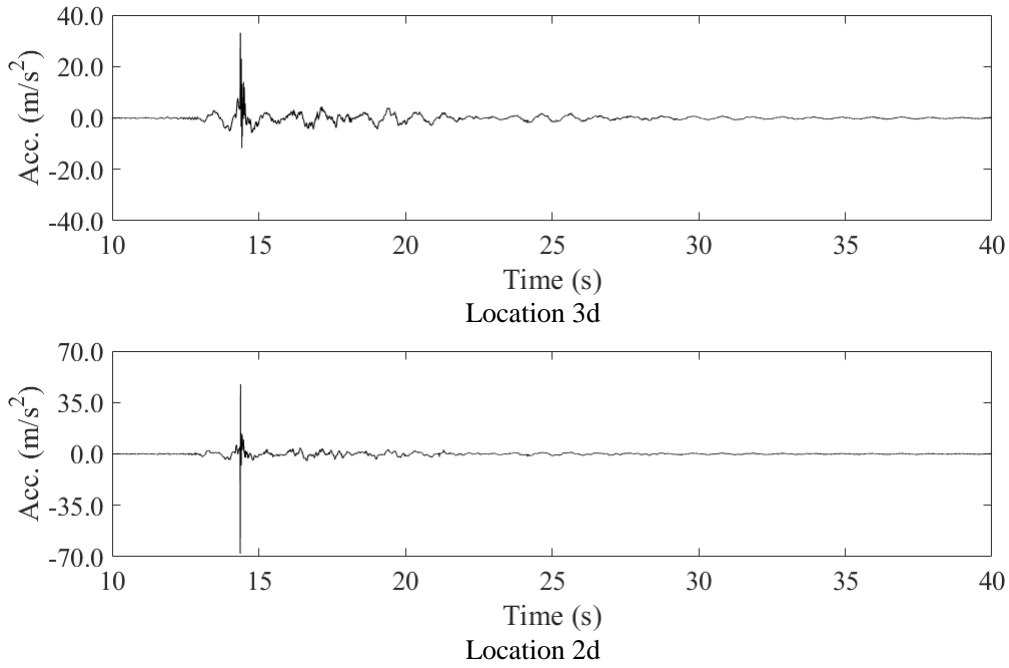


Figure 6-12 x-directional accelerations with extreme peak amplitudes in No.6 test

Table 6-8 Peak response amplitudes in the six tests

Test sequential No.	Fl.	x-dir.			y-dir.		
		Acc. (m/s ²)	Vel. ×10 ⁻¹ (m/s)	Disp. ×10 ⁻² (m)	Acc. (m/s ²)	Vel. ×10 ⁻¹ (m/s)	Disp. ×10 ⁻² (m)
1	5	3.35	3.86	4.44	Not discussed		
	4	2.96	3.32	3.82			
	3	2.67	2.49	2.77			
	2	1.99	1.32	1.37			
2	5				4.05	4.72	5.88
	4		Not discussed		3.63	4.08	5.01
	3				2.90	3.12	3.60
	2				2.07	1.76	1.81
3	5				4.92	6.10	7.64
	4		Not discussed		4.72	5.46	6.46
	3				4.48	4.20	4.60
	2				3.23	2.42	2.35
4	5	11.79	11.83	15.28	Not discussed		
	4	14.25	10.41	13.05			
	3	15.00	8.22	10.48			
	2	11.52	4.99	5.94			
5	5	9.96	8.98	11.41	10.86	11.75	16.39
	4	8.08	7.40	10.33	8.70	10.73	14.62
	3	11.54	5.61	8.18	8.15	8.31	10.88
	2	5.56	3.44	4.83	6.45	4.80	6.22
6	5	14.18	10.34	14.87	20.09	14.58	20.77
	4	22.29	9.48	13.64	17.42	12.21	17.22
	3	-	8.67	11.89	16.23	9.90	13.36
	2	-	6.53	7.28	-	7.84	10.12

6.6 Modal Properties Under the Shaking Table Tests

To investigate the changes of modal properties under different scales of ground motions, the modal identification method using the recursive Least Squares Method with a forgetting factor was employed to the recorded accelerations [2]. The identification method utilizes the single-input-four-output Auto-Regressive Exogenous (ARX) models: the input was the acceleration at Location 1d and the outputs were the accelerations at locations 2d, 3d, 4d and 5d. The forgetting factor was set at 0.998 to investigate the time variances of the 1st equivalent modal properties. Before the identification, the measured accelerations were bandpass-filtered with the bandwidth from 0.5 Hz to 2.0 Hz to fix the dimension for the ARX models to (2,2): the first 2 indicates two auto-regressive terms and the second 2 indicates three exogeneous input terms with the direct term. The identification was conducted in the horizontal direction independent of the other direction. A similar identification has already been applied to the past E-defence tests to understand the structural amplitude-dependency [3]. Figure 6-13 compares the time variances in the *x*-direction of the 1st *x*-directional mode under the Kobe waves in Nos.1, 4 and 6 tests. Then Figure 6-14 shows the time variances in the *y*-direction of the 1st *y*-directional mode under the OS2 waves in Nos.3 and 5 tests. The initial 10 s are neglected because of the warm-up period for the shaking.

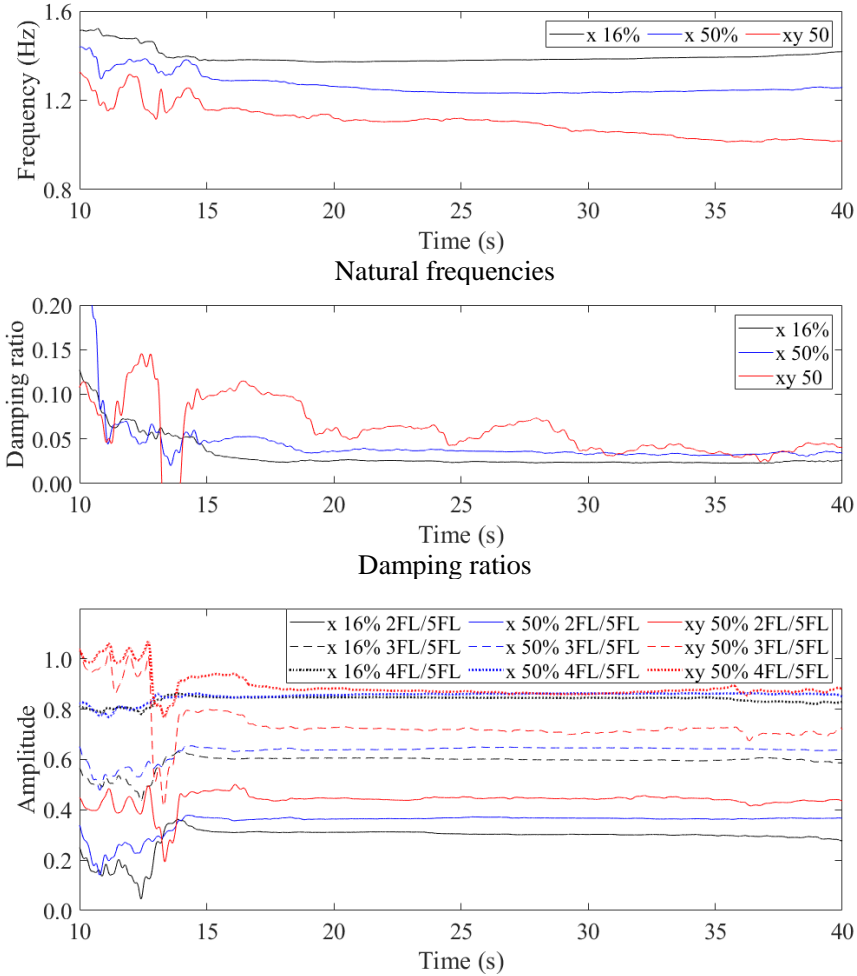
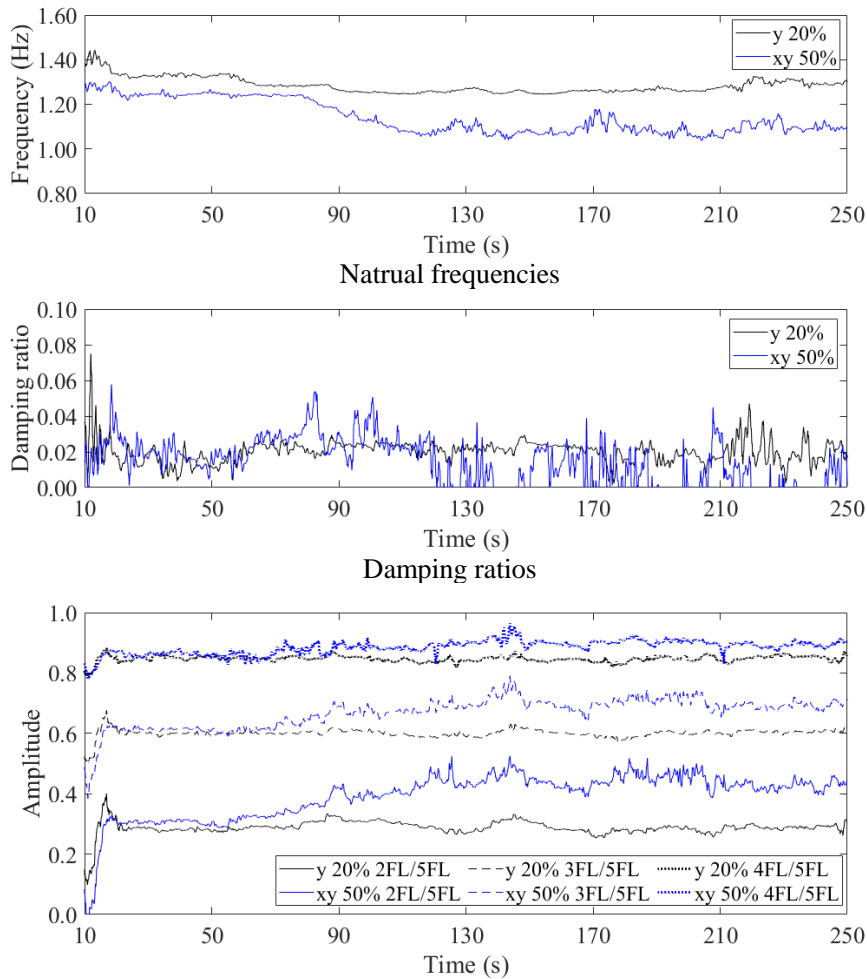


Figure 6-13 *x*-directional modal properties in the 1st mode under the Kobe waves



Mode shape amplitudes normalized by the amplitudes on the 5th floor
 Figure 6-14 y-directional modal properties in the 1st mode under the OS2 waves

As shown in Figures 6-13, the obvious decrease in the x -directional 1st natural frequency can be seen in the first 5 s (10 s to 15 s in the figure) in No.1 test when the excitation amplitude becomes large. The decreased 1st natural frequency might be caused by the invalidity of the non-structural components. In Nos.4 and 6 tests, the 1st natural frequencies in both x - and y -directions vibrate in the first 10s, it might be caused by the invalidity of non-structural damage and the structural damage. On the other hand, the 1st damping ratios in both x - and y -directions vibrate in the early 15 s under the three tests. A negative damping ratio around 13.5 s implies that the ARX model cannot understand the corresponding physical phenomena. The 1st natural frequency tends to decrease as the excitation scale increases while the relationship between the 1st damping ratio and different scales of ground motions is unclear. Under the Kobe waves, the 1st damping ratio increases when the scale of the input ground motion increases. However, the 1st damping ratio decreases when the scale of the input ground motion increases under the OS2 wave in Nos. 3 and 5 tests.

Table 6-9 compares the modal properties under different tests to the values identified from microtremor measurements. The modal properties identified during tests are averaged from 10 s to 40 s under the Kobe excitations and from 10 s to 250 s under the OS2 waves. The negative values in the damping ratios are set

as zeros when they are averaged. Since the locations where the microtremor measurements were taken are different from the locations that recorded the seismic responses, the 1st mode shape amplitudes at Locations a, b and c are averaged to compare to the amplitudes at Location d. The mode shape amplitudes are normalised to the amplitude on the 5th floor.

Table 6-9 shows that the mode shape amplitude on the 2nd floor increases in No.4 test comparing to the amplitudes in Nos.1 to 3 tests, which implies the structural damage in No.4 test. It was founded that the anchor bolts yielded in tension during No.4 test, the damage apparently softened the stiffness in the 1st story. The yielded anchor bolts were retightened after the test. As the scale of the ground motion increases, the mode shape amplitudes on the 2nd and 3rd floors become larger. The proposed seismic response prediction method assumes the mode shapes remain constant but the shaking table tests imply the limitation of the assumption in practical applications. However, the mode shapes in Nos.1 to 3 testes are consistent with the values from microtremor measurements, which implies the applicability of the proposed method when the structure is undamaged. This limited applicability is not against the objective of the proposed prediction method. The prediction method aims to provide seismic responses to improve the efficiency of building checking, building users can evaluate the structural condition by their eyes when a building has obvious structural damage.

Table 6-9 Comparison of modal properties between under microtremor measurements and earthquakes

Dir.		Natural frequency (Hz)	Damping ratio (%)	Modal amplitude normalized to 5th floor				Averaging time
				2	3	4	5	
x	Microtremor	1.65	1.0	0.32	0.60	0.84	1.00	
	1	1.40	3.2	0.29	0.59	0.84	1.00	10–40 s
	2			Not discussed				
	3			Not discussed				
	4	1.27	4.4	0.35	0.63	0.85	1.00	10–40 s
	5	1.20	4.2	0.38	0.66	0.86	1.00	10–250 s
	6	1.11	6.1	0.44	0.74	0.89	1.00	10–40 s
y	Microtremor	1.57	1.0	0.29	0.64	0.85	1.00	
	1			Not discussed				
	2	1.30	3.0	0.25	0.58	0.84	1.00	10–40 s
	3	1.28	2.0	0.29	0.60	0.85	1.00	10–250 s
	4			Not discussed				
	5	1.14	2.0	0.39	0.67	0.88	1.00	10–250 s
	6	1.04	3.9	0.48	0.67	0.88	1.00	10–40 s

6.7 Verification with Different Intensities of Ground Motions

The applicability of the proposed seismic response prediction method is tested by comparing the predicted responses to the recorded responses. Two scenarios are considered in the seismic response prediction: One assumes that an observation system is installed at the objective building. The input ground motion and the accelerations at some locations are available so that the natural frequencies and damping ratios can be updated, then the prediction method is utilized to predict seismic responses at unmonitored locations; The other scenario assumes only the input ground motion is available, then the natural frequencies and damping

ratios are modified by factors based on engineering experience as briefly introduced in Chapter 2. The second scenario requires a few sensors for the ground motion monitoring so it is economic-friendlier. Apart from the two scenarios, the seismic response prediction directly using the modal properties from microtremor measurements is firstly performed. It demonstrates the necessity of considering modal property variances in the seismic response prediction.

As shown in Figure 6-2, the sensors that recorded the seismic responses were different from the locations where the microtremor measurements were taken. Therefore, the mode shapes at Location d on each floor are approximated by the averaged mode shapes at Locations a, b and c on the same floor. Then the seismic responses at Location d can be predicted and compared to the recorded responses. In addition, the torsional modes are neglected in the mode superposition. As a result, the 1.65 Hz, 4.91 Hz and 8.39 Hz modes are used for the x -directional prediction. The 1.57 Hz and 4.79 Hz mode are used for the y -directional prediction. As noted in Section 6.4, two sets of approximated participation vector are utilized, which are the Cases 0 and 2 in Table 6-5. Although the prediction does not use the torsional mode in the mode superposition, the participation vector is approximated by using the five modes in the x -direction and four modes in the y -direction including the identified torsional modes. Since the sampling frequency was 200 Hz, the average acceleration method with the time interval of 0.005 s is utilized to solve the modal equations of motion.

6.7.1 Using unmodified modal properties

To demonstrate the influence of neglecting modal property variances on the seismic response prediction accuracy, the seismic responses are predicted by directly using the modal properties from microtremor measurements. Figures 6-15 shows the prediction results of the seismic response amplitudes in Nos.1 to 3 tests where structural damage did not occur. Then Figure 6-16 shows the prediction results in Nos.4 to 6 where structural damage occurred during the tests. Table 6-10 summarizes the averaged prediction errors. The damping ratios are assumed frequency-proportional and set as 1% in the 1st modes based on the modal identification results in Section 6.3. Since the recorded x -directional accelerations on the 2nd and 3rd floors and the y -directional acceleration on the 2nd floor had extreme peaks in No.6 test, they are not involved in the comparison.

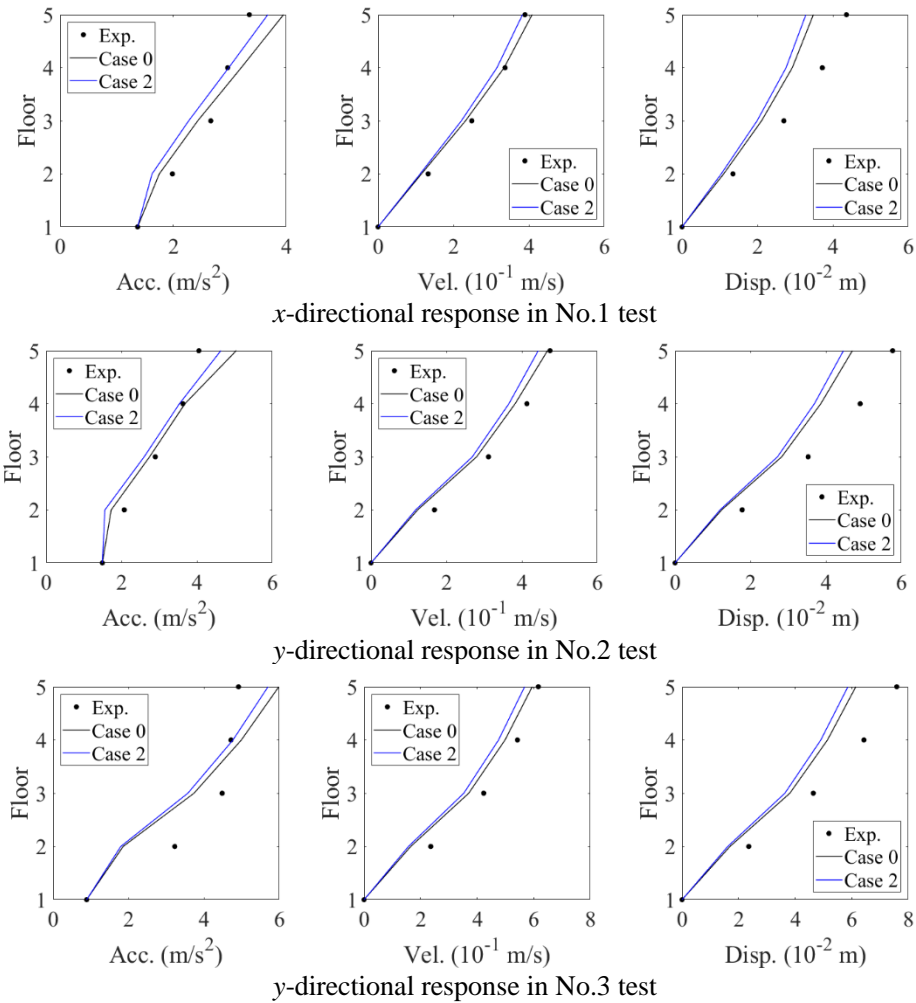


Figure 6-15 Response prediction using unmodified modal properties in tests where no structural damage occurred

In Nos.1 to 3 tests where no structural damage occurred, the averaged errors of velocity and displacement amplitudes are around 20% and the averaged acceleration amplitude errors are mostly under 10%. The accuracy is more likely a coincidence caused by the complicated interaction of evidently factors: the natural frequency and damping ratio variances; the participation vector errors and the truncation errors in the mode superposition. The errors of velocity and displacement amplitudes in Nos.1 to 3 tests are larger than the acceleration errors, which is mainly caused by the difference of the actual natural frequencies under shaking excitations and the identified ones under the microtremor. The prediction errors significantly increase in Nos.4 to 6 tests where structural damage occurred. However, the prediction accuracy in the y -direction is obviously better than x -direction even though the utilized natural frequencies, damping ratios and mode shapes have large variances. The accuracy differences in the x - and y -directions in Nos.4 to 6 tests implies the complicated interaction of the three factors.

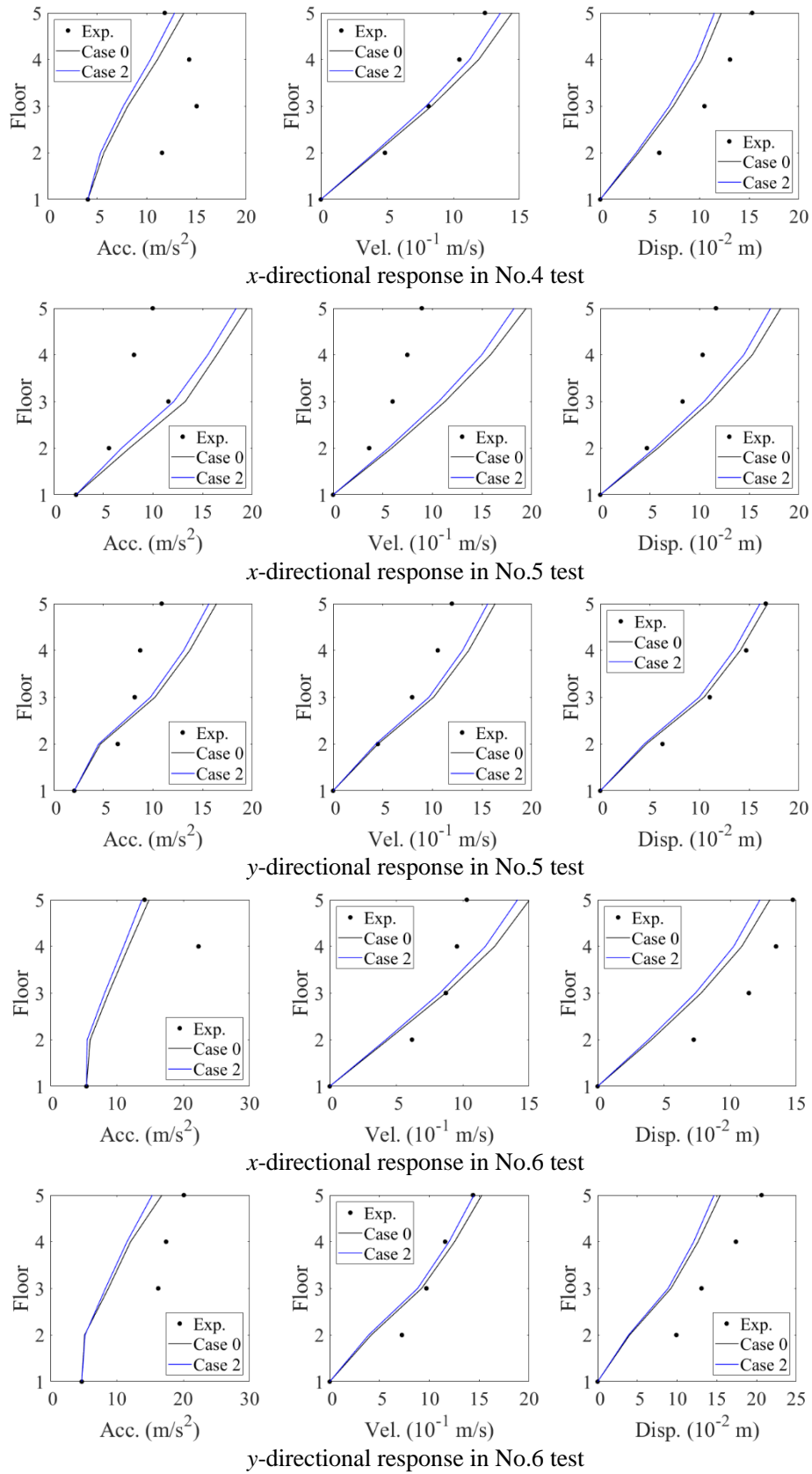


Figure 6-16 Response prediction using unmodified modal properties in tests where structural damage occurred

Table 6-10 Averaged prediction errors using unmodified modal properties

Test Seq. No.	x-dir.			y-dir.		
	Acc. (%)	Vel. (%)	Disp. (%)	Acc. (%)	Vel. (%)	Disp. (%)
1	+1	-3	-22	Not discussed		
	-6	-8	-27			
2	Not discussed			+1	-12	-24
				-6	-16	-27
3	Not discussed			-8	-14	-21
				-12	-18	-25
4	-26	+6	-27	Not discussed		
	-30	+0	-31			
5	+62	+100	+41	+27	+20	-8
	+51	+89	+33	+21	+15	-12
6	-21	+11	-28	-31	-12	-36
	-27	+5	-32	-35	-16	-39

Note: upper lines correspond to Case 0 and lower lines correspond to Case 2

6.7.2 Using updated modal properties

The averaged 1st natural frequency and the 1st damping ratio under the six tests in Table 6-9 are utilized. The natural frequencies in the higher modes are scaled down proportionally based on the decreased 1st natural frequency. The damping ratios are assumed frequency-proportional to obtain damping ratios in higher modes. The predictions of seismic response amplitudes are in Figures 6-17 and 6-18, then the averaged errors are summarized in Table 6-11.

The comparisons between Figure 6-15 to Figure 6-17, Table 6-10 to 6-11 show the significantly improved prediction accuracy especially in velocity and displacement amplitudes in Nos.1 to 3 tests where the structure was not damaged. The significantly reduced averaged velocity and displacement amplitude errors in Table 6-11 again implies that the high acceleration amplitude accuracies in Table 6-10 are just coincidences. As described in Chapter 1, some references verified their proposed prediction methods for high-rise buildings and accuracy is within 20% for amplitude evaluation on each floor [4-7]. The prediction using updated modal properties exhibit nearly the same level of error in Nos. 1 to 3 tests. The prediction differences between using approximated participation vectors from Cases 0 and 2 are small, it is because the 1st mode is most excited mode while the difference between Cases 0 and 2 is small in the 1st mode.

When structural damage occurred on lower floors in Nos.4 to 6 tests, the changes in the equivalent 1st mode shapes imply the large prediction errors. In addition, the building became nonlinear and utilized linear model in the prediction method might be inadequate. The significantly increased acceleration prediction errors suggest the limited application of the proposed prediction method for acceleration amplitude evaluation.

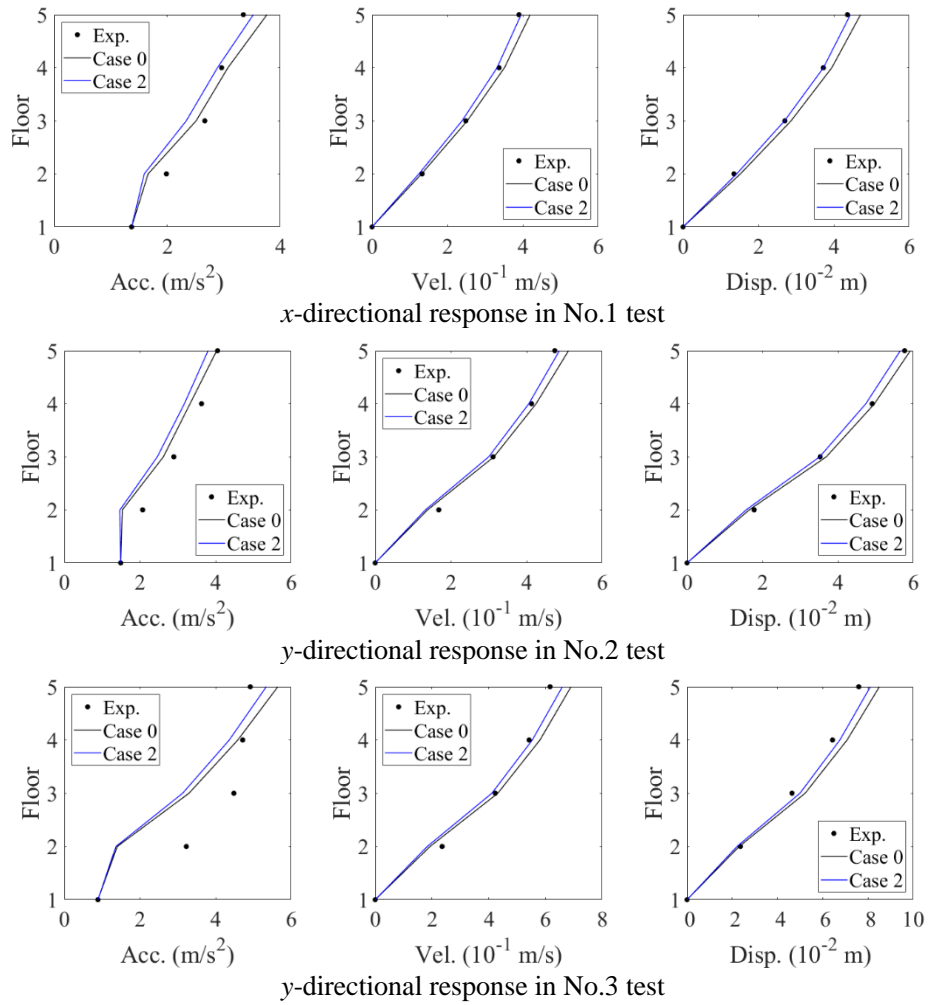


Figure 6-17 Response prediction using updated modal properties in tests where no structural damage occurred

Table 6-11 Averaged prediction errors using updated modal properties

Test Seq. No.	x-dir.			y-dir.		
	Acc. (%)	Vel. (%)	Disp. (%)	Acc. (%)	Vel. (%)	Disp. (%)
1	-1	+4	+6	Not discussed		
	-7	-2	-0			
2	Not discussed			-11	-2	-2
				-16	-6	-6
3	Not discussed			-18	+1	+8
				-22	-4	+3
4	-33	+21	+16	Not discussed		
	-37	+14	+10			
5	-30	+15	+16	-19	+7	+12
	-35	+9	+10	-23	+2	+7
6	-40	+9	+19	-51	-7	+6
	-45	+3	+13	-54	-11	+2

Note: upper lines correspond to Case 0 and lower lines correspond to Case 2

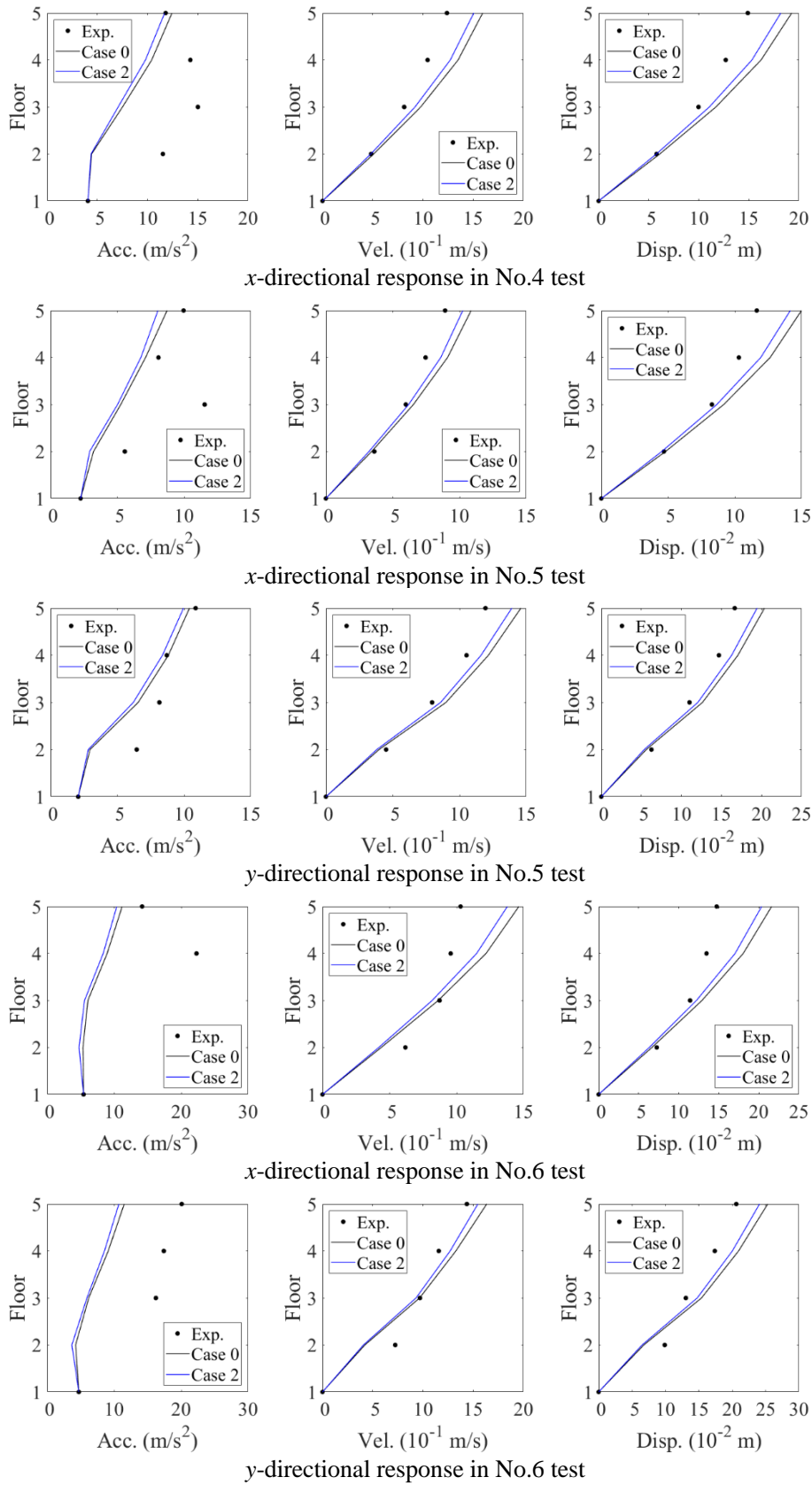


Figure 6-18 Response prediction using updated modal properties in tests where structural damage occurred

6.7.3 Using modified modal properties

One of the advantages of the proposed prediction method is that it does not necessarily require sensors installed at the measured building to obtain seismic responses at some locations. The natural frequencies and damping ratios from measurements can be modified based on existing researches. As introduced in Chapter 2, the decrease of the 1st natural frequency is generally around 10% to 20% for steel structure when no structural damage occurs. Therefore, the natural frequencies from measurements are scaled down by 15%. The damping ratios are assumed frequency-proportional and set as 2% for the prediction in Nos.1 to 3 tests. Further decreases in natural frequencies and increases in damping ratios are expected when structural damage occurs, so the natural frequencies are scaled down by 30% and the damping ratios are set as 3% for the prediction in Nos.4 to 6 tests.

When the natural frequencies are scaled down by 15%, the decreased 1st x -directional natural frequency is 1.40 Hz, which is actually identical to the identified value in No.1 test shown in Table 6-9. However, the utilized 1st damping ratio is 1% smaller. The prediction results in No.1 test help to demonstrate the influence of the damping ratio variances on the prediction accuracies. In No. 3 test, the modified 1st natural frequency is 0.05 Hz lower than the actual value while the utilized 1st damping ratio is similar. The prediction results in No.3 test help to demonstrate the influence of the natural frequency variances on the prediction accuracies. The major difference between updating and modifying modal properties is that the former considers the different changes in the x - and y -directions while the latter uses fixed factors to simultaneously adjust the utilized natural frequencies and damping ratios in the x - and y -directions. As result, modal property variances are inevitable when using modified modal properties but the variances are smaller than directly using the modal properties from microtremor measurements. The amplitude prediction results are in Figures 6-19 and 6-20, then the averaged errors are summarized in Table 6-12.

The comparisons between Figure 6-17 to Figure 6-19, Table 6-11 to 6-12 show the significantly increased prediction errors with small modal property variances in Nos.1 to 3 tests where the structure was not damaged. The 1% damping ratio variance in the 1st mode increases the averaged velocity and displacement errors from below 10% in Table 6-11 to around 20% in No.1 test in Table 6-12. On the other hand, the 0.05 Hz natural frequency variance in the 1st mode leads to more significant prediction errors in No.3 test as shown in Tables 6-11 and 6-12. The prediction accuracy in No.2 test is the best comparing to Nos.1 and 3 tests even though the utilized natural frequencies and damping ratios both have variances. When structural damage occurred in Nos.4 to 6 tests, the prediction accuracies are significantly decreased. It is because the natural frequency and damping ratio estimation becomes more difficult since they depend on the level of structural damage, which relates to the input ground motion amplitude.

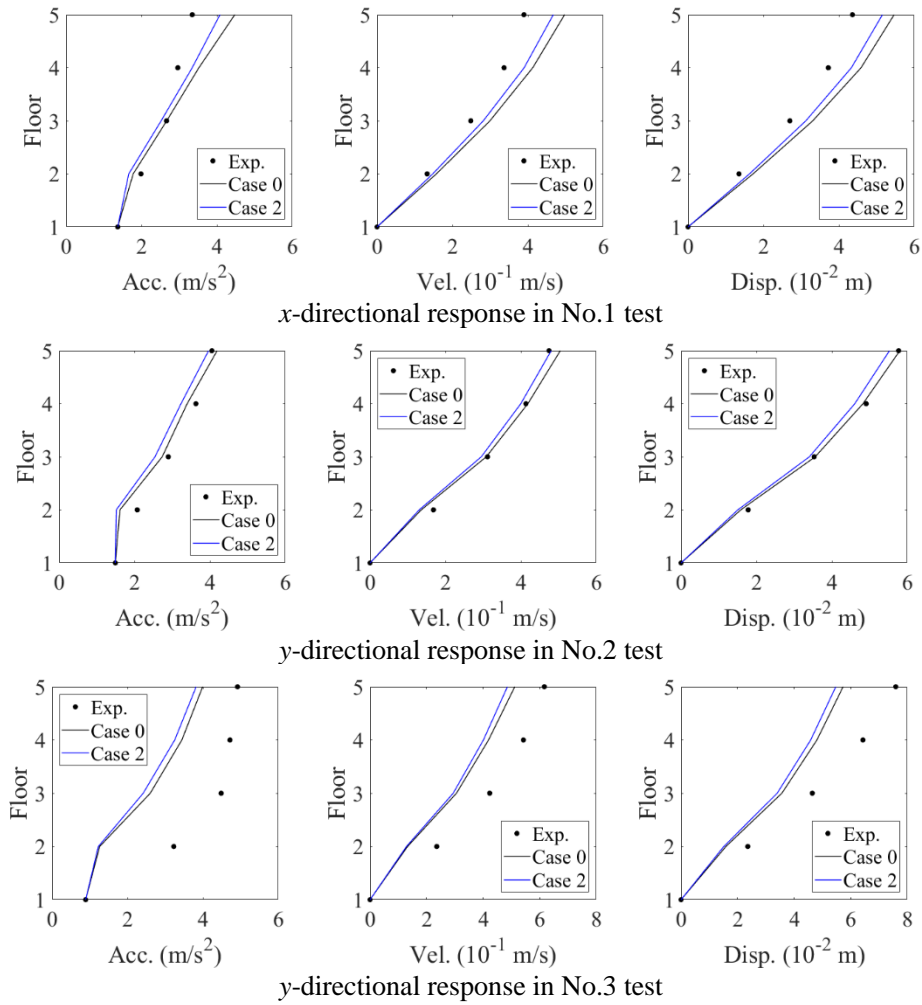
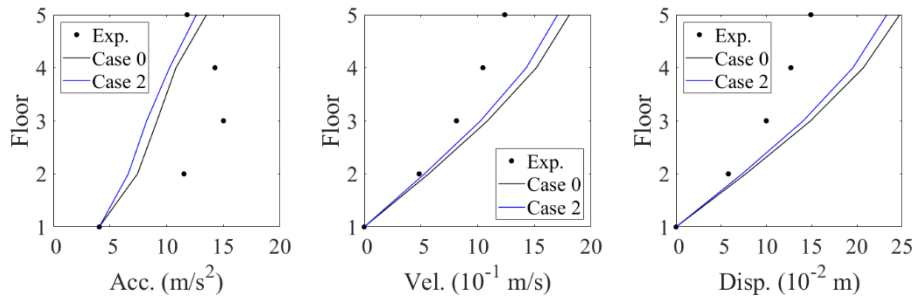


Figure 6-19 Response prediction using modified modal properties in tests where no structural damage occurred

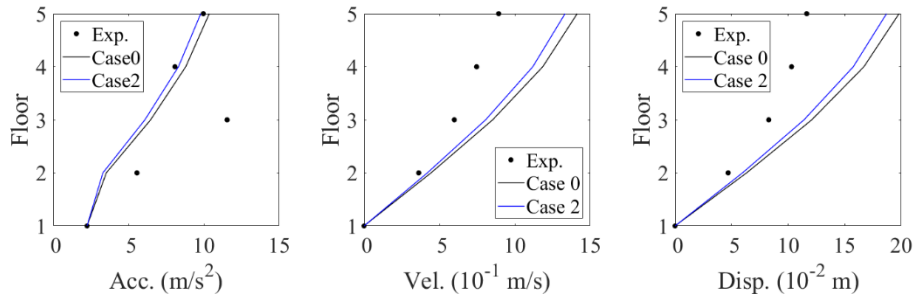
Table 6-12 Averaged prediction errors using modified modal properties

Test Seq. No.	x-dir.			y-dir.		
	Acc. (%)	Vel. (%)	Disp. (%)	Acc. (%)	Vel. (%)	Disp. (%)
1	+11	+23	+22	Not discussed		
	+3	+16	+15			
2	Not discussed			-8	-4	-5
				-13	-8	-9
3	Not discussed			-37	-28	-26
				-40	-31	-30
4	-21	+36	+48	Not discussed		
	-27	+28	+40			
5	-17	+50	+53	-24	-1	+12
	-22	+41	+45	-27	-6	+7
6	-30	+34	+31	-42	+2	+8
	-35	+26	+24	-47	-3	+4

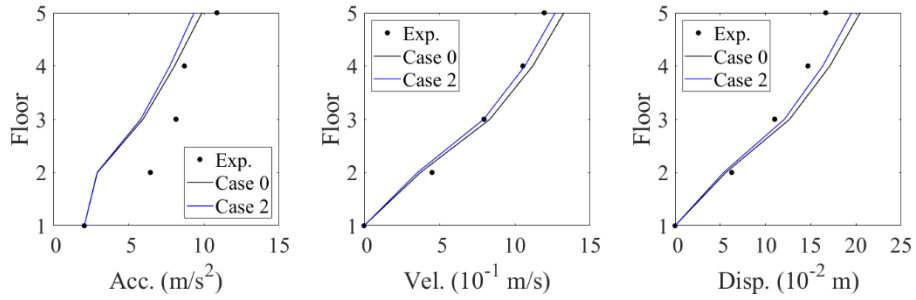
Note: upper lines correspond to Case 0 and lower lines correspond to Case 2



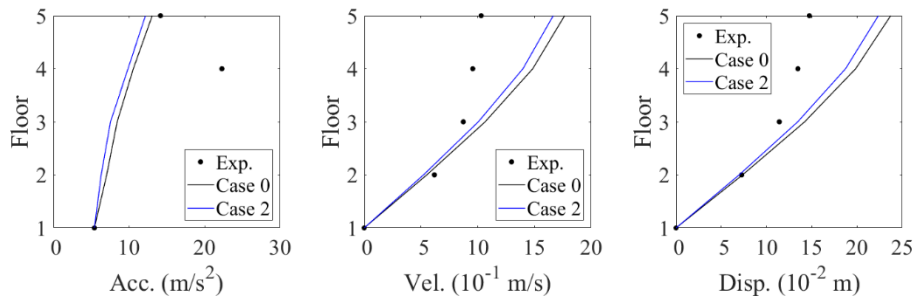
x-directional response in No.4 test



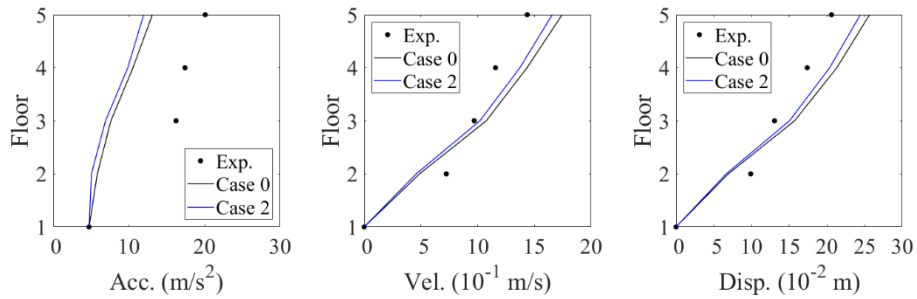
x-directional response in No.5 test



y-directional response in No.5 test



x-directional response in No.6 test



y-directional response in No.6 test

Figure 6-20 Response prediction using modified modal properties in tests where structural damage occurred

Figure 6-21 shows the relationship between the predicted acceleration amplitudes on the 5th floor and the utilized 1st natural frequency with 2% or 3% 1st damping ratio in Nos.1 to 3 tests. It helps to understand the significantly increased errors in Nos.1 and 3 tests and the small errors in No.2 test when using the modified modal properties.

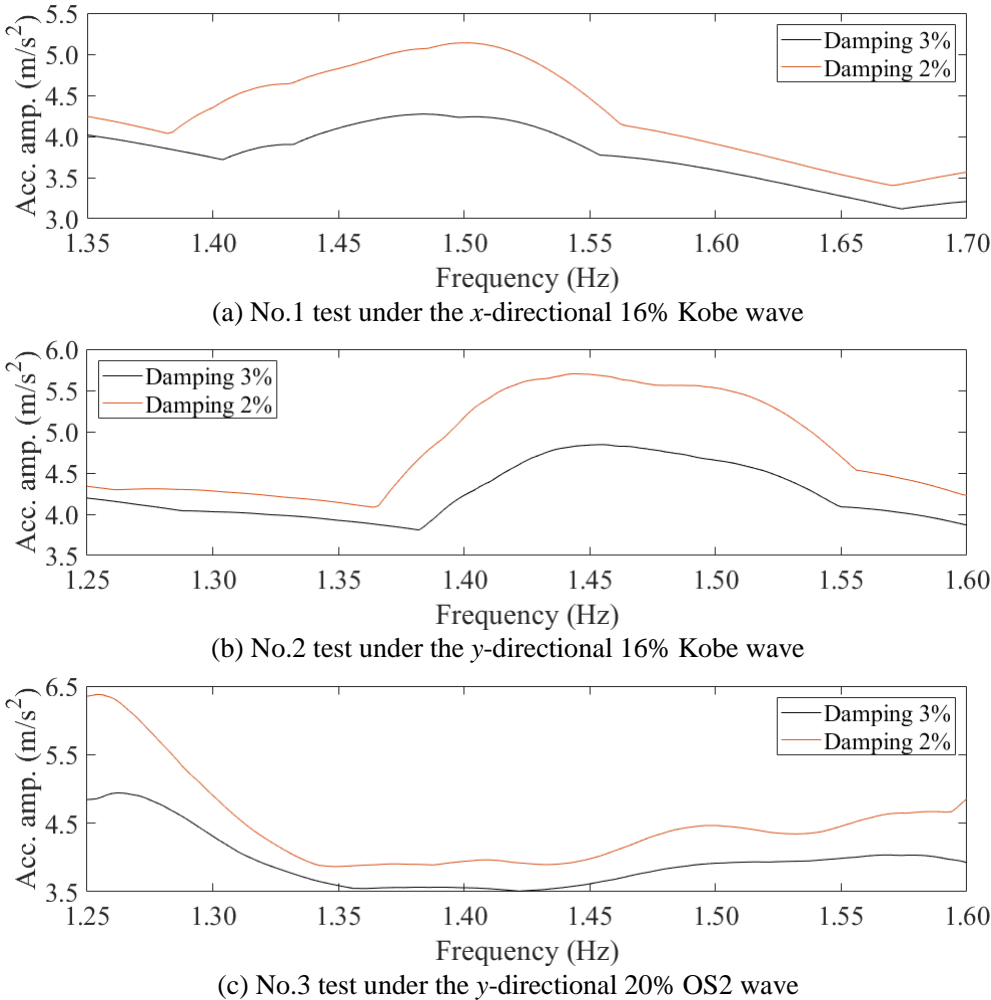


Figure 6-21 Predicted acceleration amplitudes corresponding to different natural frequencies and damping ratios

Figure 6-21(a) suggest that the influence from the 1st damping ratio variance is different under different frequency range. For example, the influence from the 1st damping ratio variance is larger when the utilized 1st natural frequency is within 1.40 Hz to 1.55 Hz in No.1 test. The influence is smaller when the frequency is within 1.35 Hz to 1.40 Hz. The prediction errors are significantly increased in No.1 test when having 1% damping ratio variance in the 1st mode because the utilized 1st natural frequency is 1.40 Hz. On the other hand, the predicted response amplitudes might be very sensitive to the 1st natural frequency variance when the frequency is within a certain range under a specific ground motion. For example, the predicted amplitudes are sensitive to the frequency variance when the frequency is within the 1.25 Hz to 1.35 Hz under the OS2 wave in Figure 6-21(c) but insensitive under the Kobe wave in Figure 6-21(b). As a result,

the prediction errors are large under the No.3 test and small under the No.2 test even though the natural frequency variances exist in the two cases.

Figure 6-21, Figures 6-17 to 6-19, Tables 6-11 and 6-12 suggest that the prediction using modified modal properties is possible to have large prediction errors. The possibility of the significantly increased prediction errors due to the small modal property variances is also implied in the seismic response spectra in Figure 6-7. For example, the responses are sensitive to the 1st natural period when it is around 0.7s under the Kobe wave in Figure 6-7. The modal property variances are inevitable when the modal properties are modified by fixed factors. Even if the modified modal properties in one direction are accurate, the modified modal properties in the other direction might be not. Therefore, it is recommended to install an observation system for the modal property updating in practical situations instead of modifying modal properties based on engineering experience to better prediction accuracy.

6.8 Conclusions

The applicability of the proposed seismic response prediction method is studied by the shaking table tests of a 4-story steel specimen. The main objective is to investigate how the modal property variances influence prediction accuracy. The considered modal property variances are the natural frequency and damping ratio variances between under measurements and an earthquake. The main conclusions of this chapter are summarized below.

- (1) The mode shapes of the specimen were obtained before the shaking table tests. The sums of approximated participation functions on both higher and lower floors are similarly close to unity when using the mode shapes on all floors. However, lower values are expected on lower floors when using a limited number of modes. On the other hand, using mode shapes on upper floors is preferable from the sums of approximated participation functions viewpoint.
- (2) The natural frequency and damping ratio variances are observed in the shaking table tests even if the specimen has no structural damage. The mode shapes under the tests are consistent with the ones from measurement when no structural damage occurred, which implies the applicability of the prediction method when the structure mostly exhibits elastic response.
- (3) The seismic response amplitude prediction errors when using the updated modal properties are around 20% on average in the tests where structural damage did not occur. The prediction results are similar when the utilized participation vectors are approximated by the mode shapes on all floors or upper floors. The averaged errors of acceleration amplitude increase to around 40% in the tests where structural damage occurred even if the equivalent modal properties are updated. The limited applicability does not influence the objective of the prediction method because it aims to provide information for building condition evaluation when no obvious damage is observed from appearance.
- (4) The seismic response prediction accuracies using modified modal properties suggest that small modal property variances might lead to large prediction errors even if structural damage does not occur. In one test, the averaged prediction error in acceleration amplitudes is increased from around 20% to around 40% when having 0.05 Hz frequency variance in the 1st mode. In another test, the averaged

prediction errors in velocity and displacement amplitudes are increased from below 10% to around 20% due to the 1% damping ratio variance in the 1st mode. Therefore, it is recommended to install an observation system to obtain input ground motions and seismic responses at some locations to update the modal properties, then the proposed seismic response prediction estimates the seismic responses at other locations.

Reference

- [1] Ikeda Y, Kurata M, Xie J (2022): Verification of multi-degree-of-freedom building modelling for seismic response prediction based on microtremor measurement, *Earthquake Engineering & Structural Dynamics*, Vol.51(7), pp.1610-1635.
- [2] Loh CH, Lin HM (1996): Application of off-line and on-line identification techniques to building seismic response data, *Earthquake Engineering & Structural Dynamics*, Vol.25, pp.269–290.
- [3] Ikeda Y (2016): Verification of system identification utilizing shaking-table tests of a full-scale 4-story steel building, *Earthquake Engineering & Structural Dynamics*, Vol.45, pp.543–562.
- [4] Ikeda Y, Hisada Y (2013): Earthquake responses on all floors in a building estimated by observation records on some restricted floor, *Journal of Japan Association for Earthquake Engineering*, JAEE, Vol. 13(4), pp.38-54 (in Japanese).
- [5] Hatada T, Ikeda Y, Hagiwara H, Nitta Y, Nishitani A (2018): Damage evaluation method based on acceleration measurement on some restricted floors, *Proceedings of the 16th European Conference on Earthquake Engineering* (Thessaloniki, Greece), 12 pages, Paper ID: 10305.
- [6] Morii T, Okada K, Shiraishi M, Sugimoto K, Terada T, Sato T, Tobita J (2016): Seismic response estimation of whole building based on limited number of acceleration records for structural health monitoring system shortly after an earthquake-system application for large shaking table test of an 18-story steel building, *Journal of Structure Construction Engineering*, AIJ, Vol.81(730), pp.2045-2055 (in Japanese).
- [7] Koderu K, Nishitani A, Okihara Y (2018): Cubic spline interpolation based estimation of all story seismic responses with acceleration measurement at a limited number of floors, *Journal of Structure Construction Engineering*, AIJ, Vol.83(746), pp. 527-535 (in Japanese).

Chapter 7

Conclusions

7.1 Summaries

For building structures, this thesis proposes a seismic response prediction method based on microtremor measurement. The prediction method estimates seismic responses at many locations on each floor. The provided information contributes to structural health monitoring when the structural damage cannot be judged from the building outlook just after an earthquake. The objective building is modelled by modal equations of motion and the modal properties are based on the identified values from microtremor measurements. The method has three advantages: (1) It does not require design documents to establish the mass, damping and stiffness matrices to formulate equations of motion; (2) It does not necessarily require instrumented sensors for the seismic response recording; and (3) It can be used for buildings that the rigid-floor assumption is not applicable to.

In Chapter 2, the dynamic characteristics of large-scale low-rise buildings are investigated by applying microtremor measurements to six commercial buildings in Japan. The identified mode shapes show the inapplicability of the rigid-floor assumption for this kind of structure. The mode shape amplitudes at the two sides of the expansion joints (EXP.Js), atria and skylights are in opposite directions in some identified modes. Local modes are also found in large areas like dining areas, and sub-areas divided by the EXP.Js, atria and skylights. As a result, the new seismic response prediction method to consider floor flexibility is expected. The identified 1st natural frequencies are different from the estimated values from the Building Standard Law in Japan. The variances vary from 40% lower to 50% higher. The identified damping ratios in 1st global modes are consistent with the commonly observed values in high-rise buildings.

In Chapter 3, the seismic response prediction method based on microtremor measurement is proposed in consideration of the dynamic natures described in Chapter 2. The proposed method measures multiple locations on each floor. The measured building is modelled as the multi-degree-of-freedom (M-DOF) linear model and the modelling assumes that masses are lumped at the measured locations to consider floor flexibility. The modal equations of motion are utilized for the seismic response prediction. The natural frequencies, the corresponding damping ratios and the mode shapes in limited modes are determined by the identified modal properties from microtremor measurements. The participation vector is approximated only by the identified mode shapes. The proposed participation vector approximation method does not require estimating the mass matrix so the prediction method does not rely on the traditional stick-shape lumped mass model. Two models with different dimensions are available based on the identification results. The two-dimensional (2D) model is recommended when a same natural frequency is simultaneously identified

in the two horizontal directions and the corresponding mode shape shows lateral-torsional coupling, or else the single-dimensional (1D) model is utilized in the seismic response prediction.

In Chapter 4, the fundamental properties of the proposed prediction method are explored by the numerical simulation of a 5-DOF model. When mode shapes at all nodes are used, the participation vector approximation has high accuracy even if only a few modes are available. The participation vector is approximated by the mode shapes at the measurement points in practical situations, which means the participation vector is approximated by the mode shapes at selected nodes. The node selection indeed influences the approximation accuracy but has less influence on lower modes. The approximation accuracy is generally improved by having more nodes (measurement points). The use of all identified modes does not necessarily produce higher accuracy in the participation vector approximation than the use of some identified modes when only limited nodes are selected. The seismic response prediction accuracy is high even if only using a few lower modes when not considering the modal property variances. However, the use of more modes does not necessarily lead to higher seismic response prediction accuracy when mode shapes at limited nodes are utilized.

In Chapter 5, the prediction method is further verified by using the numerical model of the large-scale low-rise building. The numerical model shows floor flexibility and the used mode shapes show lateral-torsional coupling with large amplitudes in both horizontal directions. In the participation vector approximation, the 2D model has higher accuracy than the 1D model because the 2D model utilizes the two directional mode shape components simultaneously to approximate the participation vector in one direction. When the input ground motion is single-directional and only the same directional responses are evaluated, the 2D model has higher seismic response prediction accuracy because of the higher participation vector approximation accuracy. However, the prediction accuracies at some locations are lower under certain ground motions when some modes with large amplitudes at those locations are neglected. The prediction accuracy using the 1D model is further decreased when the input ground motion becomes two-directional because the 1D model cannot consider the vibrations induced by orthogonal ground motions.

In Chapter 6, the prediction method is verified by the full-scale shaking table tests of the 4-story steel specimen under different scales of ground motions. The tests also explore the influences of modal property variances on prediction accuracy. The modal property variances here mean the natural frequency and damping ratio variances between under microtremor measurements and an earthquake. The microtremor measurements were taken before the tests began and the participation vector is approximated by the identified mode shapes. Based on the sums of approximated participation functions on different floors, the use of mode shapes on upper floors is preferable. The mode shapes under the tests are consistent with the ones from microtremor measurements when no structural damage occurred, which implies the applicability of the prediction method when the structure mostly exhibits elastic response. The proposed seismic response prediction method considers two scenarios in practical situations: (1) One scenario assumes an observation system is installed at the objective building so that the seismic responses at some locations are available. Then the natural frequencies and damping ratios can be updated and the prediction method evaluates the seismic responses at unmonitored locations. When using the updated modal properties, the

prediction errors of seismic response amplitudes are around 20% on average in the tests where structural damage did not occur. The prediction results are similar when the utilized participation vectors are approximated by the mode shapes on all floors or upper floors. The averaged errors of acceleration amplitudes increase to around 40% in the tests where structural damage occurred even if the equivalent modal properties are updated; (2) The other scenario assumes only the input ground motion is available and the modal properties from microtremor measurements are modified by factors based on engineering experience, the tests show that the small modal property variances are possible to cause large prediction errors. In one test, the averaged prediction error in acceleration amplitudes is increased from around 20% to around 40% when having 0.05 Hz frequency variance in the 1st mode. In another test, the averaged prediction errors in velocity and displacement amplitudes are increased from below 10% to around 20% due to the 1% damping ratio variance in the 1st mode. Therefore, it is recommended to install an observation system to update modal properties for better prediction accuracy.

Finally, the thesis concludes that: (1) The seismic response prediction method considering floor flexibility is required according to the microtremor measurements to six actual commercial large-scale low-rise buildings; (2) The seismic response prediction method based on microtremor measurement is proposed to estimate seismic responses at measured locations, multiple locations are measured on each floor to consider floor flexibility; (3) The fundamental properties of the proposed prediction method are explored by the numerical simulation of a simple model; (4) Then the applicability of the prediction method to buildings that exhibit floor flexibility is verified by the numerical simulation of a complicated model that represents a large-scale low-rise building; and (5) The performance of the prediction method in practical situations is examined by the shaking table tests.

The prediction method has high prediction accuracy when the objective building exhibits elastic response and an observation system is installed to update the natural frequencies and damping ratios from microtremor measurements. This limited applicability is still useful for the building owners and users from the structural health monitoring viewpoint because they can observe structural damage from the building outlook in the events of a strong nonlinear case.

7.2 Future Studies

The future studies relating to the proposed seismic response prediction method include two aspects. One aspect exclusively relates to the proposed prediction method and the other aspect is a general issue that different microtremor measurement-based prediction methods have in common.

In the proposed seismic response prediction method, floor flexibility is considered by setting multiple nodes on each floor. The nodes are lumped at the locations where the microtremor measurements are taken. In practical situations, every location on a floor is candidate to measure while only limited locations can be measured. The participation vector of the objective building is approximated by the mode shapes at measured locations and it is possible that different sets of measured locations lead to different approximation results. In the thesis, the influence from the selection of the measured locations, or measurement point selection, is discussed by numerical simulations. However, a theoretical analysis is

expected to further understand how the selection influence the participation vector approximation. Although the measurement points are determined solely based on the planar view of the objective building in practical situations, an optimal measurement point design is still expected.

There also exists a common problem in the microtremor measurement-based seismic response prediction method, which is the modal property variance problem. The modal property variance is a common issue when a prediction method uses mode superposition. As discussed in Chapter 6, the natural frequency and damping ratio variances are inevitable even if the building has no structural damage. The shaking table tests also reveal that small modal property variances can lead to large prediction errors. In addition, the decreased scale of the 1st modes in the horizontal directions are generally different. It is difficult to directly modify the modal properties identified from microtremor measurements by fixed factors. Nonetheless, the seismic response prediction without installing sensors at the objective building for seismic response recording is attractive and surely widen the applicability of the proposed seismic response prediction method.

Publications

Journal papers

- [1] Xie J, Ikeda Y, Kurata M (2021): Dynamic properties of large-scale low-rise commercial buildings based on microtremor measurements, *Journal of structural engineering*, AIJ, Vol. 67(B), pp.495-507. (in Japanese)
- [2] Xie J, Ikeda Y, Kurata M (2021): Multi-degree-of-freedom linear building model based on microtremor measurement for seismic response analysis, *Journal of structural engineering*, AIJ, Vol.67(B), pp.509–518. (in Japanese)
- [3] Ikeda Y, Kurata M, Xie J (2022): Verification of multi-degree-of-freedom building modelling for seismic response prediction based on microtremor measurement, *Earthquake Engineering & Structural Dynamics*, Vol.51(7), pp.1610-1635.

Conference papers

- [1] Xie J, Ikeda Y, Kurata M (2020): Dynamic Characteristic of Long Two-story Building with Large Atria and Skylights. *Annual Meeting*, Disaster Prevention Research Institute, Kyoto University, 2 pages, Paper ID: B26, <https://www.dpri.kyoto-u.ac.jp/hapyo/20/pdf/B26.pdf>. (accessed on 5 August 2022)
- [2] Xie J, Ikeda Y, Kurata M (2020): Dynamic Characteristic of Long Two-story Building with Large Atria and Skylights: *Summaries of Technical Papers of Annual Meeting Kinki Branch AIJ*, pp.77-80. (in Japanese)
- [3] Xie J, Ikeda Y, Kurata M (2020): Dynamic Characteristic of Long Two-story Building with Large Atria and Skylights. *Summaries of Technical Papers of Annual Meeting AIJ*, pp.543-544. (in Japanese)
- [4] Xie J, Ikeda Y (2021): Seismic Response Prediction of Large-scale Low-rise Buildings Based on Microtremor Measurement. *Summaries of Technical Papers of Annual Meeting Kinki Branch AIJ*, 4 pages, Paper ID: 2066.
- [5] Xie J, Ikeda Y, Kurata M (2021): Modal identification of large-scale low-rise buildings through microtremor measurements, *Proceedings of the 14th World Conference on Earthquake Engineering* (Sendai, Japan), 12 pages, Paper ID: 3b-0015.

Acknowledgements

I firstly want to express my gratitude to my supervisor, Professor IKEDA Yoshiki, for his patient guidance through my Ph.D program. He is a responsible mentor that teaches me a lot in many aspects. His knowledge and experience in engineering make my research meaningful in practice.

I'm also grateful for the kind supports and helpful suggestions from my doctoral committee members, Professor SAKAI Yuki and Professor FUJITA Kohei. It is difficult for me alone to be aware if my thesis can be understood by others and your comments help me to make my thesis easier to understand.

Then, I want to extend my appreciation to Professor KURATA Masahiro and Mrs. GAMOU Chisato. Professor KURATA is a nice person who keeps our morale high. Our office secretary, Mrs. GAMOU, has always been a strong supporter for us, especially for the foreign students, to deal with daily affairs. Life in Uji is simple and the time with the students in the office, who have graduated and those who are still working in the office, creates precious memories to me.

I would also like to thank Dr. TU Chengliang from Tsinghua University for the support in the numerical model establishment and Dr. CAO Jinjian from Purdue University for the mathematical support.

The financial support from the Chinese Scholarship Council has been very helpful for me to continue my study.

Lastly, I want to thank my parents and friends for the encouragement and support.

XIE Jinzhe
November 11th, 2022